Shyam N. Jha *Editor*

Nondestructive Evaluation of Food Quality

Theory and Practice

Springer

Nondestructive Evaluation of Food Quality

Shyam N. Jha
Editor

Nondestructive Evaluation of Food Quality

Theory and Practice

Foreword by M.M. Pandey

Springer

Editor
Shyam N. Jha
Central Institute of Post-Harvest
Engineering and Technology (CIPHET)
Agricultural Structures and Environmental Control
Ludhiana 141004
India
snjha_ciphet@yahoo.co.in

ISBN 978-3-642-15795-0 e-ISBN 978-3-642-15796-7
DOI 10.1007/978-3-642-15796-7
Springer Heidelberg Dordrecht London New York

Library of Congress Control Number: 2010937779

Cover design: eStudio Calamar S.L., Heidelberg

Printed on acid-free paper

Springer is part of Springer Science+Business Media (www.springer.com)

Foreword

Fast changing global market has unleashed tremendous activities world over to accelerate the pace of economic growth. In the process, majority try to sell their food products without assessing their quality and safety aspects on daily basis. Food adulterations nowadays are rampant to have quick economic gain, ignoring health hazards. They are in fact partly successful in their business of selling low quality foods because of lack of technologies, which can assess the food quality and safety aspect quickly and on the spot of purchase. Consumers are therefore now more conscious for quality and safety of their food they buy, but they cannot do much because presently foods are mostly tested in laboratory, and by the time report comes interest of consumer goes down, some epidemic due to food poisoning already had have taken place and the regulatory authorities are not able to do much to stop the misshappenings. Numerous research works on nondestructive and quick testing of food quality using near infrared spectroscopy, Fourier transform infrared spectroscopy, colour and visual spectroscopy, electronic nose and tongue, computer vision (image analysis), ultrasound, X-ray, CT and magnetic resonance imaging are thus being carried out worldwide.

All these technologies are different and are being applied for nondestructive evaluation of different quality attributes of food materials on-site. Many books are therefore published on each of the above topic and researchers may not be able to afford to buy and carry them all the time. I am happy to see that the book on "Nondestructive Evaluation of Food Quality: Theory and Practice" includes one chapter on each of above topic covering all aspects of theory/basics in brief, practical applications (sampling, experimentation, data analysis) for evaluation of quality attributes of food and some recent works reported in literature by the renowned scientists/professors from USA, South Korea and India. I hope the purpose of this book to guide the researchers at one platform to use any technology before and during experimentation, data analysis and reporting will be fulfilled to all in general and the new researchers coming in particular.

I warmly congratulate the editor of the book who himself is a pioneer in nondestructive methods of quality evaluation of food in India; and authors of different chapters who are well known in their own field for bringing such book on right time

through a right publisher M/S Springer Verlag, Germany. I hope the book will be publicized and distributed fast to harness the benefit of hard work of editors and authors and R & D work will be accelerated in these areas. I wish them all success in their endeavour.

Indian Council of Agricultural Research M.M. Pandey
New Delhi, India

Preface

Food quality and safety are of paramount importance for consumers, retailers as well as regulators engaged in enacting food laws. Mostly quality and safety parameters are checked using the traditional laboratory (wet-chemistry) methods, which are time consuming, laborious and leaving samples after test unfit for consumptions. Nondestructive methods, which are fast, accurate and keeping samples intact, nowadays are being increasingly tried for various kinds of food. Numerous articles and research papers are being published every year that deal with the applications of various rapid and nondestructive methods of food testing. These methods are: near infrared spectroscopy, colour and visual spectroscopy, electronic nose and tongue, computer vision (image analysis), ultrasound technology, radiography, computer tomography and magnetic resonance imaging. All these technologies are theoretically different and only a few books dealing separately with some of them are available. None of them presents all these topics at one place. This book fills the void, including one chapter on each of the above topic covering theory/basics in brief, practical applications for evaluation of quality attributes of food and some recent works reported in literature. The purpose of this book is to guide the researchers at one platform to use any technology before and during experimentation, data analysis and reporting. The editor and authors of chapters are though not responsible for any kind of loss/damage while practicing any technique or using any data reported in this book; the contents of the book would help the most the new researchers coming in this field.

The book has mainly been designed to serve as a text book for postgraduate including the Ph.D. students and new scientists having interest in these fields. It would also be useful to researchers engaged in developing fast, reliable and nondestructive methods for evaluation of food quality and safety aspects directly; and the food industries and regulators responsible to check food quality to minimize public hazards indirectly.

The nondestructive methods of evaluation of food quality involve various techniques and therefore this book could not have been possible without the help of personnel engaged in these fields. Contributions of authors of four different chapters without which this useful volume could not have been possible are highly

acknowledged. The editor wishes to acknowledge some of his colleague for reading some chapters and rendering suggestions for improvement in the manuscript.

The editor is indebted to his parents, uncle (*Lal kaka*) and the late elder brother who made him to reach such stage of editing a book of international standing. Sacrifices of my wife Bandana and two lovely daughters Priya and Preeti, especially during my 4 months stay in USA when major portions of manuscripts were prepared and editing of the same were carried out after returning to India are highly acknowledged.

Ludhiana, India Shyam N. Jha

Contents

Contributors

Rajib Bandhopadhyay Department of Instrumentation and Electronics Engineering, Jadavpur University, Kolkata 700098, West Bengal, India, rb@iee.jusl.ac.in

Nabarun Bhattacharyya Center for Development of Advance Computing (C-DAC), Kolkata 700091, West Bengal, India, nabarun.bhattacharya@cdackolkata.in

Byoung-Kwan Cho Chungnam National University, Daejeon, South Korea, chobk@cnu.ac.kr

Sundaram Gunasekaran Department of Biological Systems Engineering, University of Wisconsin-Madison, Madison, WI 53706, USA, guna@wisc.edu

Shyam N. Jha Central Institute of Post-Harvest Engineering and Technology, Ludhiana 141004, Punjab, India, snjha_ciphet@yahoo.co.in

Abhimannyu Kalne Central Institute of Agricultural Engineering, Nabibagh, Bhopal 462038, India, abhikalne7@rediffmail.com

Nachiket Kotwaliwale Central Institute of Agricultural Engineering, Nabibagh, Bhopal 462038, India, nachiket@ciae.res.in

Karan Singh Central Institute of Agricultural Engineering, Nabibagh, Bhopal 462038, India, ksingh@ciae.res.in

Chapter 1
Food Quality and Safety: An Overview

Shyam N. Jha

Food quality and safety is the foremost issue amongst the present days' consumers. Fresh fruits and vegetables are often thought of as healthful, nutritious foods having no risk of food borne illness associated with their consumption. However recent food borne illness outbreaks in countries have been traced to fresh fruits, vegetables, juices and milk. These incidences have caused producers, processors, transporters, distributors, and importers to re-evaluate quality of their fresh fruits and vegetables produce and identify the hazardous points such as production, handling and processing systems to prevent any food borne diseases.

Where fresh fruits, vegetables or any other food items are concerned, most people now are able to decide difference between a product that is of good quality and one that is not. Quality is thus an increasingly important factor in the production and marketing of these products. Consumers of majority of countries are becoming more quality conscious and the suppliers of products try to meet their choices to maintain or increase their market share. There are three Ms, i.e. Meaning, Measurement and Maintenance of quality, describing the key areas concerning quality and safety of food. The primary emphasis of this chapter is the general discussion on what food quality and safety are and how to control the critical points to produce quality and safe food.

1.1 What Is Food Quality?

The term quality stands for rated ability of a product, whether it is a food or fruits and vegetables, to perform its functions. Quality implies the degree of excellence of product or its suitability for a particular use. In other words quality can be viewed as an absence of defects in a product. So, quality means different things to different handlers within the distribution chain. Food *quality* embraces both sensory attributes that are readily perceived by the human senses and hidden attributes

S.N. Jha (✉)
Central Institute of Post-Harvest Engineering and Technology, Ludhiana 141004, Punjab, India
e-mail: snjha_ciphet@yahoo.co.in

S.N. Jha (ed.), *Nondestructive Evaluation of Food Quality*,
DOI 10.1007/978-3-642-15796-7_1,

such as safety and nutrition that require sophisticated instrumentation to measure. Quality is thus a human construct for a product comprising many properties and characteristics desired by them. Quality produce encompasses sensory properties (appearance, texture, taste and aroma); nutritive values (chemical constituents), mechanical properties, functional properties and defects. Quality is not a single, well-defined attribute but comprises many properties and characteristics.

In the ISO 9000 standard (developed by the International Standard Organization) quality is defined as "the totality of the features and characteristics of product or service that bear on its ability to satisfy stated or implied needs".

Kader (1997) defines it for fruits and vegetables as "the combination of attributes or properties that give them value in term of human food". Quality may be equated to meeting the standards required by a selective customer. In this context the customer is the person or organization receiving the product at each point in the production chain. This is important because quality is perceived differently depending on the needs and intentions of the particular customer. If some thing is not a quality product this implies that the product does not meet a certain standard that has been adopted by the customer. In this case the market price is adversely affected. Conversely, if a product is perceived to be a quality product, then it can be sold at a better price.

1.2 Quality Factors for Fresh Fruits and Vegetables

Following are the factors that can be included in any discussion of quality.

(i) Hygiene and quarantine factors:

- (a) Quarantine – passenger parasites (larvae, pupae, adults)
- (b) Consumer safety-natural toxicants, contaminants, mycotoxins (fungi etc.) microbial contaminants.

(ii) Cosmetic appearance:

- (c) Size: weight, volume, and dimensions
- (d) Shape: regularity, length, diameter
- (e) Surface texture: smoothness, waxiness, gloss
- (f) Colour: uniformity, intensity, spectral
- (g) Physiological: browning, genetic defects etc.

(iii) Texture and flavor factor:

- (h) Texture- firmness, juiciness, fibrousness
- (i) Flavor – sweetness, sourness, off flavor, off odors, etc.

(iv) Nutritional: cancer inhibitors, carbohydrates, lipids, minerals, proteins, vitamin, etc.

The ultimate objective of the production, handling and distribution of food materials is to accommodate the above factors to satisfy the consumer. While the term quality has been defined in many ways and contexts in preceding paragraph, there is little agreement as to what it is, how it can be measured, and how it relates to consumer acceptability.

1.3 Quality Orientation

Quality of food products changes as it proceeds from processors to handlers after harvest. The relative importance of different quality attributes changes from handling to purchase to consumption. Shewfelt (1999) points out that quality is often defined from either product orientation or a consumer orientation. An understanding of the different perspectives of different participants in postharvest distribution is essential in any attempt to improve the quality of a fresh fruit or vegetable for the consumer.

A product orientation views quality as a bundle of attributes that are inherent in a product and can be readily quantified throughout handling and distribution. A consumer orientation defines quality in terms of consumer satisfaction, a much less tangible and less quantifiable concept. Both orientations have strengths and limitations in the delivery of fresh items from harvest of the consumer. Selection of measurement techniques and development of product standard depend on the orientation. Failure to appreciate the differences in perspective results is barrier to improvement in fresh fruit and vegetable quality.

1.3.1 Product-Oriented Quality

Most postharvest research (physiological as well as technological) assumes a product orientation to quality. Quality is defined as a series of attributes selected on the basis of accuracy and precision of measurement. These attributes are in turn used to evaluate the effect of a breeding line or transgenic product, chemical or quarantine treatment, handling technique or system, set of storage conditions or other postharvest variables. Product-oriented quality is readily defined and clearly understood. Quality changes can be plotted as a function of time and directly related to changes occurred, such as increase in free fatty acid in oil and rancidity of rice bran during handling and storage. These data can be used to develop a mechanistic understanding of effects on loss of quality. Product-oriented quality is usually measured with analytical instruments and the data can be readily analyzed with results readily reproduced. The accuracy and precision of measurement provide "internal validity" to any scientific study. A product orientation provides a clear assessment of which treatment(s) are superior or inferior within the context of study objectives.

Product-oriented quality has its limitations however. Measurements that are less readily quantified carry less weight than those that are readily quantified. Such

biases then tend to favour handling and storage treatments that maintain appearances (a readily quantifiable attribute) over texture (less quantifiable) over flavor (very difficult to quantify). Likewise, sugar and acid measurement (readily quantified) are likely to predominate over volatile compound analysis. Instrumental methods are preferred to sensory evaluation, which is preferred over consumer testing. While generation of large dataset provides a wide range of attributes to separate effects of postharvest treatments, the results lack "external validity" or "the extent to which the test results can be generalized to market behaviour". Thus, it is not possible to determine if the significant differences observed in appearance by treatment are even detectable by many consumers much less lead to a change in purchase behavior. Likewise it is not possible to determine whether large differences in predominant volatile compounds affect flavour perception any more than small differences in compounds present in trace amounts. In addition, the product-oriented approach is unable to keep pace with changes in consumer desires and expectations.

A product orientation to quality is the best at assessing the effectiveness of change in a handling system like cultivar selection, harvest technique or postharvest treatment. It can be adjusted to become more responsive to the marketplace if the quality attributes important to consumers are known and accurate and precise measurements can be obtained.

1.3.2 Consumer-Oriented Quality

A consumer orientation to quality requires an understanding of consumer behavior and is focused at predicting product performance in the marketplace. When performed well consumer-oriented studies provide external validity, thus giving a better appreciation of potential performance in the marketplace. Such studies focus more on measuring human perception and behaviour than measurement of specific quality attributes. Measurement of consumer attitudes can be simplified to determine either acceptability (superior, acceptable or unacceptable) or willingness to purchase. Qualitative consumer studies can be used to identify quality attributes that drive acceptability at the points of purchase and consumption. Judicious coupling of quantitative consumer panels with sensory descriptive analysis can either verify or refute the accuracy of consumer statements about the critical quality attributes.

A consumer-oriented approach to quality has its own limitations. The consumer is frequently viewed as a monolith with consistent preferences. Realistically consumer preferences vary widely from one cultural or demographic perspective to another, from one consumer to another within a cultural or demographic group, or even within the same consumer depending on many factors including current mood and intended use of the product. Critical quality attributes that drive product acceptability can be more easily identified using a consumer-oriented approach, but these attributes may be difficult to measure accurately and precisely. While consumers represent only valid sources of preference or acceptability, they are not good at expressing the rationale for these preferences. Furthermore, it may be difficult to quantify these attributes during handling and storage.

A consumer orientation to quality is best at identifying consumer needs and expectations. It can be made more useful to physiologists if the consuming population can be segmented into distinct user groups, based on quality preference rather than demographic groupings and expressed as a percentage distribution of the population. It is an exact tool in assessing a particular experimental treatment within the distribution chain.

1.4 The Quality Paradox

It has been my observation that within a food handling chain, for a given product longer the shelf life, poorer is the quality delivered to the consumer. From a product orientation, this statement is counterintuitive because the longer the shelf life, the slower quality deterioration of the product during handling and storage and the more likely a consumer is to purchase and consume it at an acceptable level of quality. From a consumer orientation, evaluation of quality is of prime importance at only two points – purchase and consumption. Management decisions made within a distribution chain to extend shelf life (selection of cultivars that ship well, maturity at harvest, holding of product within the shelf life for an increase in price, use of visual grading standards, etc.) all conspire to reward improved appearances frequently at the expense of flavour.

Individual variability between fresh items within the same lot represents a quality defect from a product orientation as it interferes with the ability to accurately predict quality changes during postharvest distribution under controlled conditions. From a consumer orientation, such variability provides consumers with a greater chance for matching their needs to available product particularly reflect consumption preferences. A technique that models changes in individual items rather than modeling changes in average quality was found to be a much more effective predictor and should be an effective means of merging product and consumer orientations for studies using non destructive quality measurements.

Studies using a consumer orientation to quality are likely to provide important and sometimes unexpected results. Consumers are most satisfied with fresh items like bananas and lettuce where the purchase signals of quality are an accurate predictor of consumption quality. Dissatisfaction with fresh products appears to be a result of a faulty linkage between purchase and consumption attributes. While most consumers cite flavour as an overriding consideration when asked how they evaluate good products particularly oil, consumer tests suggest that today's consumers are much more sensitive to subtle differences in texture than colour and flavour and tend to use them as the primary limiting factors for acceptability.

1.5 Implications of Quality Orientation

Product oriented quality is well suited to meet the needs of distributors. It provides the best means of developing and assessing technical advances in postharvest handling. It is more likely to emphasize appearances leading to extended shelf life

and lower prices at the expense of flavour and disgruntled consumers. Consumer-oriented quality is better suited to produce that is sensitive to the needs of consumers. It is more likely to emphasize flavour at the expense of appearances leading to shorter shelf life, higher prices, greater losses and disgruntled distributors.

Adherence to one type of orientation with a disregard of the other can have dire consequences. The overemphasis on a product orientation to quality that has dominated the American market in fresh fruits and vegetables has bred an overreliance on appearance at sacrifice of flavour, particularly with items such as tomatoes and peaches. A good understanding of postharvest physiology and shelf life extension has not translated into greater acceptance of fruit and vegetable quality. A switch to a consumer orientation presents a different set of problems, particularly with respect to consumer variation and validity of quality measurements. A better appreciation of differences in quality orientation should lead to development of better handling systems that are more responsive to consumer desires. A distribution enterprise that is willing to incorporate a consumer-oriented approach to postharvest handling of fresh fruits and vegetables and can accept the initial losses associated with the switch is likely to become the dominant figure in produce industry. A failure of the produce industry to be responsive to consumer wants and need could lead to a decline in fruit and vegetable consumption and, in turn, less interest in postharvest research that failed to meet industry need.

1.6 Food Safety

As the common saying goes "Prevention is better than cure", it assumes utmost significance in case of food products consumed by us. Many unnoticed chemicals, which may cause irreversible damage to human in many unnoticed forms, are found in food items and drinks. Even drinking water of every place is not safe. With the publicities of these unwanted harmful adulterants through various media, there has been a growing awareness among manufacturers and consumers alike regarding the need for assuring safety of consumer products, especially foods. The introduction of highly automated manufacturing systems coupled with innovations in packaging and distribution systems has led to quicker and more efficient production and distribution. In addition, there has been a drastic shift towards food products that have higher shelf life. On the plea of safety from food, our various export consignments are rejected at foreign ports (Buchanan 1990). To avoid such situations, various agencies and bodies for certification of food products are setting up stringent quality standards.

Due to progress in science and technology – and the increasingly stringent legislation of many countries that has resulted – today's agri-foodstuffs sector must respect ever stricter standards and increasingly rigorous quality control and monitoring procedures. Yet paradoxically, over the past decade there have also been an increasing number of food alerts – artificial milk, pesticides in soft drinks, argemone oil in mustard oil – creating a genuine crisis of confidence among consumers. Research on food safety and quality must therefore be a priority.

The paradox stems from changes resulting from two factors. While the globalization of supply and commerce provides for a very varied range of produce in the shops, it inevitably increases the risk of poor quality. Also, the economic pressure for ever-growing rationalization of the complete agri-foodstuffs chain – from the farm to the supermarket shelf, including processing and transport – results in produce being sold in bulk. When there is a problem at any stage of this chain, the threat of contamination can consequently assume alarming proportions with the potential of placing large sections of the population at risk.

The agri-foodstuffs sector is now increasingly exposed to "industrial" risks. Apart from the very particular cases of BSE (or mad cow disease), which originated in the United Kingdom, or the Belgian "accident" concerning dioxin contamination, attributable to the gross negligence of a supplier of animal feed, scientists are most concerned by the much stealthier and generalised increase in the frequency of illnesses linked to microbiological contamination by Salmonella, Campylobacter and Listeria.

Another problem is the exposure to chemical elements contained in food, whose source is much more difficult to trace. These may be natural toxic products (such as mycotoxins) or a whole range of contaminants (compounds originating in pesticides, dioxins, mercury, lead, and radionuclides).

There is, therefore more attention to food safety than quality control and monitoring is required (Dean 1990). Biotechnology has opened up a vast field of exploration into new methods of agricultural production, including the creation of genetically modified plants and nutritional inventions such as so-called "functional" foods or "pharmafoods" or BT eggplant fruits.

The GMO debate is currently raging between the promoters of these innovations, who justify them in the name of the progress they bring (in particular for solving environmental problems as well as problems of hunger or food shortages in the world's poorest countries), and their opponents, who condemn a profit motive and a lack of both health and environmental precautions. But the debate is going nowhere – a situation which created yet another reason for intensifying research.

Above all, the growing emphasis now is on rapid transfer of manufactured food to the consumer, which has narrowed down the safety margins that existed for microbiological decontamination of food products. The rapid change in technology has also resulted in microorganisms gaining resistance to anti-microbial products such as antibiotics. Interestingly microorganisms that were considered safe are also now a potential threat. There is a definite need, therefore, to ensure that all food products manufactured meet appropriate safety requirements. Food safety needs to be assured for the following reasons:

(a) To prevent *spoilage* of products due to microbial growth.
(b) To prevent *health hazards* to consumers due to pathogens.
(c) To protect the consumers from harmful/hazardous chemical contamination

Besides the need to protect the consumer from hazards and protect the brand image of the manufacturer, it has become necessary to implement microbial safety

assurance programs to conform to the specific government regulations. As the world economy is becoming increasingly global, interactions between various countries in terms of exports and transfer of technology has become very important. Since different countries have different safety criteria for various consumer products, there exists an urgency and need to develop safety assurance procedures that can be applied uniformly across international borders (Corlett 1993).

1.6.1 Management of Food Quality and Safety

In fruit or vegetable market, meeting a standard to govern the production and post-production handling of product requires the appropriate quality assurance method. To maintain the standard an appropriate quality control program is required to be established. The ISO 9000 series of standard is a major helping guide to establish a standard. For every food product a clear standard is defined, as this give producer a clear indication of what actually is needed. Such standard tend to be large documents. They can be developed by producer or by marketing and retail organization for their own products.

The application of management systems like ISO 9000 and HACCP (Hazard Analysis Critical Control Point) to food safety and quality has been introduced in the industry in the developed countries and has been reviewed (Mayes 1993). ISO 9000 is a specification for quality management system, which is accepted as being applicable to all manufacturing and service industries. It requires manufacturers to define their own standards and demonstrate that they conform to them. HACCP was initially developed for identification of microbiological hazards and now is being considered as being the most cost effective means of controlling food-borne diseases and other adverse developments in the body in the form of infections and intoxications arising from physical, chemical or microbiological hazards. It is more of a self-assessment system and is aimed mainly at food safety, which will help in generating confidence in the customers.

1.6.2 Safety and the HACCP System

Product safety assurance is an exercise that covers a whole gamut of interactions between product ingredients, processing methods, manufacturing environment and the other critical areas of manufacturing process that may affect the microbiological quality and safety of the product. Due to large processing volumes and short processing time, it is nearly impossible to monitor every aspect of manufacturing process. However, it is possible to monitor certain key areas (“critical points”) where implementation of safety measures can reasonably assure the safety of the manufactured product (Bauman 1990). This is the basis for the HACCP system, which is a systematic approach for identification, assessment and control of hazards. The system offers a rational approach to the control of potential hazards in foods, which avoids the many weaknesses inherent in the inspection process or approach and

circumvents the shortcomings of reliance on end product testing. By focusing attention on the factors that directly affect the safety of a food, it also eliminates wasteful use of resources on extraneous considerations, while ensuring that the desired level of safety and quality are maintained.

1.6.3 HACCP Principles

There are basically seven principles, which summarize the theme of HACCP that are of importance from international perspective. These are:

Principle 1 Identification of the potential hazard (s) associated with food production at all stages, from growth, processing, manufacture and distribution, till the point of consumption. Assess the likelihood of occurrence of the hazard (s) and identify the preventive measures for control.

Principle 2 Determination of the point(s)/procedures/operational steps that can be controlled to eliminate the hazard (s) or minimize its likelihood of occurrence- (Critical Control Point: CCP).

Principle 3 Fixing target level(s) and tolerances, which must be met to ensure the CCP is under control.

Principle 4 Establishment of a monitoring system to ensure control of CCP by scheduled testing or observation.

Principle 5 Establishment of a mechanism for the corrective action to be taken when monitoring indicates that a particular CCP is not under control.

Principle 6 Documentation (record – keeping) concerning all procedures and records appropriate to these principles and their application.

Principle 7 Establishment of verification procedures, which include appropriate supplementary tests and procedures to confirm that HACCP is working effectively.

1.6.4 Practical Implementation of HACCP Systems

The implementation of HACCP usually involves two separate stages, namely, preliminary preparation and application of HACCP principles.

1.6.4.1 Stage 1: Preliminary Preparation

(a) Creating the HACCP team

The multi-disciplinary HACCP team should comprise of a quality assurance specialist who understands the biological, chemical or physical hazards connected with a particular product group, a production specialist who has the responsibility of looking after the whole process for manufacturing the product, an engineer who has a good knowledge of hygiene, design and operation of a

plant and equipment, a packaging specialist who has a thorough knowledge of the effect of packaging material, nature of packaging material for the desired product, a distribution specialist who has an expertise in the area of handling, storage and transportation right from production to consumer, a hygiene specialist who has the responsibility of looking at the process from hygiene and sanitation point of view with a proactive approach, and a microbiologist to identify the gray areas of microbial contamination, enumeration of microorganisms as and when required and suggest the safety measures (Codex Alimentarius Commission 1995a, b).

(b) Describe the food product

The main purpose of this section is to provide as much information as possible to the HACCP team for proper evaluation. The description must include the following:

Composition of product (e.g. list of ingredients, including description or specifications of the raw materials), characteristics of product (e.g. solid, liquid, emulsion, pH, Brix etc), processing methods (heating, smoking, cutting/slicing, freezing), packaging methods/systems (vacuum, modified atmosphere, controlled atmosphere), storage and distribution conditions, expected shelf life, instructions for use.

(c) Identification of intended use

State the intended use of the product by the consumer and the consumer target group, e.g., general public, institutional caterers, infants etc.

(d) Construct a flow diagram

The purpose of this step is to provide a clear, simple picture of all steps involved in producing the product. The flow diagram must cover all steps in the process that are under direct control of the manufacturing unit from receipt of raw materials through distribution of the finished product (Process flow chart for manufacturing of tomato puree is presented for guideline in Fig. 1.1).

(e) On – site verification of flow diagram

It is important for the HACCP team to verify the flow diagram on-site during operating hours. Any deviation must result in an amendment of the original flow diagram. If the analyses are applied to a proposed line, pre-production runs must be observed carefully.

An effective HACCP programme works only on a specific product and process and must take into account the actual procedure that is in use. For HACCP programme to be useful, data generated from an initial HACCP study needs to be constantly updated and implemented to assure maximum product safety.

1.6.4.2 Stage 2: Application of HACCP Principles

Principle 1 Identification of the potential hazard(s) associated with food production at all stages, from receiving of raw material till consumption of processed food. Assess the likelihood of occurrence of the hazard (s) and identify the preventive measures for control.

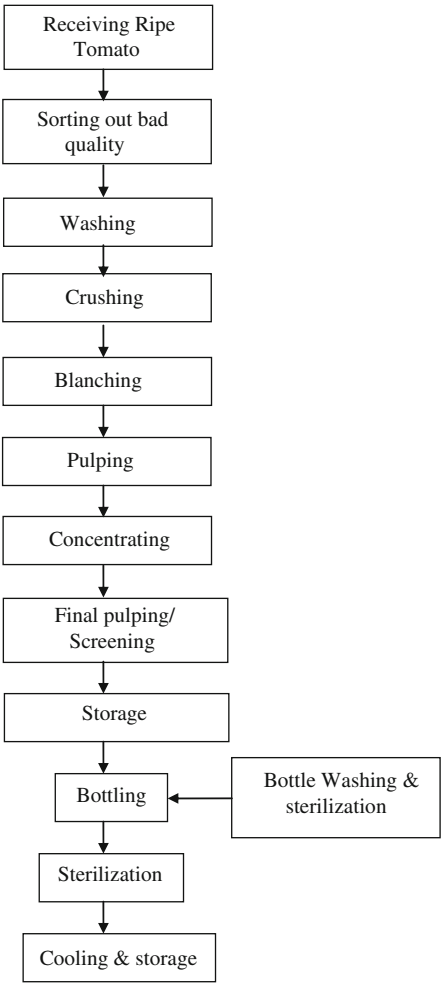

Fig. 1.1 Process flow chart for manufacturing of tomato puree

On the basis of the flow diagram generated, the HACCP team should be able to identify all the potential hazards that are expected to occur at each step. Hazards must be of the nature such that their elimination or reduction to acceptable levels is essential for the production of safe food. Once all the potential hazards have been identified, the HACCP team may then consider and describe the control measures to be adopted. There is a possibility that more than one control measure is required to control one hazard and vice versa.

Principle 2 Determination of the point, procedures/operational steps that can be controlled to eliminate the hazard(s) or minimize its likelihood of occurrence- (Critical Control Point: CCP).

The identification of CCP's requires a logical approach such as the CCP decision tree (Fig. 1.2). The sequence given in the flow diagram must be strictly followed. At each step, the decision tree must be applied to each hazard whose occurrence is probable and each control measure identified. The CCP is specific for specific product as every product by and large requires different manufacturing process and must not have unwanted or unnecessary critical points.

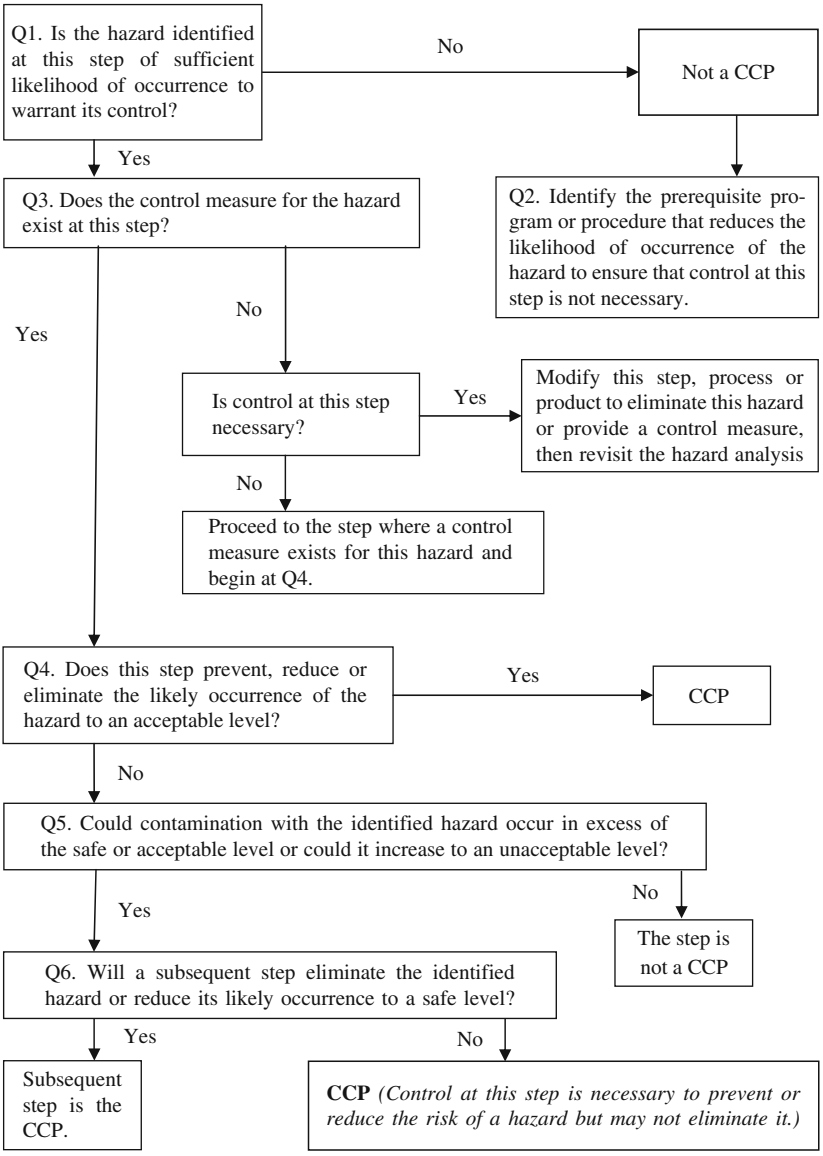

Fig. 1.2 Decision tree for identifying the critical control points

Principle 3 Fixing target level(s) and tolerances which must be met to ensure that the CCP is under control.

The critical limits for each CCP or control measure should represent some quantitative (measurable) parameters that can be measured relatively quickly and easily. For example, parameters like temperature, time, pH, preservative level, firmness, texture, appearance etc. and those levels should commensurate with requirement of food standards fixed by related regulatory authority in marketing areas

Principle 4 Establishment of a monitoring system to ensure control of the CCP by scheduled testing or observations.

The programme should describe the procedure, frequency and personnel responsible for carrying out the measurements or observations. The monitoring system could be on-line (flow rate, temperature) or off-line (measurement of total solids, carbon dioxide levels etc.). On-line systems give an immediate indication of the performance so it is desirable to have on-line continuous monitoring systems for each CCP but the same is not practically possible many times. It is therefore important for the HACCP team to ensure that the results obtained are directly relevant to the CCP and limitations if any are fully understood.

Principle 5 Establishment of mechanism for corrective action once a particular CCP is not under control.

Since the HACCP team is a multidisciplinary in nature, it should be able to specify the action once the monitoring results show a deviation in CCP. There should be facilities and planning for immediate disposition action when the CCP goes out of the specified limits.

Principle 6 Documentation concerning all raw ingredients, procedures, and steps of processing, procedures and records etc.

A comprehensive record keeping system for ingredients, processes, and product controls should be established in order to facilitate tracing and recall of the product whenever necessary. In addition, this will also help in finding and correcting deviations in CCP's. HACCP records must include the following:

- Product description and intended use
- Complete flow diagram of the process including the CCPs
- Hazards, control limits, monitoring measures and corrective action for each CCP
- Verification procedures and data.

Principle 7 Establishment of verification procedures to confirm the effective working of HACCP

Verification is necessary to ensure that the HACCP system is working correctly. Verification is defined as those activities, other than monitoring, that determine the validity of the HACCP plan and that the system is operating according to the plan. The NAS (1985) pointed out that the major infusion of science in a HACCP system

centers on proper identification of the hazards, critical control points, critical limits, and instituting proper verification procedures. These processes should take place during the development and implementation of the HACCP plans and maintenance of the HACCP system.

One aspect of verification is evaluating whether the HACCP system is functioning according to the HACCP plan or not. An effective HACCP system requires little end-product testing, since sufficient validated safeguards are built in early in the process. Therefore, rather than relying on end-product testing, firms should rely on frequent reviews of their HACCP plan, verification that the HACCP plan is being correctly followed, and review of CCP monitoring and corrective action records.

Another important aspect of verification is the initial validation of the HACCP plan to determine that the plan is scientifically and technically sound, that all hazards have been identified and that if the HACCP plan is properly implemented these hazards will be effectively controlled (Sperber 1991). Information needed to validate the HACCP plan often includes (1) expert advice and scientific studies and (2) in-plant observations, measurements, and evaluations. For example, validation of the manufacturing and packaging process for tomato puree should include the scientific justification of the heating time and temperature needed to obtain an appropriate destruction of pathogenic microorganisms (i.e., enteric pathogens) and studies to confirm that the conditions that will deliver the required time and temperature to each pack of juice.

Subsequent validations are performed and documented by a HACCP team or an independent expert as needed. For example, validations are conducted when there is an unexplained system failure; a significant product, process or packaging change occurs; or new hazards are recognized. In addition, an unbiased, independent authority should conduct a periodic comprehensive verification of the HACCP system. Such authorities can be internal or external to the food operation. This should include a technical evaluation of the hazard analysis and each element of the HACCP plan as well as on-site review of all flow diagrams and appropriate records from operation of the plan. A comprehensive verification is independent of other verification procedures and must be performed to ensure that the HACCP plan is resulting in the control of the hazards. If the results of the comprehensive verification identify deficiencies, the HACCP team modifies the HACCP plan as necessary. Individuals within a company, third party experts, and regulatory agencies carry out verification activities. It is important that if an individual is doing verification, he has appropriate technical expertise to perform this function.

1.7 Quality and Safety Determination Techniques

Methods of determining quality and safety parameters depend on their orientation of any food. It could be broadly divided into two: analytical or objective methods and subjective or sensory methods. Both methods have their own advantages and disadvantages. Analytical methods are based on product attributes, whereas, subjective

or sensory methods are consumer oriented. Safety aspects however cannot be even determined by the sensory methods. For scientific works one needs to measure attributes numerically and thus may not be variations in those perspectives. Sensory attributes changes with sensory panels, place, religion, society and so on. Practically sensory method of quality determination is better for adoption in a particular region, whereas the objective evaluation may be helpful in development of specific instruments for measuring a specific quality attribute. The objective methods are of two types: one can be said as destructive methods and the other nondestructive. Most destructive methods use small samples and utilize them during investigation. The used sample is not reusable by the consumers. Generally it is chemical analysis and used at laboratory level. It is not necessary that whatever attributes are measured in sample will be closely related with the bulk from where samples had been drawn. There must be substantial variations. Moreover infectious foods even should not be tested by the sensory panels or actual consumers from their health point of view. In nondestructive methods, samples or bulk of materials even remain untouched. It is nondestructive because samples are not destroyed. It remains intact as well for future use.

In the preceding paragraphs various facets of quality of foods, safety from food to prevent any disastrous situation by eating them and choices of their determination techniques have been discussed. Further to know the exact condition from both quality and safety perspective, quick measurement of critical responsible parameters and that too without destroying rather harming the food in any way is of paramount importance. For this purpose instrument which measure these parameters of food nondestructively and instantly are need of the hour. Lot of work in this directions using various techniques, such as machine vision system, x-ray, CT, MRI, ultrasound, near infrared (NIR) spectroscopy, Fourier transform(FT) NIR, Medium Infrared, FTIR, electronic nose etc are being carried out worldwide. Concerted efforts are required to have an accelerated development in developing countries to have their own commodity based precision Postharvest Technology to save huge postharvest losses and life of consumers by ensuring them safe foods.

References

Bauman H (1990) HACCP: concept, development, and applications. Food Technol 44:156–158

Buchanan RL (1990) HACCP: A re-emerging approach to food safety. Trends Food Sci Technol 1:104–106

Codex Alimentarius Commission (1995a). Recommended International Code of Practice – General Principles of Food Hygiene (CAC/RCP 1-1969, Rev. 2 (1985)). In: Codex Alimentarius, vol 1B, General requirements (food hygiene), pp 1–20

Codex Alimentarius Commission (1995b) Guidelines for the Application of the Hazard Analysis Critical Control Point (HACCP) System (CAC/GL 18-1993). In: Codex Alimentarius, vol 1B, General requirements (food hygiene), pp 21–30

Corlett DA (1993) Application of the HACCP system in food manufacturing for consumer safety Assurance. In: Proceedings of Symposium on Food Quality and Safety – from Manufacturers to Consumers, 12–13 May

Dean KH (1990) HACCP and food safety in Canada. Food Technol 44:172–178

Kader AA (1997) A summary of CA recommendations for fruits other than apples and pears. In: 7th International Control Atmospheric Resolution Conference University of California, Davis, pp 1–34
Mayes T (1993) The application of management systems to food safety and quality. Trends Food Sci Technol 4(7):216–219
NAS (1985) An evaluation of the role of microbiological criteria for foods and food ingredients. National Academy Press, Washington, DC
Shewfelt RL (1999) What is quality? Postharvest Biol Technol 15:197–200
Sperber WH (1991) The modern HACCP system. Food Technol 45:116–120

Chapter 2
Colour Measurements and Modeling

Shyam N. Jha

The most common property to measure quality of any material is its appearance. Appearance includes colour, shape, size and surface conditions. The analysis of colour is especially an important consideration when determining the efficacy of variety of postharvest treatments. Consumers can easily be influenced by preconceived ideas of how a particular fruit or vegetable or a processed food should appear, and marketers often attempt to improve upon what nature has painted. Recently colour measurements have also been used as quality parameters and indicator of some inner constituents of the material. In spite of the significance of colour in food industries, many continue to analyze it inadequately. This chapter deals with theory of colour, colour scales and its measurement, sampling techniques, and modeling of colour values for correlating them with some internal quality parameters of selected fruits.

2.1 Light and Colour

Among the properties widely used for analytical evaluation of materials, colour is unique in several aspects. While every material can be said to possess a specific property such as mass, no material is actually coloured as such. Colour is primarily an appearance property attributed to the spectral distribution of light and, in a way, is related to (source of radiant energy) the illuminant the object to which the colour is ascribed, and the eye of the observer. Without light or the illuminant, colour does not exist. Therefore, several factors that influence the radiation subsequently affect the exact colour that an individual perceives. Those factors are:

- spectral energy distribution of light,
- conditions under which the colour is viewed,
- spectral characteristics of the object with respect to absorption, reflection, and transmission, and
- sensitivity of the eye.

S.N. Jha (✉)
Central Institute of Post-Harvest Engineering and Technology, Ludhiana 141004, Punjab, India
e-mail: snjha_ciphet@yahoo.co.in

S.N. Jha (ed.), *Nondestructive Evaluation of Food Quality*,
DOI 10.1007/978-3-642-15796-7_2,

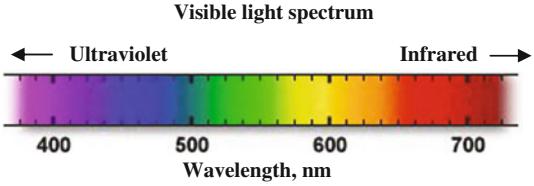

Fig. 2.1 Colour spectra of light in visible range of wavelength

Light is the basic stimulus of colours, it is important to consider the electromagnetic spectrum. Visible light forms only a small part of the electromagnetic spectrum, with a spectral range from approximately 390 nm (violet) to 750 nm (red) (Fig. 2.1). Wavelength intervals of major colour are summarized in Table 2.1. The sensitivity of the eye varies even within this narrow visible range. Under conditions of moderate-to-strong illumination, the eye is most sensitive to yellow-green light of about 550 nm (Fig. 2.2).

If the spectral distribution throughout the visible region is unequal, then the sensation of colour is evoked by radiant energy reaching the eye's retina. An equal spectral distribution makes the light appear as white. The unequal distribution responsible for colour sensation may be characteristic of the source itself; such as flame spectra (Fig. 2.2) composed of one or more monochromatic wavelengths, or may result from selective absorption by the system, which appears coloured. The latter includes several systems that show selective absorption for light and exhibit colour as a result of reflection or transmission of unabsorbed incident radiant energy. The radiant energy emitted by the radiator is characterized by its spectral quality, angular distribution, and intensity.

The following material properties, lighting of the scene and interaction of matter with light affect the total appearance of the object:

(i) Material properties:

Optical properties (spectral, reflectance, transmittance)
Physical form (shape, size, surface texture)
Temporal aspects (movement, gesture, rhythm)

Table 2.1 Breakup of wavelengths for major colours in visible range of wavelength

Colour	Wavelength interval	Frequency interval
Red	~ 700–635 nm	~ 430–480 THz
Orange	~ 635–590 nm	~ 480–510 THz
Yellow	~ 590–560 nm	~ 510–540 THz
Green	~ 560–490 nm	~ 540–610 THz
Blue	~ 490–450 nm	~ 610–670 THz
Violet	~ 450–400 nm	~ 670–750 THz

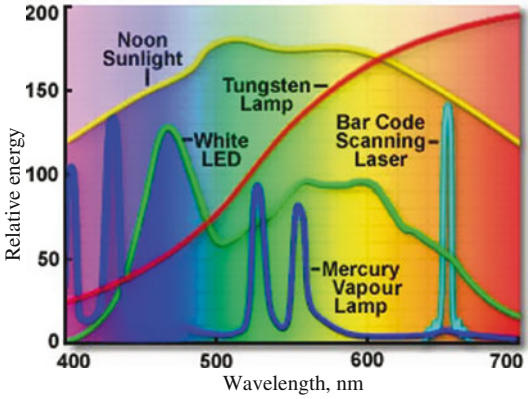

Fig. 2.2 Spectra of visible light from common light sources

(ii) Lighting of the scene:

Illumination type (primary, secondary, tertiary)
Spectral and intensity properties; directions and distributions
Colour-rendering properties

(iii) Interaction of light with matter

(a) Physical laws

When light falls on an object, it may be reflected, transmitted, or absorbed (Fig. 2.3). Reflected light is the part of the incident energy that is bounced off the object surface, transmitted light passes through the object, and absorbed light constitutes the part of the incident radiant energy absorbed within the material. The degree to which these phenomena take place depends on the nature of the material and on the particular wavelength of the electromagnetic spectrum being used. Commonly, optical properties of a material can be defined by the relative magnitudes of reflected, transmitted, and absorbed energy at each wavelength. Conservation of energy requires that sum of the reflected (I_R), transmitted (I_T), and absorbed (I_A) radiation equals the total incident radiation (I). Thus,

$$I = I_R + I_T + I_A \tag{2.1}$$

According to its transmittance properties, an object may be transparent, opaque, or translucent. Almost all food and biological products may be considered to be opaque, although most transmit light to some extent at certain wavelengths. The direction of a transmitted ray after meeting a plane interface between any two non-absorbing media can be predicted based on Snell's law:

$$n_2 \sin \theta_T = n_1 \sin \theta_i \tag{2.2}$$

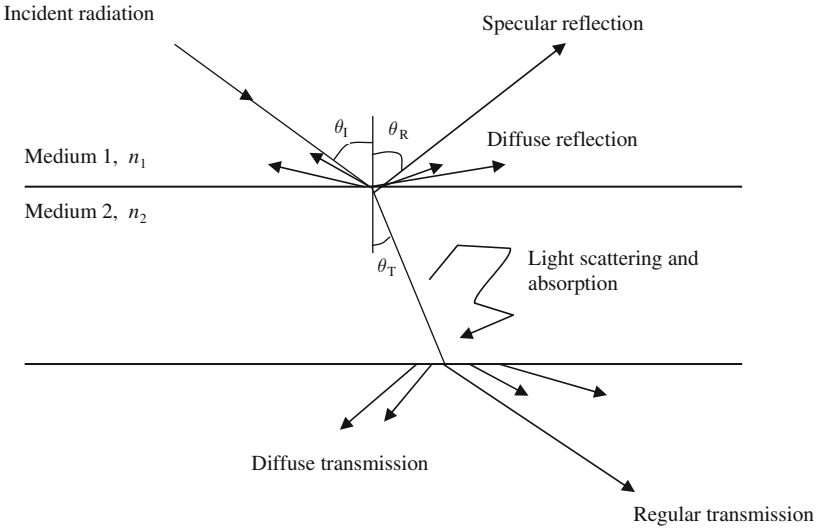

Fig. 2.3 Schematic representation of interaction of light with matter, θ_I= angle of incidence, θ_R = angle of reflectance, θ_T = angle of transmittance, n_1, n_2 = refractive index of medium 1 and 2, respectively

Beer-Lambert's law defines the attenuation of the transmitted ray in a homogeneous, non-diffusing, absorbing medium:

$$\log\ (I_T/I) = abc \tag{2.3}$$

The ratio I_T/I is known as the transmittance T and is related to absorbance A as:

$$A = \log(I/T) \tag{2.4}$$

From Eqs. (2.3) and (2.4), absorbance A can also be written as:

$$A = abc \tag{2.5}$$

where a is called the absorptivity. [if c is expressed in *mol/L* and b in *cm*, a is replaced by the molar absorptivity, ε (*L/mol.cm*).]

Various constituents of food products can absorb a certain amount of this radiation. Absorption varies with the constituents, wavelength, and path length of the light. Reflection is a complex action involving several physical phenomena. Depending on how light is reflected back after striking an object, reflection may be defined as regular or specular and diffused (Fig. 2.3). Reflection from a smooth, polished surface is called" specular" or "regular". It mainly produces the gloss or shine of the material. The basic law of specular reflection states that the angle at which a ray is incident to a surface must equal the angle at which it is reflected off the surface. Fresnel equations define the phenomenon of specular

reflection. The intensity of parallel R_{pl} and perpendicular R_{pr} components of the reflected light are:

$$R_{pl} = \left[\frac{(n_2/n_1)^2 \cos\theta_I - [(n_2/n_1)^2 - \sin^2\theta_I]^{1/2}}{(n_2/n_1)^2 \cos\theta_I + [(n_2/n_1)^2 - \sin^2\theta_I]^{1/2}} \right]^2 \tag{2.6}$$

$$R_{pr} = \left[\frac{\cos\theta_I - [(n_2/n_1)^2 - \sin_2\theta_I]^{1/2}}{\cos\theta_I + [(n_2/n_1)^2 - \sin^2\theta_I]^{1/2}} \right]^2 \tag{2.7}$$

The regular reflectance $R = R_{pl}{}^2 + R_{pr}{}^2$ and for normal incidence ($\theta = 0°$), $R_{pl} = R_{pr,}$ and hence.

$$R = \left[\frac{n_2 - n_1}{n_2 + n_1} \right]^2 \tag{2.8}$$

where n_1 and n_2 are refractive index of the medium and object, respectively: and θ_I is the incident angle (Fig. 2.3). If the material is absorbing, the refractive index is a complex number n (1-ik), where n is the real part of the complex number and k is an absorption constant, and the regular reflectance is written as:

$$R = \left[\frac{(n_2 - n_1)^2 + (n_2 k)^2}{(n_2 + n_1)^2 + (n_2 k)^2} \right] \tag{2.9}$$

When the incident light is reflected from a surface evenly at all angles, the object appears to have a flat or dull finish termed "diffuse reflection". No rigorous theory has been developed for diffuse reflectance, but several phenomenological theories have been proposed, the most popular being the Kubelka-Munk theory. The Kubelka-Munk model relates sample concentration to the intensity of the measured spectrum in a manner analogous to the way Beer-Lambert's law relates band intensities to concentration for transmission measurements. The Kubelka-Munk function $f(R_\infty)$ is generally expressed as:

$$f(R_\infty) = \frac{(1 - R_\infty)^2}{2R_\infty} = \frac{k}{s} \tag{2.10}$$

where R_∞ = absolute reflectance of an infinitely thick layer, k = absorption coefficient, and s = scattering coefficient.

Kubelka-Munk theory predicts a linear relationship between spectral data and sample concentration under conditions of constant scattering coefficient and infinite sample dilution in a non-absorbing matrix such as KBr (potassium bromide). Hence, the relationship can only be applied to highly diluted samples in a non-absorbing matrix. In addition, the scattering coefficient is a function of particle size, so samples must be prepared to a uniform fine size for quantitative valid measurements.

It is not easy to quantify diffuse reflectance measurements since sample transmission, scattering, absorption, and reflection all contribute to the overall effect. By reducing particle size and dilution in appropriate matrices, surface reflection that can give strong inverted bands is reduced and the spectra more closely resemble transmission measurements. Typically, quantitative diffuse reflectance measurements are presented in log(*I*/*R*) units, analogous to absorbance log(*I*/*T*) units for transmission measurements. Bands increase logarithmically with changes in the reflectance values. By comparison, bands in spectra displayed in Kubelka-Munk units vary as a function of the square of reflectance. This difference emphasizes strong absorbance bands relative to weaker bands.

The diffuse reflectance may be measured with respect to non-absorbing standards and converted to produce a linear relationship with concentration c as follows:

$$\log (R'/R) = \log (I/R) + \log (R') \cong ac/s \tag{2.11}$$

where R' and R – reflectance of the standard and the sample ($R' > R$), a = absorptivity, c = concentration, and s = scattering coefficient. For monochromatic radiation, *log* R' is constant and may be ignored, and Eq. (2.11) may be written as (2.12):

$$c = k + (s/a) \log (I/R) \tag{2.12}$$

where k = absorption coefficient. It should be noted that s is not a constant but depends on a number of properties of the sample such as particle size (s is inversely proportional to particle size) and moisture content. In food materials, the primary factors that influence light reflection is a phenomenon known as scattering or diffusion. If the surface of incidence is rough, incident light will be scattered in all directions. Since the incident rays strike a rough surface more than once before being reflected, they would be expected to have a lower total reflectance than those reflected from a smooth surface.

In classical optics, diffuse reflection was thought to be responsible for colour. It was also commonly believed that colour of natural objects, such as foods, plants and foliage, are seen by means of light reflected off their surfaces. It is also known that the light must be transmitted through pigment within the cells in order to produce a coloured appearance. Since most food materials are optically non-homogeneous, light entering such material is scattered in all directions. Only about 4–5% of the incident radiation is reflected off the surface of these materials as regular reflectance. The remaining radiation transmits through the surface and encounters small interfaces from within the material and is scattered back to the surface through the initial interface. This type of reflection is termed as "body reflectance". The body reflectance is nearly always diffuse and is the most significant form of reflectance for foods. Some part of the transmitted light diffuse deeper in to the material and may eventually reach the surface some distance away from the incident point.

(b) Factors affecting diffuse reflectance spectral data

Diffuse reflectance spectroscopy offers exceptional versatility in sample analysis. This versatility results from both its sensitivity and optical characteristics. Classically, diffuse reflectance has been used to analyze powered solids in a non-absorbing matrix of an alkali halide such as KBr. The sample is typically analysed at low concentrations, permitting quantitative presentation of the data in Kubelka-Munk unit. This technique yields spectra that are qualitatively similar to those produced by conventional transmittance or pellet methods. However, they exhibit higher sensitivity for quantification and are less subject to scattering effects, that cause slopping baselines in pellet measurements.

Several factors determine band shape and relative/absolute intensity in diffuse reflectance spectroscopy through their effect on the reflection/absorbance phenomena specific to the sample. These include:

refractive index of the sample,
particle size,
sample homogeneity, and
concentration.

Refractive index: Refractive index affects the results via specular reflectance contributions to diffuse reflectance spectra. With organic samples, the spectra display pronounced changes in band shape and relative peak intensities, resulting in non-linearity in the relationship between band intensity and sample concentration. For some inorganic samples, strong specular reflection contributions can even result in complete band inversions. Sample dilution in non-absorbing matrix can minimize this overlay of diffuse reflectance and specular reflectance spectra, as well as the resulting spectral distortions. In addition, accessory design can help reduce specular reflectance contributions.

Particle size: Particle size is a major consideration when performing diffuse reflectance measurements of solids. The bandwidth is decreased and relative intensities are dramatically altered as particle size decreases. These effects are even more pronounced in spectra of highly absorbing inorganic materials with high refractive indices. For these samples, specular contributions can dominate the final spectra if the particle size is too large. To acquire a true diffuse reflectance spectrum, it is necessary to uniformly grind the sample and dilute it in a fine, non-absorbing matrix. Similar preparation must be applied to the non-absorbing matrix material in order to provide an "ideal" diffuse reflector for background analysis and as a support matrix for the samples.

Sample homogeneity: The Kubelka-Munk model for diffuse reflectance is derived for a homogeneous sample of infinite thickness. However, some sample analysis methods, especially those designed for liquid sample (e.g., deposition of sample onto a powdered supporting matrix) can result in a higher concentration of sample near the analysis surface. In these circumstances, variations in relative peak intensities may be noticed. In particular, more weakly absorbing wavelengths tend to be attenuated at higher sample concentrations. To avoid these peak intensity variations it is necessary to distribute the analyte as uniformly as possible within the non-absorbing background matrix.

Concentration: One particularly important advantage of diffuse reflectance spectroscopy, especially in comparison to transmittance measurement, is its extremely broad sample-analyzing range. While it is theoretically possible to acquire usable diffuse reflectance spectra on samples of wide-ranging concentrations, practical considerations often complicate the analysis process. With high concentration samples, especially those with a high refractive index, one can expect a dramatic increase in the specular contribution to the spectral data. As a result, some sample data may be un-interpretable without adequate sample dilution. Even when samples can be measured satisfactorily at high concentrations, it is advisable to grind the sample to a very uniform and fine particle size to minimize both specular reflectance and sample scattering effects, which adversely affect quantitative precision.

From the preceding paragraphs one can say that in reality, colour is in the eye of the observer, rather than in the "coloured" object. The property of an object that gives it a characteristic colour is its light-absorptive capacity. Three items (light source, object and observer) therefore are necessary for visual perception of colour and the instrument quantifies the human colour perception in the visual observing situation and we measure them in different units, scale or specification.

2.2 Colour Scales

There are three characteristics of light by which a colour may be specified: hue, saturation, and brightness. Hue is an attribute associated with the dominant wavelength in a mixture of light waves, i.e., it represents the dominant colour as perceived by an observer. Saturation refers to relative purity or the amount of white light mixed with a hue. Brightness is a subjective term, which embodies the chromatic notion of intensity. Hue and saturation taken together are called chromaticity. Therefore, a colour may be characterized by brightness and chromaticity. There are numerous colour scales, one may even develop their own scale for uniformity in comparison of their subsequent products. The basic colours however are only three: red, green and blue, and other colours are derived by mixing these three. The light reflected off of the object passes through a red, green and blue glass filter to simulate the standard observer functions for a particular illuminant. A photodetector beyond each filter then detects the amount of light passing through each filter and these signals are displayed as X, Y, and Z values. The specifications of basic standards used in colourimetry however are based on definitions of The Commision de International de l'Eclairage (CIE) by general consent almost in all countries. Some industries however are also using Munsell System and atlas for their products.

2.2.1 CIE System

The Commission Internationale de l'Eclairage (CIE) defined a system of describing the colour of an object based on three primary stimuli: red (700 nm), green (546.1 nm), and blue (435.8 nm). Because of the structure of the human eye, all

colours appear as different combinations of these. The amounts of red, green, and blue needed to form any given colour are called the' 'tristimulus" values, *X*, *Y*, and *Z*, respectively. Using the *X*, *Y*, and *Z* values, a colour is represented by a set of chromaticity coordinates or trichromatic coefficients, *x*, *y*, and *z*, as defined below:

$$x = \frac{X}{X+Y+Z} \quad y = \frac{Y}{X+Y+Z} \quad z = \frac{Z}{X+Y+Z} \tag{2.13}$$

It is obvious from the equations above that $x + y + z = 1$. The tristimulus values for any wavelength can be obtained from either standard tables or figures. A plot that represents all colours in *x* (red)-*y* (green) coordinates is known as a chromaticity diagram (Fig. 2.4).

To understand the chromaticity diagram, the locus is superimposed, with the reference horseshoe curve obtained from a standard monochromatic light. It can be seen from this figure that the chromaticity of unripe fruits falls near the center of the CIE diagram. The position marked "c" in this diagram represents colour, which is biochromatically achromatic or hueless. Oil palm actually appears reddish black when unripe and this agrees well with colourimeter since this equipment treats both pure white and black as hueless. As the fruit starts to ripen; the locus moves from the hueless zone to the reddish red zone and ends at a point bordering the reddish orange zone. It can be seen from this diagram that the difference in chromaticity between unripe and underripe is relatively small compared to the difference in chromaticity between optimally ripe and overripe, indicating that there is a small degree of change in colour at the early stage of ripening. The distance between unripe and overripe is 0.202 compared to slightly over 0.03 between unripe and under-ripe. Hence, distinguishing unripe from underripe samples or vice versa may be difficult chromatically.

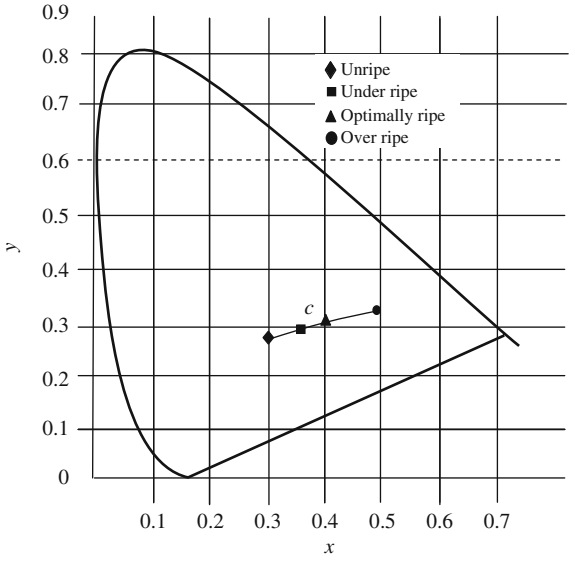

Fig. 2.4 Schematic of chromaticity diagram showing the ripeness locus of oil palm and also the location of white in illuminant "c"

Sometimes, tristimulus systems of representation of colours are not easily understood by the users in terms of object colour. Other colour scales therefore were developed to relate better to how we perceive colour, simplify understanding, improve the communication of colour differences, and be more linear throughout colour space. This gave the birth of opponent colour theory, which states that the red, green and blue responses are re-mixed in opponent coders as they move up the optic nerve in human brain. Based on this theory a 3-dimensional rectangular *L*, *a*, *b*, colour space was evolved, in which at *L* (lightness) axis – 0 is black and 100 is white, *a* (red-green) axis – positive values are red; negative values are green and zero is neutral, and *b* (blue-yellow) – positive values are yellow; negative values are blue and zero is neutral (Fig. 2.5). All colours that can be visually perceived can be plotted in this *L*, *a*, *b*, rectangular colour space.

There are two popular *L*, *a*, *b* colour scales in use today – Hunter *L*, *a*, *b*, and CIE L^*, a^*, b^*. They are similar in organization, but will have different numerical values. Hunter *L*, *a*, *b* and CIE L^*, a^*, b^* scales are both mathematically derived from *X*, *Y*, *Z* values (Table 2.2). Neither scale is visually uniform, Hunter scale is over expanded in blue region of colour space, while CIE scale is over expanded in yellow region. The current recommendation of CIE is to use L^*, a^*, b^*.

Fig. 2.5 Hunter *Lab* colour space

Table 2.2 Formulae for computation of *L*, *a*, *b*, and L^*, a^*, b^* from *X*, *Y*, *Z* values

Hunter *L*, *a*, *b*	CIE L^*, a^*, b^*
$L = 100\sqrt{\frac{Y}{Y_n}}$	$L^* = 116f\left(\frac{Y}{Y_n}\right) - 16$
$a = K_a\left(\frac{X/X_n - Y/Y_n}{\sqrt{Y/Y_n}}\right)$	$a^* = 500\left[f\left(X/X_n\right) - f\left(Y/Y_n\right)\right]$
$b = K_b\left(\frac{Y/Y_n - Z/Z_n}{Y/Y_n}\right)$	$b^* = 200\left[f\left(Y/Y_n\right) - f\left(Z/Z_n\right)\right]$

Where, Y_n is the Y tristimulus value of a specified white object. For surface-colour applications, the specified white object is usually (though not always) a hypothetical material with unit reflectance and which follows Lambert's law. The resulting L will be scaled between 0 (black) and 100 (white); roughly ten times the Munsell value. K_a is a coefficient which depends upon the illuminant (for D_{65}, which will be told in latter part of the chapter, K_a is 172.30; see approximate formula below) and X_n is the X tristimulus value of the specified white object. K_b is a coefficient which depends upon the illuminant (for $_{D65}$, K_b is 67.20; see approximate formula below) and Z_n is the Z tristimulus value of the specified white object, subscript n suggests normalized values of X, Y, Z, and

$$f(t) = \begin{cases} t^{1/3} & t > (6/29)^3 \\ \frac{1}{3}\left(\frac{29}{6}\right)^2 t + \frac{4}{29} & otherwise \end{cases} \tag{2.14}$$

The division of the $f(t)$ function into two domains was done to prevent an infinite slope at $t = 0$. $f(t)$ was assumed to be linear below some $t = t_0$, and was assumed to match the $t^{1/3}$ part of the function at t_0 in both value and slope. In other words:

$t_0^{1/3}$	=	$at_0 + b$	(match in value)
$1/3t_0^{2/3}$	=	a	(match in slope)

The value of b was chosen to be 16/116. The above two equations can be solved for a and t_0:

$a = 1/(3\delta^2) = 7.787037\ldots$
$t_0 = \delta^3 = 0.008856\ldots$

where $\delta = 6/29$. Note that the slope at the join is $b = 16/116 = 2\delta/3$

$$K_a \approx \frac{175}{198.04}(X_n + Y_n)$$

$$K_b \approx \frac{70}{218.11}(Y_n + Z_n)$$

2.2.2 Munsell System and Atlas

The Munsell colour system (Fig. 2.6) divides hue into 100 equal divisions around a colour circle. This is similar in approach to the Newton colour circle except that the circle is distorted by assigning a unit of radial distance to each perceptible difference in saturation (called units of chroma). Since there are more perceptible differences

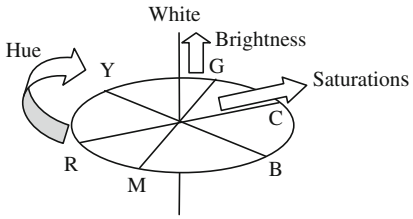

Fig. 2.6 Schematic of Munsell colour system

for some hues, the figure will bulge outward to 18 for some hues compared to only 10 for others. Perpendicular to the plane formed by hue and saturation is the brightness scale divided into a scale of "value" from zero (black) to 10 (white). A point in the colour space so defined is specified by hue, value, and chroma in the form *H*, *V* and *C*. The Munsell colour-system is therefore a way of precisely specifying colours and showing the relationships among them. Every colour has three qualities or attributes: hue, value, and chroma. A set of numerical scales with visually uniform steps for each of these attributes has been established. The Munsell Book of Colour displays a collection of coloured chips arranged according to these scales. Each chip is identified numerically using these scales. Comparing it to the chips under proper illumination and viewing conditions can identify the colour of any surface. The colour is then identified by its hue, value, and chroma. These attributes are given the symbols *H, V*, and *C* and are written in a form *H V/C*, which is called the Munsell notations. Using Munsell notations, each colour has a logical relationship to all other colours. This opens up endless creative possibilities in colour choices, as well as the ability to communicate those colour choices precisely. The Munsell system is the colour order system most widely quoted in food industry literature. Food products for which the US Department of Agriculture (USDA) recommends matching Munsell discs to be used include dairy products such as milk and cheese, egg yolks, beef, several fruits, vegetables, and fruit juices.

Other colour atlases and charts are available for use in the food industry, such as the Natural Colour System and Atlas, Royal Horticultural Society Charts, etc. These atlases and charts are used for comparison of a product colour with that of a standard colour diagram, which is also commonly practiced in the food industry. The evaluation of potato chip colour is a very good example.

Other colour scales, such as the *RGB*, *CMY*, *HSI*, *HSV*, *HLS* etc. also exist, but are very similar to the CIE system. *RGB* system is generally used in analysis of colour of an image, while others are now not in much use for measurement of colour of food items, however have been dealt in detail in Chap. 3.

2.2.3 Transformation of Colour Values from One System to Others

There are, as we have discussed above, various colour scales. These scales can be transformed from one to other forms, through simple trigonometric or mathematical

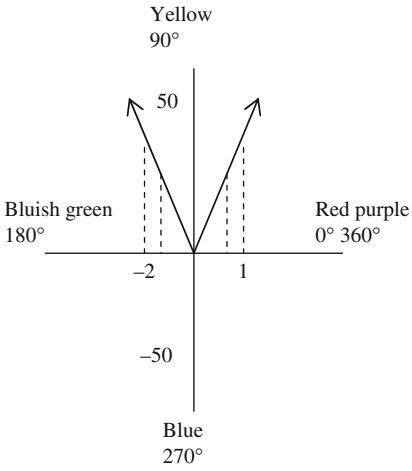

Fig. 2.7 Representation of peel hue affected by heat treatments of grape fruits. *CIE LAB* a^* and b^* values are plotted on horizontal and vertical axes respectively

functions (Eqs. 2.15, 2.16 and 2.17). A colour wheel subtends 360°, with red-purple traditionally placed at the far right (or at an angle of 0°), yellow, bluish-green, and blue follow counter clockwise at 90, 180, 270°, respectively (Fig. 2.7).

$$L = L^* \tag{2.15}$$

$$h^0 = \tan^{-1} \frac{b^*}{a^*} \tag{2.16}$$

$$C^* = \sqrt{\left(a^{*2} + b^{*2}\right)} \tag{2.17}$$

Arctangent, however, assumes positive values in the first and third and negative values in the second and fourth quadrants. For a useful interpretation, h° should remain positive between 0 and 360° of the colour shed.

Figure 2.8 shows the variation of CIE*Lab* values calculated from the oil palm image. It can be seen that both hue and chroma increase in curvilinear fashion with ripeness. The small hue and chroma values for unripe class (approximately 7.6° and 2.62, respectively) pushed the psychometric point nearer to the origin or the achromatic zone of colour. These values increased to approximately 48° in hue and 72.1 in chroma for overripe case. This location is equivalent to reddish orange colour on CIE*Lab* space. Hence, the hue-moves further away from the origin and in the upward direction as the oil palm ripens. These observations are consistent with human vision and match strongly with the trend of the ripeness locus shown in Fig. 2.4. Thus hue provides a much better discrimination compared to either *RGB* or CIE*xy* values when specifying colours of food materials. Because of this reason usually hue is chosen for colour inspection by machine.

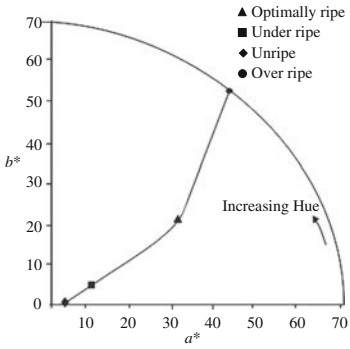

Fig. 2.8 Schematic of colourimetric plot of oil palm showing the change in hue and chroma during ripening

Unlike colourimeter, the calculation of hue using machine vision system is mathematically involved since it requires colour conversion from *RGB* to *HSl* (Hue, Saturation and Intensity) space. One way of achieving this is by firstly *I* establishing a new coordinate system, *YIQ*. The relationship between the two coordinate systems is:

$$\begin{bmatrix} Y \\ I \\ Q \end{bmatrix} = \begin{bmatrix} 0.30 & 0.59 & 0.11 \\ 0.60 & -0.28 & -0.32 \\ 0.21 & -00.52 & 0.31 \end{bmatrix} \begin{bmatrix} R \\ G \\ B \end{bmatrix} \tag{2.18}$$

Secondly, h is the rotational angle around the Q, I plane and therefore can be written as:

$$h^o = \tan^{-1}\left[\frac{I}{Q}\right] \tag{2.19}$$

Equations (2.18) and (2.19) are theoretically valid and they can be found in almost any textbook on colour and image processing. For practical reasons, $h°$ was calculated according to the Munsell's colour system, which is given by:

$$h^o = \left\{360^o - \cos^{-1}\left(\frac{-0.5\left[(R-G)+(R-B)\right]}{\sqrt{(R-G)^2+(R-B)(G-B)}}\right)\right\} \times \frac{255}{360} \; if \; B \geq G \tag{2.20}$$

or

$$h^o = \left\{\cos^{-1}\left(\frac{-0.5\left[(R-G)+(R-B)\right]}{\sqrt{(R-G)^2+(R-B)(G-B)}}\right)\right\} \times \frac{255}{360} \; if \; B < G \tag{2.21}$$

The above equation transforms *RGB* information from three-dimensional space to one-dimensional $h°$ space. In order to speed-up analysis only $h°$ values may be processed. The hue values shown in this figure are normalized to 255 for the 8-bit

machine vision system. A different approach is needed to solve this type of problem. The method investigated for this application was to treat hue distributions as features and apply multivariate discriminate technique to establish classification as discussed in Chap. 6.

2.2.3.1 Example of Transformation of CIE/Hunter *L a b* Values to Chroma (*C*) and Hue (*h*°)

Assume a practical data given in Table 2.3 for analysis of grapefruit colour after three heat treatments for quarantine control

Following subprogram may be used to compute the $h°$ and C for above data

```
Data colour
READ (* ,* ) L, a, b
C=SQRT((a* b)+(b* b))
THETA=(ATAN(b/a)/6.2832)* 360
IF a>0 AND b>=0 THEN h = THETA
IF a<0 AND b>=0 THEN h=180+THETA
IF a<0 AND b<0 THEN h=180+THETA
IF a>0 AND b<0 THEN h=360+THETA
WRITE (* ,* ) a, b, THETA, h
STOP
END
```

Table 2.3 Conversion of grapefruit *L a b* values to hue and chroma values

	Colour characteristics				
Treatment	*L*	*a*	*b*	*C*	*h*°
1	76.6	–2.0	56.0	56.0	92.0
2	74.4	2.0	56.0	56.0	88.0
3	63.0	1.2	34.0	34.0	88

2.3 Colour Measurement

It is clear by now that to see colour three things (light source, object and the observer) are needed. Similarly to measure colour three items are essential: light source, specimen object and a spectrometer (colourimeter). When we have spectrometer or colourimeter the user first goes through the operational manual of the instrument thoroughly to see the suitability for their specimen object, i.e. sample. Once suitability is judged then colour scale, illuminant and observer types, if options are available in the instrument, are selected. CIE standard illuminants are D_{50}, D_{55}, D_{65}.

2.3.1 CIE Standard Illuminants

D_{65} is a commonly used standard illuminant defined by the CIE. It is part of the D series of illuminants that try to portray standard illumination conditions at open air in different parts of the world. The subscript 65 probably is used to indicate the correlated colour temperature of 6,500 K at which it is standardized. D_{65} corresponds roughly to a mid-day sun in Western Europe/Northern Europe, hence it is also called a daylight illuminant. As any standard illuminant is represented as a table of averaged spectrophotometric data, any light source which statistically has the same relative spectral power distribution can be considered a D_{65} light source. There are no actual D_{65} light sources, only simulators. The quality of a simulator can be assessed with the CIE Metamerism index discussed elsewhere. D_{65} should be used in all colourimetric calculations requiring representative daylight, unless there are specific reasons for using a different illuminant. Variations in the relative spectral power distribution of daylight are known to occur, particularly in the ultraviolet spectral region, as a function of season, time of day, and geographic location.

2.3.2 CIE Standard Observers

CIE has standardized the observer angle of field of view. Originally this was taken to be the chromatic response of the average human viewing through a 2° angle, due to the belief that the colour-sensitive cones resided within a 2° arc of the fovea of human eye. Thus the CIE *1931 Standard Observer* is also known as the CIE *1931 2° Standard Observer*. Latter it was experimentally decided that cones were spread beyond the fovea. The experiments were repeated in 1964 resulting in 1964, 10° standard observer. Of the two sets of observer function, the 10° standard observer is recommended for better correlation with average visual assessment made with large fields of view that is typical in most commercial application.

2.3.3 Instrument Geometry

A third important aspect for selection before actual experimentation is instrument geometry. The geometry of an instrument defines the arrangement of light source, sample plane, and detector. There are two general categories of instrument geometries, directional (45°/0° or 0°/45°) and diffuse (sphere). Directional geometry typically has illumination at 45° angle and a measurement angle of 0° (meaning from top of the object or from direction perpendicular to the sample). This is called 45°/0° geometry. 0°/45° geometry has illumination at 0° and measurement at 45°. Both exclude the specular reflection in the measurement. This provides measurements that correspond to visual changes in appearance of the sample due to both changes in pigment colour and surface gloss or texture. 0°/45° instrument geometry as I think is the best for the quality determination and monitoring applications.

The fourth and the last consideration for colour measurement is the preparation and presentation of the prepared samples as discussed below.

2.4 Sample Preparation and Presentation

Availability of wide range of techniques for measurement of quality parameters, necessitates to know the suitability of characteristics of samples, i.e. whether it is liquid, solid, paste, semisolid, transparent, opaque or translucent etc for a particular technique to be employed. Complete history of the source of sample and a careful attention to proper instrument operation and consistent sample handling is required particularly for colour measurement.

2.4.1 Preparing Samples for Measurement

During sample measurement it is important to select them appropriately, using an established method of sampling, and handling all samples in a consistent manner.

(a) Selecting samples
Sample representative of the entire batch should be selected for measurement. One should always try to collect as number of varied materials as possible from different sources whose colour is to be measured and

1. Choose samples that are truly representative of the materials collected from various sources,
2. prepare samples in exactly the same manner each time they are measured. Follow standard method, if they exist such as ASTM, BIS etc, and
3. present the sample to the instrument in a standard, repeatable manner. Results obtained depend on the condition of the sample and their presentation. For established procedure, make a checklist so that laboratory personnel may simply check each step. The checklist will also help in training of new workers.

The sample must also be representative of attributes that are of interest. If samples are non-representative of the batch or are spoiled, damaged, or irregular, then the sample may be biased. While choosing a sample, select in random fashion and examine the sample to avoid biased results. If sampling procedures are adequate, a different sample selected from the same batch should result in comparable measured values.

(b) Sample handling and presentation methods
If method of measurement is established so that same procedure is used each time for specific samples or types of samples, results may be validated for comparison purposes. This also insures repeatability of results when measuring the same sample.

There are a variety of techniques that can be used in handling various forms of objects and materials so that the most valid and repeatable measurement of their appearance results. Consideration must be given to the conditions for sample preparation that are dependent upon the type of measurement to be made. For example, when measuring the colour of sample that might spill into the viewing aperture, one should hold the surface flat by using a cover glass taped over the aperture window. Other materials being measured for colour may be chopped up and placed in a glass specimen cell or made into paste and applied to a glass plate. Sheets and films should be flattened by tension or by a vacuum, if necessary.

(c) Directional samples

Averaging several measurements with rotation of the sample between readings can minimize directionality. Examination of the standard deviation displayed with the average function can guide in selecting the appropriate number of readings to average.

(d) Non-opaque samples

Non-opaque samples must have a consistent backing. A white un-calibrated tile is recommended. If the sample is such that it can be folded to give multiple layers, such as fruit leather, the number of layers for each sample should be noted.

(e) Translucent samples

Light trapped in a translucent sample can distort the colour. The thickness of the sample presented should be chosen to maximize the haze or colour difference.

(f) Granular, powdery and liquid samples

These foods in required quantity may be taken into a petri dish of known composition and characteristics and covered by other complete transparent and flat petty dish of known properties. Thickness or depth of the sample should be so maintained that it presents an opaque mass. Colour readings may be taken keeping the flat portion of nosecone of the colourimeter on the surface of the top petty dish ensuring that light thrown by the instrument neither goes out of the nosecone nor passes through the sample. Part of the light is absorbed by the sample and remaining portion (reflected from the sample) again comes back to the nosecone of the instrument for measurement and interpretation. If samples cannot be prepared to make it opaque (in case of transparent liquid sample) instruments such as tintometer, photospectrometer etc are better to use.

2.5 Error in Colour Measurement

Every measurement has a chance of error, and colour measurement is not an exception. It has possibly two source of error: first may be due to instrument and second, error in measurement. Instrumental errors are based on instrument you are using. They are enumerated below:

- Errors in absolute scales of diffuse reflectance and 0/45 radiance factor.
- Errors due to differing properties of white reference standards.

- Non-linearity of the photodetector.
- Incorrect zero level.
- Wavelength scale error.
- Specular beam exclusion error.
- Specular beam weighting error.
- Errors due to non-uniformity of collection of integrating spheres.
- Polarisation errors in the 0/45 geometry.
- Differences in methods for calculating colour data from spectral data.
- Errors due to thermochromism in samples.
- Errors due to the dependence of spectral resolution on band width, scan speed and integration time.
- Geometry difference between illumination and collection optics within the specified limits.

At present, there is no method for quantifying the effects of geometry differences (last item) and applying corrections. The method used to minimise error due to non-uniformity of collection by integrating spheres, which is to measure matt samples against matt masters and glossy samples against glossy masters, has not proved very effective. Integrating sphere errors are due to the fact that the integrating sphere is not an ideal sphere but a hemispherical sphere. There are also some baffles inside the sphere which prevent straight light from striking the detector.

Possibilities of error during measurement are due to following reasons:

(i) Nosecone of the instrument and surface of sample is not having good agreement and thus leakage of light
(ii) Samples are non-uniform, translucent or transparent and cause leakage or escape of light during measurement.
(iii) Improper alignment of colourimeter with sample surface
(iv) Surface of reference plate is not properly maintained and does not give reference values supplied by the manufacturer
(v) Error due to incorrect type of sample for the instrument

It is now clear that there are significant undetermined errors. Instrumental error, if any, should be checked and minimized with the help of manufacturer while error due to measurement will be minimized with due care by the users. Accounted errors should be measured and analysed properly for reporting.

2.6 Colour Analyses and Modeling

Colour values are generally analysed to see the colour difference in comparison with the standard specimen, to see the trends of changes with storage or processing conditions and are modeled sometimes to correlate with the specific attributes of the products. Colour difference nowadays can directly be obtained using most of the colourimeter, while for correlating colour values with any attributes; regression analyses are performed.

2.6.1 Colour Difference

Colour difference is always calculated as colour values of sample minus that of standard specimen. If ΔL^* is positive than sample is lighter than the standard. If negative, it would be darker than the standard. If Δa^* is positive, the sample is more red or less green than the standard. If it is negative, it would be greener or less red. Similarly if Δb^* is positive, the sample is more yellow or less blue than the standard. If negative, it would be bluer or less yellow. Now question arises what should be the acceptable colour difference? The simple answer is the minimum perceptible colour. What should be the acceptable tolerance? In theory the total colour difference of 1.0 is supposed to be indistinguishable unless samples are adjacent to one another. Colour difference can be computed using the following formulas.

$$\begin{aligned} \Delta L^* &= L_2^* - L_1^*, \Delta a^* = a_2^* - a_1^*, \Delta b^* = b_2^* - b_1^* \quad \text{and} \\ \Delta E_{ab}^* &= \sqrt{\left(L_2^* - L_1^*\right)^2 + \left(a_2^* - a_1^*\right)^2 + \left(b_2^* - b_1^*\right)^2} \end{aligned} \tag{2.22}$$

Where subscript 1 is for standard specimen and 2 is for sample and $E_a{}^*{}_b$ is total colour difference. It is intended to be a single number metric to have decision to pass or fail the sample. ΔE itself is not always reliable, because it is non uniform in colour space. It is therefore better, if can be, to set the tolerance limit for individual colour values.

2.6.2 Colour Modeling

Modeling is a very useful tool for (relatively) quickly and inexpensively ascertaining the effect of any system and parameters on the outcome of a process or effect of parameters. The benefit of modeling is to minimize the number of experiments that need to be conducted to know the effect of individual parameter. Models broadly can be divided into two types: theoretical mathematical model and empirical or regression model. The first one becomes more accurate and generalized while the second one is developed for a particular process or products and its accuracy depend on the accuracy in experimental values used in development and regression coefficient of determination of such models. In colour modeling majority of scientists have used the second type of modeling. Any modeling process can roughly be divided into five phases.

- First step is problem identification, i.e., what you want to predict using the developed model
- The second step consists of constructing a mathematical model for the corresponding problems. This could be in the form of differential or algebraic equations.
- In third phase the mathematical model is converted to numerical model by doing some approximation for easy solution.

- The fourth phase is the solution of the numerical model. It is generally not required if modeling is empirical or regression equation.
- Fifth and the final phase is validation of solution or predictions done by the model in real situations

2.7 Practical Applications

Numerous works on colour analyses and modeling of colour values of food materials are reported in literature, majority of them however are based on colour values extracted from the specimen's images. Some of them are covered in the Chap. 3. This chapter is limited to the most recent work on analyses of colour values acquired in terms of CIE colour scale and usually using a colourimeter.

2.7.1 Vegetables

The green colour of vegetables changes considerably during heat treatments like blanching and has been modeled using simplified kinetic mechanisms (Tijskens et al. 2001). Validation of model indicated that the formation and degradation of visible colour in vegetables is governed by processes related to the colouring compounds $\check{Z}$ like chlorophyll and chlorophilides, irrespective of the vegetables under study. This study helped in understanding of chlorophyll degradation and gave generalized information for any vegetable. But in another study (Martins and Silva 2002) on chlorophyll degradation of frozen green beans using Hunter colour values *a, b* and total colour difference in first order and reversible first order models revealed that colour is a more important parameter to asses frozen greens visual quality however chlorophyll content is not a good colour index for the same. Trends of chromatic changes of broccoli under modified atmosphere packaging (MAP) at 20°C in perforated and unsealed polypropylene film packages for a storage period of 10 days indicated using $L^*C^*h^*$ colour space diagram that the modified atmosphere (6.1% O_2 and 9% CO_2) generated inside the perforated film packages having 4 macro-holes was the most suitable in maintaining the chromatic quality of the broccoli heads (Rai et al. 2009). Postharvest life of tomatoes is limited by colour as one of the important parameters. One colour model correlates the colour level and biological age at harvest (Schouten et al. 2007). Data were analysed using non-linear regression analysis and found that biological age of tomato can well be predicted at farmers' level and can save lot of postharvest losses of tomato especially during the glut. Interestingly they also found very good correlation among the colour values and firmness of tomato.

2.7.2 Fruits

The different combinations of *L*, *a* and *b* colour values have been fitted in different form of linear models (Table 2.4) and regressed using multiple linear regression,

Table 2.4 Generalized forms of maturity index (I_m) models tested in terms of colour values (L, a, b)

Model no.	Variables	Models*
1	a, b, L	$I_m = C_1 + C_2a + C_3b + C_4L$
2	a, b	$I_m = C_1 + C_2a + C_3b$
3	a, b, $a \times b$	$I_m = C_1 + C_2a + C_3b + C_4ab$
4	a, b, a^2, b^2, $a \times b$	$I_m = C_1 + C_2a + C_3b + C_4ab + C_5a^2 + C_6b^2$
5	a^2, b^2	$I_m = C_1 + C_2a^2 + C_3b^2$
6	b, $a \times b$	$I_m = C_1 + C_2b + C_3ab$

*C_1, C_2, C_3 are models' constants.

partial least squares and principal component regressions to maturity index of mango (Jha et al. 2007, 2009). Precision of prediction using models having the parameters of a, b and their product ($a \times b$) was verified by sensory evaluation of 55 ripe mangoes and was found that the fruits predicted to be mature could ripe with high-satisfied taste while the ones predicted to be immature or over mature were mostly rejected by the panels (Jha et al. 2007). Latter a colour chart for Dusheri cultivar of mango was developed to read the maturity or ripeness level after taking the values of a and b of mango in tree using a handheld colourimeter (Fig. 2.9). It is evident from the study that internal quality parameters of mango (Jha et al. 2006b) are correlated with the colour values and can be predicted satisfactorily. Similarly a freshness index/over all quality index for five cultivars of apple was developed in which colour values are important factors (Jha 2007, Jha et al. 2010, 2010a). The relationship between colour parameters and anthocyanins of four sweet cherry cultivars using L^*, a^*, b^*, chroma and hue angle parameters (Berta et al. 2007) indicated that chromatic functions of chroma and hue correlate closely with the evolution

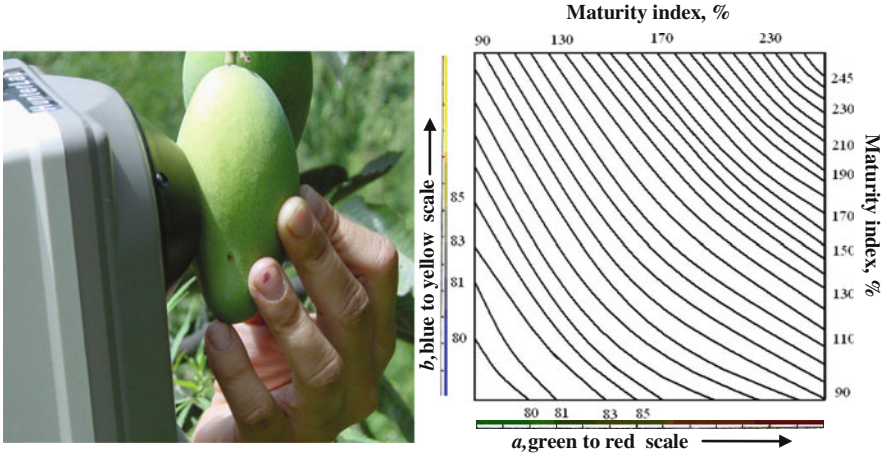

Fig. 2.9 Measurement of maturity and ripeness of mango in tree

of colour and anthocyanins levels during storage of sweet cherries and that colour measurements can be used to monitor pigment evolution and anthocyanin contents of cherries.

Tiwari et al. (2008) used response surface methodology to develop the empirical model to study the effect of ozonation on orange juice colour degradation and found that predicted colour values obtained using model equations were in good agreement with the experimental values. Mathematical equations using *L*, *a*, and *b* developed by Atilla (2007) for predicting the optimum roasting degree of hazelnut and reported that *a* and *L* values gave high r^2 and obtained three-dimensional nonlinear equations to determine the optimum roasting degree based on time and temperature.

The above paragraphs indicate that significant attempts have been made to model colour values or combination thereof for prediction of various surface as well as internal quality parameters of various fruits and vegetables. Very limited work however on modeling of colour values of other foods such as food grain, oilseeds etc. are reported for prediction of their quality parameters. The coefficient of determination of these models may not be sometimes as high as it is expected. In such cases one may try to obtain the complete spectra of specimen instead of individual colour values (*L*, *a*, *b* etc.) in the visible range of wavelength (400–700 nm) and develop models using the absorption or reflectance data (Jha et al. 2006a, 2005).

References

Atilla S (2007) The use of 3d-nonlinear regression analysis in mathematical modeling of colour change in roasted hazelnuts. J Food Eng 78:1361–1370

Berta GA, Ana PS, Jose MP et al (2007) Effect of ripeness and postharvest storage on the evolution of colour and anthocyanins in cherries (*Prunus avium* L.). Food Chem 103:976–984

Jha SN (2007) Final report (RPF III) of research project on development of nondestructive methods for quality evaluation of apple. Central Institute of Post-Harvest Engineering and Technology, Ludhiana, India

Jha SN, Chopra S, Kingsly ARP (2005) Determination of sweetness of intact mango using visual spectral analysis. Biosyst Eng 91(2):157–161

Jha SN, Chopra S, Kingsly ARP (2007) Modeling of color values for nondestructive evaluation of maturity of mango. J Food Eng 78:22–26

Jha SN, Chopra S, Kingsly ARP (2009) On-farm nondestructive determination of maturity of intact mango fruit. Indian Journal of Horticulture 66(3): 353–357

Jha SN, Kingsly ARP, Chopra S (2006a) Nondestructive determination of firmness and yellowness of mango during growth and storage using visual spectroscopy. Biosyst Eng 94(3):397–402

Jha SN, kingsly ARP, Chopra S (2006b) Physical and mechanical properties of mango during growth and storage for determination of maturity. J Food Eng 72(1):73–76

Jha SN, Rai DR, Gunasekaran S (2010) Visual spectroscopy and colour modeling for nondestructive evaluation of quality of apple. J of Agric Engineering – accepted

Jha SN, Rai DR, Sharma R (2010a) Physico-chemical quality parameters and overall quality index of apple during storage. J Food Sci and Technol – accepted

Martins RC, Silva CLM (2002) Modeling colour and chlorophyll losses of frozen green beans (*Phaseolus vulgaris* L.). Int J Refrig 25:966–974

Rai DR, Jha SN, Wanjari OD et al (2009) Chromatic changes in broccoli (*Brassica oleracea italica*) under modified atmospheres in perforated film packages. Food Sci Technol Int 15(4):387–395

Schouten RE, Huijbeb TPM, Tijskens LMM et al (2007) Modeling quality attributes of truss tomatoes: linking colour and firmness maturity. Postharvest Biol Technol 45:298–306

Tijskens LMM, Schijvens EPHM, Biekman ESA (2001) Modeling the change in colour of broccoli and green beans during blanching. Innov Food Sci Emerg Technol 2:303–313

Tiwari BK, Muthukumarappan K, Donnell CPO et al (2008) Modeling colour degradation of orange juice by ozone treatment using response surface methodology. J Food Eng 88(4): 553–560

Chapter 3
Computer Vision Systems

Sundaram Gunasekaran

Food quality is of paramount consideration for all consumers, and its importance is perhaps only second to food safety. By some definition, food safety is also incorporated into the broad categorization of food quality. Hence, the need for careful and accurate evaluation of food quality is at the forefront of research and development both in the academia and industry. Among the many available methods for food quality evaluation, computer vision has proven to be the most powerful, especially for nondestructively extracting and quantifying many features that have direct relevance to food quality assessment and control. Furthermore, computer vision systems serve to rapidly evaluate the most readily observable foods quality attributes – the external characteristics such as color, shape, size, surface texture etc. In addition, it is now possible, using advanced computer vision technologies, to "see" inside a food product and/or package to examine important quality attributes ordinarily unavailable to human evaluators. With rapid advances in electronic hardware and other associated imaging technologies, the cost-effectiveness and speed of computer vision systems have greatly improved and many practical systems are already in place in the food industry. Thus, many of the quality evaluation operations are now done in a fairly routine basis at speeds matching the production and high throughput requirements of the food industry. As the technology matures and finds more mainstream applications, further growth will be in improving and speed under challenging food processing environments – dusty, wet, hot etc. Turn-key applications that would require only moderate operator intervention will be further developed, which can operate trouble-free for prolonged durations. New advances in terms of non-visible defect detection and hyperspectral imaging will continue to evolve and bring additional computer vision innovations to the food industry, which would require intensive research and developmental work by many new scientists and technologists.

S. Gunasekaran (✉)
Department of Biological Systems Engineering, University of Wisconsin-Madison,
Madison, WI 53706, USA
e-mail: guna@wisc.edu

S.N. Jha (ed.), *Nondestructive Evaluation of Food Quality*,
DOI 10.1007/978-3-642-15796-7_3,

3.1 Computer Vision System

Computer vision, also known as machine vision or computer image processing, is the science that develops the theoretical and algorithmic basis by which useful information about an object or scene can be automatically extracted and analyzed from an observed image, image set, or image sequence. It is a branch of artificial intelligence technique and deals with simulating human vision. We see an object and perceive its optical characteristics based on the reflected light received from the object being illuminated by natural or artificial light. Thus, in essence the task of a computer vision system is to simulate human visual perception process illustrated in Fig. 3.1.

The essential components of a typical computer vision system are:

a. computer, which is analogous to the human brain,
b. sensor or camera, which is analogous to the human eyes,
c. illumination system, which facilitates image capture,
d. frame grabber/digitizer, which digitizes the image information from the camera, and
e. monitor(s), which displays the acquired and/or processed images.

The use of digital cameras eliminates the need to use a separate frame grabber in the computer. A schematic of a computer vision system is presented in Fig. 3.2.

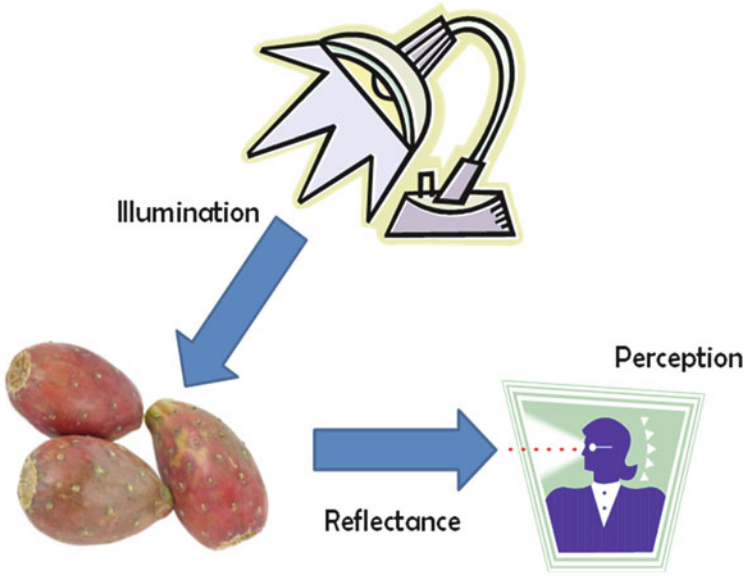

Fig. 3.1 Schematic illustration of the process of human vision perception

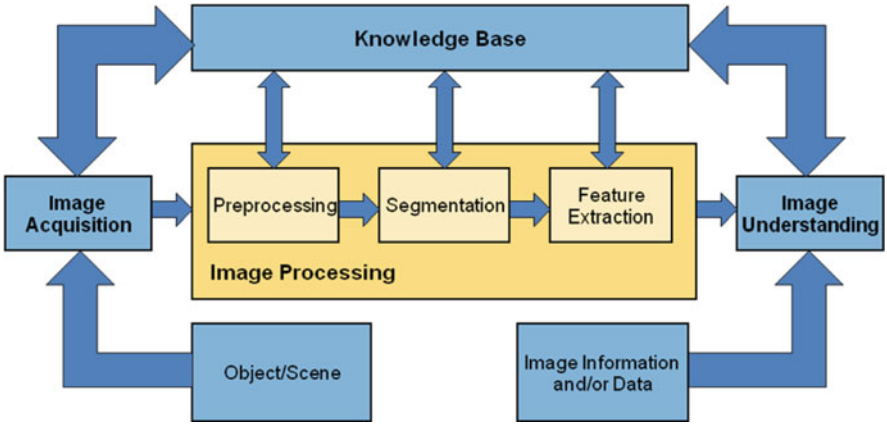

Fig. 3.2 Basic steps in computer image processing (Panigrahi and Gunasekaran 2001)

A typical computer vision task involves a series of steps, which can be grouped into three major tasks as depicted in Fig. 3.3. These include:

a. image acquisition, which deals with such issues/components as illumination, camera, digitizer, etc.,
b. image processing, which encompasses preprocessing, segmentation, and feature extraction, and
c. image understanding, which entails image recognition and interpretation.

Each of these sub-tasks is as important as the other two, and the success of a good computer vision system, then depends on the success of all these sub-tasks

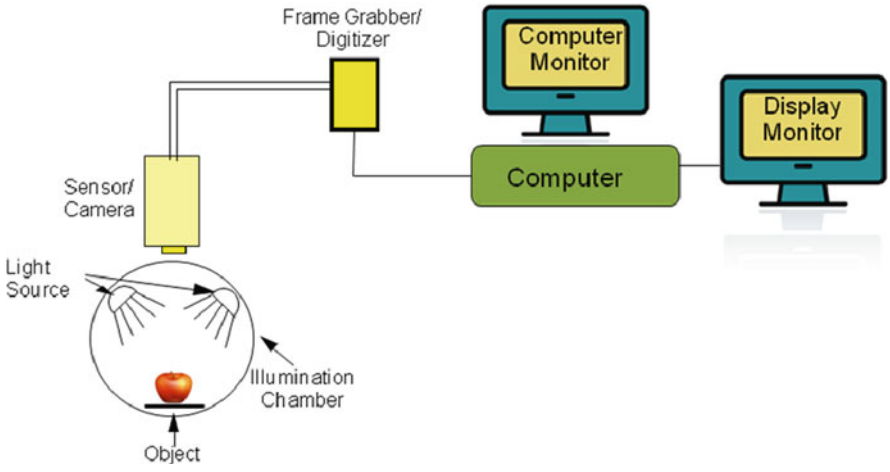

Fig. 3.3 A typical computer vision system (Panigrahi and Gunasekaran 2001)

working in harmony. For example, an image acquired with utmost care will not yield useful information if faulty processing methodologies are used; and if interpretation of properly acquired and processed image is erroneous, all the time and money invested in image acquisition and processing becomes worthless. Thus, all these sub-tasks are closely linked with knowledge base available about the system studied and the image features that are relevant for evaluating product quality of interest.

3.2 Image Acquisition

Capturing image for processing is the foremost activity in machine vision system. It requires outmost care and manner which can be used repeatedly and image should be without any shades. A good light source or illumination system and a camera are important gadgets for acquiring a good digital image for processing.

3.2.1 Digital Image

A digital image is a spatial representation of an object or scene. A monochrome image is a two-dimensional (2-D) light-intensity function, $I(x, y)$ where the value or amplitude of intensity I at spatial coordinates (x, y) is typically proportional to the radiant energy received in the electromagnetic band to which the sensor or detector (the camera) is sensitive in a small area around the point (x, y). As far as the computer is concerned, the image is a matrix (x, y) of numeric values, each representing a quantized image intensity value. Each matrix entry is known as a pixel (short for picture element). The total number of pixels in an image is determined by the size of the 2-D array used in the camera. Most commonly used cameras have a spatial resolution of 1024×768 or better; the higher the resolution, the larger the image size. For example, camera spatial resolution of 1280×960 produces an image size of 1 Mb. The recent explosion in digital technology now makes possible to have image sizes greater than 12 Mb. The intensity of a monochrome image is known as gray level. The limit on gray level is that it is positive and finite. The gray level interval (from low to high) is called a gray scale. A common practice is to shift this interval numerically to the interval $(0, L)$ where the lowest value 0 represents pure black and the maximum value L represents pure white. All intermediate values are shades of gray varying continuously from black to white. For example, when an 8-bit integer is used to store each pixel value, gray levels range from 0 to 255 (i.e., 2^0-1 to 2^8-1).

Inferring an object's size, shape, position, orientation and other attributes from the spatial distribution of gray levels requires the capability to infer which pixels belong to the object and which do not. Then, from the pixels that belong to the object, it requires the capability to identify the object features of interest. Algorithms have been developed to translate the gray levels of a pixel in a way that accentuates the desired information.

In the case of color images, the image intensity is represented by three components denoting red, green, and blue (in the RGB system) or hue, saturation, and intensity (in the HSI system). Various color scales and relationships among them have already been discussed in Chap. 2 and further details of the color digital image are presented in a latter section.

3.2.2 Illumination

The prerequisite for any vision application is that the features to be examined can be seen in the image. Therefore, despite all the progress in image analysis/processing algorithms, the performance of the camera and illumination subsystem can greatly affect the success and reliability of a computer vision application. A well-designed lighting and illumination system is essential for the accuracy and success of image analysis by enhancing image contrast. Good lighting will improve feature discrimination and reduce processing time and hardware requirements. Thus, it is almost always cheaper to improve lighting than to enhancing image processing algorithms. Food materials are nonhomogeneous, randomly oriented; and may be dirty. Furthermore, singulation of objects, i.e., the ability to present objects one at time under the camera for image acquisition is often difficult. Therefore, we have to cope with objects that touch, overlap, and someway occlude hiding and/or casting a shadow during image acquisition. Overall, computer vision applications in the food industry are faced with unusual challenges, compared to those in other industries, for example in the automobile industry, when designing proper illumination systems.

Selecting appropriate light sources and identifying suitable configurations for the light sources so as to obtain the highest quality images is the essence of proper illumination for a computer vision system. The geometry of the imaging system should be well known. This requirement is especially important for dimension measurements. When the viewing geometry is more complicated, either because of the non-planar image surface or non-perpendicular imaging angle, measurements are more difficult and require determining the geometry of the imaging system. Most lighting arrangements can be grouped as either front-lighting or back-lighting. The front-lighting option (Fig. 3.3) is best suited for obtaining surface characteristics of an object, while back-lighting (Fig. 3.4) is best for subsurface features. For example, using back-lighting internal stress cracks in corn kernels (Gunasekaran et al. 1987), watercore in apples (Upchurch and Throop 1994), and cracks in eggs (Elster and Goodrum 1991), automatic recognition of Fuji apples at harvest (Bulanon et al. 2002), and separating black walnut meat from shell (Jin et al. 2008). The appropriateness of a well-designed illumination system can be evaluated by the suitability of acquired images for successful further processing. The most commonly used illumination systems and their associated advantages and disadvantages are summarized in Table 3.1.

A wide variety of light sources and lighting arrangements are available. Most general computer vision applications are implemented using either incandescent or

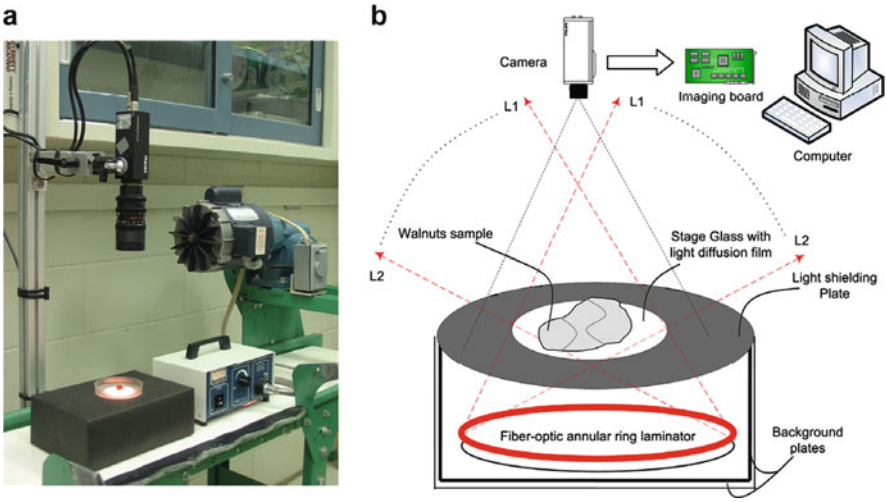

Fig. 3.4 A backlit imaging system (**a**) and it's schematic (**b**) used for separating black walnut meat from its shells. L1 and L2 represent the range between which rays penetrate the glass stage covered with light diffusion film. The camera captures only a part of the scattered light from both the sample and the diffusion film (Jin et al. 2008)

florescent lighting. However, use of polarizers and polarized light can improve the light intensity contrast, eliminate unwanted glare and minimize diffuse reflectance. This is especially suitable for transparent and translucent objects. Since an object's color depends on illumination, color measurements are easily affected by changes in the color temperature of an incandescent bulb. Thus, measuring brightness information, such as density or color values, requires a very stable illumination source and sensor. Bright specular reflections may cause saturation, blooming or shifts in image magnification. Sometimes the color of two objects will appear similar under one light source but much different under another. So, a number of light sources of different spectral responses must sometimes be tried when attempting to maximize image contrast for the best possible results. For multiple or brightly colored fruits and vegetables, a multiple spectral lighting system is needed to assure accuracy over a large spectral range. Spectral reflectance properties of products should be considered when developing an appropriate illumination system (lighting and viewing geometries, light sources and sensor components) to obtain maximum discrimination power. The spectral output of different light sources can be obtained from respective manufacturers.

For on-line evaluations where speed of operation becomes an important criterion, global uniformity (i.e., the same type of feature should look the same wherever it appears in the image) is essential. This means that brightness and color values are the same and thus it requires uniform, consistent image illumination. Furthermore, the optomechanical construction of a camera and illuminator should withstand environmental conditions such as mechanical vibrations and dust common in industrial

Table 3.1 Comparison of different illumination systems (Courtesy, Machine Vision Society of Manufacturing Engineers, Dearborn, MI)

System	Advantages	Disadvantages
Diffuse Front Illumination	• Soft, fairly non-directional • Reduces glare on metallic surfaces • Relatively easy to implement	• Edges of parts may be fuzzy • Low contrast on monocolor parts
Directional Front Illumination	• Easy to implement • Good for casting shadows • Fibre optic delivery in many configurations	• May create unwanted shadows • Illumination is uneven
Light Tent	• Eliminates glare • Eliminates shadows	• Must surround workpiece • Can be costly • Size can be a problem
Collimated Back Lighting	• Produces very sharp edges for accurate gauging	• Difficult to implement if material handling interferes • May be too bright for camera without neutral density filters
Dark Field Illumination	• Illuminates defects • Provides a high contrast image in some applications	• Does not illuminate flat smooth surfaces
Diffuse Backlighting	• Easy to implement. • Creates silhouette of part • Very high contrast image • Low cost	• Edges of parts may be fuzzy • Difficult to implement if material handling interferes
Low Angle Illumination	• Shows topological defects	• Single source will produce uneven lighting across surface
Polarized Front Illumination	• Eliminates glare	• Reduces amount of light into the lens significantly
Polarized Backlighting	• Highlights certain types of features or defects in translucent materials • Relatively easy to implement	• Only works for birefringent features. • Edges of parts may be fuzzy • Difficult to implement if material handling interferes
Strobed Illumination	• Crisp image with no blurring • Can be area, fibre optic, or light emitting diode (LED) • Very long lifetime	• More costly than standard sources • Requires accurate timing with camera • Must be shielded from personnel
Structured Light	• Shows 3-D information • Produces high contrast on most parts • Laser frequency can be easily band pass filtered	• Lasers above 5 mW pose safety issue • Hard to image on some metals and black rubber
Coaxial Lighting	• Eliminates shadows • Uniform illumination across FOV	• Complicated to implement • Harsh illumination for shiny surfaces

applications. Strobe lighting is useful for on-line applications to virtually arrest the motion to aid in acquiring images without worrying about image "blur" due to image motion. The strobe repetition rate should be selected to match the speed of object motion. A strobe unit designed for machine vision use must be able to withstand continuous operation with repetition rates of 30 times a second.

3.2.3 Camera

The camera is the sensor for capturing the image information in a computer vision system. It functions similar to the eyes in human vision. Charge coupled device (CCD) cameras have been used for nearly all computer imaging applications since their introduction in the early 1960s. There have been many developments based on the CCD technology. The complementary metal-oxide semiconductor (CMOS) technology was introduced in the mid-1990s. Both CCD and CMOS technologies are based on arrays of light-sensitive pixels (or photosites), which gather photons of light and convert them to a visible image. How this process works has profound influence on the qualities and capabilities of the image sensors. Many varieties of black-and-white and color cameras are commercially available. The optical resolutions available with CMOS sensors have improved tremendously over the last few years. Resolutions are now high enough and run at fast enough frame rates to enable electronic pan, tilt, and zoom in cameras. Because of how they capture light, CMOS imagers offer lower dark (junction) current and enable applications like high-definition television (HDTV) where CMOS image sensors capture considerably better pictures (in terms of signal-to-noise ratio and dynamic range) at HDTV rates. CMOS architecture allows for random pixel access and window-of-interest readout for applications requiring image compression, motion detection, or target tracking.

When selecting an appropriate camera, it is important to match the requirements for a particular application with capabilities of a camera. In addition, the following parameters are also critical when selecting a suitable camera: resolution, signal-to-noise ratio, signal output, minimum illumination required, analog or digital output, and additional camera adjustment capabilities.

3.3 Image Processing

The basic steps in image processing are image preprocessing, segmentation, and feature extraction (Fig. 3.3). The purpose of image preprocessing or image conditioning is to enhance the quality of the acquired image, which is often degraded by distortion and noise in the optical and electronic systems of the input device. Image preprocessing steps include one or more of the following: noise reduction, geometrical

correction, gray-level correction and correction of defocusing. These steps are typically applied uniformly and are context-independent.

Image segmentation refers to the process of partitioning a composite image into component parts or objects. Proper segmentation is very critical. Often, the first step in assuring successful segmentation is control of background uniformity. For monochrome images, segmentation normally is performed by examining the gray scale histogram – a bar chart of the number of pixels in the image at different gray levels. Segmentation algorithms are based on discontinuity or similarity of the gray-level values. Discontinuities in image gray scale indicate sharp changes in image brightness such as the background or the object. In general, autonomous segmentation is one of the most difficult tasks in image processing. A real-time adaptive thresholding is preferably used for on-line evaluation with line-scan cameras. Adaptive thresholding algorithms of x-ray images for quarantining selected fruits are presented in Jiang et al. (2008)

Segmented image constitutes raw pixel data of the image boundary or a region of interest in the image. The image representation as boundary or region should be selected based on the intended application. For example, boundary representation is appropriate for image size and shape characterization; the region representation is suitable for evaluating image texture and defects.

The feature extraction step is the key in deciphering require image data from the composite image information. Feature extraction facilitates obtaining some quantitative information of interest, which is then processed in conjunction with the knowledge base available for the feature studied. The "knowledge" of the features in consideration is also critical at this stage in designing appropriate algorithms to extract information pertaining to the desired feature(s).

3.3.1 Knowledge Base

At all steps during image processing, interaction with the knowledge base enables more precise decision-making. Thus, knowledge about the system being studied should be an integral component of an image processing system. Without an appropriate knowledge base, the vision system cannot "think" and make intelligent decisions (Gunasekaran and Ding 1994). This problem is further complicated by the fact that the output of a vision sensor is a complex combination of many parameters: size, shape, texture, color, etc. Some requirements for intelligent decision making are: (1) ability to extract pertinent information from a background of irrelevant details, (2) ability to learn from examples and generalize this knowledge and apply it in different circumstances and (3) ability to make inferences from incomplete information.

Expert systems, neural networks and fuzzy logic are some methods of building knowledge bases into computer memory, enabling recognition and interpretation of image data and to provide on-line control capabilities. The image understanding part of the computer vision system is inherently tied with the completeness and

accuracy of the valid knowledge base available for the product(s) and the feature(s) being studied. The successful image understanding step will lead to the ultimate goal – translating image data into information useful for further action such as process/machine control. Applying neural networks and/or fuzzy logic in conjunction with computer vision systems is rapidly growing and commercial systems are available for quality sorting of fruits and vegetables (Benhanan et al. 1992, Blasco et al. 2007, Ozer et al. 1995, Riquelme et al. 2008, Saito et al. 2003).

3.3.2 Pattern Recognition

A pattern is a quantitative or structural description of an object or some other entity of interest in an image. In general, a pattern is formed by one or more image features. Pattern recognition by computer involves techniques for assigning patterns to their respective classes automatically and with as little human intervention as possible.

In machine recognition of image patterns and shapes, generally two approaches are used: (1) statistical or decision-theory approach in which features are extracted and subject to statistical analysis and (2) syntactic or structural approach in which image primitives are selected and subjected to syntax analysis.

The statistical or decision-theory approach is the traditional approach to pattern recognition that has been studied since the 1960s. The system (Fig. 3.5) consists of two parts, analysis and recognition. In the analysis part, a set of image features that are judged to be non-overlapping (or as widely apart as possible) in the feature space is chosen (Wong 1994). A statistical classifier (e.g., based on a fuzzy logic or neural network system) is designed and trained with the chosen set of features to obtain the appropriate classifier parameters. In the recognition part, an unknown image is filtered or enhanced in the preprocessing stage, followed by feature detection and classification. This approach, however, does not describe or represent structural information in a pattern which is often desirable or necessary for certain applications as, for example, when the number of classes is so large or the given pattern is very complex. In these circumstances, the number of features required is probably very large, making the statistical approach impractical.

In the syntactic or structural approach, complex patterns are decomposed into subpatterns and recursively into sub-subpatterns and so on, until meaningful primitive patterns (analogous to features in the statistical approach) can be reliably extracted from them (Wong 1994). This approach allows us to describe and represent the input pattern, in addition to classifying it into a specific class. This approach has attracted much attention in the recent development of pattern recognition research.

3.3.3 Image Morphology

Image morphology refers to the geometric structure within an image which includes size, shape, particle distribution and texture characteristics. A general approach in

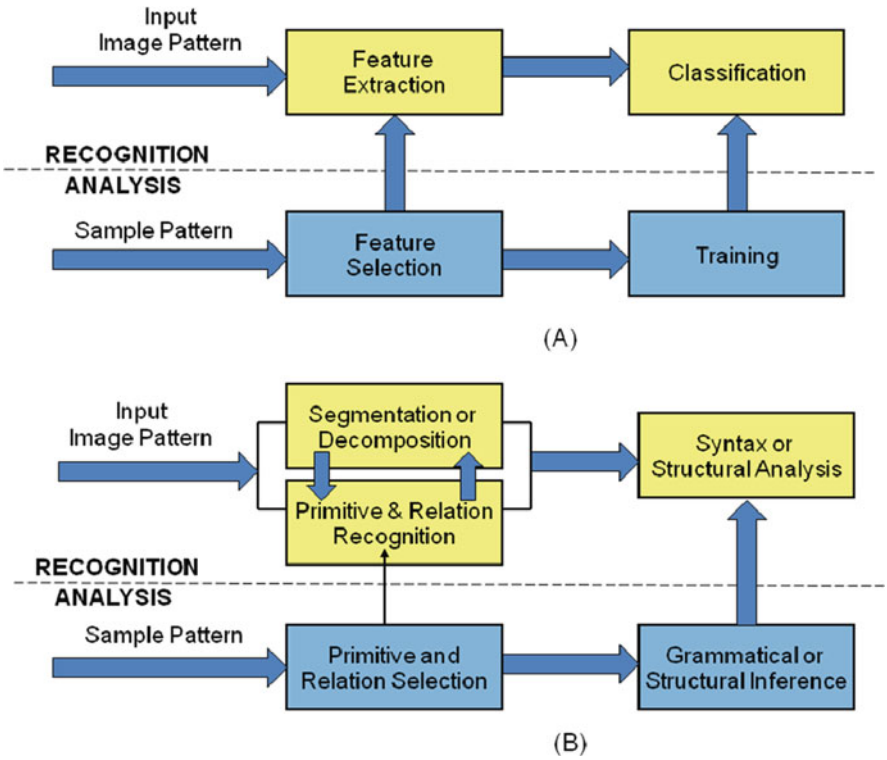

Fig. 3.5 Pattern recognition systems: (**a**) statistical and (**b**) syntactic (Panigrahi and Gunasekaran 2001)

analyzing image morphology is to transform the given image to another where the information represented in the transformed image is more easily understood. For example, investigations of the shape of objects in a binary image often use thinning algorithms. Reducing an object to a minimal set of pixels representing an invariant of the object's geometrical shape is called thinning. A skeleton is a line-thinned caricature of the binary image that summarizes the shape and conveys information about its size, orientation and connectivity (Gonzalez and Woods 1992). An image resulting from the thinning process has fewer black pixels representing the object and is, therefore, easier to manipulate. An example of thinning operation is illustrated in Fig. 3.6. If the main goal of thinning is data reduction and exact reconstruction of the original image is not essential, many techniques are available that yield acceptable skeleton representations. However, if close or exact reconstruction is desired, care must be taken in choosing an appropriate algorithm.

The morphological approach has been successfully applied to a wide variety of problems. The power and usefulness of some basic morphological processing algorithms have been illustrated by McDonald and Chen (1990). Morphological processing for isolated, non-touching objects is easily done using commercial packages

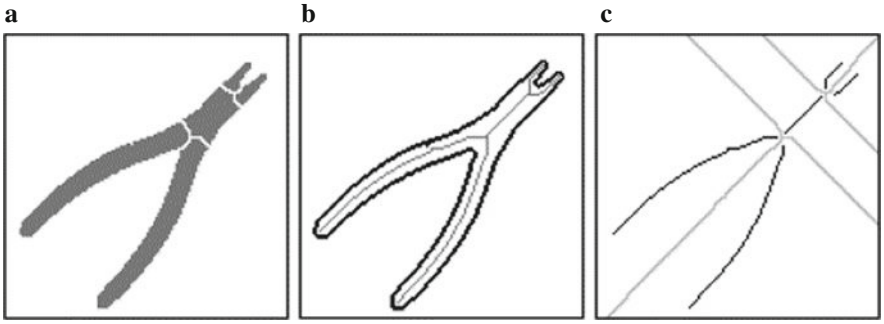

Fig. 3.6 Illustration of morphology evaluation of an object (**a**), its outline (**b**), and line-thinned image (**c**) (Di Ruberto and Cinque 2009)

which can perform object counting and dimensional measurements, etc. However, touching and overlapping objects pose problems unique to the products being examined. Thus separate algorithms and procedures need to be developed. McDonald and Chen (1991) developed a morphological algorithm to separate connected muscle tissues in an image of beef ribeyes. Ni and Gunasekaran (1998, 2004) used image thinning in conjunction with a syntactic approach to evaluate the morphology and integrity of touching and overlapping cheese shreds (Fig. 3.7). The algorithm performed very well with less than 10% error in individual shred length measurements.

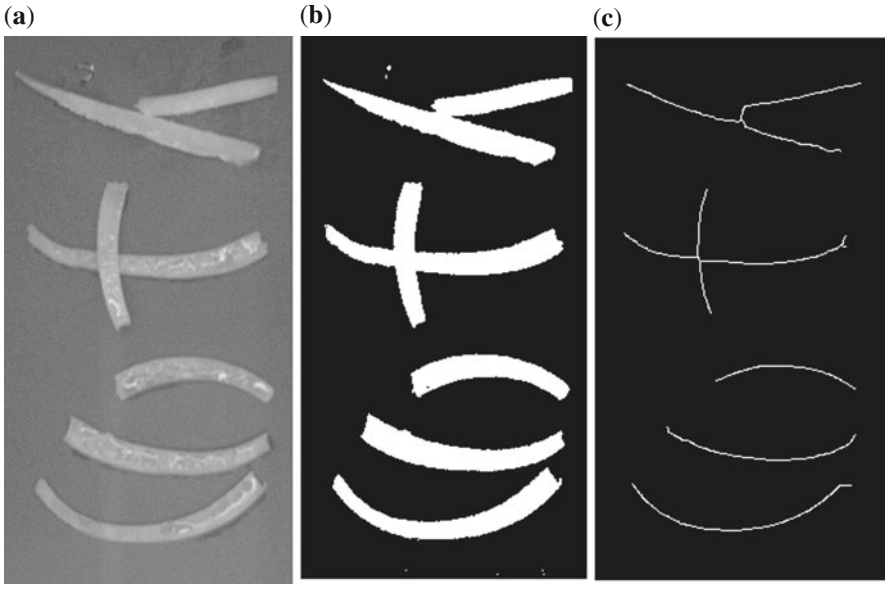

Fig. 3.7 Morphological image processing for evaluating integrity of cheese shreds. (**a**) Cheese shreds, (**b**) binary images of cheese shreds, and (**c**) line-thinned image of cheese shreds (Ni and Gunasekaran 1998)

Evaluation of an image skeleton was also used to characterize granular foods that may agglomerate (Ros et al. 1995). Smolarz et al. (1989) used morphological image processing to define structural elements of extruded biscuits and then to discriminate biscuit type. Morphological features have been used to separate touching grain kernels (Anami et al. 2009, Zhang et al. 2005) and to classify cereal grains such as wheat, barley, oats, and rye (Majumdar and Jayas 2000a, b). Dell'Aquila (2009) used external and internal morphology of seeds determined from their X-ray images to sorts them according to their physiological quality.

3.3.4 Shape Feature Extraction

Food material shape feature is very useful as it is often closely related to quality. Due to the demands of high quality, automated food shape inspection has become an important need for the food industry. Due to large inhomogeneities of food materials, however, such invariant shape features cannot be used to detect local defects. In many cases, therefore, the invariant feature extraction methods cannot accurately distinguish between damaged and undamaged categories. Panigrahi et al. (1995) evaluated invariant moments and fractal geometry for shape classification of corn. Variant shape extraction methods (position, orientation and scale) are gaining popularity for food material shape inspection (Lai et al. 1986).

In the variant method, the edge contour of the inspected object is transformed to a given position, orientation and scale. Then the shape features are extracted from every local edge point. Statistical model-based variant feature extraction method has been used for shape inspection of corn kernels. This was based on a reference shape, a transformed average shape of some undamaged corn kernels. After the reference shape was obtained, the shape of kernels being inspected was compared with the reference shape.

Ding and Gunasekaran (1994) proposed a new algorithm with improved ability to adjust object location, orientation and scale to determine the edge contour of a number of food materials for shape evaluation. This multi-index active model-based feature extractor is based on a reference shape comparison principle. The basic idea is to first transform and adjust a set of undamaged training objects to a certain location, orientation, and scale to obtain the "average of transformed good object edge contour" known as the reference shape. The second step is to transform and adjust each object to the same location, orientation, and scale. Then the shape of the objects under inspection can be compared with the reference shape to identify any significant deviations. Corn kernel and animal cracker shape inspection is used as example food materials to illustrate this method. Some recent advances in object contour and shape detection are available in literature (Ferrari et al. 2006, Schindler and Suter 2008).

Beyer et al. (2002) evaluated the image contour shape of sweet cherry (*Prunus avium* L.) Using digitized images of individual fruit in front view (onto ventral suture) and side view, they described the contour of Sam variety of sweet cherry

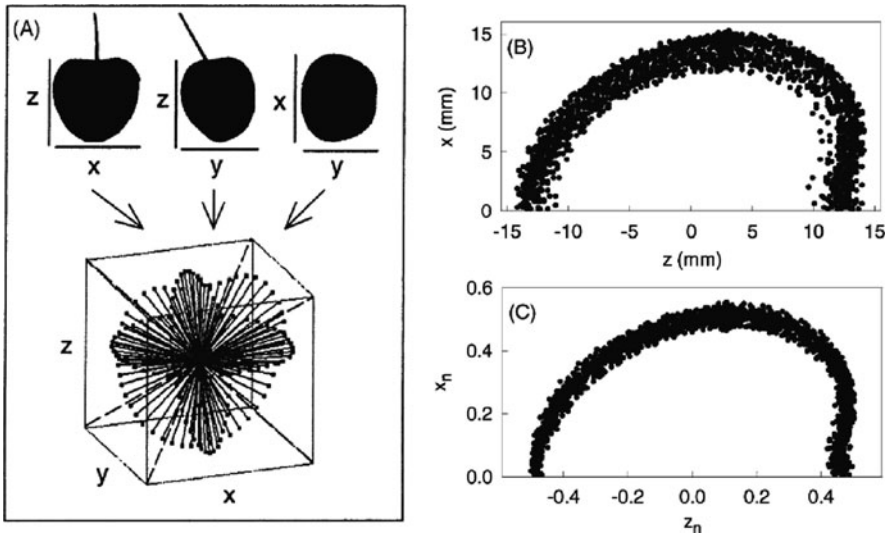

Fig. 3.8 Shape contour measurement. (**a**) Overall image data acquisition scheme, (**b**) scatter plot of left-half of Sam variety of mature sweet cherry fruit contour in x-z perspective (front view), and (**c**) same as (**b**) but normalized for fruit height (Beyer et al. 2002)

fruit in front view (x, z-perspective) (Fig. 3.8). Their results are useful for various applications including for such determinations as: fruit symmetry, changes of fruit shape with development, effects of environmental factors (year, site, etc.) or differences in fruit shape among cultivars. For example, they determined that the shape of a single cultivar did not differ significantly during later stages of fruit development (Fig. 3.9), between two different sites or two different growing seasons. However, fruits of different cultivars are significantly different. Furthermore, the relative depth of the pedicel cavity and the height to width ratio of fruit are two major determinants of sweet cherry fruit shape.

3.3.5 Image Texture

Texture is characterized by the spatial distribution of gray levels in a neighborhood. For most image processing purposes, texture is defined as repeating patterns of local variations in image intensity, which is too fine to be distinguished as separate objects at the observed resolution. Thus, a connected set of pixels satisfying a given gray-level property which occurs repeatedly in an image region constitutes a textured region. A simple example is a repeated pattern of dots on a white background.

Image texture can be used to describe such image properties as smoothness, coarseness, and regularity (Gonzalez and Woods 1992). There are three approaches to study image texture characteristics: statistical, structural and spectral. Statistical methods are used extensively in texture classification, identifying the given textured

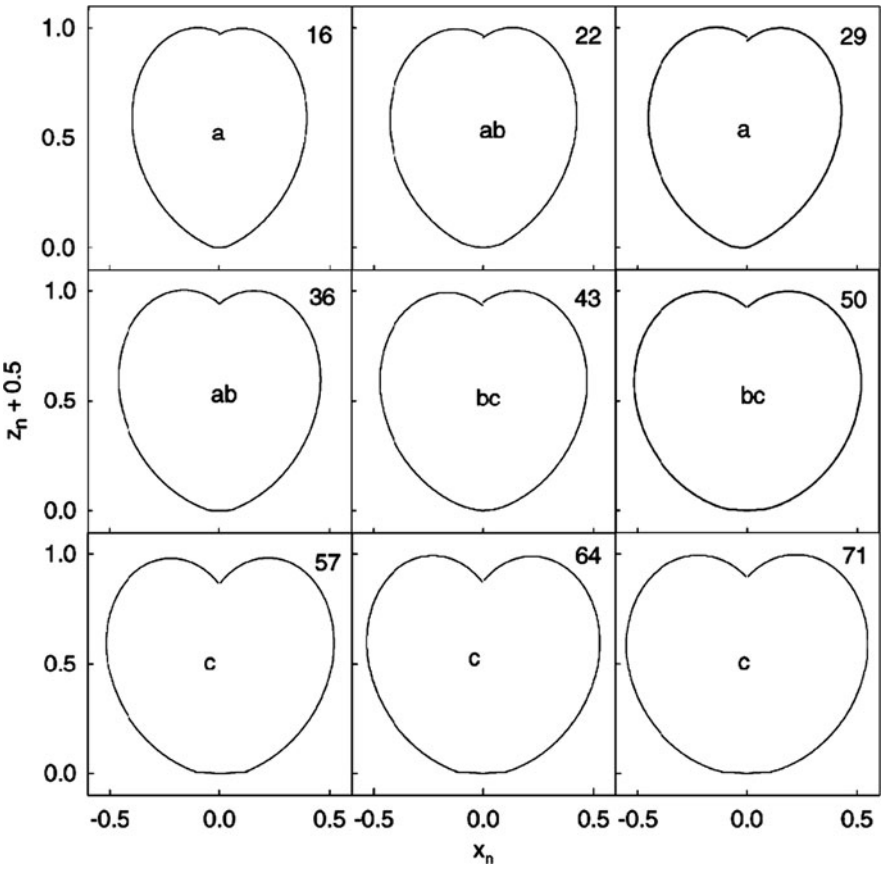

Fig. 3.9 Effect of development on the average shape (front-view) of Sam variety sweet cherry on different days (the number in each frame) after full bloom. The frames identified with same letters are not statistically different (Beyer et al. 2002)

region from a given set of textured classes. Image data such as mean, standard deviation and moment (a measure of the frequency of occurrence of pixels of a given gray level within a particular image region) are used to study smoothness, coarseness, graininess, etc. Techniques are also available to study additional image texture characteristics such as entropy (randomness) and uniformity.

Structural techniques of image texture analysis deal with the arrangement of image primitives such as the description of texture based on regularly updated parallel lines. Spectral methods are based on the Fourier transform to study the global periodicity of an image. For example, presence of high frequencies in the frequency image may represent a coarse texture. Gonzalez and Woods (1992) have further described the structural and spectral methods in some detail.

An overview of image texture analysis methods are presented in Fig. 3.10. Many of these methods have been reviewed in detail by (Zheng et al. 2006). Image texture

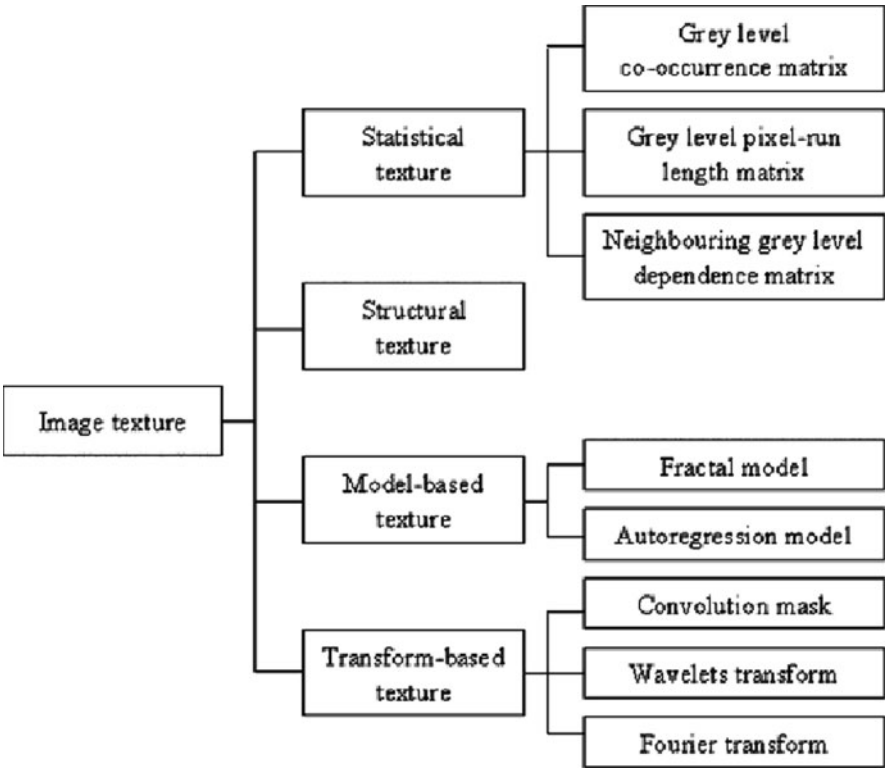

Fig. 3.10 Overview of different image texture analysis methods (Zheng et al. 2006)

analysis can be performed using either monochrome or color image data. Zayas (1993) used gray-scale image characteristics to study bread crumb grain properties. Tan et al. (1994) used HSI space image texture properties to evaluate corn extrudate characteristics. Image texture of meat samples of different tenderness have been reported to differ allowing computer vision-based evaluation of tenderness in meat (Tan 2004). Image texture of beef muscles is considered to be correlated with that of beef tenderness (Fig. 3.11).

3.4 Color Image Processing

Color is an important property of biological and food products as it plays a major role in evaluating their quality. The basic differences between a gray level and a color computer imaging system are in the camera, frame grabber, and display monitor – camera should be a color camera; frame grabber/digitizer should be capable of handling color information; and display monitor should be a color monitor capable of displaying color information.

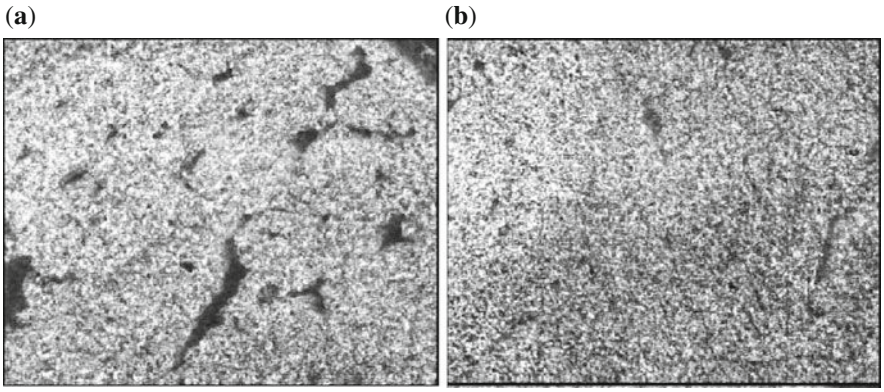

Fig. 3.11 Image texture (saturation images) of a more tender (**a**) and less tender (**b**) meat (Tan 2004)

Color computer vision systems represent image information in terms of color coordinates. The Commission Internationale de l'Eclairage (CIE) defined three new hypothetical light sources, x, y, and z, which yield positive matching curves. If we are given a spectrum and wish to find the corresponding X, Y, and Z quantities, we can do so by integrating the product of the spectral power and each of the three matching curves over all wavelengths. The weights X, Y, Z form the three-dimensional CIE XYZ space. Often it is convenient to work in a 2D color space.

This is commonly done by projecting the 3D color space onto the plane $X + Y + Z = 1$, yielding a CIE chromaticity diagram. The projection is defined as:

$$x = \frac{X}{X + Y + Z} \tag{3.1}$$

$$y = \frac{Y}{X + Y + Z} \tag{3.2}$$

$$z = \frac{Z}{X + Y + Z} \tag{3.3}$$

3.4.1 RGB Color Space

The *RGB* space is a three-dimensional color space whose components are the red, green, and blue intensities that make up a given color. The additive color model used for computer graphics is represented by the *RGB* color cube, where *R*, *G*, and *B* represent the colors produced by red, green and blue phosphors, respectively. For example, scanners read the amounts of red, green, and blue light that are reflected from or transmitted through an image and then convert those amounts into digital

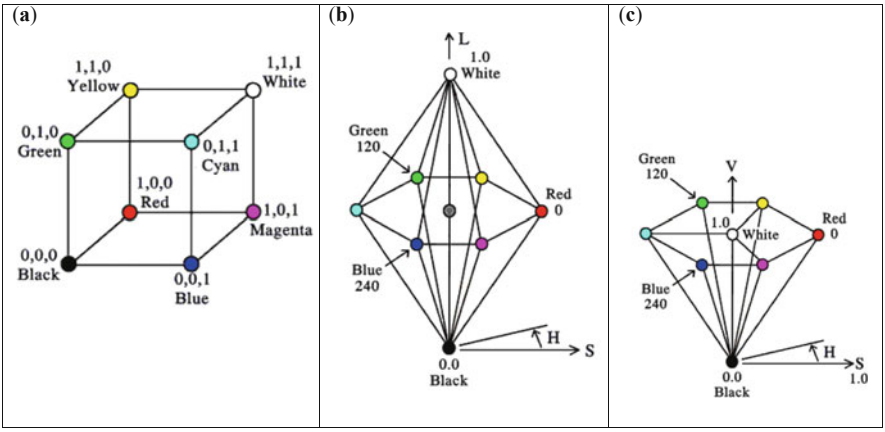

Fig. 3.12 Different color spaces used in representing color images. (**a**) RGB, red-green-blue; (**b**) HLS, hue-lightness-saturation; and (**c**) HSV, hue-saturation-value

values. Information displayed on a color monitor begins with digital values that are converted to analog signals for display on the monitor. The analog signals are transmitted to the phosphors on the face of the monitor, causing them to glow at various intensities of red, green, and blue (the combination of which makes up the required hue, saturation, and brightness of the desired colors). Any color expressed in RGB space is some mixture of three primary colors: red, green, and blue. Most RGB-based color spaces can be visualized as a cube as in Fig. 3.12, with corners of black, the three primaries (red, green, and blue), the three secondaries (cyan, magenta, and yellow), and white. The RGB color cube sits within the CIE *XYZ* color space. The groups of color spaces within the *RGB* base family include: *RGB* spaces and *HSV* and *HLS* spaces.

In RGB system, the three color components are the three primary or fundamental colors red, green, and blue, which are light generated by a monochromatic light source at 700 nm, 435.8 nm and 546.1 nm, respectively. Different combinations of these primary colors produce various secondary colors, the spectral primary system RGB to define any color by combining red, green, and blue. The chomaticities *r*, *g*, and *b* (normalized red, green and blue) are defined similar to *x*, *y*, and *z* above with *R*, *G*, and *B* values used in place of *X*, *Y*, and *Z* values, respectively. *RGB*-based color spaces are the most commonly used color spaces in computer graphics, primarily because they are directly supported by most color displays and scanners. *RGB* color spaces are device-dependent and additive. *RGB* technology is fine for acquiring, storing and displaying the image, but processing the image in *RGB* space is computationally intensive and algorithmic implementation is complex (Travis 1998). Moreover, *RGB* color coordinate is a poor way to represent images based on human vision because people do not think of color in terms of combinations of red, green and blue. *RGB* processing mimics human color perception so poorly that some operations leave objectionable color artifacts and cannot be implemented as

RGB images at all. For example, examining the red information of the *RGB* image of yellow-colored food does not help determine in any meaningful way an object's color.

3.4.2 HSV and HLS Color Space

HSV (hue, saturation, and value) space and *HLS* (hue, lightness, and saturation) space are transformations of *RGB* space that can describe colors in terms more natural to an artist. *HSV* is sometimes also known as *HSB* space, for hue, saturation, and brightness. These two spaces can be thought of as being single and double cones, as shown in Fig. 3.12. The value component in HSV describes the brightness. In both color spaces, a value of 0 represents the absence of light, or black. In *HSV* space, a maximum value means that the color is at its brightest. In *HLS* space, a maximum value for lightness means that the color is white, regardless of the current values of the hue and saturation components.

CMYK is another color system which uses Cyan, Magenta, and Yellow as its primary colors, and is commonly used in color printing industry. This system is based on light that we see reflected off surfaces such as the printed page, and these are the colors of ink used by the printing industry. From these, all of the other colors can be made, and when they are mixed together in equal parts, they make black. Printers always add black ink (the shorthand for which is "K") as a fourth color because it comes out darker, and it is more efficient to print one spot of black than to print the three primary colors on top of each other. It is best if RGB computer display images are converted into CMYK images for printing purposes."

3.4.3 Color Image Processing Applications

Appropriate color camera and digitizers are definitely very critical for color imaging systems. As emphasized earlier selection of the appropriate light source (illumination source) is very critical. In addition to several other considerations when selecting a gray level-based imaging system, two more factors need to be taken into account when selecting light sources, especially for the color imaging system: color rendering index and color temperature/chromaticity of the light source.

Calibration of a color computer imaging system is essential to handle, process, and display color precisely. However, many end users or developers, unfortunately, have not practiced color calibration. Many times, it is assumed that all components are working satisfactorily. In many cases, however, a small deviation of calibration of one component can introduce errors in the final result provided by the color computer imaging. For example, if a color camera looking at an orange puts out the color information as yellow or red instead of orange, then serious error is introduced.

Color computer imaging technology is extensively applied to numerous food-related applications which can be broadly grouped into color evaluation, defect

detection and texture evaluation of different food products including dairy, meat, fish, fruit, vegetables and others. This variety of applications, however, presents challenging color image processing issues. These applications can be discussed under two broad image processing categories – color segmentation and image analysis and understanding.

3.4.4 Color Segmentation

In processing color images, segmentation refers to isolating or separating a homogenous or desirable region of interest in the image. Removal of a background from an image is a simple example. Segmentation is also used to identify and quantify all sorts of defects, diseases, and other abnormalities. The segmentation problem in color image processing is more complex than in the gray-scale applications. A color image is comparable to three gray-level images having color information contained in three color components, e.g., red, green and blue. Thus, segmentation is more time-consuming and involved for color images. Of course, the level of complexity depends significantly on a given application. The inherent random variability of quality attributes of raw materials (agricultural products) for food products further adds to the complexity of segmentation of color images of many food products.

Thresholding based on histogram is used for applications that separate background from the object or separate two or three dissimilar contrasting regions in the image. One requirement is that there should be a good amount of color difference among the regions to be segmented. Sometimes investigation is necessary to choose the appropriate color coordinate for performing segmentation. To evaluate the color of French fries, for example, removing background information from the French fries was required (Chtioui et al. 1998).

Use of adaptive thresholding techniques for a histogram-based segmentation is also recommended for food images. They promise higher accuracy and robustness than a fixed (global) threshold. Adaptive thresholding techniques can adapt to changes in lighting and spectral characteristics of an object as well as the background. Therefore, they are well suited for real-world applications and most food quality evaluation applications. The description of different adaptive thresholding techniques including other traditional image segmentation techniques such as region growing, clustering and region merging can be found in literature (Chtioui et al. 1998, Panigrahi et al. 1995).

The neural network technology, with its associated advantage of being fault-tolerant intelligent, has been used for unsupervised segmentation of color images (Pandya and Macy 1996). Unsupervised neural networks are best suited for real world images. They do not need supervision or teacher as do supervised neural networks in order to conduct segmentation. Self organizing map (SOM) has been extensively studied for unsupervised image segmentation. This type of neural network can work for multidimensional data such as a color image having three-dimensional color information. It preserves the image topography and

simultaneously maintains its spatial relationships. Though applications of SOM networks or other neural networks for food image segmentation have not been reported extensively in the literature, the success of their applications on natural color images (Iivarinen 1998) and other multidimensional pattern recognition techniques (Uchiyama and Arbib 1994) clearly reinforces the potential success of neural network technologies for image segmentation of food products.

3.4.5 Image Analysis and Understanding

In analyzing color images of food, the exact techniques for image analysis and understanding differ from application to application. For example, an image analysis and understanding algorithm developed for color classification of corn might not work fully with high accuracy for potatoes or potato products. This provides additional challenges and requires investigation for developing successful applications.

Selecting appropriate color coordinates for analyzing a given food color image is very critical. For color evaluation of edible beans, Chtioui et al. (2003) evaluated both *RGB* as well as *HLS* coordinates. Both sets of coordinates provided accuracy up to 100% in classifying beans in three color groups. To identify and quantify fat in meat images, *RGB* color space was used with a rectangular prism and Mahalano bois distance criteria (Gerrard et al. 1996). *RGB* color coordinates were used for locating citrus fruits for harvesting (Jimenez et al. 2000) and RGB color space was utilized along with Bayes' decision theory for image partitioning and subsequent color classification of stoned fruits (Singh et al. 1993).

The potential of artificial intelligence technologies, such as neural networks and fuzzy logic, has also been explored for image classification and understanding purposes. Both neural network and fuzzy logic techniques are intelligent, adaptive and fault-tolerant (Du and Sun 2006) and they complement each other. Neural networks are a new paradigm of computing or information processing inspired by biological models. For color classification of French fries, Chtioui et al. (1998) condensed both hue and saturation histogram information by two separate back-propagation neural networks. The condensed color information was then fed as input to another neural network. The maximum color classification accuracy obtained by this modular network was 96% for classifying a given French fry sample into three color groups (Chtioui et al. 1998). (In this case, neural networks were used in a modular format.) Similarly, another probabilistic neural network was used for color classification of French fry samples into three color groups: medium, light and dark. A few multistructure neural network classifiers were used to classify four varieties of pistachio nuts with an average classification of accuracy of 95.9% (Ghazanfari et al. 1996). Detection of blood spot and dirt staining on eggs was performed with an accuracy of 85.6 and 80%, respectively, using neural networks (Patel et al. 1998).

Similarly, fuzzy logic is another intelligent information processing mathematical paradigm for dealing with uncertainty, vagueness and ambiguity. Fuzzy logic has

been successfully used for real-world complex image classification and understanding (Du and Sun 2006). It was used to diagnose tomato disease and to analyze and classify other biological and agricultural images (Panigrahi 1998). Extending its use to classify and evaluate food images is definitely very encouraging.

Rough sets theory, similar to fuzzy logic technology, has also been used for defect detection and quality evaluation of edible beans based on their color. The maximum classification accuracy achieved was 99.6% (Chtioui et al. 2003). A knowledge-based discrimination function was adopted for dissemination of corn kernel properties along with a learning vector quantization network resulting in a classification accuracy of up to 93% (Steenoek et al. 2001).

The complementary characteristics of neural networks and fuzzy logic have created a new technique called "neuro-fuzzy" system. Neuro-fuzzy techniques have been used to classify disease in soybean seed with a maximum accuracy of 95%. Other applications of neural networks and fuzzy logic for image segmentation and classification can be found (Panigrahi 1998).

3.5 Non-visible Computer Imaging

Though the majority of computer imaging technology uses the visible spectrum (380–700 nm), the non-visible electromagnetic spectrum also has potential for use in computer imaging. These non-visible bands include X-ray, ultraviolet (UV), near infrared (NIR) and infrared (IR).

3.5.1 Fluorescent Imaging

Most food products or raw materials of food products can use fluorescent imaging. For most cases of fluorescent imaging, the wavelengths used range from the far end of UV (300 nm) to the far end of VIS (700 nm). Intensified CCD cameras have been used for this type of application. Because of the low amount of signals available, these intensified CCD cameras work better than a conventional CCD camera. Low-light cameras have the capability to vary the time of integration of image information from 1/60 or 1/130 s to several minutes. By integrating a weak fluorescent signal for a longer time, a quality fluorescent image is obtained.

The introduction of BCCD has also generated another viable option for acquiring quality fluorescent and NIR images. The spectral sensitivity of a BCCD camera is significantly higher than that of intensified CCD and conventional CCD cameras, especially in the UV and NIR ends of the visible spectrum.

3.5.2 NIR Imaging

NIR images can be very valuable for food quality evaluation. For imaging purposes, the NIR waveband can be divided into two groups, 700–1,100 nm and above 1,100 nm.

Because of the higher sensitivity of BCCD cameras in the lower NIR region, they can be used for NIR imaging of food products. Similarly, some monochrome CCD cameras have relatively high sensitivity in the lower NIR region. Though the sensitivity of monochrome CCDs in the 900–1,100 nm zone is not as high as that of a BCCD, there is a big difference in cost. Thus, depending on the application, one needs to choose which to use. Note that before using a monochrome CCD camera for NIR imaging, the IR filter in front of the CCD sensor head must be removed. It is also highly recommended that the sensitivity curve of the camera be obtained from the manufacturer to verify that the camera is appropriate for the application.

NIR imaging can also be achieved by using a liquid crystal tunable filter. Tunable filters can be easily coupled to a standard CCD detector to produce digital images at any wavelength within 400–1,100 nm. It has no moving parts. Since it is capable of acquiring images at many wavelengths, it can be used to generate multi-spectral images. Note that the quality of the image still depends on the sensitivity of the CCD detector used.

NIR images based on 700–1,100 nm can be used for detecting defects and for mapping moisture (970 nm) and protein (1,020 nm) in food products. An example is detecting defects in peaches. A monochrome CCD camera with a band pass filter centered at 750 nm (with a bandwidth of 40 nm) produced the images. The images were further analyzed for placing a peach into one of eight classes based on different defects. The classification error based on NIR images was 31% compared to 40% obtained with color images (Miller and Delwiche 1991).

The NIR spectrum (700–2,500 nm) is sensitive to chemical constituents e.g., protein, moisture, oil of food and agricultural products. Though NIR spectroscopic techniques have been used for quality evaluation of food products, NIR imaging could provide additional spatial information that is not available from traditional spectroscopic signals. For example, the NIR spectroscopy can be used to measure the overall protein, oil, or moisture content; whereas, the NIR images will show the distribution of such constituents within the food material. Therefore, NIR imaging may replace NIR spectroscopy for some applications. It is more likely that NIR imaging/visible imaging may be used in conjunction with visible/NIR spectroscopy. Park et al. (1996) integrated multispectral imaging (using 542, 571, 641, 700, 726, 847 nm) with visible/NIR spectroscopy (417–965 nm) for inspection of poultry carcasses.

NIR images above 1,100 nm can be obtained using Indium-Gallium-Arsenide (InGaAs) based cameras available from Sensors Unlimited (Princeton NJ). Area cameras are sensitive to 900–1,700 nm and line-scan cameras are sensitive to 800–2,200 nm. Both cameras produce analog and digital output including RS-170. They can be operated at room temperature, thus eliminating the need for cooling (Miller and Delwiche 1991). These capabilities show tremendous promise for integrating non-visible NIR technology into evaluation and analysis of food composition and constituents in a non-destructive manner. Most food constituents such as protein, oil, water, starch, sucrose, glucose and other chemicals based on hydrogen-carbon bonds have been evaluated by spectroscopic methods. NIR imaging would provide additional spatial information that spectroscopy cannot provide. With these capabilities, functional or compositional images of food products can be acquired which can

help quality evaluation and inspection and also provide valuable information on the interaction of food components that could be very valuable for product development and quality evaluation.

3.5.3 Infrared (IR) Imaging

Focal plane array thermal infrared cameras without liquid nitrogen cooling (using a stirring cycle-based cooler instead) are now available. They are compact, easy to use and provide better spatial resolution and thermal sensitivity. They are sensitive to the thermal infrared band (3–5 μm) and can capture images at 30 frames/s with 12-bit dynamic ranges. With emissivity and atmospheric correction capabilities, they can create thermal images of food products. IR cameras can also measure temperatures from –10 to 1,500°C. Thus, IR cameras promise another rapid and non-destructive technique for food quality evaluation, especially for characterizing thermal properties, thermal mapping and moisture-related studies. IR imaging was used to estimate the internal temperature of chicken meat after cooking (Ibarra et al. 1999).

3.5.4 X-Ray Imaging

X-rays are a part of the electromagnetic spectrum. They contain high energy and can be used for non-destructive imaging. Recently, the development of film-less and low energy X-ray detectors has created expanded possibilities for X-ray imaging, also known as radiography, for food and agricultural applications. It has been dealt in detail in the Chap. 5.

3.5.5 Hyperspectral Imaging

Hyperspectral imaging (HSI) combines conventional imaging and spectroscopy to simultaneously acquire both spatial and spectral information from an object. Thus, a typical HSI system consists of both a digital camera and a spectrograph (Fig. 3.13). It is also known as chemical or spectroscopic imaging. Originally developed for remote sensing applications, this technology has recently emerged as a powerful process analytical tool for rapid, non-contact, and non-destructive food analysis. Since spectroscopic data are obtained in addition to the optical properties, HSI offers several advantages such as providing spatial and spectral information along with data pertaining to multiple constituents of food systems. In addition, HSI is sensitive to even minor system components (Table 3.2). Thus, a spectrum for each pixel can be obtained along with a gray scale or tonal image for each narrow band. Hyperspectral images, also known as hypercubes, are made up of hundreds of contiguous wavebands for each spatial position of the object. Consequently, each pixel in a hyperspectral image contains the spectrum of that specific spot. The image data

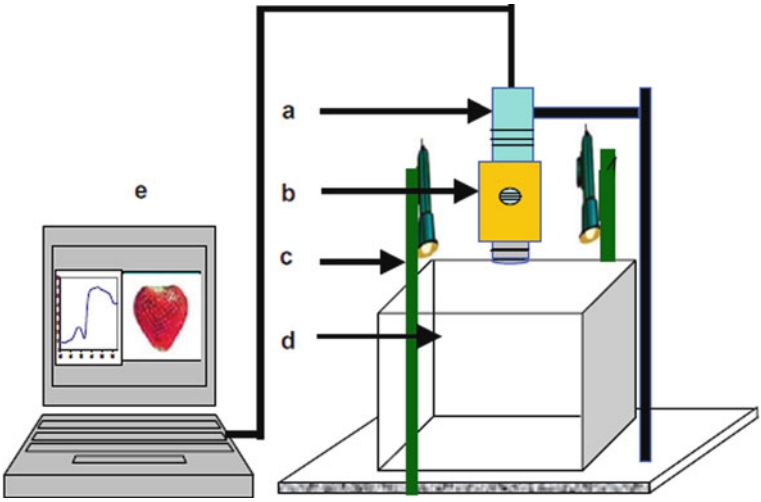

Fig. 3.13 A schematic of hyperspectral imaging system. (**a**) CCD camera, (**b**) spectrograph, (**c**) halogen lighting unit, (**d**) white nylon tent, and (**e**) computer and image acquisition software (ElMasry et al. 2007)

Table 3.2 Advantages of hyperspectral imaging compared to conventional color imaging (RGB) and near-infrared spectroscopy (NIRS). Based on (Gowen et al. 2007)

Feature	RGB	NIRS	HSI
Spatial information	x		x
Spectral information		x	x
Multi-constituent information	Limited	x	x
Sensitivity to minor components			x

contains 3-D information comprising two spatial and one wavelength dimension, as illustrated in Fig. 3.14. The *hypercube* allows for the visualization of biochemical constituents of a sample, separated into particular areas of the image, since regions of a sample with similar spectral properties have similar chemical composition. Thus, the resulting spectrum can be considered a fingerprint useful to characterize the composition of that particular pixel. HSI has been successfully evaluated for food quality applications (Kim et al. 2001). HSI systems have been used to detect fecal contamination in apples (Kim et al. 2002a), skin tumors in chicken carcasses (Kim et al. 2002b), feces on the surface of poultry carcasses (Park et al. 2002, 2004, 2005), cucumber chilling damage (Cheng et al. 2004), and caps of white mushrooms (*Agaricus bisporus*), which can be used for non-destructive monitoring of damaged mushrooms on the processing line (Gowen et al. 2008).

Hyperspectral imaging operates under simultaneous reflectance (400–675 nm) and transmittance (675–1,000 nm) modes. It has been studied for non-destructive and non-contact sensing of surface color and bloater damage in whole pickles. An

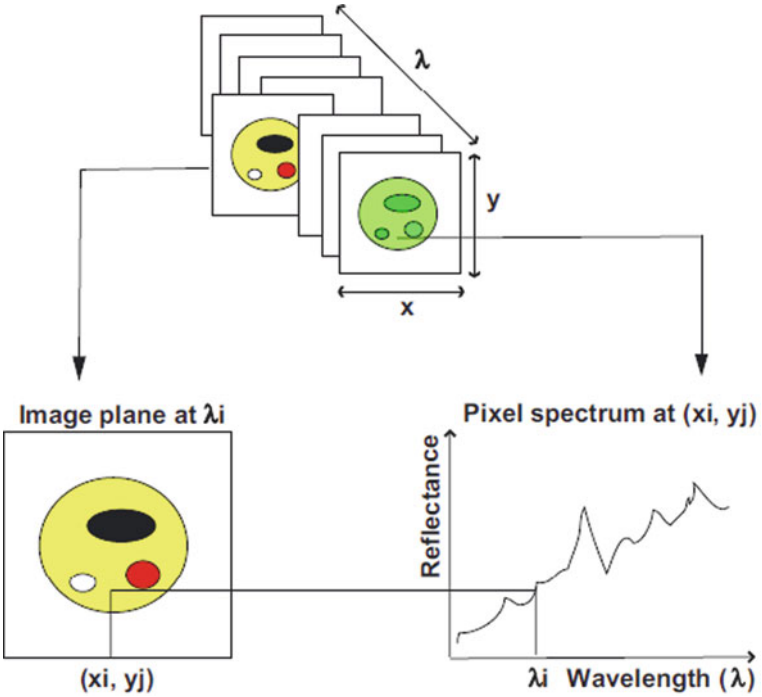

Fig. 3.14 Hyperspectral image contains a 3-D array of image data (hypercube) pertaining to two spatial (x_i, y_j) and on wavelength (λ_i) dimension at different *i-j* image planes (Gowen et al. 2007)

overall defect classification accuracy of 86% was achieved, compared with an accuracy of 70% by the human inspectors. With further improvement, the hyperspectral imaging system could meet the need of bloated pickles detection in a commercial plant setting (Ariana and Lu 2010). A visible/near-infrared hyperspectral imaging system has also been used to predict tenderness of cooked beef with a 96.4% accuracy (Fig. 3.15) (Naganathan et al. 2008).

Hyperspectral imaging in the visible and near-infrared (400–1,000 nm) regions was tested for nondestructive determination of moisture content, total soluble solids, and acidity in strawberry. Moreover, for classifying strawberry based on ripeness stage, a image texture analysis was also conducted (ElMasry et al. 2007).

3.6 On-Line or Moving Scene Analysis

Most computer vision systems designed are concerned primarily with static scenes. However, the perception of visual motion plays an important role in many emerging computer vision applications. Input to a dynamic or moving scene analysis system is a sequence of image frames taken from a changing world. The camera used to

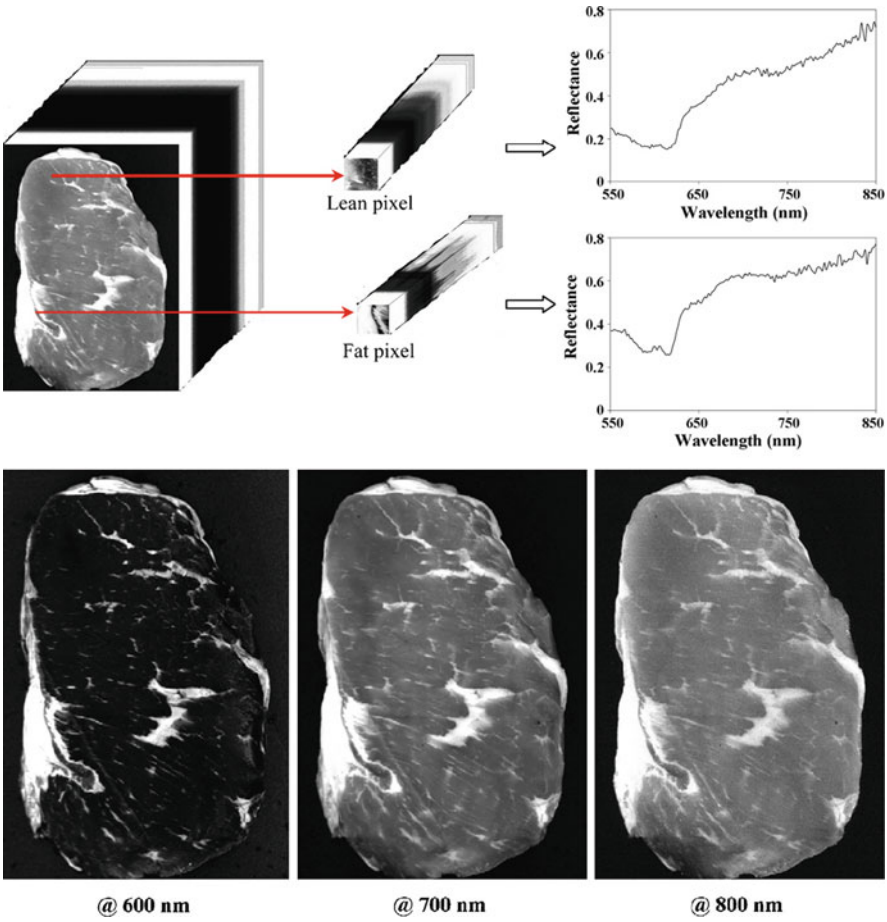

Fig. 3.15 A hyperspectral image of a beef-steak. *Top row*: typical spectral signatures of lean and fat pixels; *bottom row*: images of at selected wavelengths (Naganathan et al. 2008)

acquire an image sequence may also be in motion. Each frame represents an image of the scene at a particular instant in time. Changes in a scene may be due to the motion of the camera, the motion of objects, illumination changes, or changes in an object's structure, size or shape. It is usually assumed that changes in a scene are due to camera and/or object motion. A system must detect changes, determine the motion characteristics of the observer and the objects, characterize the motion using high-level abstraction, recover the structure of the objects and recognize moving objects.

Depending on the design of the imaging system, different image processing techniques are required. In the food industry, the most common design is that of stationary camera and moving objects. Image input is a frame sequence represented

by $F(x, y, t)$ where x and y are the spatial coordinates in the frame representing the scene at time t. The value of function F represents the intensity of the pixel.

In many applications, an entity, a feature or object, must be tracked over a sequence of frames. If there is only one entity in the sequence, the problem is easily solved. With many entities moving independently in a scene, tracking requires the use of constraints based on the nature of the objects and their motion. A number of real-time visual tracking systems have been reviewed by Morris and Trivedi (2008). Due to inertia, however, the motion of a physical entity cannot change instantaneously. If a frame sequence is acquired at a rate such that no dramatic change takes place between two consecutive frames, then no abrupt change in motion can be observed for most physical objects. This has been the basis of most on-line applications currently available in the food industry. The important factor is then to set the image acquisition rate fast enough to minimize image blur so the analysis of image data can take place frame by frame. Real-time image processing boards and real-time processors are available to assist in on-line real-time computer vision applications (Ahmad et al. 1999).

For a continuous stream of material flowing down a conveyor belt, a computer vision system can be designed using a line-scan camera for image acquisition. A line-scan camera contains a 1-D array of photosensitive sites. The line-scan camera is suitable for fairly fast moving object scenes. In addition to higher speed, line-scan cameras offer high resolution and the ability to handle infinitely long image scenes. A new breed of cameras, known as time delay and integrate (TDI) cameras, are line-scan cameras using CCD image sensor technology to gain an increase in speed or sensitivity of up to 100 times that of conventional cameras while providing exceptional spatial resolution (Ni et al. 1997). A 2-D image can be produced if there is relative motion between the camera and the object of interest. The columns of information from the line-scan camera are usually stored sequentially in a framestore allowing interpretation of returned data as a 2-D image. The author's research team is currently evaluating such an on-line system to evaluate the quality of shredded cheese. The run-length coding (binarizing an image in which each pixel is a 1 or 0) of the binary image is used to identify object locations in the scene (a string of 1s represent an object's presence). Syntactic pattern recognition technique was used in the image interpretation step.

Use of strobe lighting is also an effective technique for acquiring on-line information from a moving scene. To obtain a complete image of the scene under strobe lighting, the strobe firing must be synchronized with camera and image acquisition. Lack of synchronization will appear as partially light and/or partially or totally dark digitized images. The most straightforward strobe and image acquisition synchronization is where an object present is a signal typically generated by a photo eye or a proximity switch device. In this technique, the strobe light is fired immediately on an object's arrival, so the amount of object placement uncertainty in the direction of travel is reduced significantly. However, this technique requires high-precision object sensors, a special television camera with the capability of scan inhibit and an electronic circuit that synchronizes the various timing signals. Ni et al. (1997) used

a strobe light to avoid image blur during image acquisition to examine individual grain kernels. The kernels were traveling at a modest speed of 6.5 m/min.

A hyperspectral-multispectral line-scan imaging system was developed for differentiation of wholesome and systemically diseased chickens. In-plant testing was conducted for chickens on a commercial evisceration line moving at a speed of 70 birds per minute. This line-scan imaging system is ideal for directly implementing multispectral classification methods developed from hyperspectral image analysis (Chao et al. 2007).

General requirements for on-line applications are throughput (speed), accuracy, consistency, durability, diversification, flexibility and adaptability. Considerations of these conditions and constraints have to be given at all stages of system design and development. Speed of evaluation is perhaps the most striking requirement. For example, Tao et al. (1995) estimated that an on-line apple grading system may have to examine at least 3,600 fruit/min. They described a computer vision system sorting 3.5 million fruit in an 8-h day, which consisted of two separate lighting units with eight cameras and one processing and control console unit. This type of machine is being widely installed in the packing industry for sorting apples, citrus, peaches, tomatoes and various other fruits and vegetables.

References

Ahmad IS, Reid JF, Paulsen MR, Sinclair JB (1999) Color classifier for symptomatic soybean seeds using image processing. Plant Dis 83:320–327

Anami BS, Savakar DG, Biradar VS (2009) Identification of multiple grain image samples from tray. Int J Food Sci Technol 44:2452–2458

Ariana DP, Lu RF (2010) Evaluation of internal defect and surface color of whole pickles using hyperspectral imaging. J Food Eng 96:583–590

Benhanan U, Peleg K, Gutman PO (1992) Classification of fruits by a Boltzmann perceptron neural network. Automatica 28:961–968

Beyer M, Hahn R, Peschel S et al (2002) Analysing fruit shape in sweet cherry (*Prunus avium* L.). Sci Hortic 96:139–150

Blasco J, Aleixos N, Molto E (2007) Computer vision detection of peel defects in citrus by means of a region oriented segmentation algorithm. J Food Eng 81:535–543

Bulanon DM, Kataoka T, Ota Y et al (2002) Segmentation algorithm for the automatic recognition of Fuji apples at harvest. Biosyst Eng 83:405–412

Chao K, Yang CC, Chen YR et al (2007) Hyperspectral-multispectral line-scan imaging system for automated poultry carcass inspection applications for food safety. Poult Sci 86(11):2450–2460

Cheng X, Chen YR, Tao Y, Wang CY, Kim MS, Lefcourt AM (2004) A novel integrated PCA and FLD method on hyperspectral image feature extraction for cucumber chilling damage inspection. Transactions of the Asae 47:1313–1320

Chtioui Y, Panigrahi S, Backer LF (2003) Self-organizing map combined with a fuzzy clustering for color image segmentation of edible beans. Trans ASAE 46:831–838

Chtioui Y, Panigrahi S, Marsh R (1998) Conjugate gradient and approximate Newton methods for an optimal probabilistic neural network for food color classification. Opt Eng 37:3015–3023

Dell'Aquila A (2009) Development of novel techniques in conditioning, testing and sorting seed physiological quality. Seed Sci Technol 37:608–624

Di Ruberto C, Cinque L (2009) Decomposition of two-dimensional shapes for efficient retrieval. Image Vis Comput 27:1097–1107
Ding K, Gunasekaran S (1994) Shape Feature – extraction and classification of food material using computer vision. Trans ASAE 37:1537–1545
Du CJ, Sun DW (2006) Learning techniques used in computer vision for food quality evaluation: a review. J Food Eng 72:39–55
ElMasry G, Wang N, ElSayed A (2007) Hyperspectral imaging for nondestructive determination of some quality attributes for strawberry. J Food Eng 81:98–107
Elster RT, Goodrum JW (1991) Detection of cracks in eggs using machine vision. Trans AASAE 34:307–312
Ferrari V, Tuytelaars T, Van Gool L (2006) Object detection by contour segment networks. Computer vision – ECCV 2006, Pt 3, proceedings 3953:14–28
Gerrard DE, Gao X, Tan J (1996) Beef marbling and color score determination by image processing. J Food Sci 61:145–148
Ghazanfari A, Irudayaraj J, Kusalik A (1996) Grading pistachio nuts using a neural network approach. Trans ASAE 39:2319–2324
Gonzalez RC, Woods RE (1992) Digital image processing addison. Wesley Publishing Co., Reading, MA
Gowen AA, O'Donnell CP, Cullen PJ et al (2007) Hyperspectral imaging – an emerging process analytical tool for food quality and safety control. Trends Food Sci Technol 18:590–598
Gowen AA, O'Donnell CP, Taghizadeh M et al (2008) Hyperspectral imaging combined with principal component analysis for bruise damage detection on white mushrooms (Agaricus bisporus). J Chemom 22:259–267
Gunasekaran S, Cooper TM, Berlage AG et al (1987) Image processing for stress cracks in corn kernels. Trans ASAE 30:266–271
Gunasekaran S, Ding KX (1994) Using computer vision for food quality evaluation. Food Technol 48:151–154
Ibarra JG, Tao Y, Walker J et al (1999) Internal temperature of cooked chicken meat through infrared imaging and time series analysis. Trans ASAE 42:1383–1390
Iivarinen J (1998) Unsupervised image segmentation with the self-organizing map and statistical method, SPIE conference on intelligent robots and conmputer vision XVII, Bellingham, WA, pp 516–525
Jiang JA, Chang HY, Wu KH et al (2008) An adaptive image segmentation algorithm for X-ray quarantine inspection of selected fruits. Comput Electron Agric 60:190–200
Jimenez AR, Ceres R, Pons JL (2000) A survey of computer vision methods for locating fruit on trees. Trans ASAE 43:1911–1920
Jin FH, Qin L, Jiang L et al (2008) Novel separation method of black walnut meat from shell using invariant features and a supervised self-organizing map. J Food Eng 88:75–85
Kim S, Schatzki T (2001) Detection of pinholes in almonds through X-ray imaging. Trans ASAE 44:997–1003
Kim MS, Chen YR, Mehl PM (2001) Hyperspectral reflectance and fluorescence imaging system for food quality and safety. Transactions of the Asae 44:721–729
Kim MS, Lefcourt AM, Chao K, Chen YR, Kim I, Chan DE (2002a) Multispectral detection of fecal contamination on apples based on hyperspectral imagery. Part I. Application of visible and near-infrared reflectance imaging. Transactions of the Asae 45:2027–2037
Kim MS, Lefcourt AM, Chen YR, Kim I, Chan DE, Chao K (2002b) Multispectral detection of fecal contamination on apples based on hyperspectral imagery: Part II. Application of hyperspectral fluorescence imaging. Transactions of the Asae 45:2039–2047
Lai FS, Zayas I, Pomeranz Y (1986) Application of pattern-recognition techniques in the analysis of cereal-grains. Cereal Chem 63:168–172
Majumdar S, Jayas DS (2000a) Classification of cereal grains using machine vision: IV. Combined morphology, color, and texture models. Trans ASAE 43:1689–1694

Majumdar S, Jayas DS (2000b) Classification of cereal grains using machine vision: I. Morphology models. Trans ASAE 43:1669–1675
Mcdonald TP, Chen YR (1990) Separating connected muscle tissues in images of neef carcass ribeyes. Trans ASAE 33:2059–2065
Mcdonald TP, Chen YR (1991) Visual characterization of marbling in beef ribeyes and its relationship to taste parameters. Trans ASAE 34:2499–2504
Miller BK, Delwiche MJ (1991) Peach defect detection with machine vision. Trans ASAE 34:2588–2597
Morris BT, Trivedi MM (2008) A survey of vision-based trajectory learning and analysis for surveillance. IEEE Trans Circuits Syst Video Technol 18:1114–1127
Naganathan GK, Grimes LM, Subbiah J et al (2008) Visible/near-infrared hyperspectral imaging for beef tenderness prediction. Comput Electron Agric 64:225–233
Ni HX, Guansekaran S (2004) Image processing algorithm for cheese shred evaluation. J Food Eng 61:37–45
Ni H, Gunasekaran S (1998) A computer vision method for determining length of cheese shreds. Artif Intell Rev 12:27–37
Ni B, Paulsen MR, Liao K et al (1997) Design of an automated corn kernel inspection system for machine vision. Trans ASAE 40:491–497
Ozer N, Engel BA, Simon JE (1995) Fusion classification techniques for fruit quality. Trans ASAE 38:1927–1934
Pandya AS, Macy RB (1996) Pattern recognition with neural networks in C++. CRC Press, Boca Raton, FL, pp 394–434
Panigrahi S (1998) Neuro-fuzzy systems: applications and potential in biology and agriculture. AI Appl 12:83–95
Panigrahi S, Gunasekaran S (2001) Computer vision. In: Gunasekaran S (ed) Nondesctructive food evaluation: techniques to analyze proeprties and quality. Marcel Dekker, New York, NY, 39–98
Panigrahi S, Misra MK, Bern CJ et al (1995) Background segmentation and dimensional measurement of corn germplasm. Trans ASAE 38:291–297
Park B, Chen YR, Huffman RW (1996) Integration of visible/NIR spectroscopy and multispectral imaging for poultry carcass inspection. J Food Eng 30:197–207
Park B, Lawrence KC, Windham WR, Buhr RJ (2002) Hyperspectral imaging for detecting fecal and ingesta contaminants on poultry carcasses. Transactions of the Asae 45:2017–2026
Park B, Lawrence KC, Windham WR, Smith DP (2004) Multispectral Imaging system for fecal and ingesta detection on poultry carcasses. Journal of Food Process Engineering 27:311–327
Park B, Lawrence KC, Windham WR, Smith DP (2005) Detection of fecal contaminants in visceral cavity of broiler carcasses using hyperspectral imaging. Applied Engineering in Agriculture 21:627–635
Patel VC, McClendon RW, Goodrum JW (1998) Color computer vision and artificial neural networks for the detection of defects in poultry eggs. Artif Intell Rev 12:163–176
Riquelme MT, Barreiro P, Ruiz-Altisent M (2008) Olive classification according to external damage using image analysis. J Food Eng 87:371–379
Ros F, Guillaume S, Rabatel G et al (1995) Recognition of overlapping particles in granular product images using statistics and neural networks. Food Control 6:37–43
Saito Y, Hatanaka T, Uosaki K et al (2003) Neural network application to eggplant classification. Knowledge-Based Intellignet Information and Engineering Systems, Pt 2, proceedings 2774:933–940
Schindler K, Suter D (2008) Object detection by global contour shape. Pattern Recognit 41:3736–3748
Singh N, Delwiche MJ, Johnson R (1993) Image analysis methods for real-time color grading of stone fruits. Comput Electron Agric 9:71–84
Smolarz A, Vanhecke E, Bouvier JM (1989) Computerized image-analysis and texture of extruded biscuits. J Texture Stud 20:223–234

Steenoek LW, Misra MK, Hurburgh CR et al (2001) Implementing a computer vision system for corn kernel damage evaluation. Appl Eng Agric 17:235–240
Tan JL (2004) Meat quality evaluation by computer vision. J Food Eng 61:27–35
Tan J, Gao X, Hsieh F (1994) Extrudate characterization by image-processing. J Food Sci 59:1247–1250
Tao Y, Chance L, Liu B (1995) Full-scale fruit vision sorting system design – factors and considerations. Food Processing Automation Conference IV, ASAE, Chicago, IL, pp 14–22
Travis M (1998) Image processing goes color. Comput Graph World:99–101
Uchiyama T, Arbib MA (1994) Color image segmentation using competitive learning. IEEE Trans Pattern Anal Mach Intell 16:1197–1206
Upchurch BL, Throop JA (1994) Effects of storage duration on detecting watercore in apples using machine vision. Trans ASAE 37:483–486
Wong EK (1994) Syntactic image pattern recognition. In: DoughertyER (ed) Digital Image processign methods. Marcell Dekker, New York, NY, pp 167–195
Zayas IY (1993) Digital image texture analysis for bread crumb grain evaluation. Cereal Foods World 38:760
Zhang G, Jayas DS, White NDG (2005) Separation of touching grain kernels in an image by ellipse fitting algorithm. Biosyst Eng 92:135–142
Zheng CX, Sun DW, Zheng LY (2006) Recent applications of image texture for evaluation of food qualities – a review. Trends Food Sci Technol 17:113–128

Chapter 4
Electronic Nose and Electronic Tongue

Nabarun Bhattacharyya and Rajib Bandhopadhyay

Human beings have five senses, namely, vision, hearing, touch, smell and taste. The sensors for vision, hearing and touch have been developed for several years. The need for sensors capable of mimicking the senses of smell and taste have been felt only recently in food industry, environmental monitoring and several industrial applications. In the ever-widening horizon of frontier research in the field of electronics and advanced computing, emergence of electronic nose (E-Nose) and electronic tongue (E-Tongue) have been drawing attention of scientists and technologists for more than a decade. By intelligent integration of multitudes of technologies like chemometrics, microelectronics and advanced soft computing, human olfaction has been successfully mimicked by such new techniques called machine olfaction (Pearce et al. 2002). But the very essence of such research and development efforts has centered on development of customized electronic nose and electronic tongue solutions specific to individual applications. In fact, research trends as of date clearly points to the fact that a machine olfaction system as versatile, universal and broadband as human nose and human tongue may not be feasible in the decades to come. But application specific solutions may definitely be demonstrated and commercialized by modulation in sensor design and fine-tuning the soft computing solutions. This chapter deals with theory, developments of E-Nose and E-Tongue technology and their applications. Also a succinct account of future trends of R&D efforts in this field with an objective of establishing co-relation between machine olfaction and human perception has been included.

4.1 Electronic Nose (E-Nose)

E-Nose is an instrument, which mimics the sense of smell of biological system. Basically, this device is used to detect and distinguish complex odor at low cost. In the parlance of food and agro produces, human expert panel and conventional

N. Bhattacharyya (✉)
Center for Development of Advance Computing (C-DAC), Kolkata 700091, West Bengal, India
e-mail: nabarun.bhattacharya@cdackolkata.in

S.N. Jha (ed.), *Nondestructive Evaluation of Food Quality*,
DOI 10.1007/978-3-642-15796-7_4,

analysis techniques such as Gas Chromatography (GC), High Performance Liquid Chromatography (HPLC) etc, characterize aroma of any substance. Both techniques have some difficulties. In case of human expert panel, it is a costly process since it requires trained people who can work for only short period of time. Also additional problems such as subjectivity of human response to odors and the variability between individuals are to be considered. On the other hand, the analytical instruments for characterization of aroma involve high cost and require knowledgeable people to operate those instruments, elaborate sample preparation and long time for analysis. E-Nose provides a low cost, non-invasive and rapid method of objective aroma measurement.

4.1.1 Nose in Biological System

Odours are sensations that occur when compounds (called odorants) stimulate receptors located in the olfactory epithelium at the roof of nasal cavity. Odorants are hydrophobic, volatile compounds with a molecular weight of less than 300 Da. Humans can recognize and distinguish upto 10,000 different substances on the basis of their odour quality. Odorant receptors (OR) in the nasal cavity detect and discriminate among these thousands of diverse chemical traces. The olfactory region of each of the two nasal passages in human is a small area of about 2.5 cm^2 containing in total approximately 50 million primary sensory receptor cells.

The olfactory region (Fig. 4.1) consists of cilia projecting down out of the olfactory epithelium into a layer of mucous which is about 60 μm thick. This mucous layer is a lipid-rich secretion that bathes the surface of the receptors at the epithelium

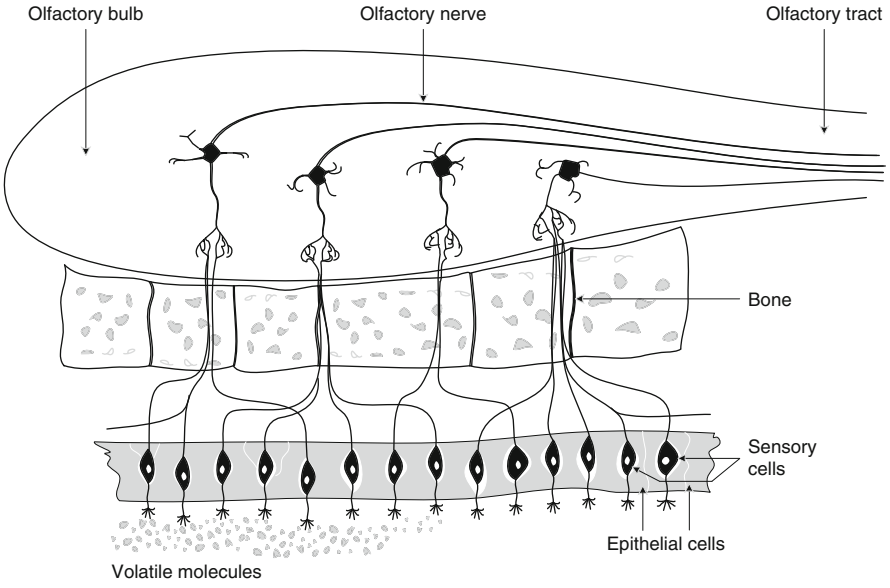

Fig. 4.1 Biological olfactory system

surface. The mucous layer is produced by the Bowman's glands which reside in the olfactory epithelium. The mucous lipids assist in transporting the odorant molecules as only volatile materials that are soluble in the mucous can interact with the olfactory receptors and produce the signals that our brain interprets as odor. Each olfactory receptor neuron has 8–20 cilia that are whip-like extensions 30–200 μm in length. The olfactory cilia are the sites where molecular reception with the odorant occurs and sensory transduction (i.e., transmission) starts.

Researchers in olfactory study have shown that every neuron in the olfactory bulbs participates in the generation of olfactory perception. In other words, the salient information about the stimulus is carried in some distinctive pattern of bulb wide activity and not in a subset of specific neurons. In the absence of a stimulus, the pattern of activity across the olfactory bulb has "chaotic" characteristics. However, upon receiving a stimulus the chaotic behavior rapidly assumes a cross-bulbar pattern. This pattern need not be the same each time for the same odour, but may change its characteristics depending upon the previous stimulus. This system allows for odorant conditioning, and also explains how we can be sensitive to odours we have never previously experienced.

4.1.2 Odour Receptor and Odorant Relationship

An individual odorant can bind to multiple receptor types and structurally different odorants can bind to a single receptor. Specific patterns of activation generate signals that allow us to discriminate between the vast numbers of different smells. The physicochemical attributes of odorants that induce specific odour sensations are not well understood yet.

Odorants vary widely in structure and include many chemical classes including organic acids, alcohols, aldehydes, amides, amines, aromatics, hydrocarbons, nitrides, phenols etc. to state a few. The signals induced by the interactions of odorants with OR's in the olfactory epithelium are transmitted to the olfactory bulb and ultimately to the brain. Most odorant sensations are produced by mixtures of hundreds of odorants rather than by a single compound. Human have limited capacity to identify single odorants in mixtures with three to four components being maximum.

Odour classification scheme based on adjective descriptors has been standardized by American Society for Testing and Materials and some of the sample vocabulary used are given in Table 4.1.

Table 4.1 Some samples of ASTM descriptive categories used for general odour quality characterization

Fragrant	Floral	Chemical	Eggy	Metallic
Sweety	Cheesy	Varnish	Fermented fruit	Malty
Fruity (citrus)	Beery	Sour milk	Chalky	Woody
Eucalyptus	Chocolate	Strawbery	Maple	Fishy
Soapy	Molasses	Urine-like	Nutty	Aromatic
Garlic	Cologne	Clove-like	Fried fat	Burnt, smoky

Although, good progress has been made in our knowledge of olfactory physiology and bio-chemistry, the fundamental relationship between odour quality and molecular property is still poorly understood. Even slight alteration in the chemical structure of an odorant can induce profound changes in odour quality. Current structure – activity model in olfaction are, for the most part, simply collection of disparate facts with no unifying theme. Furthermore, they have inadequate predictive accuracy. As a consequence, the basic logic necessary to develop a comprehensive odour classification scheme based on particular features of molecules remain elusive.

4.1.3 Concept of E-Nose

An electronic nose is an instrument that is designed to detect and discriminate among complex odours using a sensor array (Bhattacharyya et al. 2005). The sensor array consists of non specific sensors that are treated with a variety of chemical materials. The sensor array is exposed to the volatile (Wickremasinghe et al. 1979) molecules and as soon as smellprint (or fingerprint) is generated from sensor array. Patterns or fingerprints from known odours are used to construct the database and train a pattern recognition (Shaffer et al. 1998) system so that unknown odours can be classified and identified. This is classical concept of electronic nose. However in a broader sense, electronic nose instruments are composed of three elements, namely: (i) sampling handling system, (ii) detection system and (iii) data processing system (Fig. 4.2)

(i) Sample handling systems

Sample handling is a critical step affecting the analysis by electronic nose. The quality of the analysis can be improved by adopting an appropriate sampling technique. To introduce the volatile compounds present in the headspace

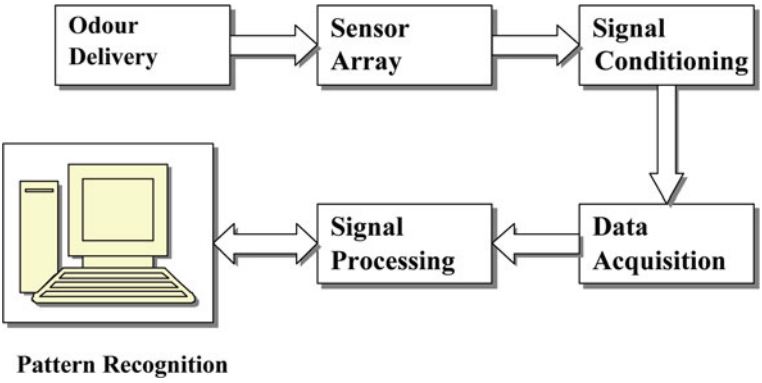

Fig. 4.2 Block diagram representation of electronic nose system

(HS) of the sample into the e-nose's detection system, several sampling techniques as below have been used in electronic nose.

(a) Static headspace (SHS) technique

SHS technique consists of placing the sample in a hermetically sealed vial and, once equilibrium has been established between the matrix and the gaseous phase, sampling from head space (HS) starts. Sample temperature, equilibration time, vial size and sample quantity are the main parameters that have to be optimized. Because of the poor repeatability of manual HS injection, it is recommended that an automatic HS sampler be used.

(b) Purge and trap (P&T) technique:

P&T and different headspace techniques have been used in some applications to increase sensitivity, since they provide a pre-concentration of volatile compounds. In these systems, the volatile components are purged by a stream of inert gas and trapped onto an adsorbent. In the case of P&T, the gas flow is injected through the sample, whereas, in the case of Dynamic head space (DHS), only the HS is purged with the gas.

(c) Solid-phase micro extraction (SPME) technique:

SPME is a user-friendly pre-concentration method. The principle involves exposing a silica fibre covered with a thin layer of adsorbent in the HS of the sample in order to trap the volatile components onto the fibre. The adsorbed compounds are desorbed by heating and introduced into the detection system. Apart from the nature of the adsorbent deposited on the fibre, the main parameters to optimize are the equilibration time, the sample temperature and the duration of extraction. This technique has a considerable concentration capacity and is very simple because, unlike P&T or DHS, it does not require especial equipment.

(d) Stir bar sorptive extraction (SBSE) technique:

SBSE, a magnetic bar coated with polymers, is held in the HS for sampling. Its loading capacity is much higher than that of SPME. Even though it has been developed only recently, SBSE is a promising extraction technique when very high sensitivity is required.

(e) Inside-needle dynamic extraction (INDEX) technique:

INDEX is also a pre-concentration technique. Its needles contain an absorbing polymer phase very much like a fixed bed. The volatile compounds are forced through the needle by repeated aspiration/ejection motions of the syringe plunger. The potential advantage of this system compared to SPME is its mechanical robustness and the possibility of increasing the amount of absorbing polymer as well as the surface area available for adsorbing volatile compounds.

(f) Membrane introduction mass spectrometry (MIMS) technique:

MIMS is a sample handling system used in mass spectrometry (MS) based e-noses. This technique allows the direct introduction of specific compounds of a liquid or gas sample into a mass spectrometer. A thin membrane is installed between the sample and the ion source of a mass spectrometer in such a way

that some compounds dissolve in the membrane, diffuse through it and, finally, evaporate directly into the ion source.

(ii) Detection system

The most complicated part of electronic olfaction process is odour capture and sensor technology to be deployed for such capturing. Any sensor that responds reversibly to a chemical in gas or vapour phase has the potential to be developed in an electronic nose format. Early electronic noses used either polished wires in contact with porous rods saturated with different electrolytes or thermistors coated with materials such as gelatin, fats or polymers. In the 1980s, advances were made with the appearance of chemically sensitive sensors and developments in electronics and computing. Some of the essential or desirable properties of the chemical micro-sensors to be used in electronic nose are summarized as follows.

- *Selectivity*: The chemical sensor must respond to a range of chemical species to be detected.
- *Sensitivity*: The chemicals to be detected may be present in the concentration range of ppm or ppb. The sensor should be sufficiently sensitive to detect small concentration level of gaseous species within a volatile mixture
- *Speed of response*: In order to be used for online measurements, the response time of the sensor should be in the range of seconds.
- *Reproducibility*: The individual sensor element should be reproducible in their manufacture and response characteristics. This will reduce the task of calibrating each sensor element before use. Fabrication processes used to make a single sensor must be compatible with the manufacture of an array of reasonable size. Additionally, the sensors should have an inherently linear response characteristic.
- *Reversibility*: The sensor should be able to recover after exposure to gas.
- *Portability*: Devices should be small so that small sample volumes can be used. The power consumption should be low so that the device can be operated with a battery, making the sensor portable.

Table 4.2 presents a list of sensor types and associated measuring principles used for electronic nose. Out of all types of sensors, conducting polymer, metal oxide semiconductor and bulk acoustic devices are most commonly used in commercial electronic noses. Brief descriptions of some commonly used sensors (Fig. 4.3) are discussed below.

(a) Conducting polymer micro-sensors

Physical and electrical properties of conducting polymers are altered significantly by a selective interaction with some chemical species. Hence, conducting polymers have been widely used in thin-film gas sensors, such as those found in commercially available artificial noses. Conducting polymer gas sensors have a number of properties that make them attractive for commercial use. Sensors can be fabricated easily by electro-polymerization in a controlled

Table 4.2 Sensor types and measurement principles

Measuring principle	Sensor type	Common materials used
Chemoresistors	Metal oxides	Doped tin di-oxide, zinc oxide, tungsten trioxide
	Conductive polymers	Polypyrrole, polyaniline, polythiophene
	Conductive oligomers	Short chain length conductive polymers
	Conductive material loaded polymers	Carbon particles in non-conductive polymers.
	Self-organising films	Discotic liquid crystals
	Macrocyclic compounds	Phthalocyanines
Mass sensitive devices	Surface and bulk acoustic devices	Poly (siloxanes), charged polyelectrolytes, fluoropolymers, polyalkanes, hydrophilic polymers, calixarenes and other cavitands, chiral polymers, metal phosphonates, conducting polymers, lipids, self assembled monolayers
Field effect devices	Metal insulator semiconductors or metal oxide semiconductors	Catalytic metals such as palladium, platinum and iridium, as well as other metals
Electrochemical devices	Oxidation or reduction catalysts	Precious metal and carbon with concentrated liquid electrolyte and counter electrode
Pellistors	Catalytic combustion devices	Platinum, palladium or alloys of the two
Fibre optic systems	Polymer bids on fibre optic bundles	Fluorescent, solvochromic dyes to detect solvation of vapours in the polymer
Intrinsic molecular parameters	Mass spectrometer, ion mobility or pulsed spectroscopy instrumentation	

manner using a wide range of basic monomers. Different chemicals can be added during the process of polymerization. The monomers react with these chemicals during the process of polymerization to give a wide range of polymer material. Additionally, different electrolytes and solvents during the process of electro-polymerization give rise to polymers with different properties. Different polymers show non-overlapping selectivity towards different chemicals, hence an array of polymer sensors can be used to generate a pattern of response to distinguish different gas species. Polymer films respond reasonably rapidly and

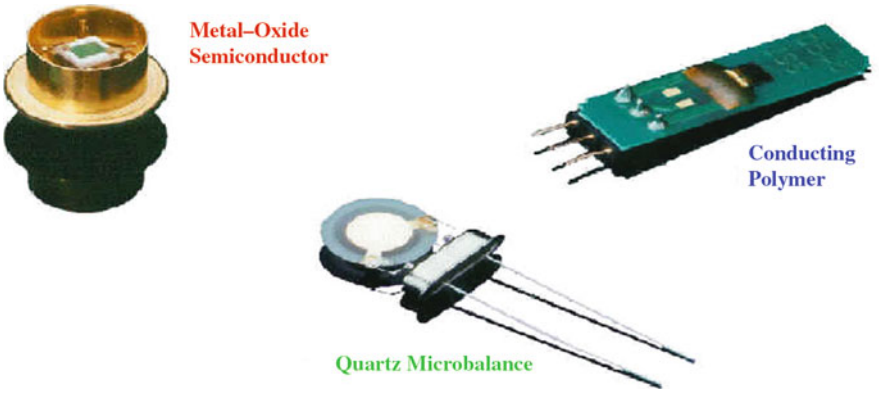

Fig. 4.3 Commonly available e-nose sensors

reversibly at room temperature to some chemicals. Thus, the advantages of the conducting polymer based sensors are:

- excellent reproducibility,
- eide selectivity,
- high sensitivity,
- wide range of applications,
- stable,
- low power,
- Operate at ambient temperature.

(b) Metal oxide sensors

Metal oxide sensors are based on semiconducting sensing elements, e.g., tin oxide, which shows a change of resistivity on exposure to certain analytes. Basic features of these sensors are:

- these are semiconducting sensing elements made from a metal oxide film, e.g., tin oxide,
- they operate in the range from 300 to 500°C,
- these sensors require O_2 to function,
- volatiles undergo redox reactions at the sensor surface, resulting in a change of conductivity across the sensor,
- selectivity can be modified by doping the metal oxide (e.g., with Pd, Pt) or modifying the operating temperature of the sensor,

Advantages of metal oxide sensors are: longevity, sensitivity, low response to RH, wide range of applications and large response and good discriminating power

(c) Bulk acoustic wave (BAW) sensors

BAW sensors are piezoelectric devices based on quartz crystal oscillators. The quartz crystal is coated with a range of materials that selectively adsorb

analytes, which results in changes in the frequency of oscillation. Basic features of BAW Sensors are:

- quartz crystal can be coated with a wide range of different selective coating films,
- on adsorbing analytes the additional mass of the film results in a change in the frequency of oscillation of the sensor, and
- a typical sensor has an operating frequency of about 10 MHz.

Advantages of BAW sensors are: high selectivity, able to measure both polar and non-polar species, stable over a wide temperature range, low power (low mW), low sensitivity to humidity, high stability, good reproducibility, and well characterized coating chemistry

(d) Optical sensors

Optical sensing is very versatile as it can allow simultaneous collection of intensity and wavelength information, and encompasses a range of techniques (absorbance, reflectance, fluorescence, refractive index and colorimetry). The most popular is fluorescence on absorption and colorimetric measurements. Fluorescence techniques generally utilise optical fibres; although these can be used directly, most chemical sensor applications use them to direct the light source to the sensing element, which can be fabricated on the fibre or coated onto an inert substrate. Most commonly the distal face or tip of the fibre is coated. Total internal reflection fluorescence (TIRF) and fibre optic evanescent wave (FOEW) sensors rely on evanescent field excitation; this takes place on an unclad but coated circumference wall of the fibre. The distal tip conveys the resultant light to a detector. The first optical E-nose used individual fibre optic strands coated with fluorescent polymer dyes. Different polymer/dye gradients led to differences in the sensing properties.

iii) Data processing system

The sensor response is stored in the PC through data acquisition card and these data sets are analyzed to extract information. The details techniques are discussed in 4.1.4 & 4.1.5.

4.1.4 Advanced Signal Processing

In a machine olfaction system, two major building blocks are the (1) sensors and (2) the pattern classification engine. Interfacing electronics, signal conditioning and data acquisition circuits provide the crucial link between these two blocks. Olfaction sensors have a wide range of transduction mechanisms as described earlier. But, at the output of these sensors, what is required is an electrical signal (say, voltage or current) proportional to the gas/liquid exposure on the sensor surface. Interface circuits convert the sensor output parameters to the electrical signal for further processing. In chemoresistor sensor, a change in resistance is obtained when exposed to the odour particles. A voltage divider or a Wheatstone bridge circuit can be used as the basic interface circuit. Interfacing circuits of QCM or SAW devices

are required to measure shift in the resonance frequency and frequency counters can do the job. What follows the interfacing circuits is the signal-conditioning block which is basically analogue conditioning of the electrical signal through five sequential stages such as (1) buffering (2) amplification (3) filtering (4) conversion and (5) compensation. In the machine olfaction system developed by C-DAC, USB compatible data acquisition cards of National Instruments have been used and the cards have got these entire signal conditioning features built-in into the hardware. Data acquisition involves gathering signals from measurement sources, i.e., sensors and digitizing the signal for storage, analysis, and presentation on a personal computer (PC). Data acquisition (DAQ) systems are available in many different PC technologies for flexibility and application-specific customization. Various options in this regard include Peripheral Component Interconnect (PCI), PCI eXtensions for Instrumentation (PXI), PCI Express, PXI Express, Personal Computer Memory Card International Association (PCMCIA), Universal Serial Bus (USB), Institute of Electrical and Electronics Engineers (IEEE 1,394), parallel, or serial ports for data acquisition in test, measurement, and automation applications. Signal preprocessing means extraction of relevant information from the responses obtained and preparation of this information for multivariate pattern analysis (Wall et al. 2003). The major aspects of this preprocessing are: (a) baseline identification and manipulation/determination, (b) compression, (c) normalization or final preprocessing. Baseline is basically the sensor response to a reference analyte and proper accommodation of the same into the actual sensor response is expected to provide compensation due to drift, scaling and enhancement of contrast and better identification. Three different techniques of baseline manipulation are (a) differential, (b) relative and (c) fractional. Compression (Pan et al. 2008) is a preprocessing stage where the response of sensor array is utilized as a feature (Distante et al. 2002) vector or a fingerprint by reducing the number of descriptors. Normalization is the final leg of preprocessing where techniques are applied to operate on the sensor signal to compensate for sample-to-sample variations due to change in analyte concentration and drift in the sensors. Alternately, entire database of a single sensor can be operated upon and scaling of sensors can be effected. The former technique is known as local method and the latter as global method.

The responses generated by an array of olfaction sensors are processed using a variety of techniques. The pattern recognition engine may be developed using both parametric and non-parametric methods. Parametric methods are commonly referred to as statistical approaches and are based on the assumption that the sensor data set may be represented as a probability distribution function. The non-parametric methods do not assume any probability distribution function and deal with biologically inspired techniques, viz., artificial neural networks (ANN) (Haykin 2001) and expert systems. Researchers use both supervised and unsupervised learning (Poggio and Girosi 1990) methodologies for the pattern recognition system. There are many algorithms for analysis of an electronic nose data. Steps involved in processing of signal data are depicted in a block diagram (Fig. 4.4) and described briefly hereunder.

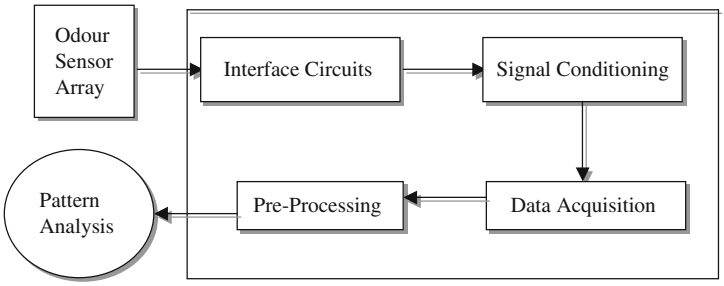

Fig. 4.4 Block diagram of signal processing system

(i) Interface circuits:

Various kinds of interface electronics are used for electronic nose. They are: voltage dividers, wheatstone bridge measurements, AC impedance spectroscopy for chemoresistors; detection of change in frequency of oscillation for Acoustic Wave Devices; and monitoring of variation of volt-amp characteristics for field effect devices.

(ii) Signal conditioning:

The electrical signal generated by sensor interface circuits is not adequate for acquisition by computer. The signals from sensors must be further processed through the analog signal conditioning steps as below.

(a) Buffering: Generally operational amplifiers in voltage follower mode are used for buffering stage to ensure proper isolation of the sensor to rest of the circuit.

(b) Amplification: The electrical signal available at the output of the buffer stage needs to be amplified so that signal level becomes suitable for analog to digital conversion. Integrated instrumentation amplifiers with high input impedance and common mode rejection ratio are generally used in this stage of electronic nose circuit.

(c) Filtering: Analog filters are used to remove unwanted frequency components from the sensor signals. Both active and passive filters have found application in electronic nose circuits depending on type of sensors and the application for which the nose is used.

(d) Compensation: A number of special functions may be implemented with analog circuits to compensate for deficiencies, non-linearity in sensor's response and reduce the computational load of a subsequent digital processing stage. These circuits perform various functions including linearization, integration, differentiation, logarithmic conversions, peak to peak and phase detection, temperature compensation etc. Operational amplifier based circuits are used in this stage.

(iii) Data acquisition

Output of signal conditioning module is directly fed to data acquisition stage of electronic nose system. For a PC-supported system, PCI compatible add on

cards are generally used. For hand held versions, special intelligent cards using advanced microcontrollers are used for capturing the conditioned data from sensor array. The data acquisition module should digitize with a resolution of 12-bits or higher at sample rate up to 250 kSamples/s. For most of e-nose applications, much slower sample rate serves the purpose. The PCI data acquisition cards come with Win32 application source code, device drivers and full register programming details and also possess on board memory for efficient processing. Application software is developed on virtual instrumentation or other platforms to communicate effectively with the intelligent data acquisition cards.

(iv) Signal pre-processing

Signal preprocessing means extraction of relevant information from the responses obtained and preparation of this information for multivariate pattern analysis. The major aspects of this preprocessing are:

(a) baseline identification and manipulation/determination,
(b) compression, and
(c) normalization or final preprocessing.

(a) Baseline identification: Baseline is basically the sensor response to a reference analyte and proper accommodation of the same into the actual sensor response is expected to provide compensation due to drift, scaling and enhancement of contrast and better identification. Three different techniques of baseline manupulation are: (a) differential, (b) relative and (c) fractional.

In differential technique, the preprocessed response is the difference between the dynamic sensor response and the baseline reference. The differential technique may be represented mathematically as below.

$$y_s(t) = (x_s(t) + \delta_A) - (x_s(0) + \delta_A) = x_s(t) - x_s(0) \tag{4.1}$$

where

$x_s(0)$ and $x_s(t)$ = The sensor responses at 0th and "t" th instants of the sniffing cycle,

δ_A = Additive noise or drift,

$y_s(t)$ = The pre-processed response.

In the relative method, the preprocessed response is obtained by dividing dynamic sensor response along with multiplicative drift with baseline reference again along with this drift. In this case, the preprocessed response may be mathematically represented as follows.

$$y_s(t) = \frac{x_s(t)(1 + \delta_M)}{x_s(0)(1 + \delta_M)} = \frac{x_s(t)}{x_s(0)} \tag{4.2}$$

Where δ_M = Multiplicative drift in the sensors.

In fractional technique, baseline reference is subtracted from the dynamic response and the result is divided by the baseline reference to obtain the fractional manipulation. The pre-processed sensor response in this method would be as follows.

$$y_s(t) = \frac{x_s(t) - x_s(0)}{x_s(0)} \tag{4.3}$$

Although choice of a particular technique is dependent on the sensor, its technology and application, the fractional technique mentioned above seems to be the best for adaptation to pattern recognition study and in all the multivariate data analyses carried out under the present thesis; fractional technique of baseline manipulation has been used. Fig. 4.5 shows the dynamic response $y(t)$, the baseline reference $y(0)$ values with odour input pulse time.

(b) Compression: Huge amount of data is generated in each sniffing cycle by the sensor array and the data acquisition system from the transient dynamics of the sensor output. Compression is a preprocessing stage where the response of sensor array is utilized as a feature vector or a fingerprint by reducing the number of descriptors. Transient or dynamic fingerprint is obtainable and transient compression technique such as (a) sub-sampling methods, (b) parameter extraction methods, (c) system identification method which is employed for compression. In (a), the dynamic information is obtained by sampling the sensor transient response at different times during the exposure of the sensor. In (b), the transient response is compressed using a number of descriptors primarily the rise time, maximum and minimum responses, slopes and off

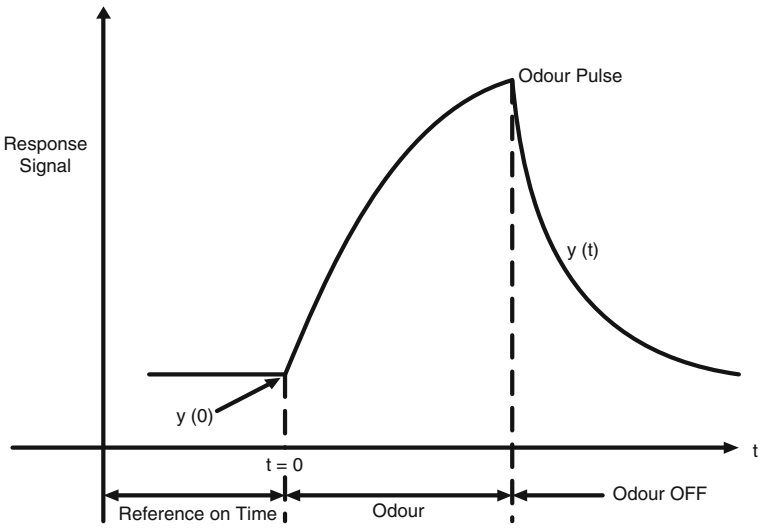

Fig. 4.5 Odour response curve

integral of the sensor curve $\sum \Delta y\,(t)$. In (c), model response curve is attempted to be fitted with the obtained one. The model curve is obtained by standard techniques such as auto regression. In the e-nose system developed and experimented with, the maximum value vector from the sensor output data has only been considered for data analysis.

The data matrix stored in the computer in each sniffing cycle will consist of a mixture of both baseline as well as actual sensor responses as shown below:

$$A = \begin{bmatrix} b_{11} & b_{12} & \cdots & b_{18} \\ b_{21} & b_{22} & \cdots & b_{28} \\ \vdots & \vdots & \cdots & \vdots \\ b_{h1} & b_{h2} & \cdots & b_{h8} \\ S_{11} & S_{12} & \cdots & S_{18} \\ S_{21} & S_{22} & \cdots & S_{28} \\ \vdots & \vdots & \cdots & \vdots \\ S_{m1} & S_{m2} & \cdots & S_{m8} \end{bmatrix}$$

Sensor baseline responses during headspace generation During Sampling

Sensor responses when exposed to tea odour during sampling

In the above data matrix, the segment b_{11} to b_{h8} represents baseline responses of the sensors during headspace generation and S_{11} to S_{m8} represents the sensor responses when exposed to tea odour during sampling. Here the number of sensor is considered as eight (8).

In most of the e-nose studies, maximum value of S_{ij} for each column is found out and a vector M is formed with these maximum values. So,

$$M = [S_{i1\,\max} \cdots\cdots\cdots\cdots S_{i8\,\max}] \tag{4.4}$$

This maximum value vector is the feature set for each sniffing cycle, which, in turn, is presented to the pattern classification software.

(c) Normalization: Normalization is the final leg of preprocessing where techniques are applied to operate on the sensor signal to compensate for sample-to-sample variations due to change in analyte concentration and drift in the sensors. Alternately, entire database of a single sensor can be operated upon and scaling of sensors can be effected. The former technique is known as local method and the latter as global method. Normalization requires certain known responses and related parameters to form a database, which also include the concentration of the sample with a specified odour. If each odour pulse (or sniff as is commonly known) produces the feature vector (response), the conventional normalization process can be adopted for a straightforward analysis to be followed. However in e-nose system, the global normalization procedure is generally followed. This procedure may be divided in two categories:

- Sensor auto scaling in which the distribution of responses of each sensor across the entire database is set to have zero mean value and unit standard deviation
- Sensor normalization in which the range of values of each sensor is set to be between 0 and 1. If the sensor output is highly non-linear with very wide range of response values, logarithmic transforms may be used. Another transform, called Box–Cox transform is sometimes used to compensate for the non-linearity.

4.1.5 Intelligent Pattern Recognition

The responses generated by an array of odour sensors may be processed using a variety of techniques. The pattern recognition (Gutierrez-Osuna 2002) engine may be developed using both parametric and non-parametric methods. Parametric methods are commonly referred to as statistical approaches and are based on the assumption that the sensor data set may be represented as a probability distribution function. The non-parametric methods do not assume any probability distribution function and deal with biologically inspired techniques, viz., artificial neural networks (ANN) (Kermani et al. 2005) and expert systems. Researchers use both supervised and unsupervised learning methodologies for the pattern recognition system. In supervised learning method, an unknown odour is tested against a knowledge base of known descriptors or classes. For unsupervised learning, pattern recognition engine learns to discriminate different samples without being presented with corresponding descriptors just like mammalian olfactory system. Commonly used techniques, up-to-date algorithms and future trends in pattern analysis for electronic nose are summarized in Table 4.3. Details of these statistical techniques are available in separate books, yet some of them have been described in brief in Chap. VI

Table 4.3 Various pattern recognition methods and multivariate techniques used in electronic nose

Statistical methods	Quantitative Pattern analysis	Supervised	MLR, PLS
		Unsupervised	PCA, CA
		Supervised	DFA, PCR
Biologically inspired methods	ANN	Unsupervised	SOM
		Supervised	MLP, PNN, RBF, LVQ
	Fuzzy methods	Supervised	FIS, FNN, FCM
		Self-supervised	ART, Fuzzy ARTMAP
	Others	Self-supervised	GA
		Supervised	NFS, wavelets

PCA, principal component analysis; PLS, partial least squares; MLR, multiple linear regression; PCR, principal component regression; DFA, discriminant function analysis; LDA, linear discriminant analysis; ANN, artificial neural network; SOM, self organizing map; GA, genetic algorithm; ART, adaptive resonance theory; RBF, radial basis function; NFS, neuro fuzzy system.

4.1.6 Application of Electronic Nose

Several successful applications of the electronic nose have been published. There are five categories of use for electronic nose in food control. These are (i) process monitoring, (ii) shelf life investigation (Boothe and Arnold 2002), (iii) freshness evaluation (O'Connell et al. 2001), (iv) authenticity assessment, and (v) other quality control studies.

4.1.6.1 Food Process Monitoring

Numerous successful applications of the electronic noses to the monitoring of flavor and aroma components along a food production process have been published. Aroma production along grape must fermentation has been monitored during bioconversion (Pinheiro et al. 2002). In this study, the muscatel aroma was chosen because the profile formed as a result of yeast metabolism is complex, being composed of many compounds. These differ from each other in concentration, chemical and organoleptic properties and contribute to the overall muscatel aroma.

During the curing process (García et al. 2005), e-nose have been used to identify spoiled Iberian hams. The sensors involved were tin-oxide semiconductor thin films, some of which were doped with metal catalysts such as Cr and In. A good discrimination (success rate of 100%) of two types of Iberian hams (spoiled and unspoiled) was obtained through the statistical methods of PCA and probabilistic ANN (PNN).

E-noses have been also applied to bioprocess monitoring where microbiological processes (Marilley et al. 2004) are involved in food production, i.e. to screen the aroma generation of lactic acid bacteria strains in the production of cheese and other fermented dairy products.

During the winemaking process (Cynkar et al. 2007), unpleasant organoleptic taints arise from *Brettanomyces* yeasts spoilage. The two main components of the taint are 4-ethylphenol (4EP) and 4-ethylguaiacol (4EG). The existing procedures to monitor spoilage due to *Brettanomyces*/*Dekkera* sp. are time-consuming and expensive, making it difficult for wine makers to monitor their wines at all stages of production. Consequently, there is a need for a rapid and cost-effective screening method to monitor the levels of 4EP and 4EG in wine.

MOS based e-nose (Air Sense) also has been applied for monitoring the changes in aroma profile of tomato (Pani et al. 2008) slices during air dehydration processes. Two kinds of samples (untreated and osmodehydrated in corn syrup) were studied. E-nose data analysis by means of PCA was able to characterize the process aromatic fingerprint, which could be helpful to understand and parameterize the degradative events caused by dehydration.

Lebrun et al. (2008) undertake a study to discriminate between mango fruit maturity by volatiles using a FOX 4,000 e-nose (comprising 18 metallic oxide sensors) and GC. Three different mango fruit varieties (*Mangifera indica* L.) were harvested at different maturities and at different sizes. Immediately after harvest (green) or

after 1 week of ripening at room temperature (ripe), fruit were homogenized or left intact and evaluated by the e-nose or by GC for aroma and other volatiles as well as for soluble solids and acids. Volatile data from the different harvest maturities and ripening stages were discriminated by using discriminant function analysis (DFA). Both the e-nose and GC were able, in most cases, to separate fruit from different harvest maturities (at both the green and ripe stages) as well as discriminate green from ripe fruit and fruit from the different varieties within a maturity stage.

During black tea manufacturing, tealeaves pass through a fermentation in which the grassy smell is transformed into a floral smell. Optimum fermentation is extremely crucial in deciding the final quality of finished tea and it is very important to terminate the fermentation process at the right time. (Bhattacharya et al. 2008) presented a study on real-time smell monitoring of black tea during the fermentation process using an e-nose (8 MOS sensors array) as well as prediction of the correct fermentation time. Different time-delay neural networks (TDNNs) and self-organizing map (SOM) methods for the prediction of optimum fermentation were used and both the methods appear to be suitable for the purpose. However, the combined SOM- and TDNN-based prediction algorithm proved to be the better alternative as the computational complexity is relatively less. The results showed excellent promise for the instrument to be used for the on-line prediction of optimum fermentation time by the industry.

Quantification of tea quality is a very complex problem because of the presence of innumerable compounds (Anon 2010) and their multidimensional contribution in determining the final quality of tea. Black tea that is produced at processing (Banerjee 1993) plants is tasted by expert human panels called "tea tasters," and the gradation of tea is done on the basis of marks that are given by these tasters. With tea being a widely consumed (Willson and Clifford 1992) beverage worldwide with an expanding market, tea quality (Dutta et al. 2003a) estimation is mostly commercially oriented, and region-specific customer taste and demand are kept in mind by the tasters during quality identification (Lozano et al. 2006). Furthermore, human panel tasting is highly subjective with numerous problems like inaccuracy and non repeatability and is laborious and time consuming due to various human factors like individual variability, decrease in sensitivity due to prolonged exposure, infection, and adverse mental state at times.

MOS based electronic nose has been developed for tea aroma characterization (Mahanta and Baruah 1989) at CDAC, Kolkata, India. The block diagram for the electronic nose setup is shown in Fig 4.6.

Electronic-nose-based aroma and flavor categorization (Kawakami et al. 2004) of black tea (Bhattacharyya et al. 2007) has been attempted, and promising results have been obtained. An electronic nose has the potential to eliminate problems that are associated with human panel tasting, and, if this instrument is standardized for the quality characterization of tea, it may serve as a very useful gadget for fast, reliable, noninvasive, continuous, and real-time monitoring of the aroma of finished tea (Bhuyan and Borah 2001).

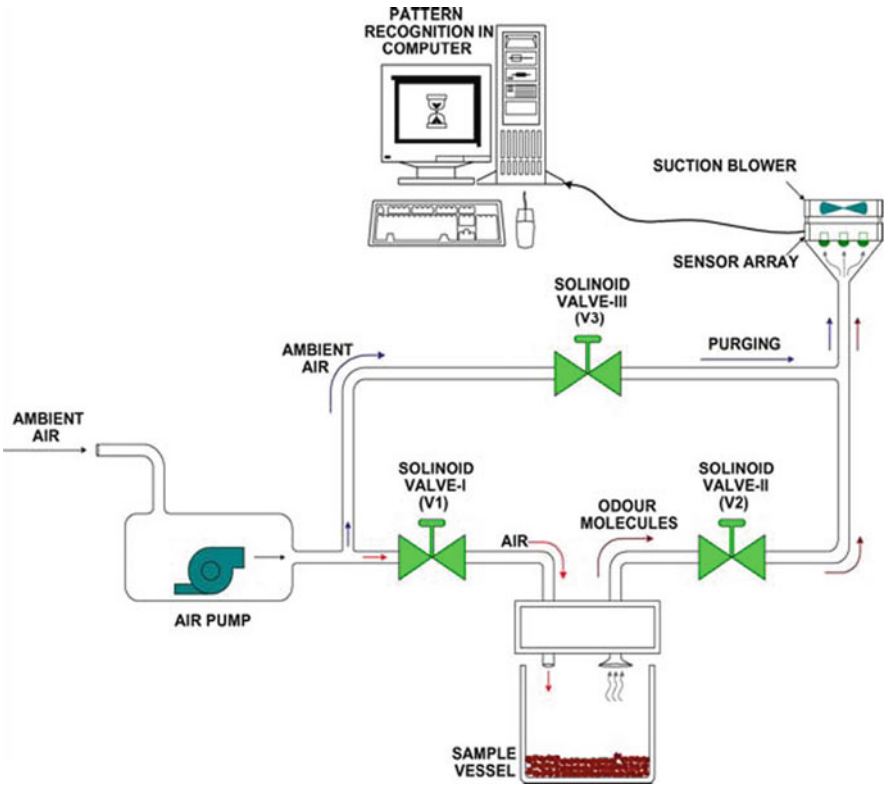

Fig. 4.6 Internal structure of electronic nose

4.1.6.2 Shelf-Life Investigation

Monitoring and controlling ripeness is a very important issue in fruit and vegetables management since it is a very important quality indicator for consumers. Many methods to monitor fruit ripeness have already been proposed but they are not useful for packing houses and most of them require the destruction of samples used for analysis. Therefore, predictions of shelf-life (Brezmes et al. 2001) ripeness state are mainly based on practical experience. In this skeleton, e-noses have proved to be promising tools for fruit ripeness assessment.

In the survey it is found that, an e-nose based on arrays of differently coated Quartz Microbalance (QMB) has been used to discriminate between volatile organic compounds (VOCs) formed during the post-harvest ripening of apples (Herrmann et al. 2002). In this study, the compounds aldehydes and esters were monitored

The performance of a QMB coated by modified metalloporphyrins and related compounds based e-nose (LibraNose) and a MS-based e-nose for tomato aroma (Berna et al. 2004) profiling was evaluated. In the first experiment, the changes in tomato aroma profiles of two different cultivars were monitored during shelf-life

(days 1, 8, 12 and 19). The score plot of PCA for the e-nose measurements showed a slight shift along the first principal component corresponding to an increasing number of days of shelf-life. However, the tomato aroma profiles measured on days 1 and 8 could not be discriminated by the e-nose.

In addition to the evaluation of fruit and vegetables ripeness states, other e-noses applications to shelf-life investigation have been performed in cheese (Benedetti et al. 2005, Riva and Mannino 2005), milk (Labreche et al. 2005) and oil samples (Cosio et al. 2007, Mildner-Szkudlarz et al. 2008).

4.1.6.3 Freshness Evaluation

Freshness is another important quality property in the food industry. Since a number of different VOCs are generated for the period of storage of foods the electronic noses have shown their budding in predicting freshness or spoilage of different food raw material and products. It also major finding in foods where volatile releases during storage due to rapid degradation by bacterial processes, such as fish (Di Natale et al. 2001, Du et al. 2002, Olafsdottir et al. 2005, Chantarachoti et al. 2006,Korel et al. 2001), oysters (Tokusoglu and Balaban 2004), shrimps, eggs (Dutta et al. 2003b), soybean curds and meats (El Barbri et al. 2008).

4.2 Electronic Tongue

The Electronic Tongue (E-Tongue) is an instrument that measures and compares tastes (Ivarsson et al. 2001b). Chemical compounds responsible for taste are perceived by human taste receptors, and sensors of electronic instruments detect the dissolved compounds. Like human receptors, each sensor has a spectrum of reactions different from the other. The information given by each sensor is complementary and the combination of all sensors results generates a unique fingerprint. Most of the detection thresholds of sensors are similar or better than those of human receptors. In the biological mechanism, taste signals are transducted by nerves in the brain into electric signals. E-tongue sensors process is similar: they generate electric signals as potentiometric variations. Taste quality perception and recognition is based on building or recognition of activated sensory nerve patterns by the brain and on the taste fingerprint of the product. This step is achieved by the e-tongue's statistical software which interprets the sensor data into taste patterns. The electronic tongue uses taste sensors to receive information from chemicals on the tongue and send it to a pattern recognition system. The result is the detection of the tastes that compose the human palate. The type of taste that is generated is divided into five categories sourness, saltiness, bitterness, sweetness, and umami (deliciousness). Sourness, which includes HCl, acetic acid, and citric acid are created by hydrogen ions. Saltiness is registered as NaCl, sweetness by sugars, bitterness, which includes chemicals such as quinine and caffeine are detected through $MgCl_2$, and umami by monosodium glumate from seaweed, disodium in meat/fish/mushrooms.

4.2.1 Tongue in Biological System

Taste buds are small structures on the upper surface of the tongue, soft palate, upper esophagus and epiglottis that provide information about the taste of food being eaten. These structures are involved in detecting the five elements of taste perception: salty, sour, bitter, sweet, and umami (or savory). Parts of the food are dissolved in saliva and come into contact with small openings in the tongue epithelium, called taste pores or taste receptors. These are located on top of the taste receptor cells that constitute the taste buds. The taste receptor cells send information detected by clusters of various receptors and ion channels to the gustatory areas of the brain via the seventh, ninth and tenth cranial nerves. Taste receptor cells, with which incoming chemicals from food and other sources interact, occur on the tongue in groups of 50–150. Each of these groups forms a taste bud, which is grouped together with other taste buds into taste papillae. The taste buds are embedded in the epithelium of the tongue and make contact with the outside environment through a taste pore. Slender processes (microvilli) extend from the outer ends of the receptor cells through the taste pore, where the processes are covered by the mucus that lines the oral cavity. At their inner ends the taste receptor cells synapse, or connect, with afferent sensory neurons, nerve cells that conduct information to the brain. Each receptor cell synapses with several afferent sensory neurons, and each afferent neuron branches to several taste papillae, where each branch makes contact with many receptor cells. The afferent sensory neurons occur in three different nerves running to the brain – the facial nerve, the glossopharyngeal nerve, and the vagus nerve. Taste receptor cells of vertebrates are continually renewed throughout the life of the organism.

The human tongue on an average has 2,000–8,000 taste buds, implying that there are hundreds of thousands of receptor cells. However, the number of taste buds varies widely. For example, per square centimetre on the tip of the tongue, some people may have only a few individual taste buds, whereas others may have more than one thousand; this variability contributes to differences in the taste sensations experienced by different people. Taste sensations produced within an individual taste bud also vary, since each taste bud typically contains receptor cells that respond to distinct chemical stimuli – as opposed to the same chemical stimulus. As a result, the sensation of different tastes (i.e., salty, sweet, sour, bitter, or umami) is diverse not only within a single taste bud but also throughout the surface of the tongue.

(i) Basic tastes

For a long period, it has been commonly accepted that there are a finite number of "basic tastes" by which all foods and tastes can be grouped. Just like with primary colors, these "basic tastes" only apply to the human perception, i.e., the different sorts of tastes the human tongue can identify. Up until the 2000s, this was considered to be a group of four basic tastes. More recently, a fifth taste, savory, has been proposed by a large number of authorities associated with this field.

(a) Bitterness: It is the most sensitive of the tastes, and is perceived by many to be unpleasant, sharp, or disagreeable. Common bitter foods and beverages

include coffee, unsweetened cocoa, South American "mate", marmalade, bitter melon, beer, bitters, olives, citrus peel, many plants in the Brassicaceae family, dandelion greens and escarole. Quinine is also known for its bitter taste and is found in tonic water.

(b) Saltiness: Saltiness is a taste produced primarily by the presence of sodium ions. Other ions of the alkali metals group also taste salty, however the further from sodium the less salty is the sensation. The size of lithium and potassium ions most closely resembles those of sodium and thus the saltiness is most similar. In contrast rubidium and cesium ions are far larger so their salty taste differs accordingly.

(c) Sourness: Sourness is the taste that detects acidity. The mechanism for detecting sour taste is similar to that which detects salt taste. Hydrogen ion channels detect the concentration of hydronium ions that are formed from acids and water. The most common food group that contains naturally sour foods is the fruit, with examples such as the lemon, grape, orange, and sometimes the melon. Wine also usually has a sour tinge to its flavor. If not kept correctly, milk can spoil and contain a sour taste.

(d) Sweetness: Sweetness, usually regarded as a pleasurable sensation, is produced by the presence of sugars, some proteins and a few other substances. Sweetness is often connected to aldehydes and ketones, which contain a carbonyl group. Sweetness is detected by a variety of G protein coupled receptors coupled to the G protein gustducin found on the taste buds. At least two different variants of the "sweetness receptors" need to be activated for the brain to register sweetness. The compounds which the brain senses as sweet are thus compounds that can bind with varying bond strength to two different sweetness receptors.

(e) Umami: Umami, popularly referred to as savoriness, has been proposed as one of the basic tastes sensed by specialized receptor cells present on the human and animal tongue. Umami is a loanword from Japanese meaning roughly "tasty", although "brothy", "meaty", or "savory" have been proposed as alternative translations.

4.2.2 Concept of Electronic Tongue (E-Tongue)

Mechanism involved for taste recognition in human and electronic tongue shows the same three levels: the receptor level [taste buds in humans, lipid membrane or novel metal sensors in the electronic tongues], the circuit level [neural transmission in humans, transducers in the electronic tongues], the perceptual level [cognition in the thalamus in humans, statistical analysis by software in the electronic tongues].

(i) Receptor level

At the receptor level, to detect dissolved organic and inorganic compounds the sensor-probe assembly is used by the electronic tongue. Each probe shows cross-sensitivity and selectivity so that each sensor could concurrently

contribute to the detection of most substances found in the liquid matrix. These sensors are composed of an organic coating sensitive to the species to analyze in the samples and a transducer that allows converting the response of the membrane into signals that will be analyzed

(ii) Circuit level

At the circuit level, the sample is quantified, digitized and results are recorded. Electroanalyical methods can be used for measuring the result, which use both active and passive to study an analyte through the observation of potential and/or current. Potentiometry measures the potential of a solution between two electrodes passively, affecting the solution very little in the process. Voltammetry applies a constant and/or varying potential at an electrode surface and measures the resulting current with a three-electrode system. Coulometry uses applied current or potential to completely convert an analyte from one oxidation state to another. In this experiment the total current passed is measured directly or indirectly to determine the number of electron passed

(iii) Perceptual level

At the perceptual level, perception is done in the computer with the using of an electronic tongue system. Depending upon the application for which it is applied, the data analysis can produce a variety of information. Exploratory data analysis can be performed using different statistical methods such that PCA (Shlens 2009), LDA (Balakrishnama and Ganapathiraju 2009) etc. on the data set, to correlate collected data.

4.2.3 Application of Electronic Tongue

At CDAC Kolkata, electronic tongue (E-Tongue) for determining the briskness/strength of the black tea liquor (Ivarsson et al. 2001a) has been developed. The major quality attributes which determines the qualities of black tea are briskness/strength, flavour, aroma and colour. Human experts called "tea taster" usually evaluate tea quality, and conventionally assign scores on a scale of 1–10, depending on the major quality attributes of the tea sample. A virtual instrumentation based E-Tongue has been developed using voltammetry (Parra et al. 2006) technique for correlating the briskness/strength of tea liquor with the "tea taster" mark. In this work an array of selected electrodes were immersed into black tea liquor-samples for analyzing the tea samples and computational model has been developed to correlate the measurements with the tea taster's briskness/strength scores. With unknown tea samples, encouraging results have been obtained with more than 90% classification rate. The block diagram of developed electronic tongue is shown in Fig. 4.7 and laboratory prototype is presented in Fig. 4.8.

In addition an electronic tongue has a potential to classify three kinds of grape wine. Hong et al. (2008) shows that test recognition rate has reached 100% in the experiment of grape wine recognition.

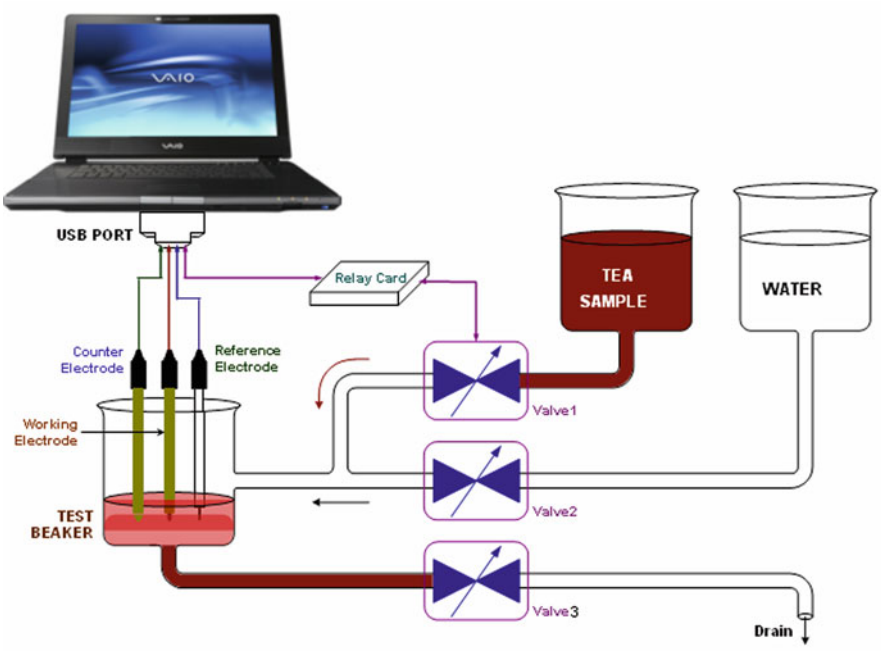

Fig. 4.7 Internal structure of electronic tongue

In the survey, it is found that, an electronic tongue developed based on nano structured films and impedance spectroscopy have been successful in detecting trace amounts of impurities in water and distinguishing similar complex liquids, such as different wines and coffees (Ferreira et al. 2007).

Robertsson et al. (2004) shows the problem of extracting the important information from a complex response from an electronic tongue sensor. A wavelet transform is used in this approach and the approximation coefficients are extracted as features and classified using a minimum distance classifier (MDC). Two experimental setups have been performed; water and milk, and the bacteriological growth are monitored.

For ageing testing electronic tongue has been helped and quality can be improved with the help of electronic tongue (Robertsson and Wide 2005) shows overall identification of different stages in the ageing process of baby food product.

(a) Commercial availability of E-Nose and E-Tongue

Nowadays instrument has been developed called as Electronic nose, for classification of odours in different application area such as food processing, shelf-life investigation, food freshness evaluation, and food authenticity assessment and food quality control studies. Some manufacturers call their devices "electronic nose", whereas others avoid mentioning this term eve if there product operates in a similar way. The following electronic noses are available in market.

Fig. 4.8 Laboratory prototype of electronic tongue at C-DAC, Kolkata, India

- FOX 2,000, 3,000, 4,000
- PEN 3
- GDA 2
- i-PEN
- Gemini
- Cybernose
- ZNose 4,200, 4,300, 7,100
- Astree
- Smart Nose 2,000
- LibraNose 2.1
- Artinose

(b) Commercially available Electronic Tongue:

- Mobile static version
- Astree.

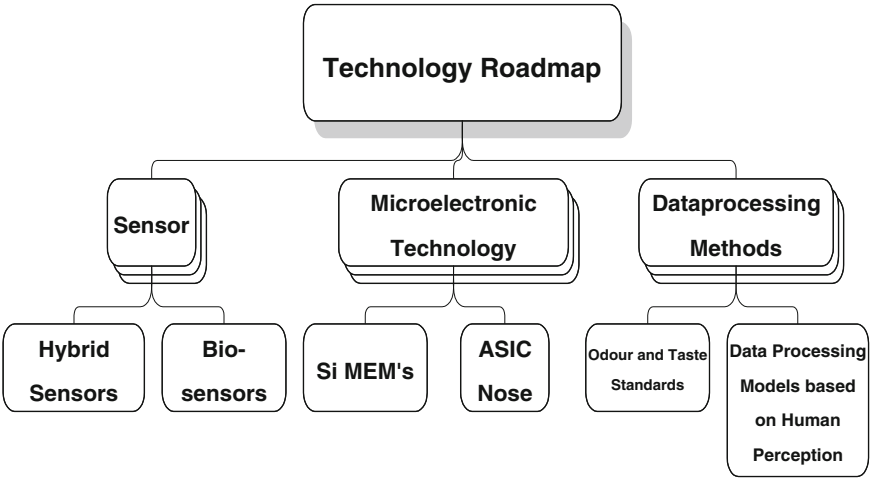

Fig. 4.9 Technological roadmap of electronic nose and tongue

4.3 Future Trends

Future technological roadmap is shown in Fig. 4.9. The developmental trend will continue for the next decade also. This period should see the transfer of some of the current research efforts of universities and R&D organizations into new commercially deployed applications. Advances in other related fields of technology would also logically influence electronic nose technology in terms of improvement of sensors, microelectronics and data processing techniques as reviewed below.

4.3.1 Sensor Technology

- Development of hybrid sensors.
- Development of Bio-sensors, Nano-sensors and Nano-bio sensors
- More intelligent sensor structure design for eliminating effects of temperature and humidity.

4.3.2 Microelctronic Technology

- Silicon micromachining techniques for sensor arrays.
- Development of miniaturized sensor array by micromachining techniques for less power consumption.Application Specific Integrated Circuits (ASIC) for electronic nose.
- Integration of sensor and electronic circuitry on same chip.
- Development of mass production facility for microelectronics required for electronic nose.

4.3.3 Data Processing Methods

- Establishment of odour and taste standards and odour data-sets.
- Development of new dynamic methods using transitory sensor signals and adaptive filters close to human perception
- Customization efforts for newer applications.

References

Anon (2010) www.tocklai.net

Balakrishnama S, Ganapathiraju A (2009) Linear discriminant analysis: a brief tutorial. http://www.zemris.fer.hr/predmeti/kdisc/bojana/Tutorial-LDA-Balakrishnama.pdf

Banerjee B (1993) Tea production and processing. Oxford & IBH, New Delhi, India

Benedetti S, Sinelli N, Buratti S et al (2005) Shelf life of crescenza cheese as measured by electronic nose. J Dairy Sci 88:3044

Berna AZ, Lammertyn J, Saevels S et al (2004) Electronic nose systems to study shelf life and cultivar effect on tomato aroma profile. Sens Actuators B Chem 97:324

Bhattacharyya N, Bandyopadhyay R, Bhuyan M et al (2005) Correlation of multi-sensor array data with "tasters" panel evaluation for objective assessment of black tea flavour. In: Proceedings of ISOEN, Barcelona, Spain

Bhattacharyya N, Seth S, Tudu B et al (2007) Detection of optimum fermentation time for black tea manufacturing using electronic nose. Sens Actuators B Chem 122:627–634

Bhattacharya N, Tudu B, Jana A et al (2008) Preemptive Identification of Optimum Fermentation Time for Black Tea Using Electronic Nose. Sens Actuators B Chem 131:110–116

Bhuyan M, Borah S (2001) Use of electronic nose in tea industry. In: Proceedings of EAIT, IIT Kharagpur, India, pp 848–853

Boothe DDH, Arnold JW (2002) Electronic nose analysis of volatile compounds from poultry meat samples, fresh and after refrigerated storage. J Sci Food Agric 82:315–322

Brezmes J, Llobet E, Vilanova X et al (2001) Correlation between electronic nose signals and fruit quality indicators on shelf-life measurements with pinklady apples. Sens Actuators B Chem 80:41

Chantarachoti J, Oliveira ACM, Himelbloom BH (2006) Portable electronic nose for detection of spoiling Alaska pink salmon (*Oncorhynchus gorbuscha*). J Food Sci 71:S414

Cosio MS, Ballabio D, Benedetti S et al (2007) Evaluation of different storage conditions of extra virgin olive oils with an innovative recognition tool built by means of electronic nose and electronic tongue. Food Chem 101:485

Cynkar W, Cozzolino D, Dambergs B et al (2007) Feasibility study on the use of a head space mass spectrometry electronic nose (MS e-nose) to monitor red wine spoilage induced by *Brettanomyces yeast*. Sens Actuators B Chem 124:167

Di Natale C, Olafsdottir G, Einarsson S et al (2001) Comparison and integration of different electronic noses for freshness evaluation of cod-fish fillets. Sens Actuators B Chem 77:572

Distante C, Leo M, Siciliano P et al (2002) On the study of feature extraction methods for an electronic nose. Sens Actuators B Chem 87:274–288

Du WX, Lin CM, Huang T et al (2002) Potential application of the electronic nose for quality assessment of salmon fillets under various storage conditions. J Food Sci 67:307

Dutta R, Hines EL, Gardner JW et al (2003a) Tea quality prediction using a tin oxide-based electronic nose: an artificial intelligence approach. Sens Actuators B Chem 94:228–237

Dutta R, Hines EL, Gardner JW (2003b) Non-destructive egg freshness determination: an electronic nose based approach. Meas Sci Technol 14:190

El Barbri N, Llobet E, El Bari N et al (2008) Electronic nose based on metal oxide semiconductor sensors as an alternative technique for the spoilage classification of red meat. Sensors 8:142

Ferreira EJ, Pereira RCT, Mattoso LHC et al (2007) Random subspace method for analysing coffee with electronic tongue. EMBRAPA Instrumentacao Agropecuaria Sao Carlos. Electron Lett 43:1138–1139

García M, Aleixandre M, Horrillo MC (2005) Electronic nose for the identification of spoiled Iberian hams. Spanish on Conference Electron Devices, Tarragona, pp 537–540

Gutierrez-Osuna R (2002) Pattern analysis for machine olfaction: a review. IEEE Sen J 2: 189–202

Haykin S (2001) Neural networks: a comprehensive foundation, 2nd ed. Pearson Education Asia, Hong Kong

Herrmann U, Jonischkeit T, Bargon J et al (2002) Monitoring apple flavor by use of quartz microbalances. Anal Bioanal Chem 372:611

Hong M, Weiguang W, Zongnian G et al (2008) Application of neural networks to identify wine based on electronic tongue. In: Computational Intelligence and Industrial Application (PACIIA) 1:896–900

Ivarsson P, Holmin S, Krantz-Rülcker C et al (2001a) Discrimination of tea by means of a voltammetric electronic tongue and different applied waveforms. Sens Actuators B Chem 76:449–454

Ivarsson P, Kikkawa Y, Winquist F et al (2001b) Comparison of a voltammetric electronic tongue and a lipid membrane taste sensor. Anal Chim Acta 449:59–68

Kawakami M, Sarma S, Himizu K et al (2004) Aroma characteristics of Darjeeling tea. In: Proceedings of International Conference O-CHA (Tea) Culture Science, Shizuoka, Japan, pp 110–116

Kermani BG, Schiffman SS, Nagle HT (2005) Performance of the levenbermarquardt neural network training method in electronic nose applications. Sens Actuators B Chem 110:13–22

Korel F, Luzuriaga DA, Balaban MÖ (2001) Objective quality assessment of raw tilapia (*Oreochromis niloticus*) fillets using electronic nose and machine vision. J Food Sci 66:1018

Labreche S, Bazzo S, Cade S et al (2005) Shelf life determination by electronic nose: application to milk. Sens Actuators B Chem 106:199

Lebrun M, Plotto A, Goodner K et al (2008) Discrimination of mango fruit maturity by volatiles using the electronic nose and gas chromatography. Postharvest Biol Technol 48:122

Lozano J, Santos JP, Aleixandre M et al (2006) Identification of typical wine aromas by means of an electronic nose. IEEE Sens J 6:173–178

Mahanta PK, Baruah S (1989) Relationship between process of withering and aroma characteristics of black tea. J Sci Food Agric 46:461–468

Marilley L, Ampuero S, Zesiger T et al (2004) Screening of aroma-producing lactic acid bacteria with an electronic nose. Int Dairy J 14:849

Mildner-Szkudlarz S, Jeleń HH, Zawirska-Wojtasiak R (2008) The use of electronic and human nose for monitoring rapeseed oil autoxidation. Eur J Technol 110:61

Olafsdottir G, Chanie E, Westad F et al (2005) Prediction of microbial and sensory quality of cold smoked Atlantic salmon by electronic nose. J Food Sci 70:S563

O'Connell M, Valdora G, Peltzer G et al (2001) A practical approach for fish freshness determinations using a portable electronic nose. Sens Actuators B Chem 80:149–154

Pan SY, Hsieh BZ, Lu MT et al (2008) Identification of stratigraphic formation interfaces using wavelet and fourier transforms. Comput Geosci 34:77–92

Pani P, Leva AA, Riva M et al (2008) Influence of an osmotic pre-treatment on structure-property relationships of air-dehydrated tomato slices. J Food Eng 86:105

Parra V, Arrieta AA, Fernández-Escudero JA et al (2006) E-tongue based on a hybrid array of voltammetric sensors based on phthalocyanines, perylene derivatives and conducting polymers: discrimination capability towards red wines elaborated with different varieties of grapes. Sens Actuators B Chem 115:54–61

Pearce TC, Schiffman SS, Nagle HT et al (2002) Handbook of machine olfaction. Wiley-VCH, Weinheim

Pinheiro C, Rodrigues CM, Schäfer T et al (2002) Monitoring the aroma production during wine-must fermentation with an electronic nose. Biotechnol Bioeng 77:632

Poggio T, Girosi F (1990) Networks for approximation and learning. Proc IEEE 78:1481–1497

Riva M, Mannino S (2005) Shelf-life monitoring and modeling by e-nose and image-analysis. Italian Food Beverage Technol 42:11

Robertsson L, Wide P (2004) Analyzing bacteriological growth using wavelet transform. In: Instrumentation and Measurement Technology Conference (IMTC), Como, Italy 2:854–859

Robertsson L, Wide P (2005) Improving food quality analysis using a wavelet method for feature extraction. In: Instrumentation and Measurement Technology Conference (IMTC), Ottawa, ON 1:93–97

Shaffer RE, McGill RA, Rose-Pehrsson SL (1998) Probabilistic neural networks for chemical sensor array pattern recognition: comparison studies, improvements, and automated outlier detection. Naval Research Labarotary, Washington, DC, NRL Formal Report 6110-97-9879

Shlens JA (2009) Tutorial on principal component analysis. http://www.snl.salk.edu/~shlens/pub/notes/pca.pdf

Tokusoglu O, Balaban M (2004) Correlation of odor and color profiles of oysters (*Crassostrea virginica*) with electronic nose and color machine vision. J Shellfish Res 23:143

Wall ME, Rechtsteiner A, Rocha LM (2003) Singular value decomposition and principal component analysis. In: Berrar DP, Dubitzky W, Granzow M (ed) A practical approach to microarray data analysis. Kluwer, Norwell, MA, pp 91–109

Wickremasinghe R, Ekanayake LA, Rajasingham CC et al (1979) Changes in polyphenols, amino acids and volatile compounds during fermentation and firing in orthodox processing of tea. J Nat Sci Council Sri Lanka 7:5–9

Willson KC, Clifford MN (1992) Tea: cultivation to consumption. Chapman & Hall, London

Chapter 5
Radiography, CT and MRI

Nachiket Kotwaliwale, Abhimannyu Kalne, and Karan Singh

Quality control is an important aspect of food production and processing for providing foods of acceptable nutritional value, and safety of products. Several characteristics such as size, shape, density, maturity, moisture content, oil content, flavor, firmness, tenderness, color, defects, blemishes, etc., are routinely used in the quality control of agricultural and biological food products. Until recently, most analytical techniques used in quality control required isolation of the food component of interest. The original properties of the product are, therefore, destroyed during sample preparation and analysis. Oftentimes, such analyses are expensive, time consuming, and require sophisticated instrumentation, and hence are not suited for "on-line" quality control of food products. Recent progress in the development of instrumentation utilizing the some physical, optical, acoustic and electromagnetic properties of food products has provided several nondestructive techniques for quality evaluation. Many such methods are highly sensitive, rapid, and reproducible, and have been successively used in routine "on-line" quality control of a large number of samples.

Quality evaluation is important for establishing price at various stages in marketing. Size, weight vis-à-vis density, product color vis-à-vis appearance, physical and pathological damage are the major factors influencing quality. These factors mainly depend on variety, environmental conditions during growth, processing, packaging and storage practices. Quality of a food product depends on many properties, such as, physical, mechanical, optical, electrical, magnetic, electro-magnetic, etc. The non-destructive part, generally carried out by the producer/grower or the first buyer, includes separation of material based on size and specific gravity. Rotary or oscillatory sieves with or without aeration will separate larger and/or smaller material from the desired size. Aeration helps by blowing away the lighter impurities of the crop. It is therefore a common practice to draw a small weighed sample from the crop lot, break each grain/fruit/nut and inspect it manually. Typically a sample of 0.1% of the saleable load is recommended. The method is time consuming and

N. Kotwaliwale (✉)
Central Institute of Agricultural Engineering, Nabibagh, Bhopal 462038, India
e-mail: nachiket@ciae.res.in

S.N. Jha (ed.), *Nondestructive Evaluation of Food Quality*,
DOI 10.1007/978-3-642-15796-7_5,

labor intensive; therefore it is a common practice to draw a samples even smaller than 0.1% of the traded lot. Such a small sample may not be a true representative of the lot. Taking a larger sample for destructive quality determination is also not possible from the seller's point of view, because this causes loss of saleable quantity. Sometimes destructive method becomes more subjective and quality of same crop can be assessed differently at different points of sale. Moreover, trained taste panels are expensive, slow and in most cases only reliable when the product has reached the eating stage. Further, quality determination through trained taste panel and some other methods of quality determination require cutting, crushing, breaking, thus damaging the tested commodity and therefore, quality of a lot can only be judged based on the drawn sample. Last century witnessed development of many types of equipment to separate agricultural commodity based on one or combination of similar (mostly physical) properties. Though effective, use of these equipments requires multiple handlings to determine overall grade of the commodity. Using multiple sensors, all the grade parameters of a commodity can be determined on one platform and then separation can be effected based on overall quality. The computer-controlled devices can also be flexible enough to accommodate similar or altogether different commodities.

X-ray imaging or radiography is one of the most successful techniques for non-destructive determination of internal quality. Radiography of agricultural materials for quality determination is an upcoming field showing promising results for some nuts, fruits, and grains. X-rays, because of their high energy, can penetrate through many objects. However there are differences in penetration through different materials due to the differences in the material properties. Photons in an X-ray beam, when pass through a body, are either transmitted, scattered or absorbed. Radiography intends to capture the difference in transmitted X-ray beam, due to material difference, in form of a visual contrast in the image. This contrast can be a measure of spatial and quantitative distribution of a certain material(s) within a composite of materials. The radiography technique can not only determine the extent of internal damage but can also estimate volume of different internal features. Besides two-dimensional radiography, used in medicine, and linescan radiography, applied on grading machines, X-ray computed tomography (CT) is another powerful technique from a research point of view. It is a proven method for evaluating a cross-section of an object using a movable X-ray source and detector assembly to accumulate data from a thin projected slice of sample. One of the major problems associated with use of X-rays is that high-energy electromagnetic radiations, like X-rays, can ionize and kill biological cells. It is therefore mandatory to provide a shield between the radiation source and people working in the vicinity. Equipment designed for radiography, therefore, needs to fulfill functional as well as radiation safety requirements. Magnetic Resonance Imaging (MRI) is another non-invasive technique that allows detecting and follow-up the development of storage disorders over time. MRI employs static magnetic fields and radio frequencies in order to obtain images of proton (^{1}H) mobility in biological systems. The signal comes from water or fat present in the sample. The intensity of this signal depends on the dynamic characteristics of the aqueous protons, which are modeled by three parameters: the proton density (NH), the spin-lattice relaxation time T_1 and the spin–spin relaxation

time T_2. Two instrumental parameters also determine the signal amplitude: the echo time (TE), between the initial 90° excitation pulse and the observation of the echo signal, and the repetition time TR, between each of the successive excitations needed to acquire the image. Nuclear magnetic resonance is sensitive to the existence of mobile water, oil and sugar, which are major components of agricultural materials therefore it has a high potential for use in various internal quality factors, such as bruises, dry regions, worm damage, stage of maturity, and presence of voids, seeds and pits (Chen et al. 1989, McCarthy 1994).

Radiography, CT and MRI techniques give an output in form of images and decision making has been, historically, with human intervention. Experts, knowing the anatomy of the object of interest could make decision about the internal quality, i.e. presence and physical dimensions of any abnormality, foreign object etc. With advent of computers, the digital image processing technique has evolved which not only allows safe storage of images but quick retrieval, enhancement of features, comparison and use of many mathematical and/or stochastic tools for decision support. In fact the techniques of CT and MRI are possible just because of very strong computational powers of modern computers. The images generated in radiography, CT and MRI are monochromatic and do not represent the optical properties of the features. It is therefore necessary to correlate different feature attributes to grayness and bunch size of different pixels or pixel bunches (2-D image) or voxels (3-D image).

This chapter gives description of history, development, theory, equipment and many related aspects about X-ray imaging (Radiography), Computed Tomography (CT) and Magnetic Resonance Imaging (MRI). To explain the theory and applications, many figures, images have been included, some of which are downloaded from internet. The information has been downloaded from the internet over a long period of time and from the sources which are no longer active, hence their sources are not provided. It is expected that with time to come, noninvasive techniques like radiography, CT and MRI would be used extensively for quality detection and referencing services for agricultural commodities. Online sorting based on digital radiography is also likely to get place in agricultural pack-houses, especially for high priced and export commodities. This chapter is intended for academicians, researchers, students and entrepreneurs embarking into the exciting field of 'INSIGHT'.

5.1 Radiography

X-ray radiation was discovered by Wilhelm Conrad Röntgen in 1895. He found that X-rays are generated by bombarding electrons on a metallic anode. Figure 5.1 shows radiograph which is believed to be the first known radiograph.

X-rays are produced when a fast moving electron, emanated from a heated cathode, impinges on a heavy metal anode. There are generally two types of X-ray emission (Fig. 5.2); (i) Bremstrahlung – A free electron is attracted to the nucleus, to conserve momentum, a photon is created with an energy dependent upon change

Fig. 5.1 Presumably first radiograph

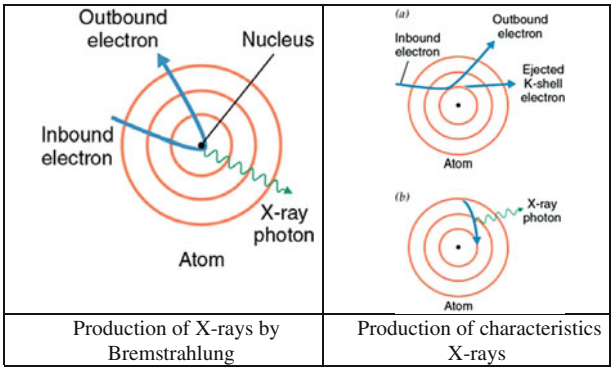

Fig. 5.2 Production of X-rays

in electron's trajectory; (ii) K-shell or characteristic X-rays – electron from cathode dislodge orbital electrons in the target material and produce excited atoms which is stabilized by X ray emission.

Generally less than 1% of the energy received by the anode is converted into X-rays. The X-rays, emitted from the focal spot travel in a conical beam shape through a window in the X-ray tube. Efficiency, quantity, quality and energy of produced X-rays generally depend upon the anode material. A material with higher atomic number will produce more X-rays. X-rays (or Röntgen rays) are a form of electromagnetic radiation with a wavelength in the range of 10–0.01 nm, corresponding to frequencies in the range 30–30,000 PHz (1 PHz = 1E15 Hz).

X-ray imaging techniques have mainly been developed for medical, particle and material physics. With this in mind, the use of X-ray imaging techniques in the agricultural and food industries has not been exploited to its fullest potential. As a sub-surface technique, X-ray radiation can give three-dimensional information about the spatial density differences and changes of the atomic number within a sample (Zwiggelaar et al. 1996).

5.1.1 Properties of X-Ray

Short electromagnetic waves, such as X-rays, behave like particles as well as waves while interacting with matter. These particles are discrete bundles of energy and are called photons or quantum. If a photon has 15 eV or more energy, it is capable of ionizing atoms and molecules, and it is called "ionizing radiation". An atom is ionized when it loses an electron. Short electromagnetic waves, such as X-rays, interact with matter as if they were particles rather than waves. Energy of a photon is given by $E = h\nu$, where h is Plank's constant (4.13×10^{-18} keV·s or 6.62×10^{-34} J·s), and ν is frequency of photon wave ($\nu = \frac{c}{\lambda}$, where c is speed of light 3×10^{8} ms^{-1}, and λ is wavelength). Rearranging and substituting values of h and c we get $E = \frac{12.4}{\lambda}$.

5.1.2 Attenuation Coefficient

The photons in a soft X-ray beam, when passed through an object, are either transmitted, scattered (Compton scattering) or absorbed (photoelectric collision). As a result, the energy of incident photons reduces exponentially (Curry et al. 1990) and is given by

$$I = I_0 e^{-\mu_m z \rho} \tag{5.1}$$

Where, I is the energy of photons exiting through a body in keV; μ_m is mass attenuation coefficient in mm^2 g^{-1}; ρ is material density in g mm^{-3}; and z is thickness in mm through which the X-rays pass. The mass attenuation coefficient for a material is a function of the atomic number of the absorbing material and incident photon energy. The exiting photon energy depends on material properties, including thickness. If the absorbing material consists of more than one element, the mass attenuation coefficient of the composite material will be a function of mass attenuation coefficients of individual elements and their mass fraction in the path of the photon beam (Hubbell and Seltzer 1995). Radiography intends to capture the difference in transmitted X-ray photons, due to material difference in the form of a visual contrast in the image. Attenuation coefficient of a material changes with thickness when measured under polychromatic X-rays (Paiva et al. 1998, Kotwaliwale et al. 2006). Buzzell and Pintauro (2003) defined 'R-value' for a material as the ratio of

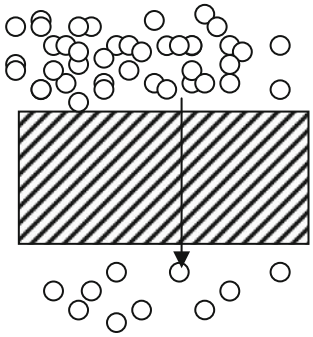

Fig. 5.3 Energy and number of photons attenuate as they pass through a matter

the attenuation coefficient at low-energy level to that at high-energy level. Figure 5.3 represents attenuation of X-ray beam when passing through a material.

5.1.3 Components Used in X-Ray Imaging

In any type of X-ray imaging, there are four basic elements: (i) X-ray source; (ii) X-ray converter; (iii) imaging medium and (iv) casing for imaging medium. The X-ray converter, e.g. phosphor screen, stops X-rays from reaching the imaging medium and produces a visible output proportional to the incident X-ray photons. The imaging medium, e.g. photographic medium captures the image while the casing protects the imaging medium from surrounding visible radiations.

X-ray Tube: Radioactive substances and X-ray tubes are the two sources of X-rays. In X-ray tubes, X-rays are generated by interactions between the energetic electrons and atoms of the target. Bombardment must take place in a vacuum to prevent ionization of air. The X-ray source is one of the most important system components in determining the overall image quality. Whereas, the radioactive substances may generate monochromatic X-rays (almost all the photons having same energy level), X-ray tubes generate polychromatic beam. The literature shows that X-ray tubes of different types have been used as X-ray sources in radiography of agricultural produce. The variations in tubes are in the maximum tube voltage, current, focal spot size, window material, electrode material, tube cooling system etc. Major parts of an X-ray tube (Fig. 5.4) are: evacuated envelop (special glass or metal tube), heated tungsten filament or cathode, anode, tungsten target attached to the anode, electron focusing cup and high voltage power supply.

Imaging medium: Historically, X-ray imaging has been done on photographic plates or films. In general, the acquisition of X-ray images can be either film-based or digital. In film-based X-ray imaging, which is similar to that of conventional photography, the X-ray is transmitted through the inspected object and a sensing film is exposed to form the object image. After developing the film, an X-ray image with high resolution can be obtained. Digital images by scanning of film radiographs have been reported by many researchers. This technique helped in performing digital

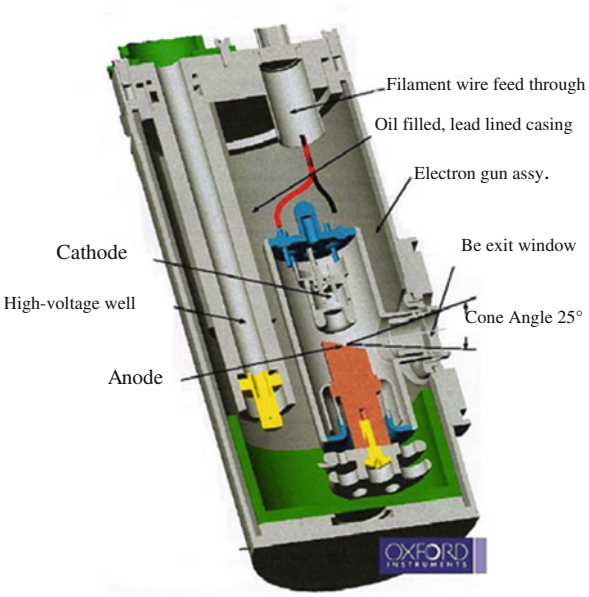

Fig. 5.4 Cut-away view of the X-ray tube (Courtesy: Oxford Instruments, USA)

image processing and electronic storage of radiographs. Different resolutions and bit depths have been reported for different products.

Photographic plate: The detection of X-rays is based on various methods. The most commonly known methods are a photographic plate, X-ray film in a cassette, and rare earth screens. In earlier periods a photographic plate was used to produce radiographic images. The images were produced right on the glass plates. Film replaced these plates. Since photographic plates are sensitive to X-rays, they provide a means of recording the image, but require a lot of exposure (to the patient), so intensifying screens were devised. They allow a lower dose to the patient, because the screens take the X-ray information and intensify it so that it can be recorded on film positioned next to the intensifying screen. The object to be radiographed is placed between the X-ray source and the image receptor to produce a shadow of the internal structure of that particular body. X-rays are partially blocked ("attenuated") by dense tissues, and pass more easily through soft tissues. Areas where the X-rays strike darkens when developed, causing bones to appear lighter than the surrounding soft tissue.

Photostimulable phosphors (PSPs): An increasingly common method is the use of photostimulated luminescence (PSL) wherein photostimulable phosphor plate (PSP plate) is used in place of the photographic plate. After the plate is X-rayed, excited electrons in the phosphor material remain "trapped" in "colour centres" in the crystal lattice until stimulated by a laser beam passed over the plate surface. The light given off during laser stimulation is collected by a photomultiplier tube and the resulting signal is converted into a digital image by computer technology, which gives this process its common name, computed radiography (also referred to

as digital radiography). The PSP plate can be reused, and existing X-ray equipment requires no modification to use them.

Scintillators: Some materials such as sodium iodide (NaI) can "convert" an X-ray photon to a visible photon; an electronic detector can be built by adding a photomultiplier. These detectors are called "scintillators", filmscreens or "scintillation counters". The main advantage of using these is that an adequate image can be obtained while subjecting the patient to a much lower dose of X-rays.

Direct semiconductor detectors: Since the 1970s, new semiconductor detectors have been developed (silicon or germanium doped with lithium, Si(Li) or Ge(Li)). X-ray photons are converted to electron-hole pairs in the semiconductor and are collected to detect the X-rays. When the temperature is low enough, it is possible to directly determine the X-ray energy spectrum; this method is called energy dispersive X-ray spectroscopy (EDX or EDS); it is often used in small X-ray fluorescence spectrometers. These detectors are sometimes called "solid state detectors". Detectors based on cadmium telluride (CdTe) and its alloy with zinc, cadmium zinc telluride, have an increased sensitivity, which allows lower doses of X-rays to be used.

Scintillator plus semiconductor detectors (indirect detection): With the advent of large semiconductor array detectors it has become possible to design detector systems using a scintillator screen to convert from X-rays to visible light which is then converted to electrical signals in an array detector. Indirect Flat Panel Detectors (FPDs) are in widespread use today in medical, dental, veterinary and industrial applications.

X-ray Camera: Using digital X-ray scanning sensors, digitized X-ray images can be acquired and analyzed in real time since this allows for online inspection of materials, the applications of digital X-ray imaging in industries have increased significantly in recent years. Two types of digital cameras are typically used; line-scan cameras and 2-D camera. In a line scan cameras, relative movement of sample and camera is required to acquire a digital radiograph. Two types of arrangements exist for 2-D radiography; a digital plate comprising of X-ray converter, CCD or CMOS array and casing replaces the conventional 'film cassette' this plate is then read through a image reader, alternatively, digital X-ray cameras giving instantaneous or 'on-line' read-out are also available. X-ray digital camera typically has a two-dimensional photodiode array or CMOS having pixels spaced apart in a sensing area. A scintillator screen, placed in direct contact with the photodiode array, converts incident X-ray photons to light, which in turn is detected by the photodiodes. A graphite window shields against ambient light and protects the sensitive electronics from accidental damage (Fig. 5.5).

The analog signal from the photodiode sensor is digitized. Resolution of digitization, number of A/D channels, dynamic range (defined as the maximum signal divided by the read noise), type of frame grabber required, frame rate are some of the variable features that decide quality of the camera (Kotwaliwale et al. 2007a).

Shield: X-rays in the range of 10–50 keV are about 10,000 times more energetic than visible light. Due to its high energy content, the photons can penetrate almost all materials. These electromagnetic radiations also have ionization properties that

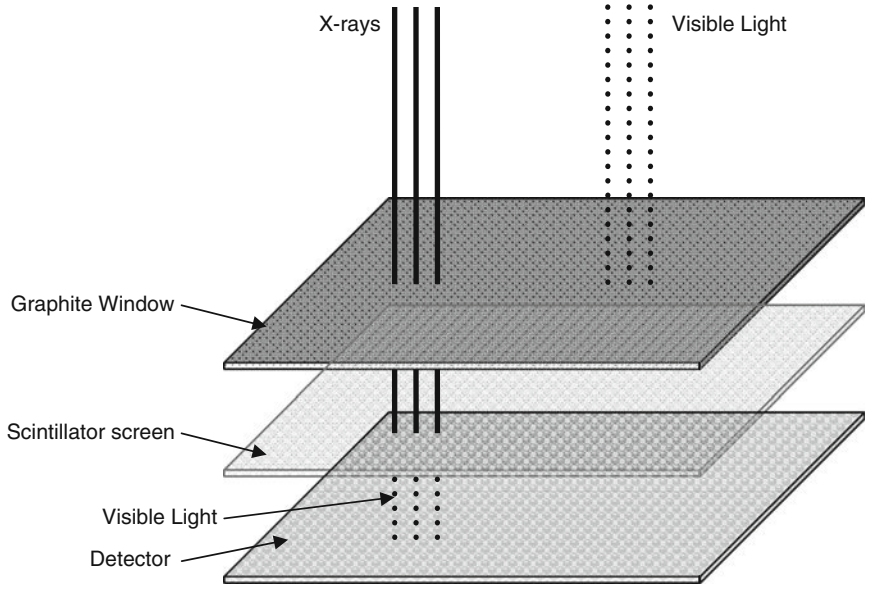

Fig. 5.5 Layout of detector and screen

can kill biological cells and hence a proper shielding is required while dealing with X-rays.

Maximum dose gets generated when the X-ray tube operates on its peak voltage and current. In thicker shields, a phenomenon of buildup from scattering must be accounted for. The thicker and taller is the shield, the larger the build up of scatter component. Also, the energy of the source affects the contribution of the scatter factor to the exposure range. For primary X-rays, the buildup due to shielding transmission is given as:

$$B_x = 1.67 \times 10^{-5} \frac{Hd^2}{DT} \tag{5.2}$$

where, B_x = shielding transmission, H = maximum permissible dose equivalent (mrem/h), d = distance between X-ray source and reference point (m), D = absolute dose index rate (rad m^2/min), and T = area occupancy factor.

The effect of material thickness on the penetration of neutrons as a modified form of Eqn. 5.1 is given as:

$$I(z) = BI_0 e^{-\sum_t z} \tag{5.3}$$

where $\sum_t$ is the macroscopic total cross section for neutrons, and B is build-up factor. The build-up factor could be expressed in a form of $B(\mu \cdot z) = 1 + \mu \cdot z$ and thus:

$$I(z) = (1 + \mu z) I_0 e^{-\sum_t z} \tag{5.4}$$

Approximating $\sum_t$ by μ for X-rays we get

$$I(z) = (1 + \mu z) I_0 e^{-\mu \cdot z} \tag{5.5}$$

This equation could be solved for z to get the thickness of shield required to reduce radiation dose by a desired factor.

Shield thickness to protect against this dose is determined using two approaches. A safe reduction of photon energy through shielding is considered as one million times reduction, i.e., $\frac{I}{I_0} = 10^{-6}$:

Approach I – Incorporating buildup due to shield, thus Eqn. 5.1 becomes

$$I = I_0 (1 + B_x) e^{-\mu_m z \rho} \tag{5.6}$$

A conservative estimate of B_x is 1.148×10^{-9} calculated at a distance of 0.25 m away from source of 3 MeV, 2 mA, 1 cm diameter electron beam and area occupancy factor of 1. Equation. 5.6 is then solved for shield thickness, z.

Approach II – Using Eq. 5.5 and solving for shield thickness, z.
(Mass attenuation coefficient of P_b for 50 keV, μ_m= 6.74 cm^2 g^{-1}. Linear attenuation coefficient $\mu = \mu_m{}^*$ Density $\rightarrow$ 6.74 cm^2 g^{-1} * 11.35 g/cm^3 = 76.49 cm^{-1}.)

The Imaging process: As shown in Fig. 5.6 and 5.7, the object for which radiograph is generated lies between X-ray tube and imaging medium. This is in contrast to the photography where light source and camera are normally in the same direction compared to object of photography. This situation poses a limitation that the imaging medium (film or camera's sensing area) should be larger than the object. The line scan detectors help alleviate this problem to some extent (at least there is a freedom in one dimension). Further, the distance between object and imaging

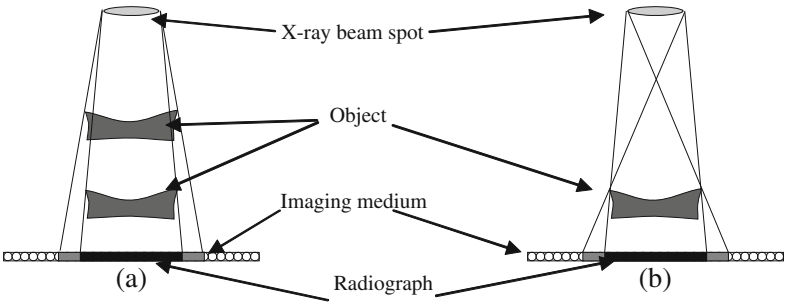

Fig. 5.6 Deviation in image size due to distance of subject from imaging medium (**a**) and geometric unsharpness due to size of beam spot (**b**)

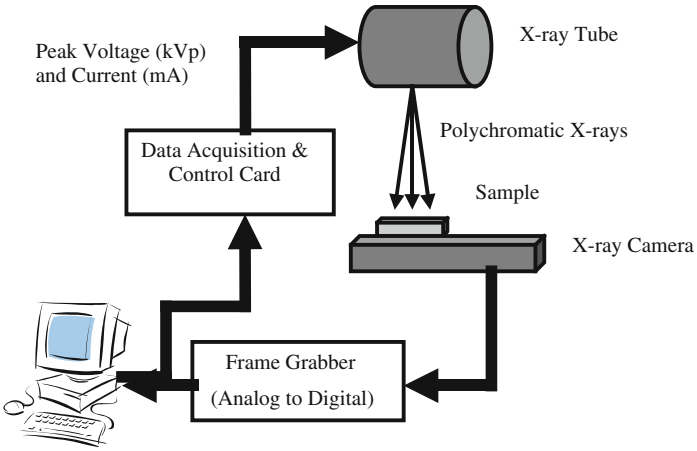

Fig. 5.7 Schematic of the X-ray digital imaging equipment setup

medium is also very vital if the dimensions of features in the radiographs have any significance the study. The spot size of X-ray beam at the source should be as small as possible. Possible artifacts due to distance from object to imaging medium and due to larger spot size are shown in Fig. 5.6.

5.1.4 X-Ray Digital Imaging Equipment

Schematic of a typical equipment setup is shown in Fig. 5.7. The equipment consists of an X-ray tube that generates polychromatic X-rays, an X-ray camera, a computer and data acquisition and control card(s) for communication between equipment and computer.

5.1.5 Applications of X-Ray Imaging in Non-destructive Quality Evaluation

Many applications are reported using human intervention for making decisions about presence of defects in various commodities like apples, mango, onion, meat, pistachio nuts, almonds, wheat, pecans, grains etc. (Diener et al. 1970, Han et al. 1992, Thomas et al. 1995, Keagy et al. 1996, Schatzki et al. 1997, Casasent et al. 1998, Abbott 1999, Arslan et al. 2000, Kim and Schatzki 2000, Casasent et al. 2001, Kim and Schatzki 2001, Haff and Slaughter 2004, Karunakaran et al. 2004, Tollner et al. 2005, Neethirajan et al. 2006a, Fornal et al. 2007, Kotwaliwale et al. 2007b, Narvankar et al. 2009) X-ray with energy ranging from 15 to 80 kVp at various current levels has been reportedly used. However, higher energy of 100 kVp has been found not suitable for radiography of food products. The X-ray exposure time as high as 90 s has been reported while taking the exposure on film.

Defect inspection and classification have been difficult problems in the development of non-destructive sorting systems for fruits and vegetables. This is because various types of defective tissues with differing severity, as well as other features, may occur on the agricultural products due to unpredictable natural environmental conditions, insects, pathogens, or physiological disorders. Spectral imaging, machine vision and pattern recognition techniques are considered effective tools to identify defective tissues on fruits and vegetables. Before introduction of digital imaging and image processing the decision system for identification of desired or undesired features has been manual. Computer based image processing system has given a support to the decision system and made it possible to quickly identify the features for opening a prospect for online sorting. Different types of image processing algorithms have been adopted for enhancement of images to aid decision on attributes. The image processing algorithms have been improving with improvement in computational skills and hardware. Whereas the initial works included morphological image processing techniques to enhance features of interest, the recent approaches use stochastic and advanced techniques leading to automatic decision support. Some primary image processing algorithms like image subtraction have been suggested to determine relative movement of live insects infesting the kernels. Figure 5.8 shows an X-ray based system used for sorting of mangoes. The unit is typically similar to the devices used at airports for scanning of passenger baggage. Figure 5.9 shows radiographs of pecans distinctly showing some kind of abnormalities which were otherwise invisible from outside. X-ray images of some more agricultural products are shown in Fig. 5.10.

Dual energy X-ray imaging: Dual energy X-ray imaging is a method for producing images with different contrast characteristics. Two images, produced with short time between exposures, and with different contrast properties are obtained using two exposures with different kVp. Using these two images makes it possible, for instance, to subtract the bone structures produced in the low-kVp image from the high-kVp image, thus generating a “soft tissue image”. Inversely, visualizing high attenuating regions can be improved by subtracting the high-kVp image from the low-kVp image. Figure 5.11 shows a schematic of DEXA setup.

Dual energy X-ray imaging is an alternative technique to simple transmission X-ray imaging. A small contrast in a X-ray transmitted image can be enhanced by a suitable selection of two X-ray photon energies (Zwiggelaar et al. 1997). Dual

Fig. 5.8 X-ray based sorting system for mangoes (Courtesy: CEERI, Chennai, India)

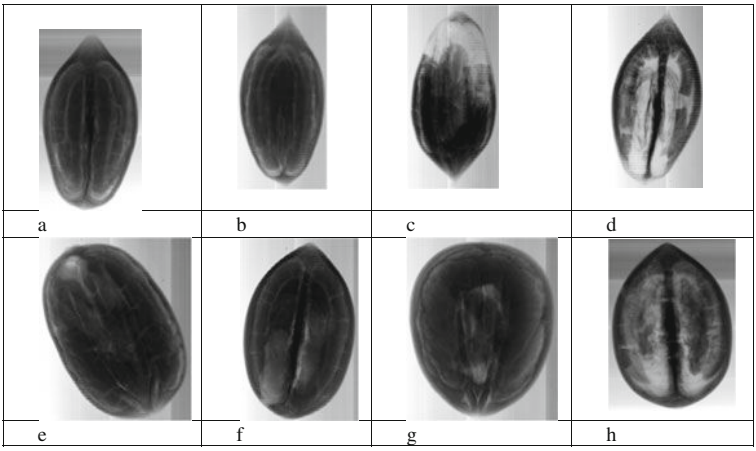

a – Good nut; b – Good nut with shucktight; c – Nut with mechanical damage; d – Nut with shriveled nutmeat; e – Insect damage to one cotyledon from inside; f – visible insect hole; g – Insect damage and insect; h – Hollow nut.

Fig. 5.9 X-ray images of some pecans with different visible attributes

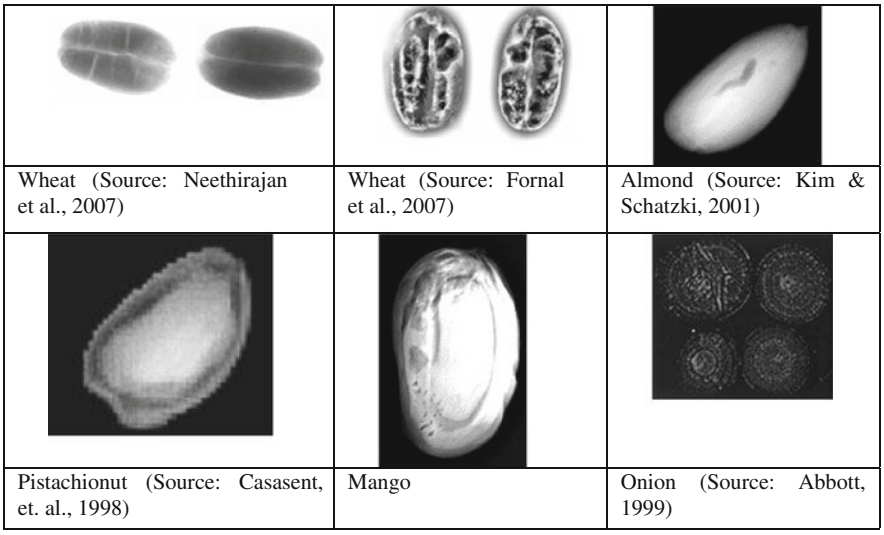

Wheat (Source: Neethirajan et al., 2007)	Wheat (Source: Fornal et al., 2007)	Almond (Source: Kim & Schatzki, 2001)
Pistachionut (Source: Casasent, et. al., 1998)	Mango	Onion (Source: Abbott, 1999)

Fig. 5.10 Radiographs of some agricultural commodities showing internal artifacts

energy X-ray imaging has been successfully used to detect glass contamination in horticultural peat (Ayalew et al. 2004); to evaluate meat tenderness (Kroger et al. 2006), to classify vitreousness in durum wheat (Neethirajan et al. 2007) and to predicts carcass composition from live sheep and chemical composition of live and dead sheep (Pearce et al. 2009). DEXA has been used to study composition of pork carcasses and to predict bone mineral content in live pigs, for predicting total weight and the amount of lean and fat in lamb carcasses and their primal cuts, to assess meat fat content.

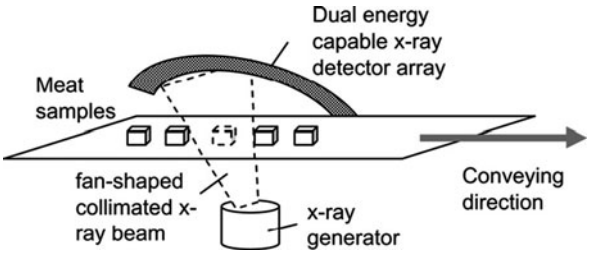

Fig. 5.11 Principal layout of DEXA scanner (Source: Kröger et al. 2006)

5.2 Computed Tomography (CT)

The technique of X-ray computed tomography (CT) enables the acquisition of two-dimensional X-ray images of thin "slices" through the object. CT, originally known as computed axial tomography (CAT or CT scan) and body section rentenography, is an imaging method employing tomography. The basic principle behind CT is that the internal structure of an object can be reconstructed from multiple X-ray projections of an object. Figure 5.12 shows an illustration of a CT scanner. The first commercially viable CT scanner was invented by Godfrey Newbold Hounsfield in Hayes, England at Thorn EMI Central Research Laboratories using X-rays. Hounsfield conceived his idea in 1967, and it was publicly announced in 1972. Allan McLeod Cormack of Tufts University, MA, USA independently invented a similar process and they shared a Nobel Prize in medicine in 1979. The first prototype took 160 parallel readings through 180 angles, each 1° apart, with each scan taking a little over 5 min. A large computer required almost 2.5 h to process the images from these scans by algebraic reconstruction techniques.

The first practical CT instrument was developed in 1971 by Dr. G. N. Hounsfield in England and was used to image the brain. The projection data were acquired in approximately 5 min, and the tomographic image was reconstructed in

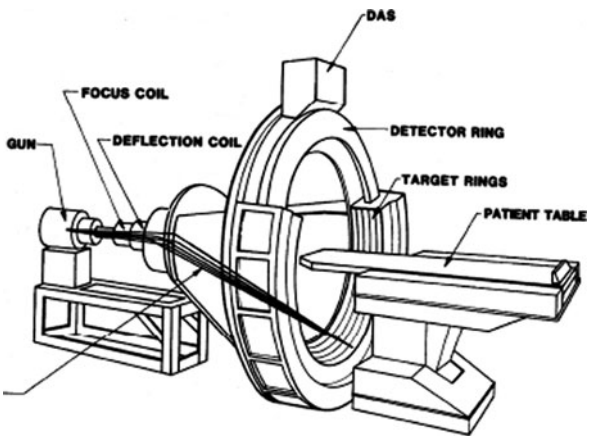

Fig. 5.12 CT scan machine schematic (Source: Cuningham and Judy 2000)

approximately 20 min. Since then, CT technology has developed dramatically, and CT has become a standard imaging procedure for virtually all parts of the body in thousands of facilities throughout the world.

5.2.1 Generations of CT

Several generations of scanners have been developed which differ in tube-detector configuration and scanning motion (Table 5.1) (Canadian Association of Medical Radiation Technologists CT Imaging 1-Theory textbook).

In the first and second generation designs, the X-ray beam was not wide enough to cover the entire width of the 'slice' of interest. A mechanical arrangement was required to move the X-ray source and detector horizontally across the field of view. The first and fourth generation of CT are compared graphically in Fig. 5.13. In the 3rd and 4th generation designs, the X-ray beam is able to cover the entire field of view of the scanner. This avoids the need for any horizontal motion; an entire 'line' can be captured in an instant. This allowed simplification of the motion to rotation of the X-ray source. Third and fourth generation designs differ in the arrangement of the detectors. In 3rd generation, the detector array is as wide as the beam, and must therefore rotate as the source rotates. In 4th generation, an entire ring of stationary detectors is used. Figure 5.14 shows a modern CT scanner with the cover

Table 5.1 Generations of CT scanners

Generation	Configuration	Detectors	Beam	Minimum scan time
First	Translate-rotate	1~2	Pencil thin	2.5 min
Second	Translate-rotate	3~52	Narrow fan	10 s
Third	Rotate-rotate	256~1,000	Wide fan	0.5 s
Fourth	Rotate-fixed	600~4,800	Wide fan	1 s
Fifth	Electron beam	1,284 detectors	Wide fan electron beam	33 ms

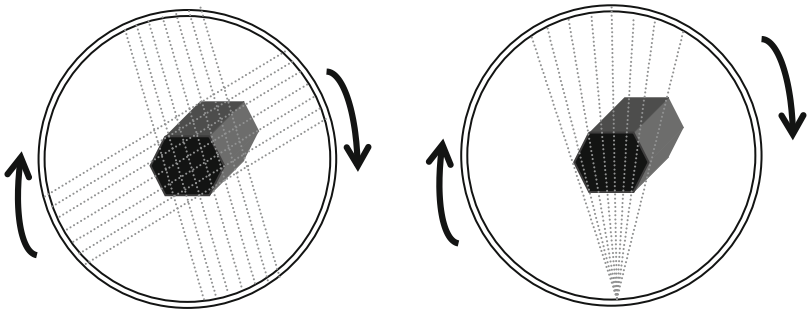

Fig. 5.13 Configuration of two generations of CT

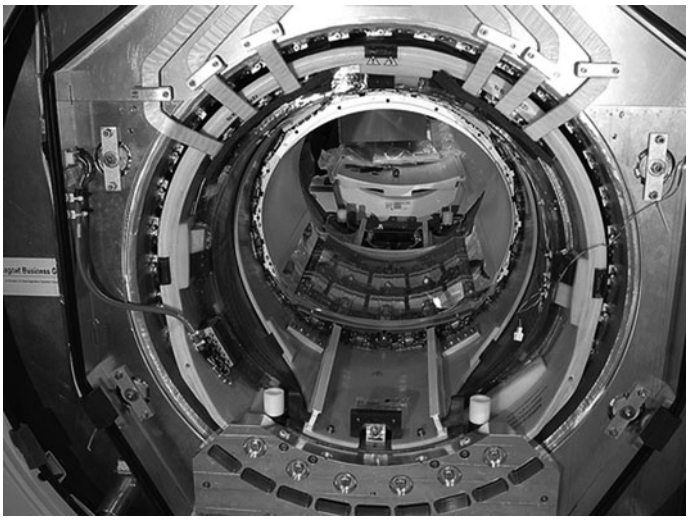

Fig. 5.14 CT scanner with cover removed to show the principle of operation

removed, demonstrating the principle of operation. The X-ray tube and the detectors are mounted on a ring shaped gantry. The object is placed in the center of the gantry while the gantry rotates around them. In this arrangement, the machine has a broad fan-shaped X-ray beam with rotating source and detectors.

Instead of rotating a conventional X-ray tube around the object, the Electron Beam CT (EBCT) machine houses a huge vacuum tube in which an electron beam is electro-magnetically steered towards an array of tungsten X-ray anodes arranged circularly around the object. Each anode is hit in turn by the electron beam and emits X-rays that are collimated and detected as in conventional CT. The lack of moving parts allows very quick scanning, with single slice acquisition in 50–100 ms. However, the equipment is exorbitantly expensive.

Helical, also called spiral, CT was introduced in the early 1990s. In helical CT the X-ray sources (and detectors in 3rd generation designs) are attached to a freely rotating gantry. During a scan, the table moves the object smoothly through the scanner; hence the X-ray beam follows a helical path (Fig. 5.15). It was the development of two technologies that made helical CT practical: slip rings to transfer power and data on and off the rotating gantry, and the switched mode power supply powerful enough to supply to the X-ray tube, but small enough to be installed on the gantry. The major advantage of helical scanning compared to the traditional shoot-and-step approach, is speed; a large volume can be covered in 20–60 s. This is advantageous for a number or reasons: (1) often the patient can hold their breath for the entire study, reducing motion artifacts, (2) it allows for more optimal use of intravenous contrast enhancement, and (3) the study is quicker than the equivalent conventional CT permitting the use of higher resolution acquisitions in the same study time. The data obtained from spiral CT is often well-suited for 3D imaging

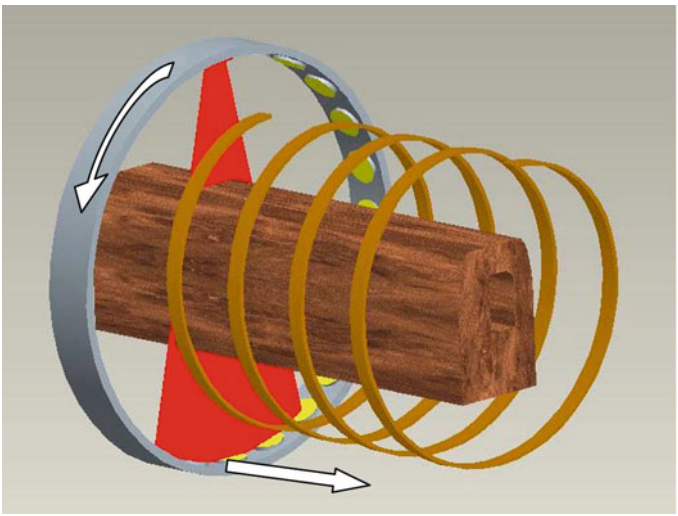

Fig. 5.15 Spiral CT Arrangement

because of the lack of motion mis-registration and the increased out of plane resolution. All other factors being equal, helical CT has slightly lower z-axis resolution than step-and-shoot.

Multislice CT scanners are similar in concept to the helical or spiral CT but there are more than one detector rings. There could be 64 or more detector rings in this type of scanners. Recent models have up to three rotations per second and isotropic resolution of 0.35 mm voxels with z-axis scan speed of up to 18 cm/s. The major benefit of multi-slice CT is the increased speed of volume coverage. This allows large volumes to be scanned.

Inverse geometry CT (IGCT) is a novel concept which is being investigated as refinement of the classic third generation CT design. Currently the technique is proven at laboratory level only. IGCT reverses the shapes of the detector and X-ray sources. The conventional third-generation CT geometry uses a point source of X-rays, which diverge in a fan beam to act on a linear array of detectors. In multidetector computed tomography (MDCT), this is extended in 3 dimensions to a conical beam acting on a 2D array of detectors. The IGCT concept, conversely, uses an array of highly collimated X-ray sources which act on a point detector. By using a principle similar to electron beam tomography (EBCT), the individual sources can be activated in turn by steering an electron beam onto each source target.

The rationale behind IGCT is that it avoids the disadvantages of the cone-beam geometry of third generation MDCT. As the z-axis width of the cone beam increases the quantity of scattered radiation reaching the detector increases and the z-axis resolution is degraded because of the increasing z-axis distance that each ray must traverse. This reversal of roles has extremely high intrinsic resistance to scatter, and

by reducing the number of detectors required per slice, it makes the use of better performing detectors (e.g. ultra-fast photon counting detectors) more practical. Because a separate detector can be used for each 'slice' of sources, the conical geometry can be replaced with an array of fans, permitting z-axis resolution to be preserved.

5.2.2 CT Number

In CT system, the studied object is irradiated from specific directions by an X-ray source. The intensities of X-rays going through the object are measured by detectors, digitized, and used in the reconstruction of a digital image of the test object using CT numbers. The CT number is defined in equation below. The CT number is based on linear X-ray absorption coefficients and, in general, is expressed by brightness data in an image. In the case of k = 1,000, the CT number is called a Hounsfield unit.

$$\text{CT number} = (\mu - \mu_w) \times \frac{k}{\mu_w} \tag{5.7}$$

where, μ = object linear X-ray absorption coefficient (m^{-1}); μ_w = linear X-ray absorption coefficient of water (m^{-1}); k = constant (1,000).

Ogawa et al. (1998) computed Hounsfield numbers as CT numbers, and the measuring range was from –1,000 to +4,000 with the CT number for air being –1,000 and the CT number for water being 0.

5.2.3 CT Image Generation and Processing

Pixels in an image obtained by CT scanning are displayed in terms of relative radiodensity. The pixel itself is displayed according to the mean attenuation of the tissue(s) that it corresponds to on a scale from –1,024 to +3,071 on the Hounsfield scale. Pixel is a two dimensional unit based on the matrix size and the field of view. When the CT slice thickness is also factored in, the unit is known as a Voxel, which is a three dimensional unit. The phenomenon that one part of the detector cannot differ between different tissues is called the "Partial Volume Effect". Water has an attenuation of 0 Hounsfield units (HU) while air is –1,000 HU, cancellous bone is typically +400 HU. The attenuation of metallic insertions/impurities depends on atomic number of the element used: Titanium usually has an amount of +1,000 HU, iron steel can completely extinguish the X-ray and is therefore responsible for well-known line-artifacts in computed tomograms.

Windowing is the process of using the calculated Hounsfield units to make an image. The various radiodensity amplitudes are mapped to 256 shades of gray. These shades of gray can be distributed over a wide range of HU values to get an overview of structures that attenuate the beam to widely varying degrees.

Alternatively, these shades of gray can be distributed over a narrow range of HU values (called a "narrow window") centered over the average HU value of a particular structure to be evaluated. In this way, subtle variations in the internal makeup of the structure can be discerned. This is a commonly used image processing technique known as contrast compression.

Three dimensional (3D) Image Reconstruction: Because contemporary CT scanners offer isotropic, or near isotropic, resolution, display of images does not need to be restricted to the conventional axial images. Instead, it is possible for a software program to build a volume by 'stacking' the individual slices one on top of the other. The program may then display the volume in an alternative manner.

Multiplanar reconstruction (MPR) is the simplest method of reconstruction. A volume is built by stacking the axial slices (Fig. 5.16). The software then cuts slices through the volume in a different plane (usually orthogonal) as shown in Fig. 5.17. Optionally, a special projection method, such as maximum-intensity projection (MIP) or minimum-intensity projection (mIP), can be used to build the reconstructed slices. Other techniques include 3D rendering techniques like Surface rendering and Volume rendering.

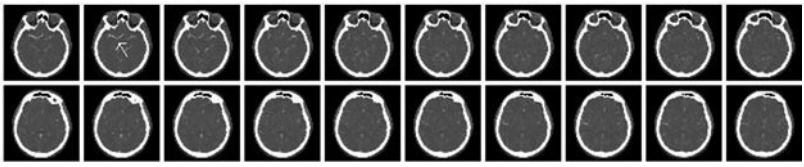

Fig. 5.16 Axial slices of brain used for stacking and building 3-D image (courtesy: Wikipedia)

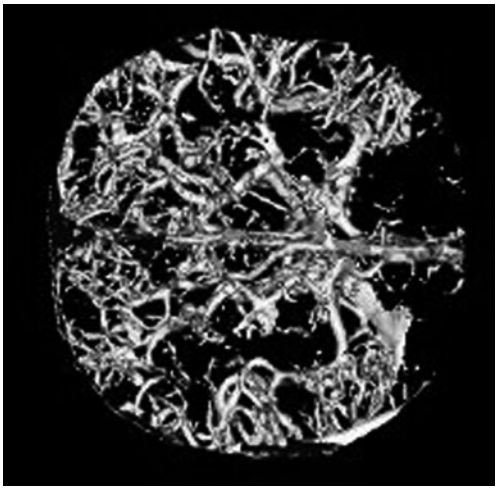

Fig. 5.17 Orthogonal slice of brain generated by the software form the 3-D image (courtesy: Wikipedia)

5.2.4 Application for Detection of Physical Foreign Materials in Foods

Application of CT in non-destructive quality detection of agricultural products is still in nascent stage. Most of research work has been carried out using medical CT scanners (Fig. 5.18) and employing software developed for analysis of human anatomy. Despite these lacunae, several successful attempts have been reported. The feature identification process is manual however use of image processing algorithms (readily available or tailored) has been reported for image enhancement and better readability. A possibility of determining chemical composition of agricultural materials has also been explored using CT. Although, changes in hardware has now considerably reduced the time required for CT scan, but it is still a matter of concern. Lim and Barigou (2004) observed that to scan a 10 mm cube over 180° in 200 discrete steps of 0.9°, it took about 30–45 min.

Sonego et al. (1995) monitored wooly breakdown of cool stored nectarines using and observed that areas exhibiting wooliness appeared darker indicating presence of gas inclusions, which were unable to absorb X-rays. Ogawa et al. (1998) used a medical CT scanner for the detection of selected non-metallic materials embedded in various fluids and food materials. The author determined detection limits for foreign materials and commented that when the volume of the foreign materials was smaller than the physical resolution of the X-ray CT scanner, small parts may be detected as foreign materials but not correctly identified as being which type of materials. They also commented that food materials possesses a range of CT number due to their inhomogenity and when CT number of a foreign material was within this range, a foreign material not detectable even if it had a volume larger than the physical resolution of the X-ray CT scanner.

Barcelon et al. (1999) produced histogram for the peach image, reflecting the frequency of the CT number of peach slice under consideration. Judging from the histogram of the image, a fresh peach had less attenuation frequency between the CT numbers ranging from – 300 to –1,000. In contrast, peaches after 2 weeks of

Fig. 5.18 Medical CT scanner being used for internal defect detection in mangoes

ripening had a considerable increase in attenuation frequency on this CT number range. This confirmed the presence of voids and a drier region that was probably developed due to the loss of moisture towards the outermost layer in the fruit. Author further determined relationship between CT number and the physicochemical contents. Further, Barcelon et al. (2000) used X-ray CT technique to analyze the internal changes associated with the ripening process of mango. They evaluated mango fruits for X-ray absorption, density, moisture content, soluble solids, titrable acidity and pH. The author commented that CT image showed visible features of the internal structural changes between the fresh and ripened mangoes. They concluded that CT number, moisture content and titrable acidity decreased significantly with postharvest ripening time, while pH and soluble solids increased with postharvest ripening time. Similarly, Haseth et al. (2007) successfully modeled dependency of CT value on chemical composition of meat and the linear relationships between sodium chloride (NaCl) and CT value.

Lammertyn et al. (2003) found a clear contrast between healthy and brown tissue of 'Conference' pears. The highest pixel intensity value of the affected tissue was still lower than the lowest pixel intensity value for unaffected tissue, and one threshold value was sufficient therefore to separate both types of tissue.

Lim and Barigou (2004) described imaging, visualization and analysis of the three dimensional (3D) cellular microstructure of a number of food products (aerated chocolate, mousse, marshmallow and muffin) using X-ray micro computed tomography. Author determined a 3D model of the foam microstructure and by combining image analysis with a stereological technique; they obtained quantitative information on a number of parameters including spatial cell size distribution, cell wall thickness distribution, air cell connectivity and degree of microstructure anisotropy. Neethirajan et al. (2006b) developed algorithms to determine total grain surface area, total airspace area, number of airflow paths, areas of the individual airflow paths and length of the individual airflow paths using CT images of five types of grains (wheat, barley, flax seed, peas and mustard). They further developed method to analyse pores that influenced fluid transport phenomenon inside grain bulks. Quality evaluation based on voids has also been attempted by Mousavi et al. (2007) who showed that from the reconstructed 3D image based on a set of 2D images, voids formed due to freeze drying could be measured in number of foods like meat, fish, chicken, potato, cheese and carrot. Leonard et al. (2008) illustrated the use of X-ray microtomography to investigate the effect of drying temperature on microstructure of a banana. 3D gray level images were formed by two phases: the pore space at low gray levels (dark voxels), and the banana skeleton at high gray levels (bright voxels). The author segmented the 3D image by assigning the value 1 to all pixels whose intensity was below a given gray tone value and 0 to others. From the 3D processed binary images the porosity was measured. Increase in drying temperature was found to lead to an increase in final porosity of the products. Figure 5.19 shows some CT images of different agricultural commodities.

X-ray microtomography is a nondestructive technique that has been used successfully for structural investigation of wide range of materials such as food materials, ceramic, metals, rock, and bones. It is an emerging technique which

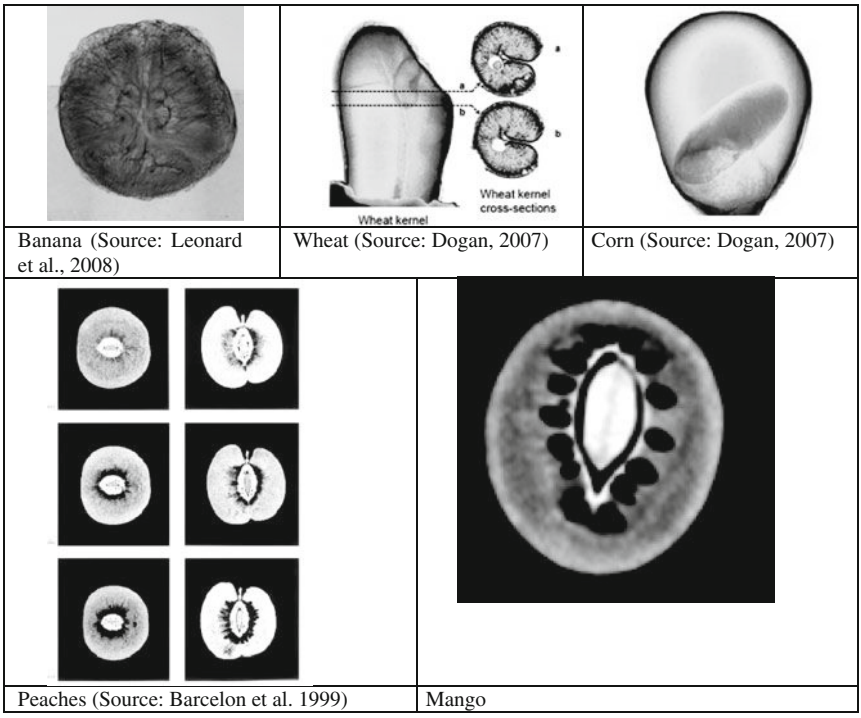

Banana (Source: Leonard et al., 2008) | Wheat (Source: Dogan, 2007) | Corn (Source: Dogan, 2007)

Peaches (Source: Barcelon et al. 1999) | Mango

Fig. 5.19 Cross-sections developed using CT 3-D models for some agricultural commodities

operates on the same basic principles as medical CT scanners, but has much higher resolution. Using microtomography, Dogan (2007) observed that physical discontinuity of protein in the soft-wheat kernels resulted in distinctly different X-ray image patterns than that of hard-wheat kernels and enabled clear discrimination between hard and soft varieties. He also tested the images for visual examination of infested kernels (wheat, corn). Images clearly indicated the presence of instars, larvae tunneled along the endosperm, as well as adults. Also presence of visually unnoticeable fissures perpendicular to crease line of wheat could be observed in the microtomographs.

5.3 Hazards of Radiation

Some common effects of X-rays are: alteration in physical properties of material (metals can be made brittle, plastics can be made stronger; transparency of material can be altered; electrical current can be induced in some semi-conductors); chemical changes (mixture of N_2 and O_2 gases gives nitrogen oxides, ethylene gas to polyethylene); biological effects (killing living organisms, preserving foods, medical applications – such as radiation oncology). All electromagnetic radiations having energy of 15 eV or more can ionize atoms.

CT is regarded as a moderate to high radiation diagnostic technique. While technical advances have improved radiation efficiency, there has been simultaneous pressure to obtain higher-resolution imaging and use more complex scan techniques, both of which require higher doses of radiation. The radiation dose for a particular study depends on multiple factors: volume scanned, patient build, number and type of scan sequences, and desired resolution and image quality. Because CT scans rely on intravenously administered contrast agents in order to provide superior image quality, there is a low but non-negligible level of risk associated with the contrast agents themselves. Certain patients may experience severe and potentially life-threatening allergic reactions to the contrast dye.

The International Commission on Radiological Protection (ICRP-60) has recommended the following to minimize hazards of radiations:

- No practice shall be adopted unless its introduction produces a positive net benefit.
- All exposures shall be kept as low as reasonably achievable
- The effective dose equivalent (whole body) to individuals working in radiation area (radiation workers) shall not exceed 2 rems (20 msv) in any 1 year and for the general public is 0.2 rem (2 msv) in a year. The above occupational limits are for adults (age > 18 years). No person under the age of 16 shall be assigned work involving ionizing radiation.
- There are three basic ways to minimize the exposure to harmful radiations:
  - Minimum exposure time: Individuals should not stay near the radiation source or the radiation source should not be kept ON for any longer than required.
  - Maximum distance from source: Individuals should stay as far as possible or practical from the source, the radiation intensity decreases with distance following inverse square law.
  - Proper shielding: It is not practically possible for radiation workers to stay far away from the radiation source. A proper shield made of lead, steel, concrete or depleted uranium is useful is protecting against radiations. The shields can be put to cover the entire radiation area or could be used as personal protective gears (gloves, apron, mask etc.)

Besides above, proper training, mock-up drills, proper design of facility for controlled access, display of danger signs etc. are some of the recommended ways to protect individuals from hazardous radiations.

5.3.1 Units Used in Radiation

The unit used to measure the energy of photons is electron volts (eV). An electron volt is the amount of energy that an electron gains as it is accelerated by a potential difference of 1 V. In the case of X-ray it is generally expressed as energy from 0.12 to 120 keV. The higher the energy the stronger is transmittance.

The unit for radioactivity is Becquerel (B_q), which is s^{-1} in SI base units, measured as decay of one nucleus per second (dps). Earlier Curie was the unit used for radioactivity which corresponds to 3.7E10 dps. The unit for absorbed dose is Roentgen (R or A.s.kg^{-1} or Coulomb.kg^{-1}), quantity of radiation which produces one electrostatic unit of positive or negative electricity per cubic centimeter (cc) of air at STP, or, quantity of radiation that will produce 2.083E09 ion pairs per cc of dry air, or radiation received in 1 h from a 1 g source of radiation at a distance of one meter; other known units for dose are Rad (J·kg^{-1}) and SI Unit Gray (Gy), 1 R = 8.72E–03 Gy, which is m^2 s^{-2} in SI base units. Equal absorbed doses from different radiations do not necessarily have equal biological effect. Therefore a term 'dose equivalent' (DE) is commonly used. The DE is equal to absorbed dose multiplied by a factor for energy distribution in tissues. The unit for DE is Sievert (sv) which is equal to Gy×F. The value of F is taken as one for gamma rays, X-rays and beta particles. A unit 'rem' was used earlier for DE, where 1 Sievert = 100 rems.

The X-ray tube current, measured in mA, refers to the number of electrons flowing per second from the filament to the target. Whereas, eV or keV is the unit to represent photon energy in X-rays, kVp is a commonly used unit to represent the peak energy of photons in the polychromatic X-ray beam generated by X-ray tube.

5.3.2 Measurement of Radiation

The term ionizing radiation refers to those subatomic particles and photons whose energy is sufficient to cause ionization in the matter with which they interact. The ionization process consists of removing an electron from an initially neutral atom or molecule. Ionizing radiation, such as X-rays, alpha rays, beta rays, and gamma rays, remains undetectable by the human senses, and the damage it causes to the body is cumulative, related to the total dose received. Since the photon is uncharged, it does not interact through the Coulomb force and therefore can pass through large distances in matter without significant interaction. The average distance traveled between interactions is called the mean free path and in solid materials ranges from a few millimeters for low-energy X rays through tens of centimeters for high-energy gamma rays. When an interaction does occur, however, it is catastrophic in the sense that a single interaction can profoundly affect the energy and direction of the photon or can make it disappear entirely. In such an interaction, all or part of the photon energy is transferred to one or more electrons in the absorber material. Because the secondary electrons thus produced are energetic and charged, they interact in much the same way as described earlier for primary fast electrons. The fact that an original X ray or gamma ray was present is indicated by the appearance of secondary electrons. Information on the energy carried by the incident photons can be inferred by measuring the energy of these electrons. The three major types of such interactions are Photoelectric absorption, Compton scattering and Pair production.

In Photoelectric absorption, the incident X-ray or gamma-ray photon interacts with an atom of the absorbing material, and the photon completely disappears; its energy is transferred to one of the orbital electrons of the atom. Because this energy

in general far exceeds the binding energy of the electron in the host atom, the electron is ejected at high velocity. The kinetic energy of this secondary electron is equal to the incoming energy of the photon minus the binding energy of the electron in the original atomic shell. The process leaves the atom with a vacancy in one of the normally filled electron shells, which is then refilled after a short period of time by a nearby free electron. This filling process again liberates the binding energy in the form of a characteristic X-ray photon, which then typically interacts with electrons from less tightly bound shells in nearby atoms, producing additional fast electrons. The overall effect is therefore the complete conversion of the photon energy into the energy carried by fast electrons. The fast electrons, detectable through their Coulomb interactions, indicate the presence of the original gamma-ray or X-ray photon, and a measurement of their energy is tantamount to measuring the energy of the incoming photon.

An incoming gamma-ray photon can interact with a single free electron in the absorber through the process of Compton scattering. In this process, the photon abruptly changes direction and transfers a portion of its original energy to the electron from which it scattered, producing an energetic recoil electron.

Pair production: The third type of interaction (pair production) occurs in gamma-ray and is possible when the incoming photon energy is above 1.02 MeV. In the field of a nucleus of the absorber material, the photon may disappear and be replaced by the formation of an electron-positron pair.

Monitoring of radiation inside a facility or monitoring the dose received by an individual are the two important aspects of radiation control. Installed or portable instruments for monitoring radiations in an area are available. The detectors used in portable instruments are ionizing chambers, Gieger Muller counters and scintillation detectors. Initially, most common detection methods were based on the ionization of gases, as in the Geiger-Müller counter: a sealed volume, usually a cylinder, with a mica, polymer or thin metal window contains a gas, a cylindrical cathode and a wire anode; a high voltage is applied between the cathode and the anode. When an X-ray photon enters the cylinder, it ionizes the gas and forms ions and electrons. Electrons accelerate toward the anode, in the process causing further ionization along their trajectory. Figure 5.20 shows one portable instrument that can measure instantaneous radiation or dose accumulated over a period of time.

Fig. 5.20 A dosimeter (make: Radcal, USA)

Common types of wearable dosimeters for ionizing radiation include:

- Quartz fibre dosimeter
- Film badge dosimeter
- Thermoluminescent dosimeter
- Solid state (MOSFET or silicon diode) dosimeter.

A real dose (dose-unit = cGy or rad) reflects something objective: The energy deposited by X-rays per gram of irradiated body-tissue. By contrast, an "effective" dose is a calculation which estimates what dose, if given to the entire body, might produce approximately the same amount of risk as would the real dose actually received by the irradiated sections. "Effective" doses (dose-unit = cSv or rem) incorporate a crude adjustment for the different types of ionizing radiation, plus "tissue weighting factors" which attempt to assess the attributable probability of fatal cancer in different organs, the additional detriment from non-fatal cancer and hereditary disorders, and the different latency periods for cancers in various tissues.

5.4 Magnetic Resonance Imaging (MRI)

MRI is based on the principles of nuclear magnetic resonance (NMR), a spectroscopic technique used to obtain microscopic chemical and physical information about molecules. Magnetic resonance imaging is an imaging modality which is primarily used to construct pictures of the NMR signal from the hydrogen atoms in an object. Due to negative connotations associated with the word nuclear in the late 1970s, the technique was called magnetic resonance imaging rather than nuclear magnetic resonance imaging (NMRI). Felix Bloch and Edward Purcell, both of whom were awarded the Nobel Prize in 1952, discovered the magnetic resonance phenomenon independently in 1946. In the period between 1950 and 1970, NMR was developed and used for chemical and physical molecular analysis. In short the MRI technique follows following steps: Put subject in big magnetic field; Transmit radio waves into subject [2~10 ms]; Turn off radio wave transmitter; Receive radio waves re-transmitted by subject; and Convert measured RF data to image.

5.4.1 Physics of MRI

Spin is a fundamental property of nature like electrical charge or mass. Spin comes in multiples of 1/2 and can be + or –. Protons, electrons, and neutrons possess spin. Individual unpaired electrons, protons, and neutrons each possesses a spin of 1/2. To understand how particles with spin behave in a magnetic field, consider a proton having spin as a magnetic moment vector, causing the proton to behave like a tiny magnet with a north and south pole. In the absence of any external magnetic field

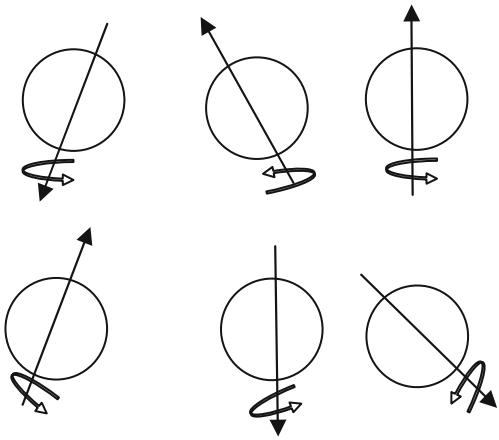

Fig. 5.21 Random orientation of nucleus

the nuclei's spin angular momentum have random orientations (Fig. 5.21) in their atomic or molecular environment.

When the proton is placed in an external magnetic field, the spin vector of the particle aligns itself with the external field (Fig. 5.22), just like a magnet would. There is a low energy configuration or state where the poles are aligned N-S-N-S and a high energy state N-N-S-S.

This particle can undergo a transition between the two energy states by the absorption of a photon. A particle in the lower energy state absorbs a photon and ends up in the upper energy state. The energy of this photon must exactly match the energy difference between the two states. The energy, E, of a photon is related to its frequency, γ, by Planck's constant ($h = 6.626 \times 10^{-34}$ J·s).

$$E = h\gamma \tag{5.8}$$

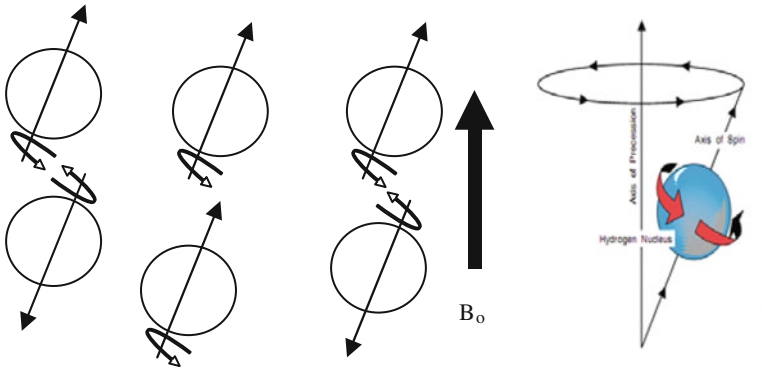

Fig. 5.22 Nucleus oriented after application of external magnetic field B_o

When the energy of the photon matches the energy difference between the two spin states, absorption of energy occurs. In NMR spectroscopy, γ is between 60 and 800 MHz for hydrogen nuclei. In clinical MRI, γ is typically between 15 and 80 MHz for hydrogen imaging.

When certain types of nuclei like protons, cabon-13 and fluorine-19 are placed in a strong static magnetic field (B_o) they absorb electromagnetic radiation in the radio frequency range. Such nuclei are said to be spin- active. The precise frequencies at which spin-active nuclei resonate can be picked up and displayed by instrument. Imposing a linear magnetic gradient on the external magnetic field causes the proton resonance frequency to vary and thus position of resonating nuclei can be determined and represented as image (Chen et al. 1989, Clark et al. 1997).

At equilibrium, the net magnetization vector lies along the direction of the applied magnetic field B_o and is called the equilibrium magnetization M_o. In this configuration, the Z component of magnetization M_Z equals M_o. M_Z is referred to as the longitudinal magnetization. There is no transverse (M_X or M_Y) magnetization here. The time constant which describes how M_Z returns to its equilibrium value is called the spin lattice relaxation time (T_1). The equation governing this behavior as a function of the time t after its displacement is:

$$M_z = M_o(1 - e^{-t/T_1}) \tag{5.9}$$

T_1 is the time to reduce the difference between the longitudinal magnetization (M_z) and its equilibrium value by a factor of e. If the net magnetization is placed along the $-Z$ axis, it will gradually return to its equilibrium position along the $+Z$ axis at a rate governed by T_1.

The time constant which describes the return to equilibrium of the transverse magnetization, MXY, is called the spin-spin relaxation time, T_2, the time to reduce the transverse magnetization by a factor of e.

$$MXY = MXY_o e^{-t/T_2} \tag{5.10}$$

Both spin lattice relaxation and spin-spin relaxation processes occur simultaneously with the only restriction being that T_2 is less than or equal to T_1.

An MR system consists of the following components: (1) a large magnet to generate the magnetic field, (2) shim coils to make the magnetic field as homogeneous as possible, (3) a radiofrequency (RF) coil to transmit a radio signal into the body part being imaged, (4) a receiver coil to detect the returning radio signals, (5) gradient coils to provide spatial localization of the signals, and (6) a computer to reconstruct the radio signals into the final image.

The signal intensity on the MR image is determined by four basic parameters: (1) proton density, (2) T_1 relaxation time, (3) T_2 relaxation time, and (4) flow. Proton density is the concentration of protons in the tissue in the form of water and macromolecules (proteins, fat, etc). The T_1 and T_2 relaxation times define the way that the protons revert back to their resting states after the initial RF pulse.

5.4.2 Image Formation

The principle behind all magnetic resonance imaging is the resonance equation, which shows that the resonance frequency ν (also known as Larmor frequency) of a spin is proportional to the magnetic field, B_o, it is experiencing.

$$\nu = \gamma B_0 \tag{5.11}$$

where γ is the gyromagnetic ratio. For hydrogen, $\gamma = 42.58$ MHz/*Tesla*.

Magnetic field gradient allows imaging position of regions of spin. A magnetic field gradient is a variation in the magnetic field with respect to position. A magnetic field gradient could be one-dimensional or multi-dimensional. The most useful type of gradient in magnetic resonance imaging is a one- dimensional linear magnetic field gradient. A one-dimensional magnetic field gradient along the x axis in a magnetic field, B_o, indicates that the magnetic field is increasing in the x direction. Here the length of the vectors represents the magnitude of the magnetic field. The symbols for a magnetic field gradient in the x, y, and z directions are G_x, G_y, and G_z.

The point in the center of the magnet where $(x, y, z) = 0, 0, 0$ is called the isocenter of the magnet. The magnetic field at the isocenter is B_o and the resonant frequency is ν_o. When linear magnetic field gradient is applied, different regions in the subject experience different magnetic fields. The result is an NMR spectrum with more than one signal. The amplitude of the signal is proportional to the number of spins in a plane perpendicular to the gradient. This procedure is called frequency encoding and causes the resonance frequency to be proportional to the position of the spin.

$$\nu = \gamma(B_o + xG_x) = \nu_o + \gamma x G_x \tag{5.12}$$

$$x = \frac{\nu - \nu_o}{\gamma G_x} \tag{5.13}$$

One of the first forms of magnetic resonance imaging to be demonstrated was backprojection. In the backprojection technique, the object is first placed in a magnetic field. A one-dimensional field gradient is applied at several angles (between 0 and 359°), and the NMR spectrum is recorded for each gradient. Once this data has been recorded the data can be backprojected through space in computer memory. After suppressing the background intensity an image can be seen. The actual backprojection scheme is called the inverse Radon transform.

The most major application of MRI is for examining human or animal anatomy, hence some important terms related to imaging and image processing are derived with reference to the subject of imaging, i.e. human body.

Imaging Coordinates: Clinical imagers do not use the *XYZ* magnetic resonance coordinate system for collection and presentation of images. Instead the anatomic coordinate system is used. In this system the axes are referenced to the body. The

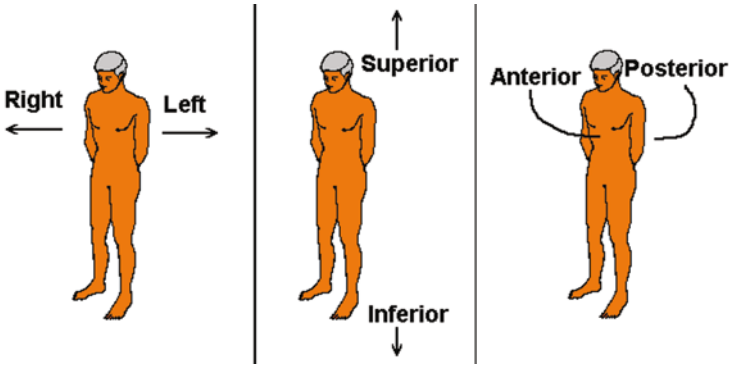

Fig. 5.23 The three imaging coordinates

Fig. 5.24 The three imaging planes

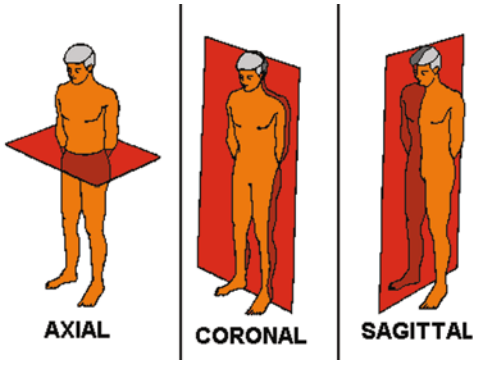

three axes are left-right (L/R), superior-inferior (S/I), and anterior-posterior (A/P) (Fig. 5.23).

Similarly, on clinical imagers the terminology *XY*, *XZ*, and *YZ* are not used to indicate the imaged planes. An imaged plane perpendicular to the long axis of the body is called an axial plane. The sides of this plane are *L/R* and *A/P*. A plane bisecting the front of the body from the back is referred to as a coronal plane. The sides of this plane are *L/R* and *S/I*. A plane bisecting the left and right sides of the body is called a sagittal plane. The sides of this plane are *S/I* and *A/P*. This has been graphically shown in Fig. 5.24.

5.4.3 Application of MRI for Quality Detection of Agricultural Produce

MRI in non-destructive quality detection of agricultural products is a new application. Most of research work has been carried out using medical MRI machines (Fig. 5.25) and employing software developed for analysis of human anatomy.

Fig. 5.25 An open MRI machine being used for MRI of mangoes

Brusewitz and Stone (1987) used a 10.7 MHz NMR sensor for measuring the MC of wheat. They showed that a ratio between the two Free Induction Decay (FID) peaks could be used to determine the MC with an error range of + 0.2%. Tollner et al. (1992) found that NMR outputs could be used to determine the MC of wheat, corn, soybean and peanut. They developed a MC prediction model using FID and spin echo measurements as independent variables. The r^2 values of the models were less than 0.97.

A fruit undergoes various changes during the maturation process. It has been shown that as a fruit becomes more mature, the water content decreases while the oil content increases. The mobility of hydrogen nuclei of water and oil may also change. These changes in the fruit may result in changes in T_1 and T_2 of water and oil in the fruit and thereby affect the NMR measurements.

Based on this, Chen et al. (1993) established an experimental protocol suitable for an on-line NMR sensor for evaluating the maturity of intact avocado fruit.

Sonego et al. (1995) monitored woolly breakdown of cool-stored nectarines (Prunus persicu) and detected the abnormality as dark areas corresponding to low proton density. However, the development of woolliness did not affect the mobility of water in the tissues of nectarines. Clark et al. (1997) reviewed many applications pertaining to the study of fruits and vegetables as well as recent developments that employ nuclear magnetic resonance principles as on-line sensors in post harvest sorting and processing situations. Authors described successful attempts of getting high resolution MR images to determine moisture content, oil content, sugar content, bruises, dry regions, watercore, worm damage, internal quality, stage maturity, etc. for various fruits and vegetables.

Kim et al. (1999) investigated the feasibility of using MRI as a quality sorting or grading technique for intact food products and to construct and test a prototype

in-line sensor utilizing high speed NMR techniques. Authors were interested in the degree to which motion influences the correlation between NMR data and quality factors in fruit. They examined two typical applications. One is the use of NMR spectral information to predict a quality factor, the measurement of oil to water ratio in avocados to predict maturity. The other application was the use of one-dimensional projections to detect the presence of a pit in cherries.

Barreiro et al. (2000) tested apples for mealiness and peaches for wooly structure using mechanical and MRI techniques. Mealy apples turned to more skewed histograms than crisp apples, while the histograms of woolly peaches turned to be more flat loosing the Gaussian appearance. This fact could be understood as a different physiological change underlying mealiness and woolliness. Gonzalez et al. (2001) studied the development of internal browning induced by high levels of carbon dioxide in controlled atmosphere storage of 'Fuji' apples. They reported that spin-spin relaxation (T_2) measurements gave images with better contrast between normal tissue and issue with internal browning than image generated using differences in proton density or spin-lattice (T_1) relaxation measurements. Authors reported that they could obtain meaningful images in 20–40 s by reducing spatial resolution and the time between repetitive scans. They concluded that the rapid development of MRI technology may, in the near future, permit MRI to be used for non-destructive detection of defects such as internal browning. However, it seems likely that the MRI equipment that would be used for such applications would be expensive and relatively sophisticated. Therefore, low-field non-imaging magnetic resonance sensing, which is lower in cost, simpler and requires less signal processing, should be thoroughly investigated to determine which defects it can detect and the detection limitations.

Core breakdown in 'Conference' pears is a storage disorder, which is characterized by brown discolouration of the tissue and development of cavities. Lammertyn et al. (2003) used MRI to monitor the development of core breakdown in 'Conference' pears during storage. Pears stored under disorder-inducing conditions were followed with MRI technique during 6 months of controlled atmosphere storage. After 2 months, incipient browning could be detected with both techniques. They also reported that the contrast between affected and unaffected tissue was higher on the MR images than on images from X-ray CT scans.

Cho et al. (2008) determined the effects of internal browning and watercore on the spin–spin relaxation (T_2) signal of whole apples. They used the non-imaging MR sensor to test apples affected by watercore, internal browning, along with unaffected apples. Marigheto et al. (2008) investigated the internal sub-cellular physiological changes associated with ripening and mealiness in apples with novel two-dimensional NMR relaxation and diffusion techniques. Authors showed that two-dimensional relaxometry reveals more subtle physiological changes than conventional one-dimensional relaxometry. In particular, it was showed by their study that the T_1 of the peak associated with the cell wall in mealy apples was much longer than that of fresh apples. ^{1}H Nuclear Magnetic Resonance (NMR) has been evaluated for use in measuring the moisture of several grains. The MC measurement is

based on the principle that the ^{1}H NMR signal intensity is proportional to the total proton numbers in the sample.

It has been shown by Aspect AI (2010) that using fast MRI techniques various internal features of fruits and vegetables could be detected. These features are not only physical like presence of a foreign body or physical/physiological damage but also certain biochemical parameters like sugar levels could be correlated to the MRI signals. Application and success of this technique has been summarized in Table 5.2. Results of some successful applications of MRI to see internal defects are shown in Figs. 5.26, 5.27, 5.28 and 5.29.

Table 5.2 Successful application of fast MRI in detecting internal features

Features	Apples	Citrus	Fresh tomatoes	Potatoes	Fresh cut fruits	Stone Fruits
Hollow/split pit	+	+	+	+		+
Pests and insects	+	+	+	+	+	+
Bruising and cracks	+	+	+	+		+
Rot	+	+	+	+	+	+
Mold damage		+	+	+	+	+
Browning	+			+	+	+
Seed size/#		+			+	
Maturity			+		+	
Sugar level	+	+	+		+	+
Mealiness/texture	+	+	+		+	+

Source: Aspect AI.

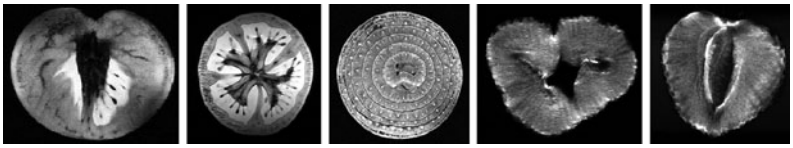

Fig. 5.26 Internal structure of tomato, onion and strawberry visible in MRI (Courtesy: http://people.web.psi.ch/kuehne/)

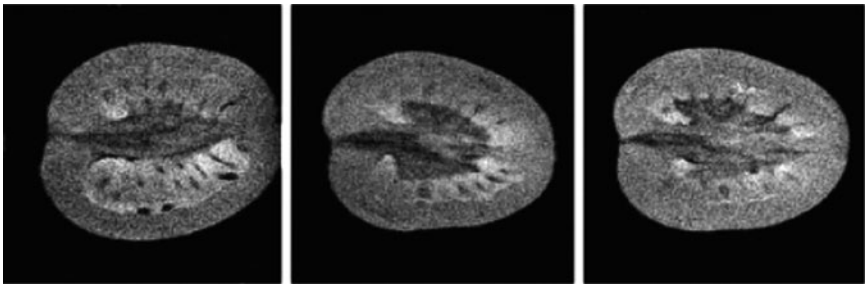

Fig. 5.27 Internal structure of tomato visible in MRI (Courtesy: Aspect AI 2010)

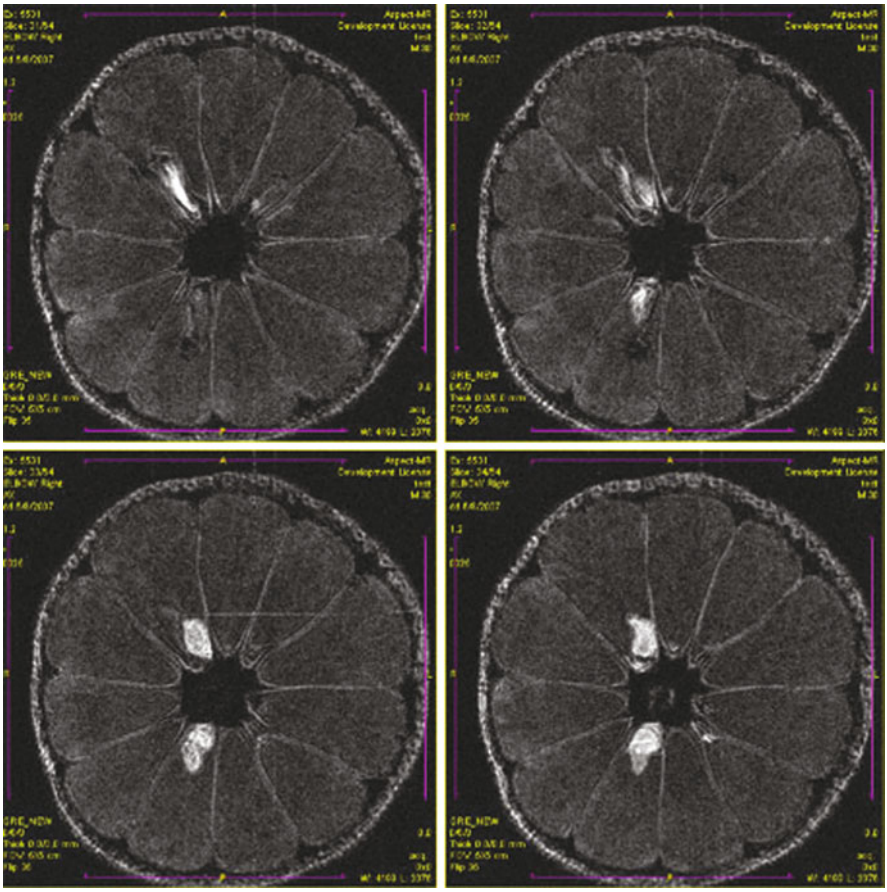

Fig. 5.28 Internal structure of citrus visible in MRI (Courtesy: Aspect AI 2010)

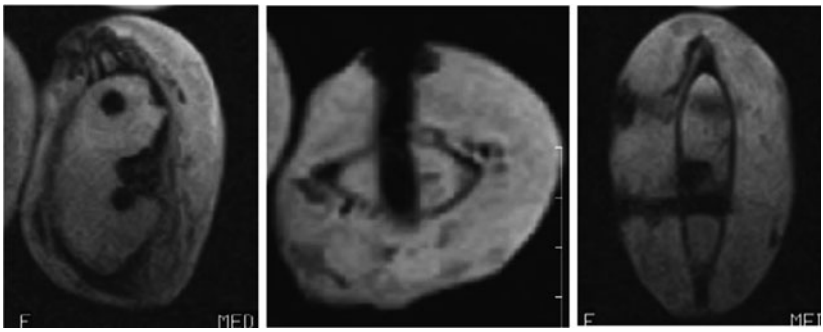

Fig. 5.29 Axial, coronal and sagittal views of mango in MRI scan showing physical and physiological disorders

5.5 Comparison of Techniques

X-rays (radiographs) are the most common and widely available diagnostic imaging technique. Small level and short duration of radiation exposure from X-rays is not harmful. The images are ready quickly. X-rays may not show as much detail as an image produced using newer, more powerful techniques. Computation in digitization of radiographs is comparatively less and there are varieties of 2-D image processing algorithms for image enhancement and automated feature detection. Some of common artifacts in radiographs are due to beam hardening, heal effect, fogging due to Compton scattering, inappropriate window material. Unsatisfactory radiographs result due to:

Density related defects: High-density defect in radiographs are caused due to overexposure or overdevelopment, while low-density defects can be observed due to underexposure or underdevelopment. The remedial action for this is viewing the image with appropriate intensity illuminator or by adjusting the exposure time suitably using characteristic curve. For appropriate development of film, developer temperature should be optimum.

Contrast problems: High contrast and low contrast are often observed in radiographs. High contrast images have limited sharpness while low contrast images are prone to have noise. Varying thickness of the object produces high subject contrast and thus high image contrast. Adjustment of voltage and use of multi film technique can help prevent high contrast. Another reason for high contrast is due to high film contrast and using lower contrast characteristics film can eliminate it. Low contrast is due to low subject contrast, low film contrast and underdevelopment of film. The respective remedies are to reduce voltage, using film with higher contrast characteristics and adjusting temperature of developer.

Poor definition: Many reasons, like (1) specimen not in contact with film (2) large focal spot (3) screens and film not in close contact (4) high film graininess and (5) too short source to film distance result into poor image definition.

Fog: Fog and scatter reduces radiographic contrast. The scatter is due to Compton scattering and fog effect on the imaging medium is undesirable. Some other causes of fog and are (1) exposure to light; (2) improper film storage condition (located close to radiation areas or presence of dust, heat, gases); (3) defective developer solution; and (4) static discharge and mishandling of film. In case of digital radiography the defects of imaging medium can be rectified by making dark current corrections.

Sampling and quantization: The quantity of digital radiographs depends on sampling, i.e. number of pixels recorded per unit dimension of the sample and quantization i.e. digitized pixel intensity/amplitude values. Better sampling and higher quantization result in more details in image but this requires higher computational power and time for processing and storage of images. Further, such images are more prone to noise.

A CT scan can show the size, shape, and position of structures that are deep inside. A CT scan costs more and takes more time than a regular X-ray. Although CT scan technique gives maximum 3-D information, it requires narrow X-ray

beam, special hardware to continuously rotate and shift the source and camera or the object, high energy X-rays, and extensive computation. For these reasons the time required for scanning an object is far more than taking one radiograph. The advantages CT poses over radiography are:

CT completely eliminates the superimposition of images of structures outside the area of interest. Because of the inherent high-contrast resolution of CT, differences between tissues that differ in physical density by less than 1% can be distinguished.

Data from a single CT imaging procedure consisting of either multiple contiguous or one helical scan can be viewed as images in the axial, coronal, or sagittal planes, depending on the diagnostic task. This is referred to as multiplanar reformatted imaging.

Although CT is a relatively accurate test, it is liable to produce artifacts such as:

- Aliasing Artifact or Streaks: These appear as dark lines which radiate away from sharp corners. It occurs because it is impossible for the scanner to 'sample' or take enough projections of the object, which is usually metallic. It can also occur when an insufficient mA is selected, and insufficient penetration of the x-ray occurs.
- Partial Volume Effect: This appears as 'blurring' over sharp edges. It is due to the scanner being unable to differentiate between overlying structures and respective HU's. The processor tries to average out the two densities or structures. This can be partially overcome by scanning using thinner slices.
- Ring Artifact: Probably the most common mechanical artifact, the image of one or many 'rings' appears within an image. This is due to a detector fault.
- Noise Artifact: This appears as gaining on the image and is caused by a low signal to noise ratio. This occurs more commonly when a thin slice thickness is used. It can also occur when the kV or mA is too low.
- Motion Artifact: This is seen as blurring which is caused by movement of live or moving object/patient. This is not so much a problem these days with faster scanning times in the use of MDCT.
- Windmill: Streaking appearances can occur when the detectors intersect the reconstruction plane. This can be reduced with filters or a reduction in pitch.
- Beam Hardening: This can give a 'cupped appearance'. It occurs when there is more attenuation in the center of the object than around the edge. This is easily corrected by filtration and software.

Unlike radiography and CT, which require ionizing radiation, MRI is based on a safe interaction between radio waves and hydrogen nuclei in the body in the presence of a strong magnetic field. A CT scan uses X rays to build up a picture. MRI uses a magnetic field to do the same and has no known side effects related to radiation exposure. MRI has much higher detail in the soft tissues. One of the greatest advantages of MRI is the ability to change the contrast of the images. Small changes in the radio waves and the magnetic fields can completely change the contrast of the image. Different contrast settings will highlight different types of tissue. Another advantage of MRI is the ability to change the imaging plane without moving the object. Most MRI machines can produce images in any plane. Presence of metal in

Table 5.3 Artifacts and their causes

Artifact	Cause
RF offset and quadrature ghost	Failure of the RF detection circuitry
RF noise	Failure of the RF shielding
B_o inhomogeneity	Metal object distorting the B_o field
Gradient	Failure in a magnetic field gradient
Susceptibility	Objects in the FOV with a higher or lower magnetic susceptibility
RF inhomogeneity	Failure or normal operation of RF coil, and metal in the anatomy
Motion	Movement of the imaged object during the sequence
Flow	Movement of body fluids during the sequence
Chemical shift	Large B_o and chemical shift difference between tissues
Partial volume	Large voxel size
Wrap around	Improperly chosen field of view
Gibbs ringing	Small image matrix and sharp signal discontinuities in an image

the samples cause malfunction during magnetic resonance imaging. MRI equipment is expensive to purchase, maintain, and operate. Like any other imaging technique there are certain artifacts NMR images which can lead to wrong identification of internal features. Artifacts are typically classified as to their source, and there are dozens of image artifacts (Table 5.3).

Radiography, computed tomography and magnetic resonance imaging are very effective methods for inspection of internal quality of various biological products. Although they differ in terms of obtainable details (Yacob et al. 2005), safety of operation, convenience, cost of machinery, sample preparation, time required for imaging and expertise required for operation, their effectiveness has been proven through plethora of research applications. These techniques are yet to find extensive place in the commercial agricultural processing but it is expected that with introduction of cheaper and faster electronic hardware, these will soon replace arduous human intervention in quality detection of agricultural products.

References

Abbott J (1999) A quality measurements of fruits and vegetables. Postharvest Biol Technol 15: 207–225

Arslan S, Inanc F, Gray JN et al (2000) Grain flow measurements with X-ray techniques. Comput Electron Agric 26(200):65–80

ASPECT AI (2010). Aspect AI: MRI applications – agriculture. http://www.aspect-ai.com/applications/agriculture.php/. Accessed 18 Jan 2010

Ayalew G, Holden NM, Grace PK et al (2004) Detection of glass contamination in horticultural peat with dual-energy x-ray absorptiometry (DXA). Comput Electron Agric 42:1–17

Barcelon EG, Tojo S, Watanabe K (1999) X-ray computed tomography for internal quality evaluation of peaches. J Agric Eng Res 73(4):323–330
Barcelon EG, Tojo S, Watanabe K (2000) Nondestructive ripening assessment of mango using an X-ray computed tomography. Agric Eng J 9(2):73–80
Barreiro P, Ortiz C, Ruiz-Altisent M et al (2000) Mealiness assessment in apples and peaches using MRI techniques. Magn Reson Imaging 18:1175–1181
Brusewitz GH, Stone ML (1987) Wheat moisture by NMR. Trans ASAE 30(3):858–862
Buzzell P, Pintauro S (2003) Dual energy X-ray absorptiometery. Department of Food Sciences and Nutrition, University of Vermont. http://nutrition.uvm.edu/bodycomp/dexa/. Accessed 6 Jan 2003
Casasent DA, Sipe MA, Schatzki TF et al (1998) Neural net classification of X-ray pistachio nut data. Lebenson Wiss Technol 31(2):122–128
Casasent D, Talukder A, Keagy P et al (2001) Detection and segmentation of items in X-ray imagery. Trans ASAE 44(2):337–345
Chen P, McCarthy MJ, Kauten R (1989) NMR for internal quality evaluation of fruits and vegetables. Trans ASAE 32(5):1747–1753
Chen P, McCarthy MJ, Kauten R et al (1993) Maturity evaluation of avocados by NMR methods. J Agr Eng Res 55:177–187
Cho BK, Chayaprasert W, Stroshine RL (2008) Effects of internal browning and watercore on low field (5.4 MHz) proton magnetic resonance measurements of T2 values of whole apples. Postharvest Biol Technol 47:81–89
Clark CJ, Hockings PD, Joyce DC et al (1997) Application of magnetic resonance imaging to pre- and post-harvest studies of fruits and vegetables. Postharvest Biol Technol 11:1–21
Cuningham IA, Judy PF (2000) Computed tomography. In: JD Bronzino (ed) The biomedical engineering handbook, 2nd edn. CRC Press, Boca Raton, FL. http://www.kemt.fei.tuke.sk/. Accessed 2 Nov 2009
Curry TS, Dowdey JE, Murry RC (1990) Christensen's physics of diagnostic radiology, 4th edn. Williams and Wilkins, Baltimore, MD
Diener RG, Mitchell JP, Rhoten ML (1970) Using an X-ray image scan to sort bruised apples. Agric Eng 51:356–361
Dogan H (2007) Nondestructive imaging of agricultural products using X-ray microtomography. Microsc Microanal 13(2):1316 CD–1317 CD
Fornal J, Jelinski T, Sadowska J et al (2007) Detection of granary weevil *Sitophilus granarius* (L.) Eggs and internal stages in wheat grain using soft X-ray and image analysis. J Stored Prod Res 43:142–148
Gonzalez JJ, Valle RC, Bobroff S et al (2001) Detection and monitoring of internal browning development in 'fuji' apples using MRI. Postharvest Biol Technol 22:179–188
Haff RP, Slaughter DC (2004) Real-time X-ray inspection of wheat for infestation by the granary weevil, *Sitophilus granarius* (L.). Trans ASAE 47(2):531–537
Han YJ, Bowers SV, Dodd RB (1992) Nondestructive detection of split-pit peaches. Trans ASAE 35(6):2063–2067
Haseth TT, Egelandsdal B, Bjerke F et al (2007) Computed tomography for quantitative determination of sodium chloride in ground pork and dry cured hams. J Food Sci 72(8): E–420–E427
Hubbell JH, Seltzer SM (1995) Tables of X-ray mass attenuation coefficients and mass energy absorption coefficients and mass energy absorption coefficients 1 keV to 20 MeV for elements $Z = 1$ to 92 and 48 additional substances of dosimetric interest. NISTIR 5632. National Institute of Standards and Technology, US Department of Commerce, Gaithersburg, MD, USA.
Karunakaran C, Jayas DS, White NDG (2004) Identification of wheat kernels damaged by the red flour beetle using X-ray images. Biosyst Eng 87(3):267–274
Keagy PM, Parvin B, Schatzki TF (1996) Machine recognition of navel orange worm damage in X-ray images of pistachio nuts. Lebenson Wiss Technol 29(1&2):140–145

Kim SM, Chen P, McCarthy MJ et al (1999) Fruit internal quality evaluation using on-line nuclear magnetic resonance sensors. J Agric Eng Res 74:293–301
Kim S, Schatzki TF (2000) Apple water-core sorting system using X-ray imagery: I Algorithm development. Trans ASAE 43(6):1695–1702
Kim S, Schatzki TF (2001) Detection of pinholes in almonds through X-ray imaging. Trans ASAE 44(4):997–1003
Kotwaliwale N, Subbiah J, Weckler PR et al (2007a) Calibration of a soft X-ray digital imaging system for biological materials. Trans ASABE 50(2):661–666
Kotwaliwale N, Weckler PR, Brusewitz GH (2006) X-ray attenuation coefficients using polychromatic X-ray imaging of pecan components. Biosyst Eng 94(2):199–206
Kotwaliwale N, Weckler PR, Brusewitz GH et al (2007b) Non-destructive quality determination of pecans using soft X-rays. Postharvest Biol Technol 45:372–380
Kroger C, Bartle CM, West JG et al (2006) Meat tenderness evaluation using dual energy X-ray absorptiometry (DEXA). Comput Electron Agric 54:93–100
Lammertyn J, Jancsok P, Dresselaers T et al (2003) Analysis of the time course of core breakdown in 'conference' pears by means of MRI and X-ray CT. Postharvest Biol Technol 29:19–28
Leonard A, Blacher S, Nimmol C et al (2008) Effect of far-infrared radiation assisted drying on microstructure of banana slices: an illustrative use of X-ray microtomography in microstructural evaluation of a food product. J Food Eng 85:154–162
Lim KS, Barigou M (2004) X-ray micro-computed tomography of cellular food products. Food Res Int 37:1001–1012
Marigheto N, Venturi L, Hills B (2008) Two-dimensional NMR relaxation studies of apple quality. Postharvest Biol Technol 48:331–340
McCarthy MJ (1994) Magnetic resonance imaging in foods. Chapman and Hall, New York
Mousavi R, Miri T, Cox PW et al (2007) Imaging food freezing using X-ray microtomography. Int J Food Sci Technol 42:714–727
Narvankar DS, Singh CB, Jayas DS et al (2009) Assessment of soft X-ray imaging for detection of fungal infection in wheat. Biosyst Eng 103:49–56
Neethirajan S, Jayas DS, Karunakaran C (2007) Dual energy X-ray image analysis for classifying vitreousness in durum wheat. Postharvest Biol Technol 45:381–384
Neethirajan S, Karunakaran C, Jayas DS et al (2006b) X-ray computed tomography image analysis to explain the airflow resistance differences in grain bulks. Biosyst Eng 94:545–555
Neethirajan S, Karunakaran C, Symonsc S et al (2006a) Classification of vitreousness in durum wheat using soft X-rays and transmitted light images. Comput Electron Agric 53:71–78
Ogawa Y, Morita K, Tanaka S et al (1998) Application of X-ray CT for detection of physical foreign materials in foods. Trans ASAE 41(1):157–162
Paiva RFD, Lynch J, Rosenberg E et al (1998) A beam hardening correction for X-ray microtomography. NDT&E Int 31(1):17–22
Pearce KL, Ferguson M, Gardner G et al (2009) Dual X-ray absorptiometry accurately predicts carcass composition from live sheep and chemical composition of live and dead sheep. Meat Sci 81:285–293
Schatzki TF, Haff RP, Young R et al (1997) Defect detection in apples by means of X-ray imaging. Trans ASAE 40(5):1407–1415
Sonego L, Ben-Arie R, Raynal J et al (1995) Biochemical and physical evaluation of textural characteristics of nectarines exhibiting woolly breakdown: NMR imaging, X-ray computed tomography and pectin composition. Postharvest Biol Technol 5:187–198
Thomas P, Kannan A, Degwekar VH et al (1995) Non-destructive detection of seed weevil-infested mango fruits by X-ray imaging. Postharvest Biol Technol 5(1–2):161–165
Tollner EW, Gitaitis RD, Seebold KW et al (2005) Experiences with a food product X-ray inspection system for classifying onions. Trans ASAE 21(5):907–912
Tollner EW, Hung YC, Upchurch BL et al (1992) Relating X-ray absorption to density and water content in apples. Trans ASAE 35(6):1921–1928

Yacob Y, Ahmad H, Saad P et al (2005) A comparison between X-ray and MRI in postharvest non-destructive detection method. Proceedings of the International Conference on Information Technology and Multimedia at UNITEN (ICIMU '05), Malaysia

Zwiggelaar R, Bull CR, Mooney MJ (1996) X-ray simulations for imaging applications in the agricultural and food industries. J Agric Engng Res, 63, 161–170

Zwiggelaar R, Bull CR, Mooney MJ (1997) Detection of "soft" materials by selective energy X-ray transmission imaging and computer tomography. J Agric Eng Res 66(3):203–212

Chapter 6
Near Infrared Spectroscopy

Shyam N. Jha

The discovery of near-infrared energy is ascribed to Herschel in the nineteenth century; the first industrial application however began in the 1950s. Initially near infrared spectroscopy (NIRS) was used only as an add-on unit to other optical devices, that used other wavelengths such as ultraviolet (UV), visible (Vis), or mid-infrared (MIR) spectrometers. In the 1980s, a single unit, stand-alone NIRS system was made available, but the application of NIRS was focused more on chemical analysis. With the introduction of light-fibre optics in the mid 1980s and the monochromator-detector developments in early 1990s, NIRS became a more powerful tool for scientific research. This optical method can be used in a number of fields of science including physics, physiology, medicine and food.

The use of NIRS as rapid and often nondestructive technique for measuring the composition of biological materials has been demonstrated for many commodities. This method is now no longer new even in the field of food; as it started in early 1970 in Japan, just after some reports from America. Even an official method to determine the protein content of wheat is available. The National Food Research Institute (NFRI), Tsukuba has since been become a leading institute in NIRS research in Japan and Central Institute of Post-harvest Engineering and Technology (CIPHET) is considered pioneer for conducting research in the field of quality determination of food using NIRS in India. The major advantages of NIR Spectroscopy are:

(i) No sample preparation

Since the bands in the near infrared (NIR) are mainly overtones and combinations they are less intense than the bands (primary vibrations) in the MIR region. Because of this, samples can be measured directly without any dilution.

(ii) No waste

Spectroscopic methods are ideal since the sample is measured directly and is retained. Thus, there is no tedious sample preparation involved and there are no waste materials such as toxic solvents.

S.N. Jha (✉)
Central Institute of Post-Harvest Engineering and Technology, Ludhiana 141004, Punjab, India
e-mail: snjha_ciphet@yahoo.co.in

S.N. Jha (ed.), *Nondestructive Evaluation of Food Quality*,
DOI 10.1007/978-3-642-15796-7_6,

(iii) Fast measurements

NIR Spectrometers can analyze the sample and calculate results in seconds, thereby providing instant answers and increasing sample throughput.

(iv) Glass containers

Glass is transparent in the NIR. Thus samples can be measured in their containers, or liquids can be easily analyzed in inexpensive disposable glass vials and test tubes.

(v) Water

Water as compared to other solutions has less absorbance in the NIR region. Thus, aqueous solutions can be measured directly, with careful control of the sample temperature.

(vi) Fibre optic sampling

High quality quartz fibre optics can be used to transmit NIR light over a long distance without significant loss of intensity. These sampling accessories are very robust and are ideally suited for use in factory environment. Using fibre optic probes, materials can be analyzed remotely in large containers and reaction vessels.

(vii) Easy and accurate analysis

Since NIR methods require no sample preparation, the amount of sampling error is significantly reduced thereby improving the accuracy and reproducibility of the measurement. Furthermore since the sample is not destroyed during the analysis the measurement can also be repeated.

(viii) Analysis Costs

In comparison with wet chemical analysis, for NIR, there is an inverse relationship with quantity and cost. The major costs for NIR are incurred during the initial implementation of the methods. Thus, as the number of samples increases the cost per analysis decreases.

(xi) Measurement in fields

Nowadays small portable and robust NIR spectrometers are available and can be carried to any site. So, one can even observe the change in behaviors of individual fruits during their growth leaving them in tree till their full maturity.

(x) Skill requirements:

NIRS technique is so robust and user friendly, that once an instrument is calibrated, the day-to-day analysis is a simple task and does not require the user to learn any elaborate procedures. It can be used very easily even by a semi or an unskilled person. It does not require special skill to operate and drawing inferences from the data.

6.1 Theory

NIR is a spectroscopic method which uses the near infrared region of the electromagnetic spectrum (from about 700 nm to 2,500 nm). It is based on molecular overtone and combination vibrations. As a result, the molar absorptivity in the NIR

region is typically quite small, but one advantage is that NIR can typically penetrate much deeper into a sample than mid infrared radiation. NIRS is therefore not only a particularly sensitive technique, but it can be very useful in probing bulk material with little or no sample preparation. The molecular overtone and combination bands seen in the NIR are typically very broad, leading to complex spectra. It therefore can be difficult to assign specific features to specific chemical components. Multivariate (multiple wavelength) calibration techniques (e.g., principal components analysis or partial least squares, which will be dealt in later part of this chapter) are often employed on absorbance, transmittance or reflectance data to extract the desired chemical information. Careful development of a set of calibration samples and application of multivariate calibration techniques is essential for near infrared analytical methods. Interactions of light with matter have already been discussed in Chap. 2, therefore, other theoretical aspects of NIR are discussed hereunder:

6.1.1 Properties of Electromagnetic Radiation

Infrared is a part of electromagnetic radiation, which is considered as a simple harmonic wave. The electric and magnetic properties of these waves are interconnected and interact with matter to give rise to a spectrum. A simple harmonic motion has a property of the *sine* wave defined by Eq. (6.1)

$$y = A \sin \theta \tag{6.1}$$

where y is the displacement with a maximum value of A, and θ is an angle varying between zero and 2π radians.

Now consider a point P traveling with uniform angular velocity ω rads^{-1} in a circular path of radius A (Fig. 6.1); P describes an angle $\theta = \omega t$ radians after t s passing Q and its vertical displacement therefore is

$$y = A \sin \omega t \tag{6.2}$$

Equation (6.2) is presented in graphical form in the right hand side of Fig. 6.1. P will return to Q after $2\pi/\omega$ s and complete one cycle in 1 s and the pattern will be repeated $\omega/2\pi$ times. This is called the frequency (ν) of the wave and the basic equation of the wave motion then may be written as:

$$y = A \sin 2\pi \nu t \tag{6.3}$$

The wavelength (λ), the distance traveled in a complete cycle, is another property of the wave. The Eq. (6.3) is required to be expressed in terms of variation of displacement with distance instead of with time. This is done by substituting $t = l/c$ where l is the distance covered by the wave in time t at velocity c. The

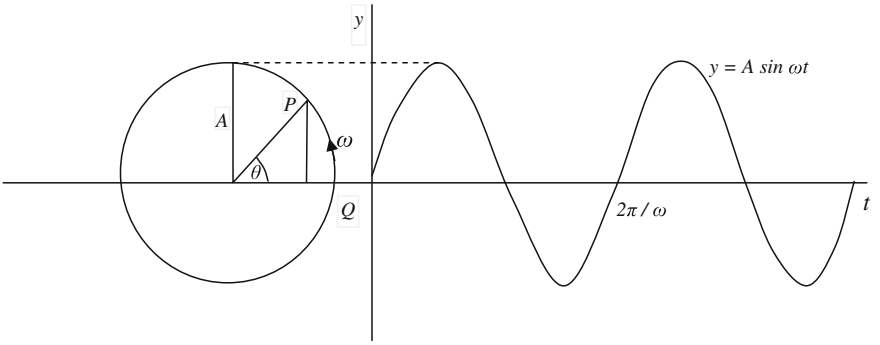

Fig. 6.1 Wave representation of electromagnetic radiation

velocity c is known as the velocity of light in vacuum and is the universal constant. The wavelength therefore may be defined as:

$$\lambda = c/\nu \tag{6.4}$$

Wavenumber ($\bar{\nu}$), defined as the reciprocal of wavelength in centimeter, is another way of expressing the character of the electromagnetic radiation. The wavenumber therefore is considered as the number of waves or cycles per centimeter of radiation. Spectroscopists describe the position of an infrared (IR) absorption band in term of wavenumber. It is directly proportional to frequency ($\nu = c\bar{\nu}$) and is related to the energy changes involved in transitions between different vibrational states.

The wave model is employed to explain many properties of electromagnetic radiation, but it fails to describe phenomenon associated with the absorption or emission of energy. It is therefore necessary to view electromagnetic radiation as a stream of discrete particles called photons with an energy proportional to the frequency of the radiation (Eq. 6.14).

6.1.2 Properties of Vibrating Molecules

(a) The harmonic oscillator

Mechanical model: To understand the harmonic oscillation of a molecule in vibration, consider a mass m at one end of a spring which is fixed at the other end. The force of gravity is constant and therefore only influence is the equilibrium point and not the motion of the masses about that point. The disturbance of the mass along the axis of the spring results in motion, which may be described by Hooke's law. This state that the restoring force F exerted by spring is proportional to distance y that it has traveled from the equilibrium position

$$F = -ky \tag{6.5}$$

where k is a force constant. The acceleration a of the mass from equilibrium is

$$a = \frac{d^2y}{dt^2} \tag{6.6}$$

and by applying Newton's second law of motion, $F = ma$,

$$\frac{md^2y}{dt^2} = -ky \tag{6.7}$$

A solution of the differential equation (6.7) is

$$y = A \sin \alpha t \tag{6.8}$$

where α is the positive square root of k/m. After one period of motion, y returns to its initial value and the *sine* wave repeats each time and αt is increased by $2\pi\nu$. From this, it may be derived as

$$\nu = \frac{1}{2\pi}\sqrt{\frac{k}{m}} \tag{6.9}$$

Putting $\alpha = \sqrt{k/m} = 2\pi\nu$ into Eq. (6.8) we get Eq. (6.3). The electromagnetic waves and mechanical oscillators therefore, by first approximation, may be described in the same terms, and the significance of spectroscopic measurements lies in the association between the frequency of radiant energy and the frequencies of molecular motions. Equation (6.9) may be modified to describe the behavior of a system consisting of two masses m_1 and m_2 connected by a spring, by substituting the reduced mass $\mu = (m_1m_2)/(m_1 + m_2)$ for m,

$$\nu = \frac{1}{2\pi}\sqrt{\frac{k}{\mu}} \tag{6.10}$$

Any system containing more than two masses follows similar or more complex equations. The vibration of a chemical bond therefore may be considered analogous to the behavior of the spring when m_1 and m_2 become the masses of two atoms and k is the force constant for the chemical bond. Using this simple mechanical model, it is possible to explain many spectral observations in the IR. For example, compound containing a carbonyl group C=O has been found experimentally to have an IR band in the region $\bar{\nu} = 1{,}500$–$1{,}900\ \text{cm}^{-1}$ (Osborne et al. 1983).

Putting $\nu = c\bar{\nu}$ and approximate values of 1×10^3 Nm^{-1} for the force constant of a double bond, 2×10^{-26} and 2.7×10^{-26} kg for the masses of carbon and oxygen, respectively, and 3×10^8 ms^{-1} for the velocity of light into Eq. (6.10), we get

$$\bar{\nu} = \frac{1}{2\times3.14\times3\times10^8}\sqrt{\frac{1\times10^3(2+2.7)\times10^{-26}}{2\times2.7\times10^{-52}}}$$

$$= 1.565\times10^5 m^{-1}, \text{or } 1565\ cm^{-1}$$

Considering the mass and spring model, it is obvious that the energy of the system undergoes cyclic conversion from potential energy to kinetic energy. The potential energy diagram for a harmonic oscillator is presented as the dotted curve in Fig. 6.2. At the equilibrium position, potential energy may be

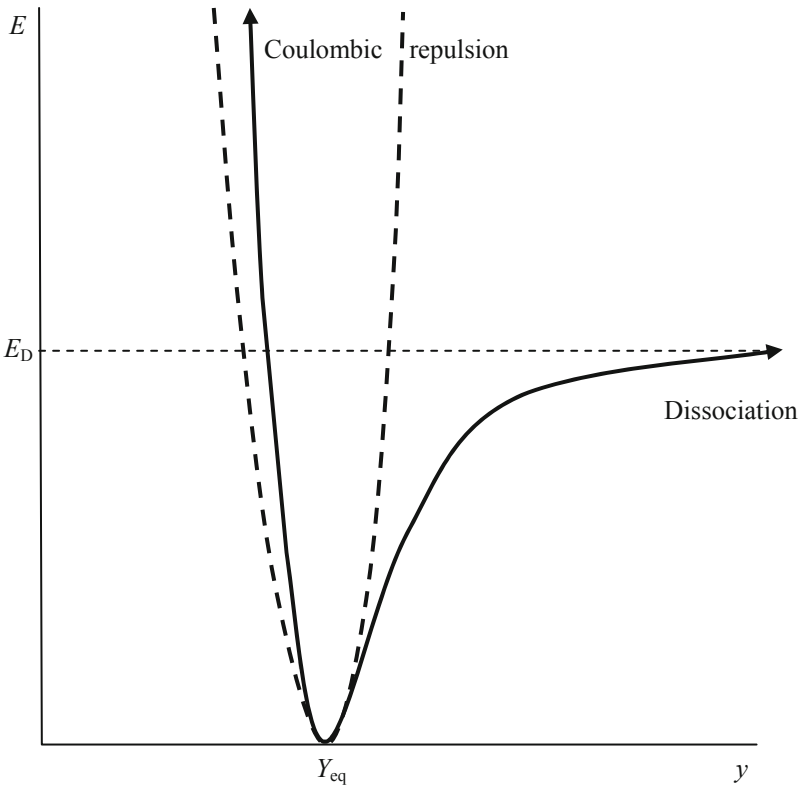

Fig. 6.2 The energy of a diatomic molecule undergoing simple harmonic motion (*dotted curve*) and anharmonic vibration (*firm curve*)

considered to be zero but as the spring is compressed or stretched by a small amount dE,

$$dE = -Fdy \tag{6.11}$$

combining Eqs. (6.5) and (6.11) we get

$$dE = kydy \tag{6.12}$$

Integrating from $y = 0$ to y

$$\int_0^E dE = k\int_0^y ydy$$

$$E = k\frac{y^2}{2} \tag{6.13}$$

The kinetic energy is zero and the total energy is potential energy at the turning point of the motion corresponding to maximum amplitude A. At the equilibrium position spring gets compressed or stretched and the energy reverts to kinetic and decreases parabolically to zero.

Quantum mechanical model: Towards the end of the 20th century experimental data were not sufficiently available to support the postulation that matter can take up energy continuously. Max Planck in 1900 proposed that the energy of an oscillator is discontinuous, changes in its content and only occur by means of transition between two discrete energy states brought about by the absorption or emission of discrete packets of energy called quanta. This idea was known as the quantum theory and the energy levels are identified by integers called quantum numbers.

When appropriate amount of energy $\Delta E = E_2–E_1$ either is absorbed or emitted by the system, transition occurs between energy levels E_1 and E_2 (Fig. 6.3). Planck further proposed that this energy takes the form of the electromagnetic radiation and frequency of that radiation is related to the energy change ΔE by the equation as follows:

$$\Delta E = h\nu \tag{6.14}$$

where h is universal Planck's constant. Equation (6.14) signifies that if a radiation beam containing a wide range of frequencies is directed onto a molecule in energy state E_1, energy will be absorbed from the beam and a transition to energy state E_2 will occur. A detector placed to collect the radiation after its interaction with the molecule shows that the intensity of the radiation

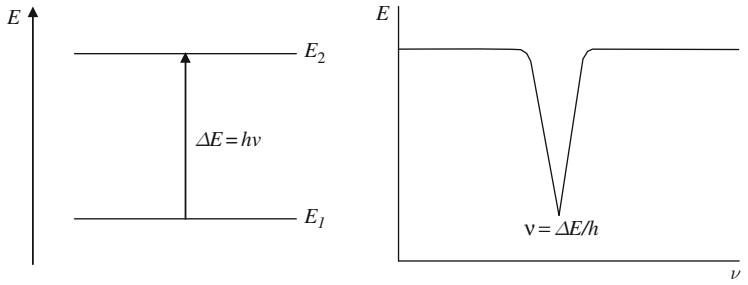

Fig. 6.3 Depiction of the quantum theory of absorption and radiation

decreases at frequency $\nu = \Delta E/h$ and all other frequencies remain undiminished and produces the absorption (Fig. 6.3). In practice, the number of energy levels for a molecule is infinite, there are many possible transitions and therefore a spectrum even from the simplest molecule would be very complex.

A molecule in space possesses many forms of energy such as vibrational energy due to periodic displacement of its atoms from their equilibrium position and rotational energy due to rotation of body about its center of gravity. Absorption of IR radiation is largely confined to molecular species for which energy differences exist between different vibrational and rotational states. The energy required to cause a change in rotational states is, however, very much smaller than for vibrational states and rotational absorption bands may only be absorbed in the case of gases. Therefore, for the study of IR spectra of solid and liquid samples, only vibration motion needs to be considered.

Vibration energies, like other molecular energies, are quantized and the allowed vibrational energies for any particular system are found by solving a series of partial differential equations known as quantum mechanical wave equation. Solution of these equations assuming a simple harmonic oscillator are found for energy levels as below (Eq. 6.15)

$$E = (\upsilon + 0.5)\, h\nu \tag{6.15}$$

where υ is the vibrational quantum number (0,1,2,. . .). From Eq. (6.15), it may be seen that the lowest vibrational energy level E_0 is at $\upsilon = 0$ is $h\nu/2$. Therefore, a molecule can never have zero vibrational energy because an atom can never be completely at rest relative to each other. E depends only on the strength of the chemical bond and the atomic masses. Prediction of E is the basic difference between wave mechanical and classical approaches to molecular vibrations. Promotion to first excited state ($\upsilon = 1$) thus requires absorption of radiation of energy, $\left(3\,h\nu/2\right) - \left(h\nu/2\right) = h\nu$; the frequency ($\nu$) of radiation that will bring about this change is identical to the vibration frequency of the bond defined by Eq. (6.10), therefore

$$\Delta E = \frac{h}{2\pi}\sqrt{\frac{k}{\mu}} \tag{6.16}$$

From Eq. (6.15) it can be seen that ΔE given by Eq. (6.16) is the energy associated with transition between any pair of adjacent levels.

Selection rules: (1) According to quantum theory, the allowed vibrational transitions are those in which υ changes by one ($\Delta\upsilon = \pm 1$).

(2) Spectral bands are observed if the vibration interacts with the radiation. Vibration due to radiation therefore is electromagnetic in origin and such interaction depends upon the existence of an electric moment across the vibrating bond. Thus, homo-nuclear diatomic molecules for example, do not exhibit vibrational absorption bands. It is sufficient, however, for polar bonds to be present molecular vibration which causes a temporarily induced dipole moment. In order to understand the anharmonicity selection rules, Mills' group at Readings University (England) used a high resolution spectrophotometer to study the NIR spectra of small molecules in the vapour phase (Holland et al. 1990).

(b) The anharmonic oscillator

Quantum-mechanical treatment of a harmonic oscillator explains the observed IR absorption bands due to fundamental modes of molecular vibration but it does not explain the presence of overtone bands in the NIR. These bands arise from transitions when $\Delta\upsilon$ is ± 2, ± 3 etc. and so are forbidden by selection rule (1) above. This anomaly is because real molecules do not obey exactly the laws of simple harmonic motion and real bonds, although elastic; do not obey Hooke's law exactly. As two atoms approach one another, Coulombic repulsion between the two nuclei causes the potential energy to rise more rapidly than the harmonic approximation predicts, and, when the interatomic distance approaches at which dissociation occurs, potential energy levels off (Fig. 6.2). It may be seen from the dotted curve in Fig. 6.2 that the success of the harmonic model stems from the fact that the two curves are almost identical at low potential energies. An empirical function due to Morse, fits the solid curve in Fig. 6.2 to a good approximation as below (Eq. 6.17):

$$E = E_d(1 - e^{-\alpha y})^2 \tag{6.17}$$

where α is a constant for a particular molecule and E_d is dissociation energy. Equation 6.17 is used to solve the wave mechanical equation. The solution for the so-called an-harmonic oscillator becomes as in Eq. (6.18).

$$E = (\upsilon + 0.5)h\nu - (\upsilon + 0.5)^2\, h\nu x - (\upsilon + 0.5)^3\, h\nu x' - \ldots \tag{6.18}$$

where x, $x'\ldots$. are small and positive an harmonicity constants which decreases in magnitude. For small values of υ, the third term and beyond in Eq. (6.18) may be ignored and then we get (Eq. 6.19)

$$E \approx (\upsilon + 0.5)h\nu - (\upsilon + 0.5)^2\, h\nu x \approx h\nu[1 - x(\upsilon + 0.5)](\upsilon + 0.5) \quad (6.19)$$

Equation (6.15) gives the same energy level as Eq. (6.19) if ν are replaced by

$$\nu' = \nu[1 - x(\upsilon + 0.5)] \quad (6.20)$$

The anharmonic oscillator thus behaves like the harmonic oscillator with an oscillation frequency which decreases steadily with increasing υ. E_0 is now ($h\nu$/2) (1–0.5x), and the energy associated with a transition from υ to υ+$\Delta\upsilon$ may be expressed as (Eq. 6.21).

$$\Delta E = h\nu[1 - (2\upsilon + \Delta\upsilon + 1)x] \quad (6.21)$$

According to selection rules $\Delta\upsilon = \pm 1, \pm 2, \pm 3, \ldots$. They are therefore same as for the harmonic oscillator but with the additional possibility of larger jumps. These are in practice of rapidly diminishing probability, and normally bands only due to $\Delta\upsilon = \pm 1, \pm 2$ and ± 3, at the most, have observable intensity. Furthermore, according to Maxwell-Boltzmann law almost all molecules in a particular sample at room temperature remains at the lowest energy level. According to this law, proportionality of molecules in an excited state n_1/n_2, where n_1 is the number of molecules in the excited state and n_2 the number of molecules in the ground state, is in the form of an exponential function (Eq. 6.22)

$$\frac{n_1}{n_2} = e^{-\Delta E/kT} \quad (6.22)$$

where k is the Boltzmann constant and T is the absolute temperature. $\Delta E = h\nu \gg kT$ at room temperature.

Three most important transitions according to above discussion in IR spectroscopy may be as:

(i) $\upsilon = 0 \rightarrow \upsilon = 1; \Delta\upsilon = +1$
$\Delta E = h\nu(1 - 2x)$
(ii) $\upsilon = 0 \rightarrow \upsilon = 2; \Delta\upsilon = +2$
$\Delta E = 2\,h\nu(1 - 3x)$
(iii) $\upsilon = 0 \rightarrow \upsilon = 3; \Delta\upsilon = +3$
$\Delta E = 3\,h\nu(1 - 4x)$

At $x \approx 0.01$, the three bands approximately lie very close to ν, 2ν, and 3ν. The line near ν is called the fundamental absorption, while those near 2ν and 3ν are called the first and second overtones, respectively. The highest wavenumber at which absorption of radiation at fundamental vibration frequencies occurs is about 4,000 cm^{-1} and the region between 4,000 and 14,300 cm^{-1} is termed as NIR in which absorption at overtones frequencies occurs. In addition to overtone bands, combination and difference bands

are possible theoretically if two or more different vibrations interact to give bands with frequencies that are the sums or differences of multiples of their fundamental frequencies as in Eq. (6.23),

$$\nu_{comb} = n_1\nu_1 \pm n_2\nu_2 \pm n_3\nu_3 \pm .... \tag{6.23}$$

where n_1, n_2,.... are positive integers. Combination bands are of very low probability unless they arise from no more than two vibrations involving bonds, which are either connected through a common item, or multiple bonds. Difference bands, which are due to absorption by molecules residing in excited vibrational states, are of very low probability at room temperature as a consequence of Eq. (6.22).

NIR region of the electromagnetic spectrum is from about 700 to 2,500 nm and whole IR range may be divided both instrumentally and functionally into near, middle and far IR (Table 6.1). The far IR is the region in which rotation absorptions occur and will not be discussed further in this chapter.

(c) Chemical assignments of near infrared bands

Modes of vibration

It is necessary to define the number of momentum co-ordinates required to describe the system for calculating the number of possible modes of vibration for a polyatomic molecule. A space is defined using three co-ordinates. To define n points in space therefore $3n$ co-ordinates are required. Three of these momentum co-ordinates define the translational motion of the entire molecule and another three the rotational motion of the same. This gives $3n$–6 co-ordinates to describe the inter-atomic vibrations. A linear molecule only requires two co-ordinates to describe the rotational motion because rotation about the bond axis is not possible. There are therefore $3n$–5 modes in this case are possible. Each of these possible vibrations is represented by a separate potential energy curve and is subjected to the selection rules described above. For a very simple molecule, it is possible to describe the nature as well as the number of vibrational modes, which, with reference to a tri-atomic molecule or group AX_2 are shown in Fig. 6.4.

Vibration is categorized either as stretching or bending. If there is a continuous change in the inter-atomic distance along the axis of the bond between the two atoms, vibration is called as stretching, which may occur symmetrically

Table 6.1 Approximate ranges of the infrared region

Region	Characteristic transitions	Wavelength range (nm)	Wavenumber (cm^{-1})
Near infrared (NIR)	Overtones combinations	700–2,500	14,300–4,000
Middle infrared (MIR)	Fundamental vibrations	2,500–5 $\times 10^4$	4,000–200
Far infrared (FIR)	Rotations	5 $\times$ 10^4–10^6	200–10

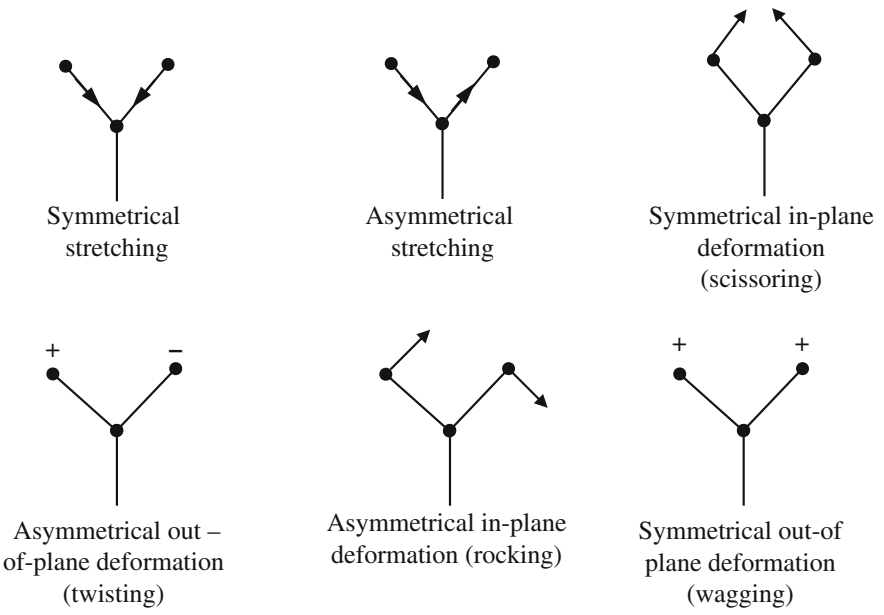

Fig. 6.4 Modes of vibration of a group AX_{2z}

in a tri-atomic group of atoms AX_2, whereas the two A–X bonds vibrate in and out together or, asymmetrically when they vibrate in opposite directions. Vibration involving a change in bond angle is known as bending and is further classified into four types: scissoring, rocking, wagging and twisting. These are also known as symmetrical in-plane deformation, asymmetrical in-plane deformation, symmetrical out-of-plane deformation and asymmetrical out-of-plane deformation, respectively (Fig. 6.4). Each of these vibration modes give rise to overtones combinations observable in the NIR. The intensity of such bands however depends on degree of anharmonicity. Bond involving hydrogen, the lightest of atoms, vibrate with large amplitude when undergoing stretching and therefore motion is deviated appreciably from harmonic. Consequently, almost all the absorption bands observed, arise from overtones of hydrogenic stretching vibrations involving AH_y functional groups or combinations thereof involving stretching and bending modes of vibration of such groups in the NIR range.

(d) Interpretation of NIR spectra

It is evident from the above discussion that the most NIR spectra may be explained by assignment of the band of overtones and combination of fundamental vibrations involving hydrogenic stretching modes. The position of fundamental bonds in the IR are very well documented (Bellamy 1975) and as a starting point, it is possible to use them for prediction of the positions of the corresponding overtone bands.

(i) Carbon-hydrogen (CH) overtone bands

The carbon-hydrogen bond is the most important organic molecules and its fundamental stretching bands lie in the region $\bar{\nu} = 2{,}972$–$2{,}843\ \text{cm}^{-1}$ for alkanes, 3,010–3,095 cm^{-1} for alkenes, and aromatic systems 3,310–3,320 cm^{-1} for alkynes. The first overtone bands in alkanes would therefore be expected to be found around $2\bar{\nu}\ \text{cm}^{-1}$ or $10^7/2\bar{\nu}$ nm $=1{,}700$ nm. The position may, however, be predicted more accurately by applying the formula (Eq. 6.24)

$$\bar{\nu} = n\bar{\nu}_0(1 - nx) \tag{6.24}$$

where $\bar{\nu}$ is the wavenumber of the overtone band, x is anharmonicity constant (0.01 as first approximation) and n is an integer which has the same value as $\Delta\upsilon$, i.e. 2 for the first overtone. Using Eq. 6.24, it is possible to construct a table of predicted wavelength and compare these with observed values. Tosi and Pinto (1972) studied NIR spectra of fifty alkanes from 1,690 to 1,770 nm and identified five bands at 1,693, 1,710, 1,724, 1,757 and 1,770 nm while Wheeler (1959) reported bands at 1,695 and 1,705 nm for methyl group and 1,725 and 1,765 nm for the methylene group. Rose (1938) reported methylene bands at 1,730 and 1,764 nm and methyl bands at 1,703, 1,707, 1,724 nm. Thereafter many researchers have identified various bands corresponding to various chemical constituents and combinations thereof.

A similar analysis may be applied to the weaker second overtone band which is expected to be around 1,150 nm. The observed position for absorption by methyl and methylene respectively are 1,190 nm and 1,210 nm (Liddel and Kasper 1933, Rose 1938) or 1,195 and 1,215 nm (Wheeler 1959). In polymers, methylene bands were observed at 1,214 nm in polyethene and 1,206 nm in nylon (Glatt and Ellis 1951). The third overtone exhibits extremely weak absorption in the region of 880 nm. The relative absorptivities of the first, second and third CH stretch overtones in case of chloroform are in the ratio of 484:22:1 (Lauer and Rosenbaum 1952). The first and second overtones of aromatic CH group are at 1,685 and 1,143 nm (Wheeler 1959), second overtone lie in the region 1,136–1,149 nm (Liddel and Kasper 1933) and first and second overtone at 1,695 and 1,143 nm (Rose 1938). Terminal methylene first overtone bands lie in the region 1,611–1,636 nm (Goddu 1960), and terminal methylene as in pent-1-yne at 1,533 nm. The presence of polar substitutes may considerably change the wave length, at which, fundamental C–H vibration and overtones occur.

More complex molecules follow the similar CH stretch overtone bands, though more complex patterns, due to the effect of C–C coupling of the chain units. Polythene exhibits bands 1,730 and 1,763 nm due to CH_2 first overtone and 1,214 due to second overtone (Glatt and Ellis 1951). Poly (2-methylpropane) exhibits bands at 1,760 and 1,210 nm due to methylene and 1,690 and 1,200 nm due to methyl; polypropene 1,750, 1,700 and 1,200 nm; polyphenylethene typical aromatic bands at 1,650 and 1,150 nm (Foster et al. 1964) The CH bands in nylon (Glatt and Ellis 1951) and proteins (Hecht

and Wood 1956) occur in the same region as similar compounds without the peptide group; e.g. 1,190, 1,700 1,730, and 1,760 nm in wheat protein (Law and Tkachuk 1977). Starch and pentosans have bands at 1,200, 1,700 1,720, 1,780 nm while wheat lipid has 1,170, 1,210, 1,720, 1,760 nm (Law and Tkachuk 1977). Fatty acids have CH_2 first overtone bands at 1,740 and 1,770 nm and =CH first overtone at 1,680 nm (Holman and Edmondson 1956).

(ii) Oxygen–hydrogen (OH) overtone bands

The NIR bands assignable to first to third overtones of OH stretch, in case of water, is at 1,450, 970 and 760 nm (Curcio and Petty 1951). The position of three bands with all OH bands is dependent on temperature and hydrogen bonding environment, although the first overtone of OH in water bound to protein was also observed at 1,450 nm. The OH first overtone bands in alcohol and phenols occur in the region 1,405–1,425 nm (Goddu 1960) with second overtone between 945 and 985 nm. Iwamoto et al. (1987) have postulated that the band in 1,450 nm region is a composite of three bands due to water molecules with no hydrogen bond, one hydrogen bond and two hydrogen bonds at 1,412 1,466, and 1,510 nm, respectively. These bands shift as a consequence of water solute interactions and hence may be useful in the study of the state of water in foods.

The effect of hydrogen bonding in carbohydrates and cyclic alcohols was studied and three bands were observed in spectra of cyclohexanol (Trott et al. 1973), α-D-glucose and glycogen (Table 6.2). The first band at about 1,440 nm in the carbohydrates was attributed to first overtone of the stretching vibration of a free OH group while those about 1,490 and 1,580 nm were due to an intra and intermolecular hydrogen bonded OH group respectively. Osborne and Douglas (1981) reported a similar effect in the case of wheat starch and the first two bands were observed at 1,450 and 1,540 nm by Law and Tkachuk (1977).

(iii) Nitrogen–hydrogen overtone bands

Overtone bands of primary amines are expected to be at about 1,500 and 1,530 nm due to NH stretch first overtone and a band at about 1,000 nm due to the second overtone. Secondary amines should have a single band at about 1,520–1,540 nm and 1,030 nm and aromatic primary amines at 1,460,

Table 6.2 Bands due to O–H stretch first overtone band (Trott et al. 1973)

	Free OH	H-bond (intra-molecular)	H-bond (inter-molecular)
Cyclohexanol	1,417	1,520	1,573
α-D-glucose	1,443	1,484	1,581
Glycogen	1,445	1,481	1,581
	1,440	1,470	1,575
Starch	1,440	1,528	1,588
	1,450	1,540	–

1,500 and 1,000 nm. No band due to the amine group would be expected in case of tertiary amines. Methylamine and dimethylamine have bands at 1,520 and 1,528 nm respectively. NH bands due to amine are not temperature sensitive though the same are displaced by hydrogen bonding. In the spectrum of nylon, for example (Glatt and Ellis 1951, Foster et al. 1964), the free NH band at 1,500 nm is shifted to 1,559 nm by hydrogen bonding. The origin of amide absorption bands was proposed by Krikorian and Mahpour (1973). Ethanamide has asymmetrical and symmetrical NH stretch first overtone bands at 1,430 and 1,490 nm while N-methyl ethanamide has a single band at 1,475 nm. Protein molecules contain peptide (-CONH-) linkage and, in some cases, free amine or amide side groups. Hecht and Wood (1956) reported an NH band at 1,550 nm whereas Law and Tkachuk (1977) observed this bands due to NH first overtone at 1,500 and 1,570 nm in wheat protein.

(iv) Miscellaneous overtone bands

A few bands other than CH, OH, or NH, which may be of importance in the NIR spectra of foods, also exists. The carbonyl group has an strong fundamental band at about 1,700 cm^{-1} and would therefore expected to have first to fifth overtones at 2,900, 1,950, 1,450, 1,160, and 970 nm. The second overtone has been observed at 1,960, 1,900–1,950, 1,920, 1,900 nm in aldehydes, ketones, esters, peptides, and carboxylic acids, respectively (Wheeler 1959). These bands are too weak and too close to the water band at 1,940 nm. Overtones of hydrogenic groups other than those discussed above should in theory be observable in simple compounds. It is possible for example to observe a very weak band at 1,892 nm due to PH in some organophosphorous compounds (Wheeler 1959). Terminal epoxides have very similar absorption properties to terminal alkenes and their first overtone band may be seen at about 1,640–1,650 nm. The observed frequency of NIR bands depends on the masses of the vibrating atoms, exchange of hydrogen for deuterium causes a shift which is a useful tool for study of NIR spectra. It is possible to assign NIR bands to combination of frequencies using Eq. 6.23. In practice, however, there are enormous number of possible combinations which can only be accounted for a very simple compounds. Kaye (1954) assigned all sixty-two possible combination bands in the case of haloforms which have simple symmetry and only a simple CH group.

(v) Carbon hydrogen combination bands

Bands in stretching and various deformations (deformed) modes involving CH group are the most important combination bands, which occur between 2,000 and 2,500 nm. A much weaker combination bands have also been observed between 1,300 and 1,450 nm and 1,000–1,100 nm. Thus, bands observed at 1,390, 2,290, 2,300, 2,340, and 2,740 nm in wheat gluten, 1,370, 2,290, 2,320, 2,490 nm in wheat starch, 1,390, 2,310, 2,340 nm in wheat lipid (Law and Tkachuk 1977), 2,314, 2,354, 2,371 nm in polyethene, 2,303, 2,349, 2,370 nm in nylon (Glatt and Ellis 1951), 1,400, 2,260, 2,310, 2,350, 2,470 nm in poly (2-methylpropane) and 1,400, 2,270, 2,310, 2,400, 2,470 nm in polypropane (Foster et al. 1964) are all CH combination bands. Holman

and Edmondson (1956) have observed bands at 2,140 and 2,190 nm in fatty acids due to *cis*-unsaturation. These bands are undoubtedly due to combination arising from =CH or CH_2 and C=C vibrations. For example =CH stretched (3,020 cm^{-1}) plus C=C stretched (1,660 cm^{-1}) gives 2,137 nm while CH_2 asymmetrically stretched (2,915 cm^{-1}) plus C=C stretched (1,600 cm^{-1}) gives 2,186 nm. The carbon hydrogen bond involving the carbonyl carbon atom of an aldehyde has a pair of characteristic fundamental vibration bands at 2,820 and 2,720 cm^{-1}, a combination of the 2,820 cm^{-1} band with the C=O band at 1,735 cm^{-1} was observed near 2,200 nm in simple saturated aldehydes.

(vi) Oxygen–hydrogen combination bands

Bands at 1,940 nm in spectrum of liquid water (Curcio and Petty 1951) and water bonded with protein at 1945 nm were observed (Hecht and Wood 1956). It is considered to be the most important absorption in the NIR spectroscopy from the analytical point of view. An OH stretched/OH deformed combination band occurs in all hydroxyl compounds, for example at 2,080 nm in ethanol (OH stretched 3,500 cm^{-1} plus OH deformed 1,300 cm^{-1}). The OH combination bands are shifted, as in case of overtone bands, with hydrogen bonding combination bands and may also be observed between OH stretched and C–O or C–C stretched (Osborne and Douglas 1981).

(vii) Nitrogen–hydrogen combination bands

Krikorian and Mahpour (1973) reported bands at 1,960, 2,000, 2,050, 2,100 and 2,150 nm which they assigned to NH asymmetrically stretched plus amide II, NH symmetrically stretched plus amide II, NH asymmetrically stretched plus amide III, NH symmetrically stretched plus amide III and twice amide I plus amide III, respectively. Primary amines would be expected to have an NH stretched/ NH deformed combination band at about 2,000 nm.

Proteins have three prominent bands in the NH combination region; at 1,980, 2,050 and 2,180 nm (Law and Tkachuk 1977). Bands at 2,058 nm and 2,174 nm were noted by Elliott et al. (1954) in the spectra of α-polypeptides. Hecht and Wood (1956) assigned the 2,060 nm band to NH stretched H bonded (3,280 cm^{-1}) plus NH deformed amide II (1,550 cm^{-1}) and the 2,180 nm band to twice C=O stretched, amide I (1,650 cm^{-1}) plus amide III (1,250 cm^{-1}). Three bands of this type were reported for secondary amides: 2,000 nm due to NH stretched plus amide II, 2,100 nm due to NH stretched plus amide III and 2,160 nm due to twice amide I plus amide III. An NH stretched /NH deformed band at 2,050 nm was observed in nylon (Glatt and Ellis 1951).

Murray (1987, 1988) traced the characteristic absorption patterns for a number of functional group by studying the NIR spectra of homologous series of organic compounds. Using this work, assignments of wavelengths in the spectra of agricultural products have been made and a concept of food composition in terms of CH, OH and NH structures was proposed.

(e) Summary on chemical assignments

Chemical assignments for NIR bands available are summarized in Fig. 6.5. Though these summaries represent only some of the important NIR bands, the degree of complexity of spectra is obvious. It is of interest to note also

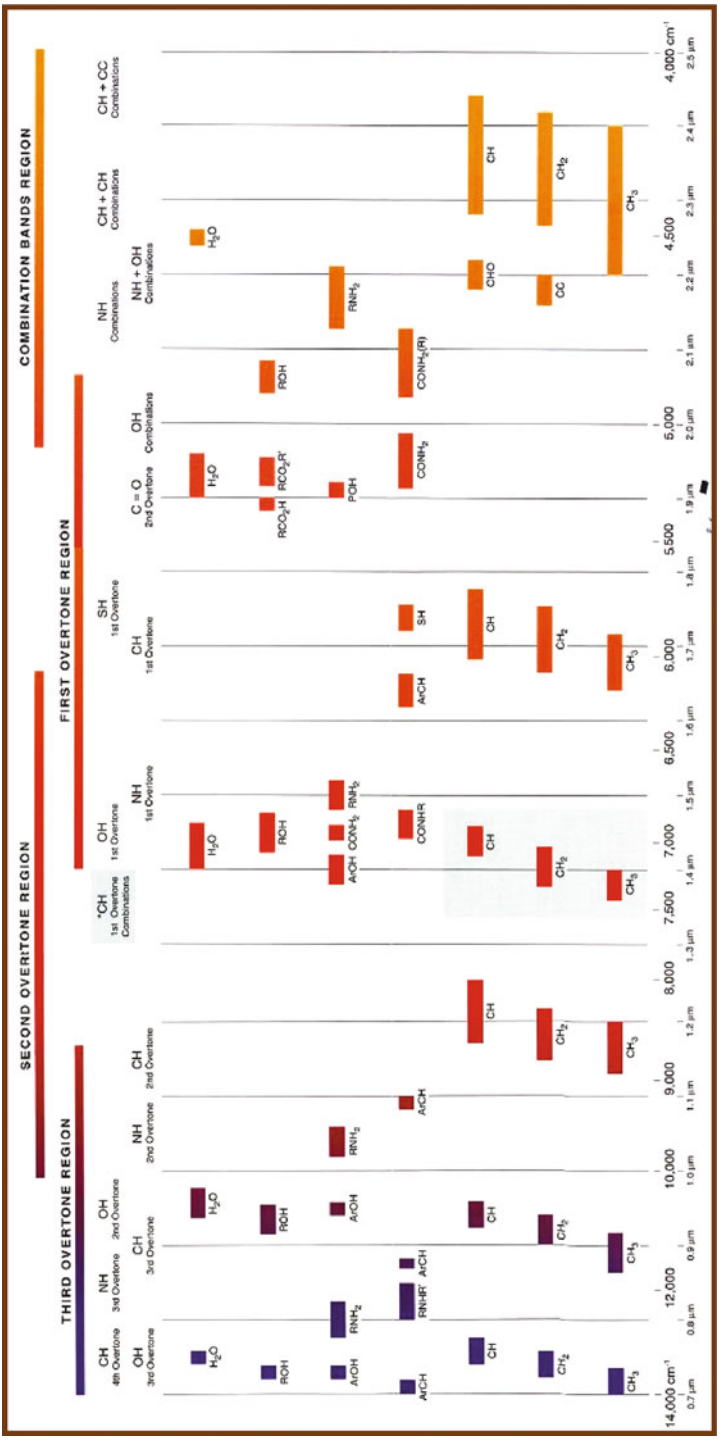

Fig. 6.5 Spectra structure correlations with NIR bands (borrowed from Central Queensland University/Camo India Limited)

that the spectral information is repeated through the successive overtones and combination regions and since the bands involved become weaker by an order of magnitude each time, this represents a useful built-in dilution series. A library of 328 NIR spectra of pure chemicals and agricultural and food products is contained in monograph by Williams and Norris (1987). Recent library is the NIRS library "NICODOM NIR Pharmaceuticals" which contains 696 NIR spectra (4,200–11,000 cm^{-1}) of active substances and excipients used in pharmaceutical industry. The sources of the samples were local pharmaceutical companies. The basic version of this library is also available in the form of a book, which contains 385 NIR spectra. Another huge library with passage of time by contribution of various researchers has also been developed as a public domain and can be reached at www.spectraonline.com.

6.1.3 NIR Imaging

In addition to chemical assignments of different NIR bands for analysis of foods and other materials, it is also being used nowadays for chemical imaging of samples. Chemical imaging is the analytical capability (as quantitative – mapping) to create a visual image from simultaneous measurement of spectra (as quantitative – chemical) spatial, and time information. The technique is most often applied to either solid or gel samples, and has applications in chemistry, biology, medicine, pharmacy, food science, biotechnology, agriculture and industry. NIR imaging is also referred to as hyperspectral, spectroscopic, spectral or multispectral imaging. Chemical imaging techniques can be used to analyze samples of all sizes, from the single molecule to the cellular level in biology and medicine, and to images of planetary systems in astronomy, but different instrumentation is employed for making observations on such widely different systems, which is beyond the scope of this book. Some work however on NIR imaging is reported in Chap. 3.

6.2 NIRS Instrumentation

Previous sections have dealt with what actually NIRS is and how is it working for quality determination. The user usually faces an increasingly difficult task in determining the most appropriate instrument for their application, be it in the laboratory, in field or in on-line application.

The generalized instrumentation used in nondestructive type of spectrometry for measurements of absorption and/or reflectance consists of a light source, wavelength selector or isolator, holder, detector and a computer (Fig. 6.6). These components, except computer (which is not considered a part of spectrometry, though an essential requirement) are connected nowadays through fibre optics cable or single thread. Wavelength isolator and detectors are combined in spectrometer. Selections of these components of NIR spectrometry are of paramount importance and therefore are discussed in brief hereunder different subheads:

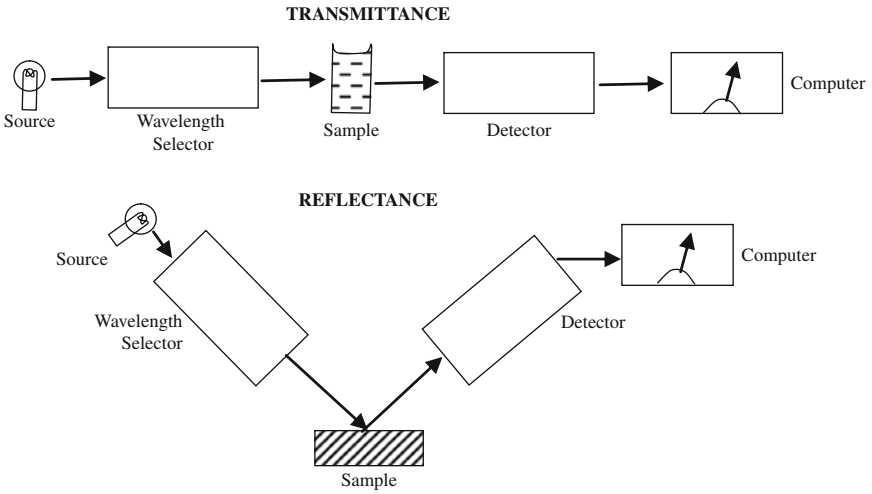

Fig. 6.6 Basic instrument layout for transmittance and reflectance measurement

6.2.1 Light Source

Common incandescent or quartz halogen light bulbs are most often used as broadband sources of near infrared radiation for analytical applications. The quartz-halogen lamp is the most popular source of NIR energy because of their widespread use for household lighting, The use of the word "energy" is more suitable in case of NIRS as compared to the "light", because NIR energy is not visible to the human eye and therefore is not light. Light-emitting diodes (LED) are the second most popular source of NIR energy. They have greater lifetime, spectral stability and reduced power requirements.

The method by which light is spectrally modulated or selected defines the optical operating principle of an NIR spectrometer. All such instruments are grouped into three categories: dispersive, interferometric and non-thermal. Devices in the first two groups generally employ broadband, thermal radiation produced by an incandescent filament. The third group consists of non-thermal or 'cold' sources where wavelength selection is inherent in the source's spectrally narrow emitting range. The resolving power of an instrument, its ability to distinguish between two close spectral elements, its transmission, the amount of light that can be admitted, are all fundamental features of the optical operating principle. The resolving power (resolution), R, is defined as $\lambda/\delta\lambda$, where $\delta\lambda$ is the resolution usually expressed in microns. The same expression can, of course, be defined in wave numbers (cm^{-1}). The solid angle of light (luminosity) admitted by the instrument, Ω, is related to P such that

$$R\Omega = \text{constant} \tag{6.25}$$

The resolution luminosity product is constant. This criterion, a figure of merit for spectrometers, has been fully developed by Jaquinot (1958). In a given instrument, resolving power has to be traded for luminosity. The higher the value of $R\Omega$ the better is the instrument.

6.2.2 NIR Spectrometers

NIR spectrometers are classified according to wavelength isolation techniques. Wavelength isolators broadly come under two groups: (i) Discrete-value and (ii) full spectrum devices. Full-spectrum spectrometers also known as "scanning instruments" produce spectra with equally spaced data, i.e. at fixed intervals across the full range from 700 to 2,500 nm. Interval may be any one number such as 1.5 nm, 2 nm, 2.2 nm etc. Discrete-value spectrometers may be further categorized by the technology used to produce narrow wavelength bands. Table 6.3 presents major wavelength-isolating technologies used in NIRS.

(i) Diodes

Light Emitting Diode Arrays (LEDA): Several light-emitting diodes (LEDs) are commercially available and are making possible the construction of multichannel or multiband NIR spectrometers, which are being used for numerous applications in the food industry. A schematic diagram of an LEDA spectrometer is shown in Fig. 6.7. Four LEDAs are systematically arranged in a matrix array. As per requirements, the bandpass of individual diodes are narrowed by adding narrow-band interference filters. A diffuser is interposed between the sample and the diode matrix to provide uniform illumination from all diodes simultaneously.

Photodiode Detector Arrays (PDA): Nowadays most of the NIR spectrometers have not a single moving part which is useful for many applications. Photodiode detector arrays (PDA) are used in such spectrometers. A basic setup of a PDA spectrometer is shown in Fig. 6.8, which is configured with a fibre-optic bundle for conducting diffusely reflected energy from the sample to the fixed grating monochromator. This instrument uses a linear diode array for measuring the reflected energy. These arrays cover the range 200–1,000 nm, but the signal becomes more noisy below 450 nm and above 900 nm.

Greensill and Walsh (2002) have developed procedures for standardizing the miniature Zeiss MMSI PDA spectrometers and Clancy (2002) has demonstrated a simple linear slope and bias correction for effective normalization of instruments and thus allowing a single master calibration to be used on all instruments (Clancy 2002). Morimoto (2002) developed two field-operable PDA instruments for determining fruit quality based on PDA technology.

Laser Diodes: The advantages of laser diode spectrometers are that the bandwidths of lasers are very narrow, and the output intensity can be very high compared to other spectrometers. A schematic diagram of a laser diode

Table 6.3 Classification of NIR spectrometers based on wavelength isolating technology

Technology	Status
Diodes	
Light emitting diode arrays (LEDA)	LEDA is a nonscanning instrument. Using these emitters, making very compact spectrometers for specialized applications requiring only a few wavelengths is possible. A limited number of light-emitting diodes are available in the market
Diodes-array detectors (DAD)	DAD spectrometers are full-spectrum instruments. DAD is used in conjunction with a fixed grating for making compact spectrometers with resolution limited only by the number of receptors in the array
Laser diodes	Laser-based instruments are wavelength limited and therefore are not full-spectrum instruments. Production of many wavelengths from laser diodes is still lagging other technologies
Filters	
Fixed	The bandpass of these filters may be as narrow as 1 nm. Fixing the plane of a narrow-band interference filter (NBIF) normal to an NIR beam provides a single wavelength band. Fixed filter spectrometers are not capable of producing full spectrum
Wedge	A wedge-interference filter (WIF) consists of two quartz plates spaced by a dielectric wedge. Moving the wedge in front of a slit produces incremental wavelength bands. Spectrometers that incorporate a WIF are full-spectrum instruments
Tilting	Tilting results in an increased band width and diminished transmission. Tilting a NBIF in a beam of parallel NIR energy produces incremental wavelength bands. Tilting-filter spectrometers, though limited to a narrow range of wavelengths are full-spectrum spectrometers
AOTF	An acousto-optical tunable filter (AOTF) is a specialized optic whose bandpass is determined by the radio frequency applied across the optic. AOTF spectrometers are full spectrum instruments
LCTF	Liquid crystal tunable filter (LCTF) spectrometers may be designed to operate in the visible, NIR, MIR and FIR range. However, the switching speed is much slower than the AOTF (maximum of 1 ms)
Prism	Prism, used in the early days of spectrometry, produce nonlinear dispersion of NIR spectrum, making it difficult to coordinate prism position with wavelength. Prism based spectrometers are full-spectrum instruments
Grating	Grating produce a near-linear dispersion with wavelength. The remaining nonlinearity can be removed with software. Spectrometers incorporating grating are said to be full-spectrum instruments
FT-NIR	Fourier transform near-infrared (FT-NIR) spectrometers produce reflection spectra by moving mirrors. Once plagued by noise modern FT-NIR spectrometers boast noise levels equivalent to grating-based instruments. FT-NIR spectrometers are full-spectrum instruments
Hadamard	This initially was made using a complex arrangement of shutters. Hadamard technology has never competed with dispersion-type instruments. This technology is capable of producing a full spectrum

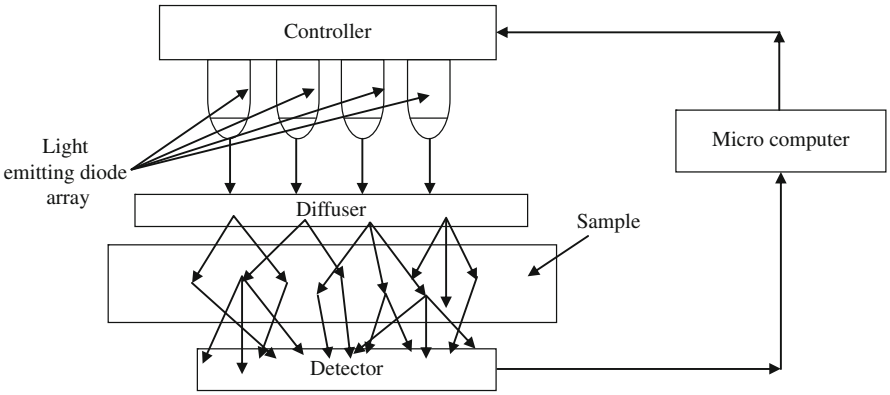

Fig. 6.7 Schematic diagram showing use of diffuser and narrow band interference filters with NIR energy emitting diodes

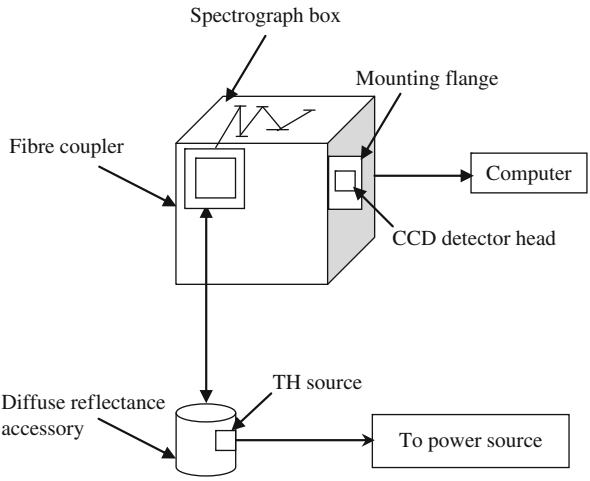

Fig. 6.8 Schematic diagram of basic setup of photodiode detector array spectrometer using a single fibre optic cable to collect spectra from a solid sample

spectrometer is shown in Fig. 6.9. The cost of laser diode has fallen much in last 25 years, but the laser diode spectrometers are still in the research stage.

(ii) Filters

Fixed Filter: A typical fixed filter spectrometer (FFS) includes filters that are useful for calibrations in high-volume food applications, such as moisture, protein, and fat. The first commercial grain NIR analyzer was made using fixed filters (FF). Today several companies produce multiple FF instruments using the fast Fourier transform for noise reduction. A schematic diagram of a fixed filter spectrometer (FFS) is shown in Fig. 6.10. It cannot do everything because FFS is capable of producing limited number of bands only; and the NIR absorptions

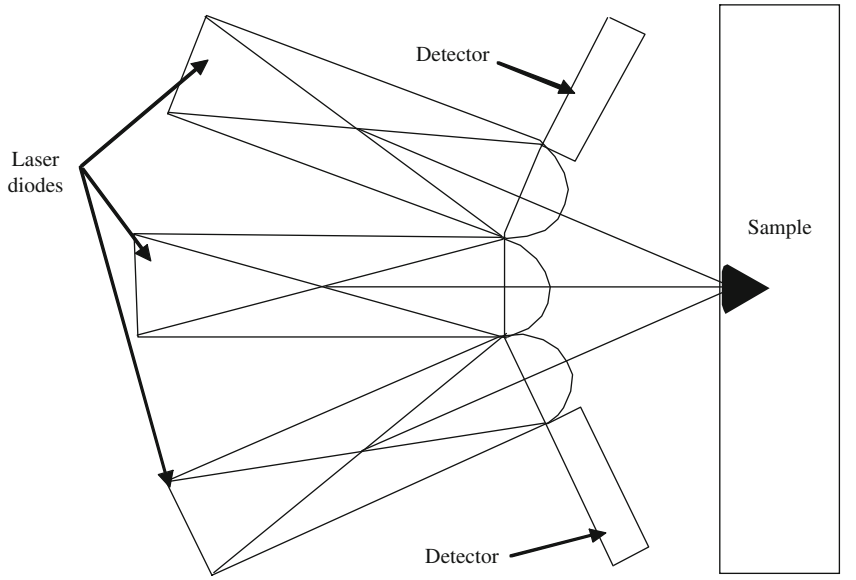

Fig. 6.9 Schematic diagram of a laser-diode arrays spectrometer for making reflection measurements

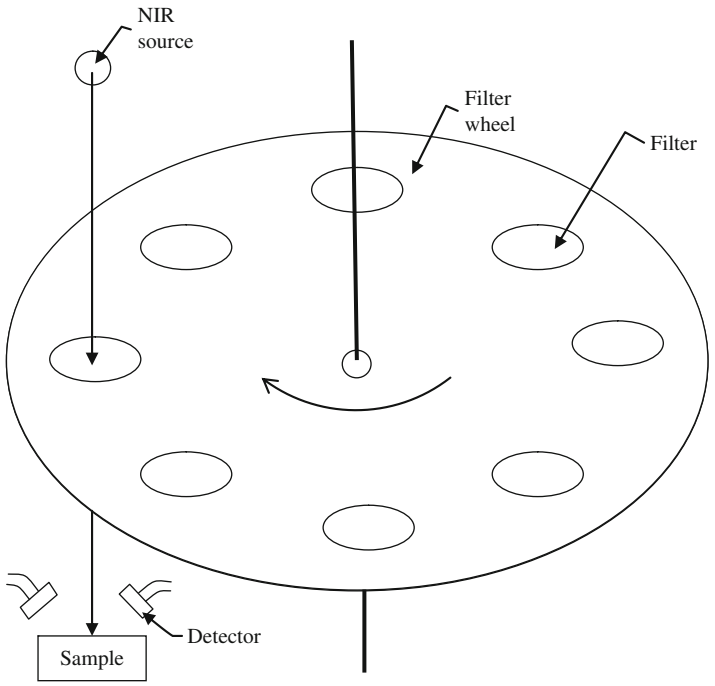

Fig. 6.10 Schematic diagram of a fixed filter spectrometer

of food and food products are broad and overlapping. Morimoto et al. (2001) since when have demonstrated that derivative calibrations can be developed with filters, a renewed interest in FFS has emerged.

Wedge-Interference Filters (WIF): This filter is similar to FF with a single exception that the optical dielectric between the plates is wedge shaped. That is, the dielectric at one end is thicker than at the other end, producing longer to shorter wavelengths, respectively. A slit between the source and the sample allows passing of a narrow band of wavelengths, with the band changing as the wedge is moved from one end to the other. WIF are also available in circular form in which the thickness of the optical dielectric varies with filter rotation. Figure 6.11 illustrates construction of a WIF spectrometer.

The recent development is a variable filter array (VFA) spectrometer. It enables to acquire NIR spectra on a variety of materials wherever they occur, whether in the production plant or in the field. It consists of an Attenuated total reflection (ATR) sample plate with an elongated pulseable source mounted close to one end and a linear variable filter attached to a detector array mounted close to the other. Use of this technology has resulted a very compact spectrometer with no moving parts and no optical path exposed to air and is able to produce NIR spectra of powders, films, liquids, slurries, semisolids, and surface. Sample cups are not required in this type of instruments and sample loading simply involves loading the ATR with a suitable thickness of material.

Tilting Filter: This filter has definite advantages over wavelength-isolation techniques. First, narrow-band NIR interference filters can be produced for any wavelength in the NIR region. Second, NIR filters characteristics can be

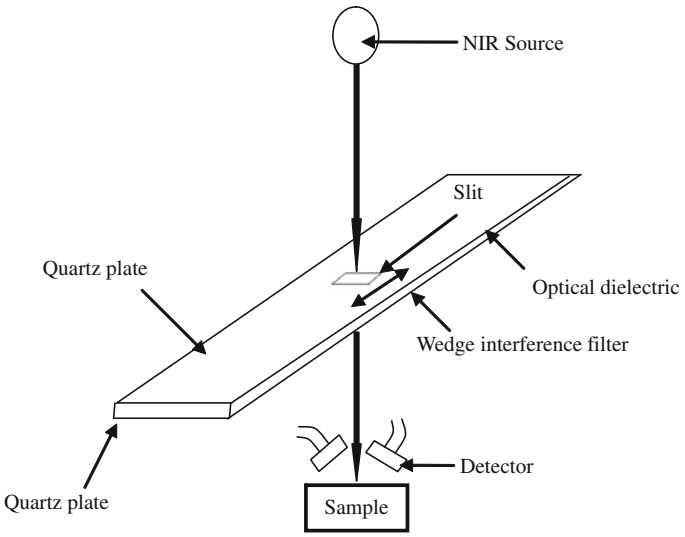

Fig. 6.11 Schematic diagram of a wedge-interference filter spectrometer. Two quartz plates hold the optical dielectric in static position

reproduced, making it much easier to duplicate spectrometers characteristics. Third, the bandpass of a filter may be increased or decreased (increasing or decreasing the energy falling on the sample, respectively) depending on the application. Spectrometers implementing narrow-band interference filters compete quite well for online and field (hand-held) applications where the objective is to measure a limited number of parameters.

Major disadvantages of tilting-filter spectrometer (Fig. 6.12) are: the relationship between angle and wavelength is nonlinear, the bandpass of the filter increases as the angle from the normal energy beam increases (clockwise or counterclockwise) and the peak transmission of the filter decreases as the angle of the filter from normal to the source beam increases (clockwise or counterclockwise), besides its expensiveness. The first three disadvantages make difficult to reproduce specifications from one instrument to another. Due to these problems this kind of spectrometers are not produced.

Acousto-optical Tunable Filter (AOTF): It is a solid-state electronically tunable spectral bandpass filter (Anon 2010). It operates on the principle of acousto-optic interaction in an anisotropic medium. The AOTF has recently reached technological maturity, moving from the research laboratory to the commercial environment (Fig. 6.13). It utilizes an anisotropic, birefringent medium for its operation. It has a relatively long acoustic interaction length,

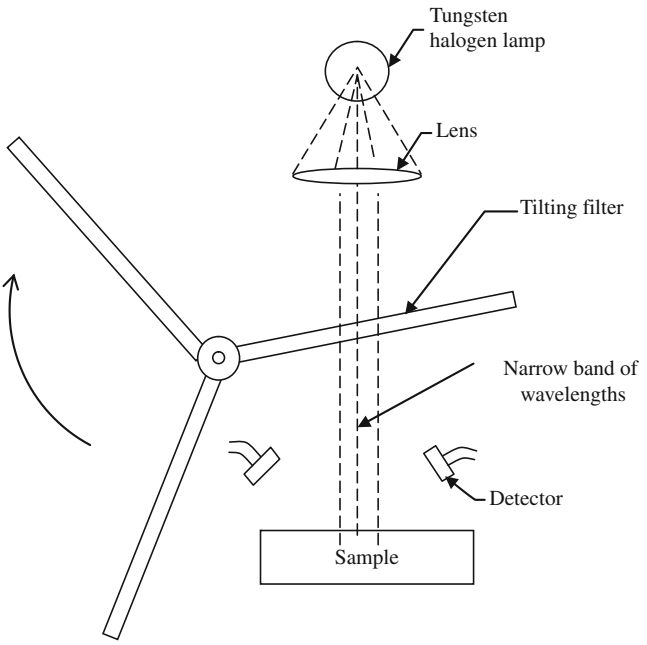

Fig. 6.12 Schematic diagram of a tilting-filter spectrometer. Three tilting filters are provided for wavelength isolation in three regions of NIR spectrum

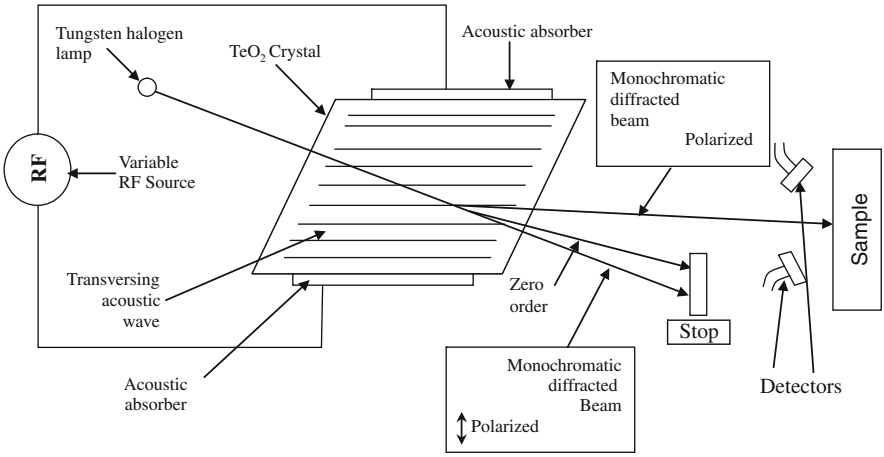

Fig. 6.13 Schematic diagram of an AOTF spectrometer

required to achieve a narrow spectral bandwidth. That one can only be achieved for a certain momentum-matching configuration, i.e., the group velocity for the extraordinary wave should be collinear with the ordinary wave. It is shown on the Fig. 6.14, where the momentum-matching vectors represent the phase velocities of the incident light k, diffracted light k_d, and acoustic waves k_a. In this geometry, the tangents for the incident and diffracted light beams are parallel to each other. Note that the two optical beams do not separate until the light propagates inside the acousto-optic medium. This long coherent buildup of the diffracted beam would be only partially beneficial to the AOTF. To a first order, any momentum mismatch, due to the light arriving at some angle from this ideal condition, is compensated by a change in the birefringence for this orientation, and thus the AOTF displays its most important characteristic: a large angle of view, which is unique among acoust-optical devices. The tuning dependence of

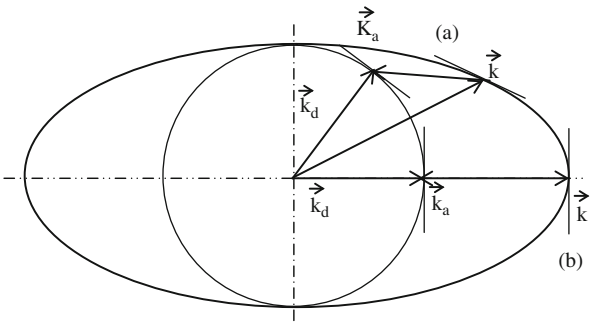

Fig. 6.14 Phase matching condition for: (**a**) non-collinear AOTF, (**b**) collinear AOTF. k, wave vector of entrance radiation; k_a, wave vector of acoustic wave; k_d, wave vector of diffracted radiation

AOTF: $F = c \times D_n/\lambda$, where F is the frequency of the radio frequency signal; $D_n = n_e - n_o$; n_e, n_o are refractive indices for extraordinary and ordinary rays; c is the constant and λ is the light wavelength

Liquid Crystal Tunable Filters (LCTF): It is a stack of polarization sensitive plates. Specific regions of the NIR spectrum are fixed by the number and thicknesses of plates usually made up of crystal quartz plates. Switching speeds from one wavelength band to another is dependent on the relaxation time of the crystal and can be as high as 50 ms. Although special crystal have been made with a switching time of 5 ms, this time far exceeds that of grating and ATOF technology and is restricted to a short sequence of wavelength. The spectral resolution is on the order of 10–20 nm, although special crystal can reduce the bandpass to 5–10 nm, which nowadays are considered not good enough. It has therefore a limited success in NIR spectroscopy, however can perform considerably well in visual region. Tilotta et al. (1987) did further development in this field and utilized liquid crystal to modulate radiation in a Hadamard spectrometer, which is considered to be the first no moving parts spectrometer.

Hadamard Spectrometer: Combination of multiplexing and dispersive spectrometers in which choice of transparent or opaque elements of multi-slit mask provides information that may be transformed into conventional NIR spectrum with Hadamard mathematics and are the basis of Hadamard-transform NIR spectrometry (HT-NIR) (Hammaker et al., 1986, Tilotta et al. 1987). Usually tungsten halogen lamp is used as a light source. The energy is first dispersed into spectral elements (wavelengths) and then collected and focused onto a focal plane. Unlike purely dispersive systems where there is only one exit slit, the focal plane of a Hadamard system implements a multislit array. Signals from this multiple-slit arrangement are collected by a single-element detector. The HT-NIR spectrometry is still not preferred one due to complex problems which are still in research stages.

Prisms: There are three types of prisms (a) polarizing (b) dispersing, and (c) reflecting, Polarizing prisms are made of birefringent materials. Dispersing (or transmission) prisms were most popular in the early development of NIR technology. Reflecting prisms were designed to change the orientation or directions (or both) of a NIR beam. Initially prism based spectrometers (Fig. 6.15) were used to acquire absorption NIR spectra in the range of 210–2,700 nm automatically (Kaye et al. 1951) by replacing photomultiplier tube with a lead sulfide (Pbs) cell and including a chopper and an electronic recorder. Absence of a digitizer for photometric signal was a major drawback of this kind of instrument.

Gratings: The first commercial gratings used were grooved by machine using a diamond ruling tool. Nowadays holographic gratings are used in this kind of spectrometer. They are made by a deposing photosensitive material onto a flat glass plate. Lasers are used to make grooves in the material, and aluminum is vacuum deposited in the grooves to make them reflective. Holographic gratings are a less efficient than the original replica gratings, but the precision of the grooves reduces scattered light. This kind of spectrometer is capable of

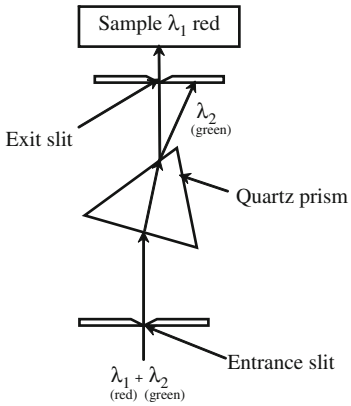

Fig. 6.15 A simple prism spectrometer

much higher resolution than prisms and is much easier to implement volumes. Schematic diagram of a grating spectrometer is shown in Fig. 6.16.

Fourier Transform-Near Infrared (FT-NIR): FT-NIR spectrometers are made using an entirely different method for producing spectra. No dispersion is involved in this method. Energy patterns set up by an interaction with a sample and reference and moving mirrors (or other optical components) produce sample and reference interferograms that are decoded using a well known mathematical technique called Fourier transformation with the help of microcomputer in the spectrometer which produces the desired spectral information to users for interpretation and further manipulations. There are two distinct advantages of FT-NIR spectrometers that make it more attractive. The first is the throughput advantage. In the absence of dispersion, the energy at the output of an FT-NIR interferometer (similar to a monochromator) can be many times greater than that obtained from a grating monochromator. The second, FT-NIR improves spectra reproducibility and wavenumber precision, which may give better accuracy in prediction using chemometrics.

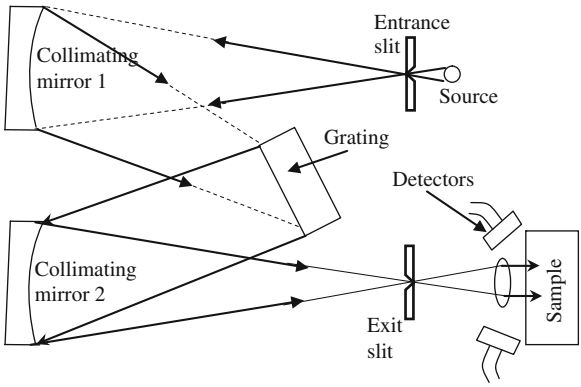

Fig. 6.16 Schematic diagram of a simple grating spectrometer

6.2.3 Infrared Detectors

Infrared detectors are divided into two types: photon detectors, comprising photoconductors and photodiodes, and thermal detectors. The latter respond to total radiated energy, irrespective of wavelength and are not efficient enough for serious use in the NIR. The response characteristics of some detectors useful in the NIR are shown in Table 6.4 and Fig. 6.17.

Responsivity (R), noise equivalent power (NEP) and specific detectivity (D*) are commonly used terms to define detectors. The responsivity (R) is expressed as:

$$R = VW^{-1} \tag{6.26}$$

where V is the root mean square (rms) output voltage and W the rms of power input.

The NEP is defined as the power input required to give an output noise voltage equal to the rms of noise voltage, whereas the inverse of the NEP is the detectivity D. When D is expressed in a normalized form for a detector of 1 cm^2 area and 1 Hz bandwidth, it is called the specific detectivity and expressed as D*. The unit of D* is cm $Hz^{1/2}$ W^{-1}. Silicon and germanium photodiodes cover the very near infrared (VNIR) part of the spectrum. These cells consist of reverse-based p-n junctions. Sufficiently energetic photons create an electron – hole pair across the boundary, producing a small potential $\approx \mu V$. Silicon detectors respond through the visible part of the spectrum and up to 1 μm, peaking at 0.85 μm. Germanium detectors peak at about 1.5 μm (Fig. 6.17).

Compound lead – salt semiconductors are the most widely used detectors in the NIR and operate in the photoconductive mode. Lead sulphide (PbS) is used over the range 1–3.6 μm and lead selenide, PbSe, is useful from 1.5 to 5.8 μm (Table 6.4). PbSe is much less sensitive than Pbs (Fig. 6.17). They are available, individually, as squares of material from 1 mm × 1 mm to 10 mm × 10 mm and can be operated at room temperature or cooled environment. Cooling shifts the sensitivity of the cell to longer wavelengths but increases the response time and signal to noise ratio.

The absorption of photons causes the creation of electron – hole pairs across the n-p junctions and electrons are excited from valence bands to conduction bands. When electrons are in this state, they can conduct electricity and the resistance of the cell falls. The decay time back to the valence bands dictates the response time of the cell, which is typically 100–200 μs for PbS and less than 1 μs for PbSe.

Lead-salt detectors are formed by chemical deposition by the precipitation of the salt. PbS is an n-type semi-conductor, rendered photo conducting by oxygen treatment. Oxide layers some 200 Å thick are grown into the semi-amorphous crystals. In effect, a two-dimensional array of n-p-n junctions is produced. Variability of crystal size and p-layer thickness means that the sensitivity and wavelength response of the cell varies over its surface. This must be taken into account in instrument design.

Another detector, with an exciting feature, is epitaxially – grown indium gallium arsenide, InGAs. This detector operates over the range 0.7–1.7 μm peaking at 1.7 μm. They are available from 1 to 6 mm diameter and are a few times more sensitive than PbS. Response times are below 1 μs. Lattice mismatch occurs at

Table 6.4 Infrared detectors and their characteristics

Types			Detectors	Spectral response (μm)	Operating temperature (K)	D^*(cm.Hz$^{1/2}$/W)
Thermal	Thermocouple, Thermopile		–	Depends on window material	300	$D^*(\lambda,10,1)=6\times10^8$
	Bolometer		–		300	$D^*(\lambda,10,1)=1\times10^8$
	Pneumatic cell		Golay cell, condenser-microphone		300	$D^*(\lambda,10,1)=1\times10^9$
	Pyroelectric detector		PZT, TGS, $LiTaO^3$		300	$D^*(\lambda,10,1)=2\times10^8$
Photon detector	Intrinsic	Photoconductive	Si	0.85–1.0	295	$D^*\approx4\times1012$
			PbS	1–3.6	300	$D^*(500,600,1)=1\times10^9$
			PbSe	1.5–5.8	300	$D^*(500,600,1)=1\times10^8$
			InSb	2–6	213	$D^*(500,1200,1)=2\times10^9$
			HgCdTe	2–16	77	$D^*(500,1000,1)=2\times10^{10}$
		Photovoltaic	Ge	0.8–1.8	300	$D^*(\lambda_p)=1\times10^{11}$
			InGaAs	0.7–1.7	300	$D^*(\lambda_p)=5\times10^{12}$
			Ex. InGaAs	1.2–2.55	253	$D^*(\lambda_p)=2\times10^{11}$
			InAs	1–3.1	77	$D^*(500,1200,1)=1\times10^{10}$
			InSb	1–5.5	77	$D^*(500,1200,1)=2\times10^{10}$
			HgCdTe	2–16	77	$D^*(500,1200,1)=1\times10^{10}$
	Extrinsic		Ge:Au	1–10	77	$D^*(500,900,1)=1\times10^{11}$
			Ge:Hg	2–14	4.2	$D^*(500,900,1)=8\times10^9$
			Ge:Cu	2–30	4.2	$D^*(500,900,1)=5\times10^9$
			Ge:Zn	2–40	4.2	$D^*(500,900,1)=5\times10^9$
			Si:Ga	1–17	4.2	$D^*(500,900,1)=5\times10^9$
			Si:As	1–23	4.2	$D^*(500,900,1)=5\times10^9$

D^* normally is expressed in format $D^*(a, b, c)$, where *a* is the temperature (K) or wavelength (μm) of radiant energy, *b* is the chopping frequency and *c* is the band width. Subscript p denotes peak wavelength in this table

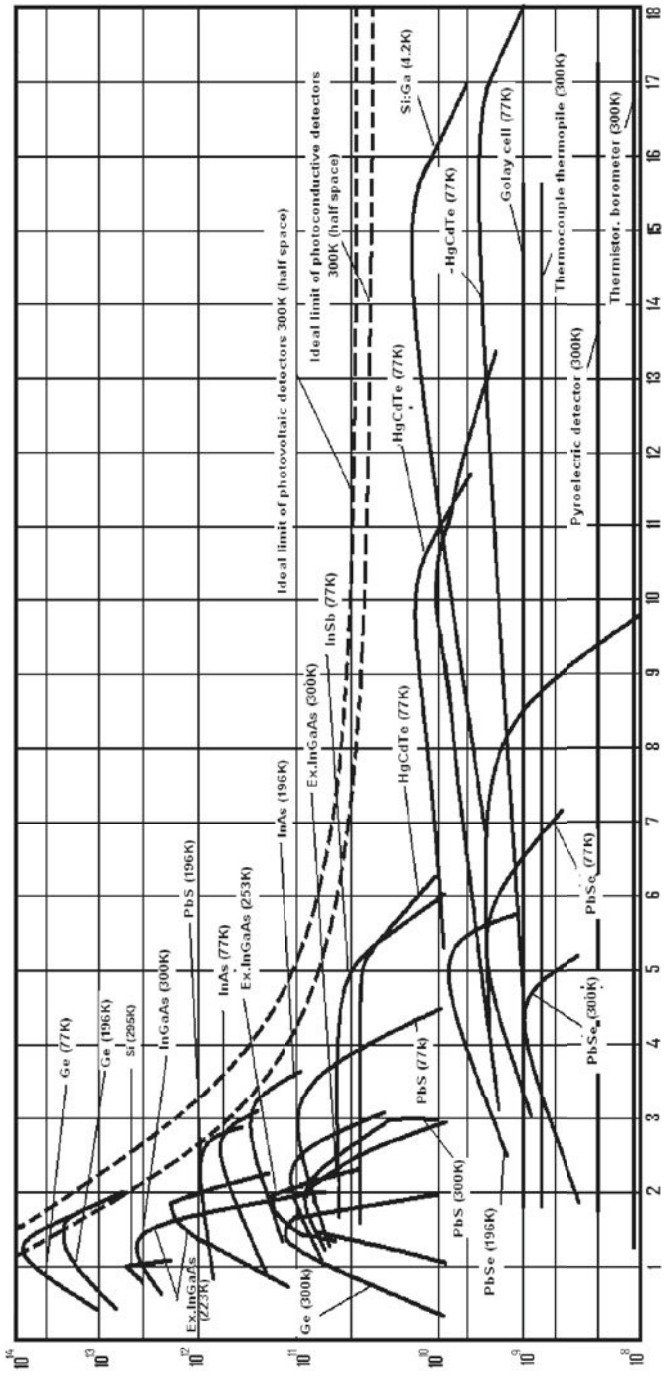

Fig. 6.17 Approximate response characteristics of different IR detectors

indium levels required to give a peak response at longer wavelengths. Although a progressive matching technique can produce such detectors, lattice strain and defects render them noisier and production costs also become higher. Performance of any detector varies with the environmental conditions in which it is used. It is very much sensitive to temperature and humidity.

6.2.4 Fibre Optics

The use of fibre optics as a means of delivery and transfer of NIR energy and information is of paramount importance. There are many situations, particularly on the production line, where the operating environment is unsuitable for sensitive equipment. This may be because of temperature, vibration, space or explosion hazards. In these situations, the ability to deliver and collect NIR energy via optical fibre is advantageous.

Principle of total internal reflection governs the science of fibre optics. It covers all aspects of transmission of light along optically transparent fibres by means of the phenomenon of total internal reflection. The transparent medium may be silica glass, plastic or any other exotic materials.

Unlike normal reflections from metallic or dielectric surface, which may be up to 99%, efficient, total internal reflection is highly efficient, typically better than 99.999% at each reflection. Even with several hundreds or several thousands of reflections per metre, significant amounts of energy can be transmitted over useful distances. The attenuation of fibre is measured in db km^{-1} or dB m^{-1}. Figure 6.18 shows the attenuation for the three most suitable fibres for NIR.

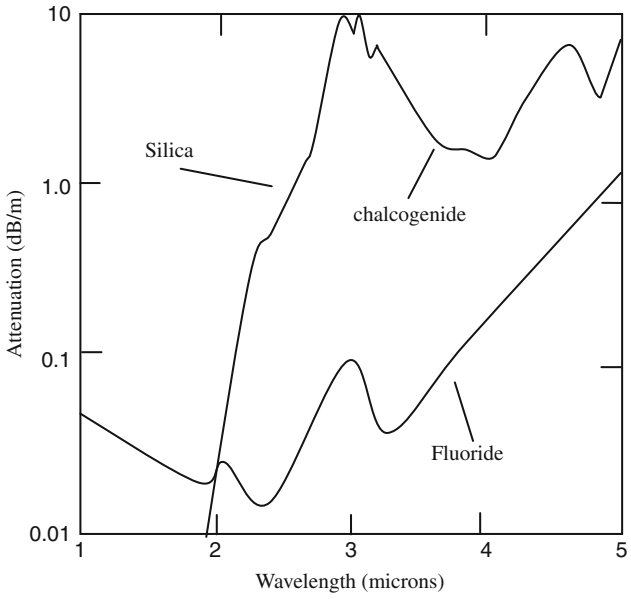

Fig. 6.18 Approximation of NIR transmission of optical fibres

Chalcogenide fibres best cover the wavelength region from 4 to 11 μm but transmission is limited to distances of a few metres. It can be seen that silica glass is ideal below 2-μm region. Zirconium fluoride is still very expensive. It offers very low attenuations, less than 1 dB km^{-1}, with theoretical performance much better than this.

(a) Optical concepts

The basic structure of a fibre is presented in Fig. 6.19. The cladding is a low index material and outer is optional and for protective purpose only. If the refractive indices of core and cladding are n_1 and n_2 where $n_1 > n_2$, an internal ray of light, incident on the boundary at an angle ϕ_1 will be partly reflected at the same angle and partly refracted into the cladding at an angle ϕ_2 according to Snell's law.

$$\frac{sin\phi_1}{sin\phi_2} = \frac{n_2}{n_1} \tag{6.27}$$

When ϕ_1 increases, a point reaches where ϕ_2 becomes 90° and no light escapes the core. The light is totally internally reflected. The complementary angle at which this occurs is known as the critical angle (θ). From Snell's law, it is defined in terms of the refractive indices as Eq. (6.28).

$$\theta = cos^{-1} n_2 / n_1 \tag{6.28}$$

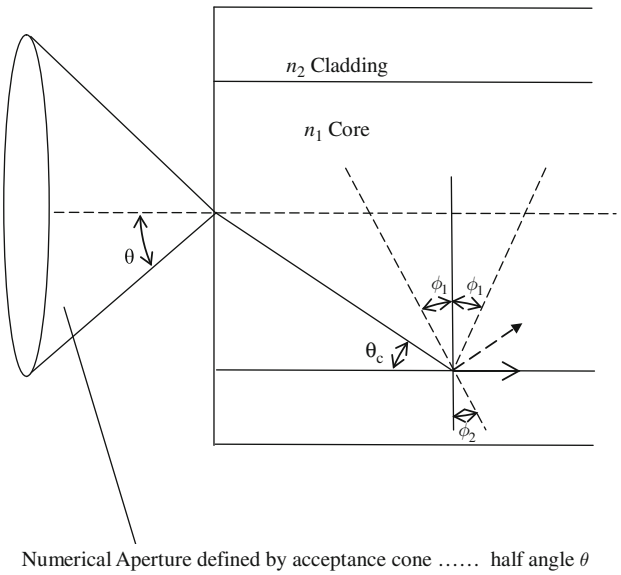

Fig. 6.19 Schematic structure of fibre showing light rays

Rays with angles less than the critical angle are totally internally reflected with high efficiency. A similar arrangement is used to calculate the maximum angle to the normal, at which light admitted to the fibre and transmitted by total internal reflection. The *sine* of this is defined as the numerical aperture (NA) as Eq. (6.29).

$$NA = \sin\theta = \frac{(n_{core}^2 - n_{clad}^2)^{1/2}}{n_{air}} \tag{6.29}$$

The angle θ defines an acceptance cone for the fibre. The square of the numerical aperture defines the light gathering capacity of the fibre. There is obviously no point in attempting to feed light onto the fibre at greater angles than this. In theory, light entering a fibre at a given angle should emerge at the other end at the same angle. However, the azimuthal angle varies rapidly with input angle and rays generally emerge on an annular cone, centred on the input angle. Scattering and inhomogeneties also causes the degradation of images.

(b) Monofilaments and bundles

Fibres are available in form of clad, single fibres (monofilament) or as bundles of filaments. Bundles are randomized, branched or structured as spatially coherent arrays for optical uniformity and mixing, for multiple input/output applications or be structured as spatially coherent arrays for imaging purpose. Core diameters normally range from 0.02 to 2 mm. Bundles are available with diameters from less than 1 to 8 mm. Monofilament fibres are less expensive and can be easier to use than bundles provided that the energy required can be imaged through the end of the fibre. Large diameter fibres are attractive for these reasons although account will need to be taken of the minimum bending radius. For a 1 mm silica glass fibre this will be approximately 150 mm. Repeated bending will cause microfractures (silica is bad for this), resulting in loss of transmission by scattering into the cladding.

Thermal and mechanical stress affects the transmission characteristics and is disastrous for accurate NIR transmission measurements. For example, a 1 mm monofilament fibre, stressed by 10% bending can change its relative transmission characteristic of about 1.8/1.9 μm ratio by as much as 0.5%. This problem can be obviated with double-beam optical design. Fibre bundles are normally made from much smaller core sizes, 30–100 μm, giving much better flexibility. The minimum bend is defined by the protective jacket. However, bundles are less efficient than monofilaments because a proportion of the incident light is lost on the cladding and interstices between fibres. Packing fractions of 35–45% are typical, but this means that more than 50% of the available energy is lost every time when light is coupled into a bundle.

6.2.5 Sample Preparation and Presentation

Two main areas of measurement, laboratory and production line, can be subdivided into solids and liquids. The former are more common and the latter usually require less sample preparation.

(i) Solids on-line

1. There may be wide variations in dimensions of some products. Generally a diffuse reflection sensor tolerates ±25 to ±50 mm random product height fluctuation at maximum sensitivity. If the height variation exceeds the observed performance of the sensor then it is necessary to plane the surface immediately prior to its passing by the target area.
2. NIR penetration is generally superficial and may range from tens of microns to a few millimeters. The penetration can be much greater at shorter wavelengths in the region 0.8–1.1 μm but currently the very near infrared (VNIR) part of the spectrum is not widely used in on-line sensing. Particularly if moisture is being measured it is important to ensure that the surface is typical of the bulk material. Surface drying in that case may be a problem. Mixing, turning or ploughing may solve these problems for granular or leaf materials up to some extent.
3. The sensor reading depends, to a small degree, on the mean orientation of the product in relation to the sensor. Generally leaf or laminar products are more problematic than granular materials and powders and thus instantaneous sensor reading may be erroneous. So, it will be useful if orientation is averaged. As the product passes under the sensor the readings will fluctuate around the correct value for the mean orientation on the production line. These fluctuations can be called 'presentation noise' and must be integrated out with an appropriate time constant. Typically a few second signals averaging may be required.
4. Product coming out from driers may contain steam and produce erroneous results, so a proper care is needed to avoid such situation.
5. It is essential that the sample patch should be filled with product and that the sensor should not be able to 'see' the transport mechanism. If gaps in the production flow are unavoidable, gauging biscuits, for example, then it is essential that the sensor should have a fast and efficient 'gating' facility.
6. An extreme case as stated above is that of vacuum-transported powders such as flour. Here, the instantaneous density is too low for a successful NIR diffuse reflection measurement. This type of situation must be avoided.

   All the product presentation problems can be minimized by intelligent location of the sensor. In practice, excellent results can be obtained.

   A limited number of applications are employed to present samples to an off-line or laboratory sensor. In case of measurement of fruits and vegetables in tree, manual sorting in laboratory or in pack house at small scale, this

arrangement seems to be more appropriate to avoid mechanical complexity of the continuous sorting system and to fit to requirements of the analyzer.

(ii) Liquids-general

The measurement of liquid is generally easier than that of solids. The Beer-Lambert absorption law is followed obeyed unless the liquid is full of particulate matter or extremely turbid. The width of the cuvette of flow-through cell can be adjusted to optimize the absorption sensitivity. Finally, it is relatively easy to adapt existing equipment to make the measurement. A simple test tube may also be used in place of cuvette for holding the liquid sample.

There is a choice between diverting a proportion of the product to an off-line instrument, or installing a cell or an insertion probe directly in the production flow in online condition. Tables 6.5 and 6.6 summarize the advantages and disadvantages of working in the laboratory environment and on-line, respectively. The profiles of some absorption features are significantly temperature dependent. Some form of corrections such as calibrated temperature correction, a chemometrically applied correction or by calculating ratio against a reference cell may be required. Two cells, with the same working gap, are maintained at the same temperature by the process stream. In this way, automatic temperature correction is achieved.

Table 6.5 Advantages and disadvantages of piping of samples in instrument

Advantages	Disadvantages
Preparation and filtering of samples are possible	There may be some difficulty in controlling flow of samples
Sampling from various points are possible	Condition of sample may change in transit
An instrument may be utilized	May not be suitable for the factory environment and only limited quantity of product can be measured
Existing laboratory spectrometers can be utilized	There is possibility of transit delay
There is possibility of stabilized temperature and pressure in the process	"Clean in place" systems are required, otherwise there is a possibility of wastage of samples

Table 6.6 Advantages and disadvantages of measurement "in place"

Advantages	Disadvantages
Fast, accurate and direct measurement	Multiple point measurement is not possible
No wastage of samples	Some form of temperature compensation might be required as control of temperatures and pressures may not be possible
Significant quantity of samples can be tested	Cleaning, maintenance and standardization of probe are difficult
Product usually remain undisturbed	

(a) Cells

Most instrument and accessory manufacturers produce a range of cells of glass or quartz. These can be of fixed-gap or adjustable types. The increasing use of fibre optic coupling has led to the development of more versatile arrangements of open-path cells and attenuated total reflectance (ATR) attachments equally suitable for immersion into laboratory beakers, or via insertion mechanisms into process streams, vats and reaction vessels. Some of these devices employ reflective surface and it is useful to note the distinction between direct transmission and retroreflection. Figure 6.20 shows two cells with the same effective absorption path. When liquid in the cell is clear and the cell is clean, there is no significant distinction between the performances of the two arrangements. However, if the liquid is cloudy, reflection cell will suffer from an apparent gap reduction as a proportion of the light is scattered back from particles or turbidity. The cloudier the contents, the shorter are the effective path. A similar problem occurs if the cell wall is dirty. With the true transmission cell this problem does not arise. Provided that the illumination and collection optics employ quasi-parallel light, the cell will have a high tolerance to particle scattering. Most of the singly- and doubly scattered light will not be collected; and will take almost a direct path through the cell. Light must be at least triply-scattered to be returned to the collection optics after significant

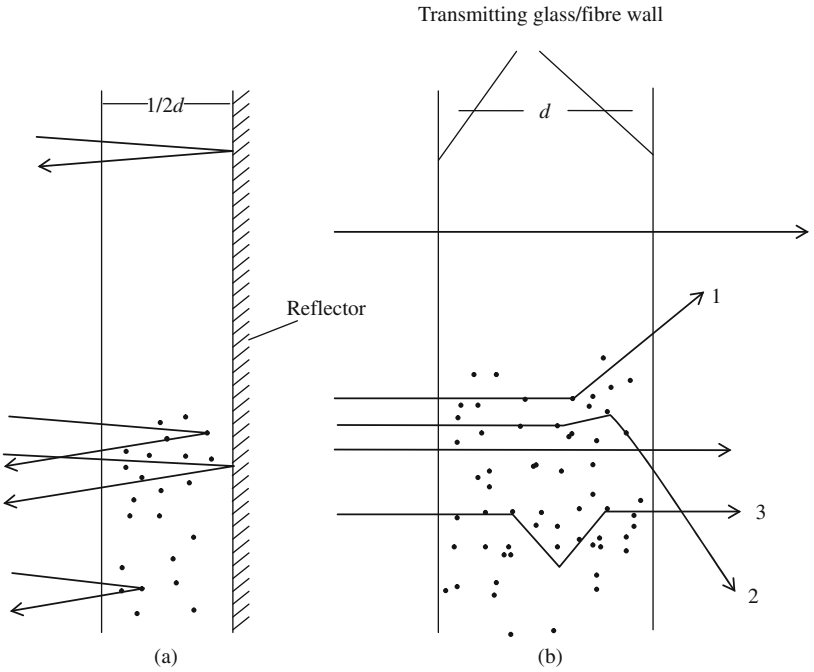

Fig. 6.20 Scattering of light by suspended particles in (**a**) reflecting and (**b**) transmitting sample holder of diameter *d*

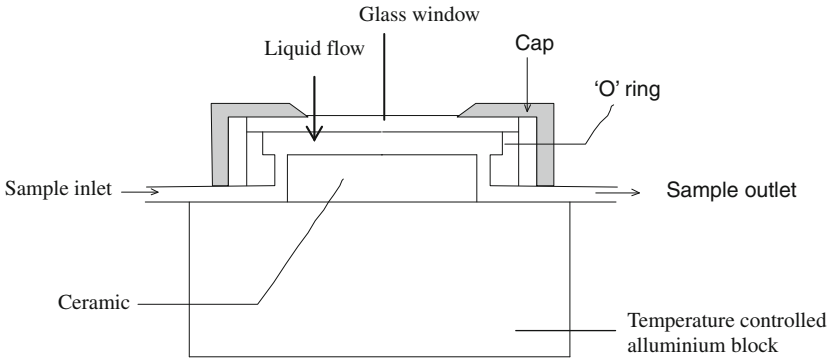

Fig. 6.21 Flowing liquid samples for acquiring transflectance data

deviation and a high level of scattering can be tolerated before this occurs. For situations, where scattering dominates, a 'path-extension ratio' which is related to effective path length through the cell, can be defined. Figure 6.21 is what is known as a transflectance cell originally developed by Technicon to fit the sample drawer of an InfraAnalyzer (Fearn 1982). Rather than using a mirror, the light is scattered back from a ceramic surface to be compatible with the diffuse reflection characteristics of the instrument. It can be noted that the term 'transflectance' also has another meaning in NIR applications. Referring to the measurement of scattering films or sheets it describes the simultaneous collection of back scattered and transmitted energy produced by the instrument. Another simple, less costly holder made of aluminum which can hold liquid samples in ordinary test tube at constant temperature (Jha and Matsuoka 2004a, b) is shown in Fig. 6.23c.

(b) Attenuated total reflection (ATR)

The phenomenon of ATR relates to what happens at the boundary between the high-and low-index materials. It can be shown from Maxwells equations (Born and Wolf 1977) that an electromagnetic disturbance exists in the low-index medium beyond the totally reflecting interface. This energy exhibits the same frequency as the incoming wave but it is evanescent and the amplitude of the electric field falls off exponentially away from the boundary.

$$E = E_o \exp(-d/D) \tag{6.30}$$

E_o is the field strength at the boundary, D is the length attenuation distance or penetration depth, and d is the actual distance. The penetration depth is proportional to the wavelength and also depends on the ratio of the refractive indices and the angle of incidence. The better the index matching, greater is the penetration depth. Also, the penetration depth is infinite at the critical angle and rapidly falls to about $\lambda/10$ at grazing incidence.

Attenuated total reflection occurs when an absorbing medium is very close to, or in contact with, the reflecting surface. The internally reflected light is

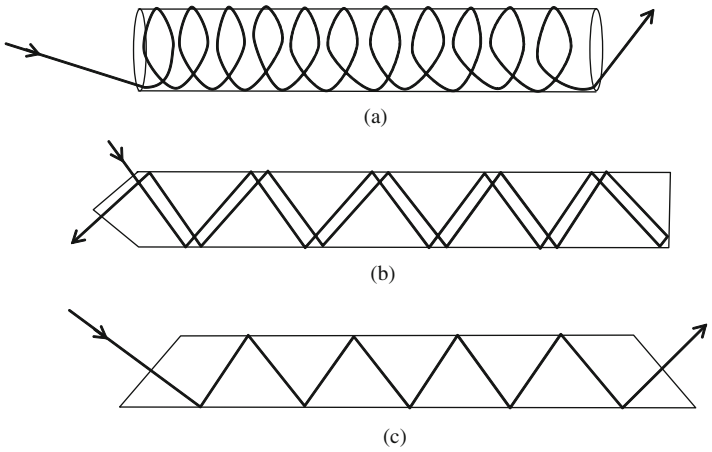

Fig. 6.22 Configurations of ATR crystal (**a**) optical fibre without cladding (**b**) double pass reflection plate (**c**) single pass reflection plate

attenuated, the energy being dissipated as a tiny amount of heat. The reflection loss does not follow a simple law and ATR spectra differ from classical absorption spectra.

As the extent of the evanescent wave is typically only a few wavelength, one reflection is equivalent to a very small transmission cell. For ATR to be useful, multiple reflections are required. There are numerous designs of rods and plates developed for specific applications and the basic concepts are shown in Fig. 6.22. The single-pass arrangement is suitable for mounting across a pipe or in an insertion probe. The double-pass system is ideal for laboratory applications where it can be lowered into a test-tube or flask. The cylindrical rod is interesting because it corresponds to a portion of an optical fibre with the cladding removed. A simple probe incorporating many reflections can be produced this way. In practical instruments, it is useful to ratio against a reference plate or crystal or similar dimensions to the absorption crystal. A clear advantage of ATR technique is the avoidance of using a cell. If the equivalent cell needs to be narrow, for example, significantly less than a millimeter, ATR may be only solution for viscous materials. A disadvantage is that the ATR crystal is vulnerable to the build-up of deposits on its surface and to abrasive substances. Currently, the ATR approach is more popular in the MIR than the NIR where absorptions are stronger and the penetration depth greater.

(iii) Presentation of solids

Solid materials may be measured in transmission or by diffuse reflectance. Measurement can be held with intact or grinded samples. Nowadays usually people prefer intact samples and nondestructive measurements such as protein measurement of whole grain. A few hundred grams of grain are run past the sample area through a cell with a gap of typically 20 mm. There are various commercially-produced sampling systems for achieving this, all deriving an

average over many measurements. For wavelengths in the region 0.8–1.1 μm, transmittances can be obtained through a few centimeters of tissue such as apple or potato, 20 mm of whole grain, 10 mm of homogenized meat or cream and a few millimeters of powders such as flour (Norris 1984). In case of diffuse reflectance measurements, the 1–2.5 μm region is usually employed. Most instruments use a similar construction. A circular quartz cover about 3.5 cm in diameter is mounted in a black plastic cylinder to form a sample holder 1 cm deep. For most substances, this depth ensures negligible transmittance.

In many cases, little preparation is required, but, it is important that the sample should be thoroughly mixed or homogenized prior to analysis. Grains and seeds need to be ground before packing into the cell, if nondestructive measurement is not a compulsion. Most substances will have a significant particle size distribution or will be a heterogeneous mixture. It is vital to prevent stratification causing either a partial separation of components in the sample or larger particles to come to the surface.

The sample should be scooped into the holder and then levelled off with the minimum disturbance. The lid of the cup, a black plastic cover, fitted with lugs to engage the other half of the cup is now placed in position. A backing plate, mounted on a rubber pad is included. This arrangement ensures constant and reproducible packing density. The window of the sample holder is brushed clean prior to insertion in the measuring instrument. Some materials such as biscuits, dough and bread can be placed directly in the sample cup after trimming to size using a knife cutter. Small samples and liquid samples can be supported on glass, fibre paper which act as a diffusely scattering matrix. This method has been used by Meurens (1984) for determining sucrose in soft drinks.

Nowadays various grain analyzers are available using these principles. Numerous holders for solid samples, especially for the individual fruit, have been developed and are in practical use in laboratory (Kawano et al. 1992, Jha and Garg 2010). Self explained photographs of some of them are presented in Fig. 6.23.

Usually commercial instruments offer their own software but increasingly systems are becoming more open with control and acquisition software running on standard Pentium computers. Standard file formats allow transfer of raw data to a range of proprietary software such as ‘Unscrambler’ for chemometric

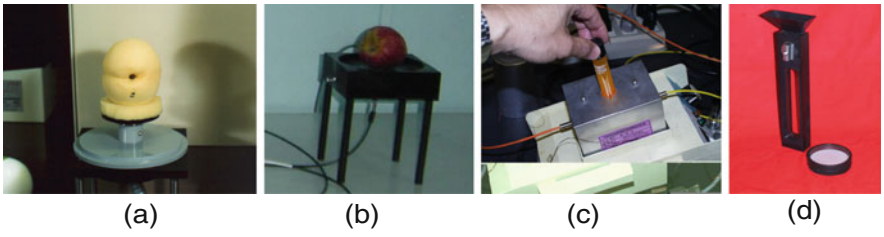

Fig. 6.23 Presentation of various types of samples (**a**) and (**b**) fruits, (**c**) liquid, (**d**) grain

analysis for spectral manipulation. Both microprocessors and associated software are evolving rapidly and the potential user is well advised to consult the trade press or specialists in the field for current information.

6.3 Multivariate Analysis

NIR spectra contain a great deal of physical and chemical information about molecules of a material. The characteristics of NIR bands can be summarized as follows.

- NIR bands are much weaker and broader than IR bands.
- NIR bands strongly overlap with each other because of their origins in overtones and combinations of fundamentals and thus yielding severe multicollinearity.
- NIR bands are difficult to assign because of overlapping of bands, complicated combinations of vibrational modes, and possible Fermiresonance.
- The NIR region is dominated by bands due to functional groups containing a hydrogen atom (e.g., OH, CH, NH). This is partly because the anharmonic constant of an XH bond is large and partly because the fundamentals of XH stretching vibrations are of high frequency.
- Band shift in NIR range is much larger for a particular band as compared to that in mid-IR spectrum because of hydrogen bonding.

From the above characteristics one may consider that NIR spectroscopy has properties that appear to be disadvantageous because NIR bands are weak and broad and overlap heavily. However, NIR spectra are still very rich in inherent information that is extracted through rigorous multivariate analyses.

Multivariate analysis in spectroscopy is a process like churning of cream to get better and larger amount of butter or *ghee* from the same amount of milk. There is no limit of independent and dependent variables. It is like ocean in which you have to dive to get some useful information as per your need and level of satisfaction. A large number of variables are considered and their effects on selected attributes are seen. To simplify the model, independent variables are reduced to a bare minimum possible number by following certain rules and techniques without scarifying the accuracy of prediction of attributes.

NIR spectroscopy is a field where multivariate calibration has shown to be an efficient tool with its ability to embed unknown phenomena (interfering compounds, temperature variations etc.) in the calibration model. Multivariate data analyses are used for a number of distinct, different purposes and have been dealt in details in Chemometrics books. The objective here is to give a brief exposure to new comers into three main aspects:

- Data description (explorative data structure modeling),
- Regression and prediction.
- Discrimination and classification

6.3.1 Data description (Explorative Data Structure Modeling)

A large part of multivariate analysis is concerned with simply "looking" at data, characterizing it by useful summaries and very often displaying the intrinsic data structures visually by suitable graphic plots. As a case in point, the data in question can be state parameter values monitored in an industrial process at several locations, or measured variables (temperature, refractive indices, reflux times, etc.) from a series of organic syntheses – in general any p-dimensional characterization of n samples.

The objective of univariate and multivariate data description can be manifold: determination of simple means and standard deviations, etc., as well as correlations and functional regression models. For example, in case of organic synthesis, interest is in observing variables, which affect the product yield the most. The variables from the synthesis could also be used to answer questions like: how correlated is temperature with yield? Is distillation time important for the refraction index? The Principal Component Analysis (PCA) method is frequently used for data description and explorative data structure modeling of any generic (n, p)-dimensional data matrix.

There are different multivariate techniques such as: PCA, Principal Component Regression (PCR), Partial Least Squares (PLS) and Multiple Linear Regression (MLR). PCA, PCR and PLS are also known as "bilinear modeling". These aspects denote a more geometrical and a more mathematical approach, respectively. One may opt, for instance, to start with the fundamental mathematics and statistics, which lie behind these methods; this is often the preferred approach in statistical textbooks.

Principal component analysis (PCA)

PCA involves decomposing one data matrix, X, into a "structure" part and a "noise" part. There is no Y-matrix, no properties, at this stage. Representing the data as a matrix, the starting point is an X-matrix with n objects and p variables, namely an $n \times p$ matrix. This matrix is often called the "data matrix", the "data set" or simply "the data". The objects can be observations, samples, experiments etc., while the variables typically are "measurements" for each object. The important issue is that the p variables collectively characterize each, and all, of the n objects. The exact configuration of the X-matrix, such as which variables to use – for which set of objects, is of course a strongly problem-dependent issue. The main up front advantage of PCA – for any X-matrix – is that one is free to use practically any number of variables for multivariable characterization. The purpose of all multivariate data analysis is to decompose the data in order to detect, and model, the "hidden phenomena". The concept of variance is very important. It is a fundamental assumption in multivariate data analysis that the underlying "directions with maximum variance" are more or less directly related to these "hidden phenomena".

6.3.2 Regression and Prediction

Regression is widely used in science and technology fields. It is an approach for relating two sets of variables to each other. It corresponds to predicting one (or several) *Y*-variables on the basis of a well chosen set of relevant *X*-variables, where *X* in general must consists of more than, say, three variables. Note that this is often related to indirect observations as discussed earlier. The indirect observation would be *X* and the property we are really interested in would be *Y*. Prediction means determining *Y*-values for new *X*-objects, based on a previously estimated (calibrated) *X*-*Y* model, thus only relying on the new *X*-data. Though, various types of analysis methods are available in statistic book, only certain important and directly usable in NIR spectral modeling/analysis such as PLS, PCR and MLR are described, in brief, hereunder.

(a) Partial least squares regression

It is also known as Projection to Latent Structure (PLS), a method for relating the variations in one or several response variables (*Y*-variables) to the variations of several predictors (*X*-variables), with explanatory or predictive purposes. This method performs particularly well when the various *X*-variables express common information, i.e. when there is a large amount of correlation, or even co-linearity.

PLS is a method of *bilinear modeling* where information in the original *X*-data is projected onto a small number of underlying ("latent") variables called PLS components. The *Y*-data are actively used in estimating the "latent" variables to ensure that the first components are those that are most relevant for predicting the *Y*-variables. Interpretation of the relationship between *X*-data and *Y*-data is then simplified as this relationship is concentrated on the smallest possible number of components.

By plotting the first PLS components one can view main associations between *X*-variables and *Y*-variables, and also interrelationships within *X*-data and within *Y*-data. There are two versions of the PLS algorithm: PLS1 deals with only one response variables at a time; and PLS2 handles several responses simultaneously. Procedure of PLS can be depicted by the Fig. 6.24.

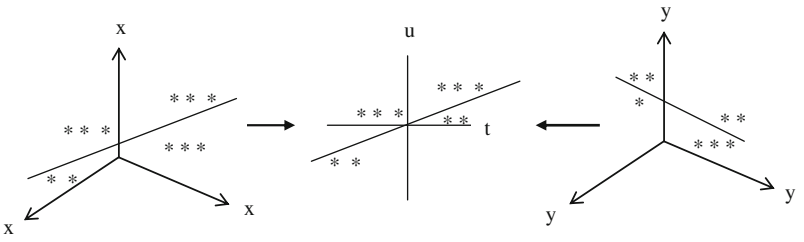

Fig. 6.24 Depiction of PLS procedure

Bilinear modeling: Bilinear modeling (BLM) is one of several possible approaches for data compression. These methods are designed for situations where co-linearity exists among the original variables. Common information in the original variables is used to build new variables that reflect the underlying ("latent") structure. These variables are therefore called latent variables. The latent variables are estimated as linear functions of both the original variables and the observations, thereby the name bilinear. PCR, PCA and PLS are bilinear methods.

$$\boxed{\text{Observations}} = \boxed{\text{Data structure}} + \boxed{\text{Error}}$$

In these methods, each sample can be considered as a point in a multidimensional space. The model will be built as a series of components onto which the samples – and the variables – can be projected. Sample projections are called *scores* and variable projections are called *loadings*.

The model approximation of the data is equivalent to the orthogonal projection of the samples onto the model. The residual variance of each sample is the squared distance to its projection.

It models both the *X*- and *Y*-matrices simultaneously to find the latent variables in *X* that will best predict the latent variables in *Y*. These PLS components are similar to principal components, and will also be referred to as *PCs*.

Principles of projection

Bearing that in mind, the principle of PCA is to find the directions in space along which the distance between data points is the largest. This can be translated as finding the linear combinations of the initial variables that contribute most to making the samples different from each other.

These directions, or combinations, are called *Principal Components* (PCs). They are computed iteratively; in such a way that the first PC is the one that carries most information (or in statistical terms: most explained variance). The second PC will then carry the maximum share of the residual information (i.e. not taken into account by the previous PC), and so on. Figure 6.25 describes PCs 1 and 2 in a multidimensional space. This process can go on until as many PCs have been computed as there are variables in the data table. At that point, all the variation between samples has been accounted for, and the PCs form a new set of coordinate axes, which has two advantages over the original set of axes (the original variables). First, the PCs are orthogonal to each other. Second, they are ranked so that each one carries more information than any of the following ones. Thus, you can prioritize their interpretation: Start with the first ones, since you know they carry more information.

The way it was generated ensures that this new set of coordinate axes is the most suitable basis for a graphical representation of the data that allows easy interpretation of the data structure.

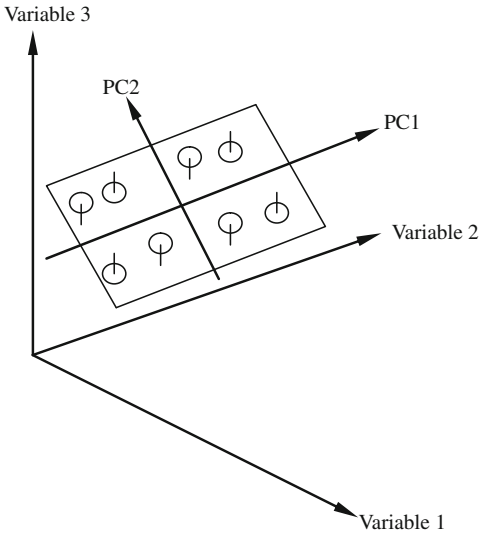

Fig. 6.25 Description of principal components

(b) Principal component regression (PCR)

PCR is a method, which suited in situations as PLS. It is a two-step method. First, a principal component analysis is carried out on the X-variables. The principal components are then used as predictors in a MLR method. The Fig. 6.26 can describe PCR procedure.

(c) Multiple linear regressions (MLR)

It is a method for relating the variations in a response variable (*Y*-variable) to the variations of several *X*-variables, with explanatory or predictive purposes. An important assumption for the method is that the *X*-variables are linearly independent, i.e. no linear relationship exists between the *X*-variables. When the *X*-variables carry common information, problems can arise due to exact or approximate co-linearity.

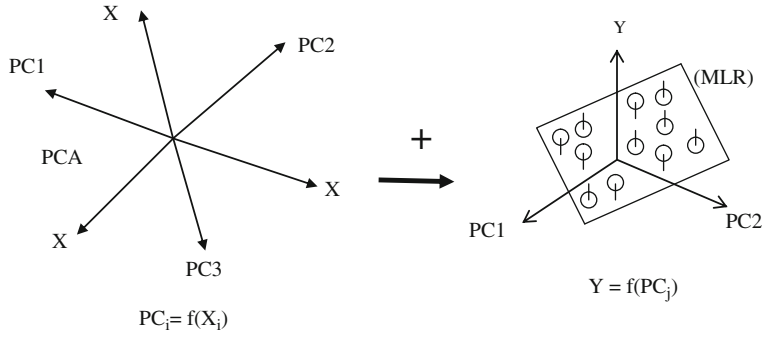

Fig. 6.26 Description of PCR procedure

In MLR, all the *X*-variables are supposed to participate in the model independently of each other. Their co-variations are not taken into account, so *X*-variance is not meaningful there. Thus the only relevant measure of how well the model performs is provided by the *Y*-variances.

6.3.3 Selection of Regression Method

Selection of regression method is of paramount importance in NIR modeling for nondestructive method of quality evaluation of foods. One should know well that which type of analysis is useful to his data for better prediction. For knowing the suitability of regression methods, knowledge of their characteristics are essential to save time. Otherwise one has to analyze data by all techniques and compare results for selection, which is again tedious and time consuming job.

In MLR the number of *X*-variables must be smaller than the number of samples. In case of co-linearity among *X*-variables, the b-coefficients are not reliable and they may be unstable. MLR tends to over fit when noisy data is used.

PCR and PLS are projection methods, like PCA. Model components are extracted in such a way that the first PC conveys the largest amount of information, followed by the second PC, etc. At a certain point, the variation modeled by any new PC is mostly noise. The optimal number of PCs – modeling useful information, but avoiding over fitting – is determined with the help of the residual variances. If difference between standard error of calibration (SEC) and standard error of prediction (SEP) as well as between biases of calibration and prediction sets of samples are minimal, one may assume model is stable. SEP is variation in the precision of predictions over several samples. It is computed as the standard deviation of the residuals and standard deviation is computed as the square root of the mean square of deviations from the mean. Bias is the systematic difference between predicted and measured values. It is computed as the average value of the residuals.

PCR uses MLR in the regression step; a PCR model using all PCs gives the same solution as MLR (and so does a PLS1 model using all PCs).

If one runs MLR, PCR and PLS1 on the same data, one can compare their performance by checking validation errors (Predicted vs. Measured *Y*-values for validation samples root mean square error of prediction, RMSEP). It can also be noted that both MLR and PCR can model only one *Y*-variable at a time.

The difference between PCR and PLS lies in the algorithm. PLS uses the information lying in both *X* and *Y* to fit the model, switching between *X* and *Y* iteratively to find the relevant PCs. So PLS often needs fewer PCs to reach the optimal solution because the focus is on the prediction of the *Y*-variables (not on achieving the best projection of *X* as in PCA).

If there is more than one *Y*-variable, PLS2 is usually the best method if you wish to interpret all variables simultaneously. It is often argued that PLS1 or PCR has better prediction ability. This is usually true if there are strong non-linearity in the data. On the other hand, if the *Y*-variables are somewhat noisy, but strongly correlated, PLS2 is the best way to model the whole information and leave noise

aside. The difference between PLS1 and PCR is usually quite small, but PLS1 will usually give results comparable to PCR-results using fewer components.

Formal tests of significance for the regression coefficients are well known and accepted for MLR. If one chooses PCR or PLS, he may check the stability of his results and the significance of the regression coefficients with Marten Uncertainty Test. However, the final model must be properly validated, preferably by a test set (alternatively with cross validation), but never with just leverage correction.

6.3.4 Modeling Error

How well does the model fit to the *X*-data and to the *Y*-data? How small are the modeling residuals? One may perhaps feel that a good modeling fit implies a good prediction ability, but this is generally not so, in fact only very rarely, that happens. To minimize such chance one should compare at least the SEC, SEP, and biases as discussed in above paragraphs.

6.3.5 Classification Analysis

Classification or sometimes it is called as discrimination of samples, deals with the separation of groups of data. Suppose that you have a large number of measurements of apples and, after the data analysis, it turns out that the measurements are clustered in two groups – perhaps corresponding to sweet and sour apples. You now have the possibility to derive a quantitative data model in order to classify these two groups. Similarly, if a food and drug inspector collects milk samples from different sources just to know which milk sample is adulterated and which not. In this case you have to assign numerical values to these two categories to make digital decision. Classification has a somewhat similar purpose, but here you typically know before the analysis a set of relevant groupings in the data set, that is to say which groups are relevant to model.

Classification thus requires a prior class description. Note that discrimination/classification deals with dividing a data matrix into two, or more groups of samples. Classification thus can be seen as a predictive method where the response is a category variable. The purpose of the analysis is to be able to predict which category a new sample belongs to. Interestingly, here also Principal Component Analysis can be used to great advantage, but there are many other competing multivariate classification methods.

(a) Classification methods

Any classification method uses a set of *features* or *parameters* to characterize each object, where these features should be relevant to the task at hand. We consider here methods for *supervised* classification, meaning that a human expert both has determined into what classes a sample may be categorized and also has provided a set of sample objects with known classes, e.g. adulterated and pure

milk. This set of known objects is called the *training set* because it is used by the classification programs to learn how to classify objects. There are two phases in constructing a classifier. In the training phase, the training set is used to decide how the parameters ought to be weighted and combined in order to separate the various classes of objects. In the application phase, the weights determined in the training set are applied to a set of objects to determine the likely classes they belong to.

If a problem has only a few (two or three) important parameters, then classification is usually an easy problem. For example, with two parameters one can often simply make a scatter-plot of the feature values and can determine graphically how to divide the plane into homogeneous regions where the objects are of the same classes. The classification problem becomes very difficult, when many parameters have to be taken into consideration. The resulting high-dimensional space is not only difficult to visualize, but so many different combinations of parameters of the space rapidly become computationally infeasible. Practical methods for classification always involve a heuristic approach intended to find a ''good-enough'' solution to the optimization problem. There are many classification methods, a few are discussed hereunder in brief:

(i) Neural networks

Among the classification methods, probably neural network methods are most widely known. The biggest advantage of neural network methods is that they are general, they can handle problems with many parameters, and they are able to classify objects well even when the distribution of objects in the *N*-dimensional parameter space is very complex. The disadvantage of neural networks is that they are notoriously slow, especially in the training phase but also in the application phase. Another significant disadvantage of neural networks is that it is very difficult to determine how the net is making its decision. Consequently, it is hard to determine which of the features of the sample being used are important and useful for classification and which are worthless. The choice of the best features as discussed below is an important part of developing a good classifier, and neural nets do not give much help in this process.

(ii) Nearest-neighbour classifiers

A very simple classifier can be based on a nearest-neighbour approach. In this method, one simply finds in the *N*-dimensional feature space the closest object from the training set to an object being classified. Since the neighbour is nearby, it is likely to be similar to the object being classified and so is likely to be the same class as that object. Nearest neighbour methods have the advantage that they are easy to implement. They can also give quite good results if the features are chosen carefully (and if they are weighted carefully in the computation of the distance.) There are several serious disadvantages of the nearest-neighbour methods. First, they (like the neural networks) do not simplify the distribution of objects in parameter space to a comprehensible set of parameters. Instead, the training set is retained in its entity as a description of the object distribution. (There are some thinning methods that can be used on the training set, but the result still does not usually constitute

a compact description of the object distribution.) The method is also rather slow if the training set has many examples. The most serious shortcoming of nearest neighbour methods is that they are very sensitive to the presence of irrelevant parameters. Adding a single parameter that has a random value for all objects (so that it does not separate the classes) can cause these methods to fail miserably.

(iii) Decision trees

Decision tree methods have also been used for solving many problems. In axis-parallel decision tree methods, a binary tree is constructed in which at each node a single parameter is compared to some constant. If the feature value is greater than the threshold, the right branch of the tree is taken; if the value is smaller, the left branch is followed. After a series of these tests, one reaches a leaf node of the tree where all the objects are labeled as belonging to a particular class. These are called axis-parallel trees because they correspond to partitioning the parameter space with a set of hyperplanes that are parallel to all of the feature axes except for the one being tested.

Axis-parallel decision trees are usually much faster in the construction (training) phase than neural network methods, and they also tend to be faster during the application phase. Their disadvantage is that they are not as flexible at modeling parameter space distributions having complex distributions as either neural networks or nearest neighbour methods. In fact, even simple shapes can cause these methods difficulties. For example, consider a simple 2-parameter, 2-class distribution of points with parameters x, y that are all of type 1 when $x>y$ and are of type 2 when $x<y$. To classify these objects with an axis-parallel tree, it is necessary to approximate the straight diagonal line that separates the classes with a series of stair-steps. If the density of points is high, many steps may be required. Consequently, axis-parallel trees tend to be rather elaborate, with many nodes, for realistic problems.

(iv) Oblique decision trees

Oblique decision trees attempt to overcome the disadvantage of axis-parallel trees by allowing the hyperplanes at each node of the tree to have any orientation in parameter space. Mathematically at each node a linear combination of some or all of the parameters are computed (using a set of feature weights specific to that node) and the sum is compared with a constant. The subsequent branching until a leaf node is reached is just like that used for axis-parallel trees.

Oblique decision trees are considerably more difficult to construct than axis-parallel trees because there are so many possible planes to consider at each tree node. As a result the training process is slower. However, they are still usually much faster to construct than neural networks. They have one major advantage over all the other methods: they often produce very simple structures that use only a few parameters to classify the objects. It is straightforward through examination of an oblique decision tree to determine which parameters were most important in helping to classify the objects and which were not used.

There are many other methods and software for classifying the samples in different categories. For example The Unscrambler has soft independent

modeling by class analogy (SIMCA) model using PCA and PLS regression for these purposes. SIMCA focuses on modeling of similarities between members of the same class. A new sample will be recognized as a member of the class, if it is similar enough to the other members; else it will be rejected. Readers are advised to consult software or relevant books which deals exclusively in these topics.

(b) Steps in developing a classifier

The choice of an algorithm for classification is in many ways the easiest part of developing a scheme for object classification. The discussion above demonstrates that there are several ''off-the-shelf'' approaches available (though there is obviously still room for improvement). There are two major hurdles to be faced before these methods can be used, though: a training set must be constructed for which the true classifications of the objects are known, and a set of object parameters must be chosen that are powerful discriminators for classification. Once a possible classifier has been identified, it is necessary to measure its accuracy.

(i) Training set

A training set must contain a list of objects with known classifications. Ideally the training set should contain many examples (typically thousands of samples) so that it includes both common and rare types. Creating a training set requires a source of true object classifications, which is usually difficult even for human experts to generate if it must rely on the same data being used by the classifier.

To construct a training set for example to identify the adulterated samples of milk, one has first to identify all possible adulterants including water and identify the more sensitive factor and accordingly simulate them giving proper weight. It is difficult but to know the adulterants it should be done. To know just whether samples are adulterated or not is easier as in this case there will be only two class and we can assign them specific values to make a separate group.

(ii) Feature selection

Adding many irrelevant parameters makes classification harder for all methods, not just the nearest neighbor methods. Training classifiers is an optimization problem in a many-dimensional space. Increasing the dimensionality of the space by adding more parameters makes the optimization harder (and the difficulty grows exponentially with the number of parameters.) It is always better to give the algorithm only for the necessary parameters rather expecting it to learn to ignore the irrelevant parameters.

One should not ask the classifier to rediscover everything you already know about the data. Not only should irrelevant parameters be omitted, but highly correlated parameters should be combined when possible to produce a few powerful features. For example, if you expect the shapes of images of a particular class of object to be similar, include a brightness-independent shape parameter rather than simply giving the classifier raw pixel values and expecting it to figure out how to extract shape information from the pixel values.

If the training process does not require too much computation, a useful approach to identify the best parameter is to train many times on subsets of the features. This method can be used in two ways, both starting from the complete list of features and reducing it by removing parameters, and starting from a minimal list, augmenting it by adding parameters. Both methods have proven effective at pruning unnecessary parameters. This procedure can be very fast if axis-parallel trees are used for the exploration.

Another useful approach with the decision tree methods is to examine directly the weights assigned to the various features. Important features are given a high weight, while unimportant features may not be used at all. This information can be used as a guide for pruning experiments.

(c) Assessing classifier accuracy

Once a potentially useful classifier has been constructed, the accuracy of the classifier must be measured. Knowledge of the accuracy is necessary both in the application of the classifier and also in comparison of different classifiers.

The accuracy can be determined by applying the classifier to an independent training set of objects with known classifications. This is sometimes trickier than it sounds. Since training sets are usually difficult to assemble, one rarely has the resources to construct yet another set of objects with known classifications purely for testing. One must avoid the temptation to train and test on the same set of objects, though. Once an object has been used for training, any test using it is necessarily biased.

We normally use five-fold cross-validation to measure the accuracy of our classifiers. The training set is divided into five randomly selected subsets having roughly equal numbers of objects. The classifier is then trained five times, excluding a single subset each time. The resulting classifier is tested on the excluded subset. Note that each training session must be completely independent of the excluded subset of objects; one cannot, for example, use the results of an earlier training session as a starting point.

The advantage of cross-validation is that all objects in the training set get used both as test objects and as training objects. This ensures that the classifier is tested on both rare and common types of objects. The cost of cross-validation is that the training process must be repeated many times, adding to the computational cost of the training. In most applications, though, the computer time necessary to repeat the training is more readily available than is the human expert time required to generate completely independent test and training sets.

6.3.6 Validation of NIR Model

Validation of a model means testing its performance on unknown set of samples, which has not been used in calibration and whose actual results or specifications are known. This new data set is called the test set. It is used to test the model under realistic, future conditions, specifically because it has been sampled so as to represent

these future conditions. Indeed if possible, one should even use several test sets. "Realistic" here means that the test set should be chosen from the same target population as the calibration set, and that the measuring conditions of both the training (calibration) set and the test set are as representative of the future use as indeed possible. However, this does not mean that the test set should be too closely similar to the training set. For instance, it will not do to simply divide the training set in two halves, provided the original set is large enough, as has unfortunately sometimes been recommended in chemometrics. This would decidedly be wrong. The brief overview below is intended only to introduce those important issues of validation which must be borne in mind when specifying a multivariate calibration. From a properly conducted validation, one gets some very important quantitative results, especially the "correct" number of components to use in the calibration model, as well as proper, statistically estimated, assessments of the future prediction error levels.

(a) Test set validation

The procedure introduced above – using a completely new data set for validation – is called test set validation. There is an important point here; one also has to know the pertinent *Y*-values for the test set, just as said for the calibration set. The procedure involved in test set validation is to let the calibrated model predict the *Y*-values and then to compare these independently predicted values of the test set with the known, real *Y*-values, which have been kept out of the modeling as well as the prediction so far. Generally predicted *Y*-values are called *Y*pred and the known, real *Y*-values as *Y*ref. (hence the term "reference" values). An ideal test set situation is to have a sufficiently large number of training set measurements for both *X* and *Y*, appropriately sampled from the target population. This data set is then used for the calibration of the model. Now an independent, second sampling of the target population is carried out, in order to produce a test set to be used exclusively for testing/validating of the model, i.e. by comparing *Y*pred with *Y*ref. The comparison results can be expressed as prediction errors, or residual variances, which now quantify both the accuracy and precision of the predicted *Y*-values, i.e. the error levels which can be expected in future predictions.

(b) Cross-validation

There is no better validation than test set validation: testing on an entirely "new" data set. One should always strive to use validation by test set. TEST IS THE BEST! There is, however, a price to pay. Test set validation entails taking twice as many samples as would be necessary with the training set alone. However desirable, there are admittedly situations in which this is manifestly not always possible. For example when the measuring of the *Y*-values is (too) expensive, unacceptably dangerous or the test set sampling is otherwise limited, e.g. for ethical reasons or when preparing samples is extremely difficult etc. For this situation, there is a viable alternative approach, called cross validation. Cross validation can, in the most favourable of situations, be almost as good as

test set validation, but only almost – but it can never substitute for a proper test set validation! And the most favourable situations do not occur very often either.

(c) Leverage corrected validation

This is a "quick and dirty" validation method. This is actually the one which was being used initially, because we had not yet introduced the concept of validation. This method uses the same calibration set to also validate the model, but now "leverage-corrected". It is obvious that this may be a questionable validation procedure; all depending on the quality of the corrections employed. Furthermore this often gives results, which are too optimistic. However, during initial modeling, where the validation is not really on the agenda yet, this method can be useful as it saves time.

6.3.7 Data Pre-processing

Detection of outliers, groupings, clusters, trends etc. is just as important in multivariate calibration as in PCA, and these tasks should in general always be first on the agenda. In this context one may use any validation method as discussed above in the initial screening data analytical process, because the actual number of dimensions of a multivariate regression model is of no real interest until the data set has passed this stage, i.e. until it is cleaned up for outliers and is internally consistent etc. In general, removal of outlying objects or variables often influences the model complexity significantly, i.e. the number of components will often change.

There are however, still a large number of applications that utilize only two or three wavelengths in routine prediction. These applications have shown that the full PLS model is sometimes inferior to a model based on a relatively small number of variables found in various methods for variable selection. This is partly due to the redundancy and the large amount of noisy, not relevant variables in NIR spectra. Recent results show that variable selection based on jack-knife estimates is a fast and reliable method with low risk of over fitting.

(i) Spectroscopic transformations

Most spectroscopists prefer to work with absorbance data, because they are more familiar with this type of data, and feel more at home interpreting absorbance spectra. Many modern multi-channel analytical instruments can provide spectra as absorbance readings, using some form of correction and transformation. If you do not know which formula is used in the instrument software, it may be wise to import the raw spectra instead and make the appropriate transformations yourself. In general it is recommended that you start by analyzing the absorbance spectra. If this does not work, then you should try to transform your data. Transmission data are often nonlinear, so they are "always" transformed into, e.g. absorbance data, using a modified logarithmic transformation. Diffuse reflectance data are "always" transformed into Kubelka-Munk units, but exceptions may be around in more

problem-specific cases. The Multiplicative Scatter Correction is another very useful transformation for spectroscopic data.

(ii) Reflectance to absorbance

We shall here assume, without loss of generality, that the instrument readings R (Reflectance), or T (Transmittance), are expressed in fractions between 0 and 1. The readings may then be transformed to apparent absorbance (Optical Density).

(iii) Absorbance to reflectance

An absorbance spectrum may be transformed to Reflectance/Transmittance directly using appropriate analysis software or even using the spectra acquisition software.

(iv) Absorbance to Kubelka-Munk

In addition the apparent absorbance units may also be transformed into the pertinent Kubelka-Munk units by performing two steps: first transform absorbance units to reflectance units, and then reflectance to Kubelka-Munk.

(v) Transmission to absorbance and back

It can be done by computing function using the expression $X = -\log(X)$ to transform X from transmission into absorbance data. $X = 10^{(-X)}$ gives transmission data again.

(vi) Multiplicative scatter correction (MSC)

Spectroscopic measurements of powders, aggregates of grains of different particle sizes, slurries and other particulate-laden solutions often display light scattering effects. This especially applies to NIR data, but is also relevant to other types of spectra; scatter effects in IR spectra may be caused by background effects, varying optical path lengths, temperature, and pressure variations. Raman spectra also often suffer from background scattering. In UV-VIS varying path lengths and pressure may cause scatter. These effects are in general composed both of a so-called multiplicative effect as well as an additive effect. Other types of measurements may also suffer from similar multiplicative and/or additive effects, such as instrument baseline shift, drift, interference effects in mixtures, etc. Multiplicative Scatter Correction is a transformation method that can be used to compensate for both multiplicative and additive effects. MSC was originally designed to deal specifically with light scattering. However, a number of analogous effects can also be successfully treated with MSC. In The Unscrambler MSC transformation can be done from the Modify – Transform menu. The idea behind MSC is that these two undesired general effects, amplification (multiplicative) and offset (additive), should be removed from the raw spectral signals to prevent them from dominating over the chemical signals or other similar signals, which often are of lesser magnitude. Thus we may well save one or more PLS-components in our modeling of the relevant *Y*-phenomena, if we were able to eliminate (most of) these effects before multivariate calibration. This, in general, will enable us to proceed with more precise and accurate modeling, based on the cleaned-up spectra. MSC can be a very powerful general pre-processing tool.

(vii) Derivatives computations

The first or second derivatives are common transformations on continuous function data where noise is a problem, and are often applied in spectroscopy. Some local information gets lost in the differentiation but the "peakedness" is supposed to be amplified and this trade-off is often considered advantageous. It is always possible to "try out" differentiated spectra, since it is easy to see if the model gets any better or not. As always however, you should preferentially have a specific reason to choose a particular transformation. And again, this is really not to be understood as a trial and error optional supermarket – experience, reflection, and more experience! The first derivative is often used to correct for baseline shifts. The second derivative is often used as an alternative to handling scatter effects, the other being MSC, which handles the same effects.

(viii) Averaging

Averaging is used when the goal is to reduce the number of variables or objects in the data set, to reduce uncertainty in measurements, to reduce the effect of noise, etc. Data sets with many replicates of each sample can often be averaged over all sets of replicates to ease handling regarding validation and to facilitate interpretation. The result of averaging is a smoother data set. A typical situation in routine applications is fast instrumental measurements, for instance spectroscopic *X*-measurements that replace time-consuming *Y*-reference methods. It is not unusual for several scans to be done for each sample. Should we average the scans and predict one *Y*-value for each sample, or should we make several predictions and average these? Both of these give the same answer, which is why averaging can also be done on the calibration data and its reference values.

(ix) Normalization

Normalization is concerned with putting all objects on an even footing. In above paragraph, we have so far mostly treated the so-called column-transformations, i.e. making specific pre-processing or transformations which act on one column-vector individually (single-variable transformations). Normalization is performed individually on the objects (samples), not on the variables (such as wavelength in NIRS). Each object vector is re-scaled – normalized – into a common sum, for example 1.00 or 100%. The row sum of all variable elements is computed for each object. Each variable element is then divided by this object sum. The result is that all objects now display a common size – they have become "normalized" to the same sum area in this case. Normalization is a row analogy to column scaling (1/SDev). Normalization is a common object transformation. For instance, in chromatography it is used to compensate for (smaller or larger) variations in the amount of analyte injected into the chromatograph. Clearly it will be of considerable help in the analytical process if this particular measurement variance can be controlled by a simple data analytic pre-processing like normalization, otherwise a whole extra PLS-component would have

to be included in order to model these input variations. There are several other data analysis problems where normalization can be used in a similar fashion.

6.4 Practical Application of NIRS

6.4.1 Quantitative Prediction

The use of near-infrared spectroscopy for predicting the composition of biological materials has been demonstrated for many commodities. Recently, it has become a useful technique for measuring soluble solids content (SSC), fruit firmness, acidity etc. (Lu and Ariana 2002, Lu et al. 2000, Lu and Peng 2006, McGlone and Kawano 1998, Peng and Lu 2007, 2006a, b). Lu (2003, 2004) developed a technique for estimating fruit firmness, based on analyzing scattering images from the fruit at multiple wavelengths in the visible and near-infrared (NIR) region. Radial scattering profiles were extracted and analysed using neural network prediction model, which gave good firmness prediction for apple fruit. Peng and Lu (2006b) further proposed a Lorentzian (LD) function with three parameters to characterize the multispectral scattering profiles of apple fruit. In analyzing hyperspectral scattering images for peach fruit, Lu and Peng (2006) utilized a two-parameter LD function for prediction of peach fruit firmness. More recently, Peng and Lu (2006b) proposed a modified Lorentzian distribution (MLD) function with four parameters to describe the entire scattering profiles, including saturation area of the spectral scattering images acquired by a compact multispectral imaging system equipped with a liquid crystal tunable filter (LCTF). Numerous investigations to quantify the natural sugars in different fruit juices have also been conducted using NIR and FTIR spectroscopy (Luis et al. 2001, Lijuan et al. 2009, Bureau et al. 2009). In one study, content of various sugars in juice of naturally ripe mango stored at –20°C was determined using FTIR spectroscopy (Duarte et al. 2002). An official method to determine the protein content of wheat was established long ago using NIRS (AACC 1983).

Now various NIR spectrometers are available and are being used commercially. Some modifications in these available spectrometers, especially for holding the intact samples, are available. In the same sample holder a test tube for holding liquid foods such as milk was also used to estimate fat content (Chen et al. 1999). Jha et al. 2006 has identified the quality parameters of mango to be used for their determination using visual and/or NIR spectroscopy. Eating quality of some ripe mangoes has also been determined in Japan with good accuracy (Saranwong et al. 2004). Numerous works for quality evaluation of other food materials using NIR spectroscopy is reported but are beyond the scope of this book to accommodate all (Jha and Matsuoka 2000, 2004b, Jha 2007, Jha et al. 2010, Jha and Garg 2010). To understand the whole process for new researchers in this field, right from experimentation to final prediction of sweetness and sourness of tomato juice (a liquid sample) (Jha and Matsuoka 2004a) and sweetness of apple (solid sample) is presented hereunder:

(a) Prediction of acid-brix ratio (ABR) of tomato juice

(i) Instrumentation

An NIR transmittance measuring unit similar to that described by Jha et al. (2001) was assembled (Fig. 6.27). The spectrometer (MMS1, Zeiss, Germany) used in this experiment has a spectral wavelength range between 311.7 and 1,124.8 nm with a spectral resolution of 3.3 nm and a 256-element photodiode array detector. The optical fibre bundle (0.5 mm diameter) contained thirty individual fibres of 70 μm diameter. Elongated and rectangular shaped detector elements allow the fibre bundle to be rearranged in a linear fashion to function as the entrance slit of the spectrometer. The halogen lamp (100 W), which had a voltage-regulating knob graduated in ten divisions for controlling the intensity of light, was used as a light source. A sample holder similar to the cell reported by Chen et al. (1999) for liquid was used in the experiment.

(ii) Materials

Good quality fully ripened tomato (cv house momotaro), cultivated hydrophonically in a greenhouse was harvested and sorted manually. Good colour (fully red) and size (big) were selected so that sufficient amounts of juice with a wide range of acid and brix values were obtained. One hundred and ten of them were numbered randomly for using in the experiment.

Tomatoes were cut in two halves and wrapped in a piece of muslin cloth (Hikari, Heiwa, Japan). A plunger type hand juicer was used to compress the wrapped tomato till juice was coming out through the wrapped muslin cloth. The flesh, skin and seeds of tomato retained in muslin cloth were thrown away. The extracted juice was thoroughly shaken and about 50 mL was filtered for experimental use, by using another piece of the same muslin cloth to minimize the suspended solid particles. A new piece of cloth was used for each sample for filtration. The sweetness and sourness of samples were measured in terms of °Brix by using a digital refractometer (Model PR-101, Atago Co., Tokyo, Japan) and acid values (titratable acid, %),

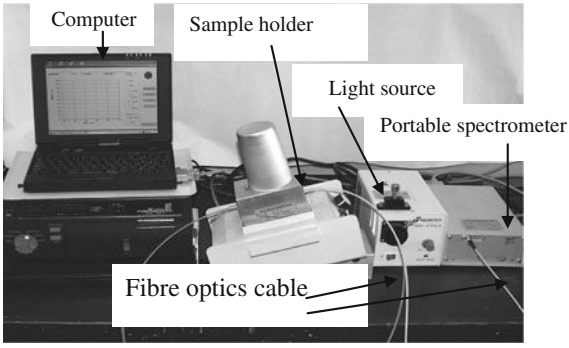

Fig. 6.27 NIR setup for measurement of transmittance of liquid samples

which were measured by an acid meter (Sourty, Model Sou-1, Shimadzu, Japan) supplied with a standard reagent. Test tubes filled with filtered juice of known acid and brix values were kept in a water-bath at 30°C for about 30 min so that all samples experienced a constant and uniform temperature before spectra acquisition because there is an appreciable effect of samples' temperature on spectra (Kawano et al. 1995). The temperature of the water-bath was set and verified by a mercury thermometer before putting the sample in it. Acid and brix values of juice samples at uniform temperature were again measured and the mean of two values, before and after keeping in water-bath, were computed. The average acid value was divided by the average brix value of the same juice to obtain acid–brix ratio (ABR), which could then be used to calibrate the NIR model.

(iii) Spectra acquisition

A test tube (12 mm diameter, 10 mL capacity) filled with tomato juice was placed into the vertical hole of an aluminum block that had a pre-set temperature of 30°C and was kept constant by a temperature controller (least count ± 0.1°C). Test tubes were covered by an aluminum tumbler to prevent any incident light and illuminated by the light (wavelength range 311.7–1,124.8 nm) from the halogen lamp (100 W) via fibre bundles (0.5 mm diameter) at one side of the block (Fig. 6.27). The transmitted energy was detected by a silicon detector at 180° to the light source at the other side of the block and was transmitted through the fibre optics (0.5 mm diameter) to the MMS1 system connected to a computer loaded with software (Japanese version Bunko, Tokyo, Japan) supplied with the MMS1 spectrometer system to acquire the spectra. The intensity of the light source was adjusted and fixed to 70% of its full capacity using the graduated knob provided for the purpose in front of the light source box. The spectra of 110 samples over the wavelength region from 311.7 to 1,124.8 nm were obtained by averaging 100 scans each of 10 ms. A ceramic plate (2 mm thickness) was held vertically in a slot cut to be exactly perpendicular to the source detector axis through the centre of the hole made in the aluminum block for holding the test tube and this plate was used as the reference material. Dark (by blocking the light) and reference spectra were acquired after every ten samples and the absorbance spectra were recorded.

(iv) Data analysis

Acquired spectra were imported to the Unscrambler (CAMO AS, Trondheim, Norway), a statistical software package, for multivariate calibration. Data of all 110 samples were plotted to inspect the nature of spectra. Three samples were identified as outliers because of their somewhat odd nature when compared with the rest of the samples. Data between the wavelengths 311.7–700 nm and outlier samples were deleted. The remaining samples (107) were split randomly into calibration (54 samples of ABR range 0.05–0.14, mean 0.094 and s.d. 0.022) and validation (53 samples of ABR range 0.06–0.15, mean 0.097 and s.d. 0.023) sets before further analysis of the spectral data between wavelengths 703.25–1,124.8 nm.

In order to search for a small and simple model, spectra between wavelength range 703.3–1,124.8 nm were divided into six separate regions with an almost equal number of data/region as: 703.3–775, 778.3–846.3, 849.5–917, 920.2–987.1, 990.3–1,056.4 and 1,059.5–1,124.8 nm. Partial least squares (PLS) regression was calculated on the original and preprocessed (treated) spectra over the whole range of wavelength (703.3–1,124.8 nm) so as to develop a calibration model for determining the ABR of tomato juice. Second derivative, multiplicative scatter correction (MSC) and smoothing were applied to the two best models and the model of the whole range of wavelength used as a preprocessing treatment in order to improve their predictability. The best amongst them, based on their standard error of calibration (SEC), correlation coefficients (R), and optimum number of latent variables (factors) used in the calculation, were selected. The optimum number of factors was selected at a minimum level of mean-squared error to avoid over fitting. The performance test of the calibration model for prediction of ABR of tomato juice was done on another set of validation samples.

(v) Results and discussion

NIR spectra

The original spectrum of tomato juice in the wavelength range between 703.3 and 1,124.8 nm is shown in Fig. 6.28. Visual inspection of the spectra did not show any obvious special characteristics that could be used in quantitative measurement, except that the relative absorbance increased with wavelength between both 925 and 975 nm; and between 1,050 and 1,125 nm. This caused an increased discrimination between the spectra. The peak and depression in the spectra around 971 and 1,053 nm, respectively, showed the strong and weak absorbance characteristics of tomato juice within this region.

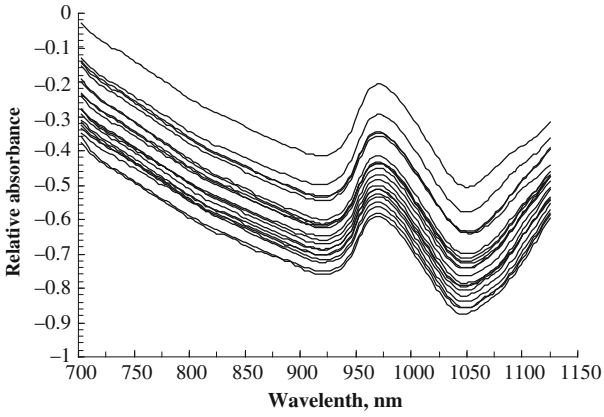

Fig. 6.28 Original spectra of tomato juice

Calibration and prediction

Different calibration models involving different sets of wavelengths were calculated for acid–brix ratio (ABR) using PLS (Table 6.7). The quality of the calibration model was quantified by the standard error of calibration (SEC), standard error of prediction (SEP) and the correlation coefficient (R) between the predicted and measured parameter. A good model should have a low SEC, a low SEP, a high correlation coefficient but also a small difference between SEC and SEP. A large difference indicates that too many latent variables (principal components) are used in the model and noise is modelled (Lammertyn et al. 1998). The SEC and SEP values decreased with data sets from higher wavelengths except over the wavelength range 849.5–917 nm, whereas the correlation coefficients (R) followed the reverse trend (Tables 6.7 and 6.8). Among the sets of wavelengths tested, the SEC, SEP and bias values were found to be the lowest

Table 6.7 Statistical results of PLS regression of different sets of wavelengths for determining the acid-brix ratio of tomato juice of calibration and validation samples' sets (Jha and Matsuoka 2004b)

		SEC/SEP[a]		Bias		Correlation	
Wavelength range (nm)	Factor	Calibration	Validation	Calibration	Validation	Calibration	Validation
703.3–775.0	8	0.105	0.112	0.005	0.004	0.80	0.74
778.3–846.3	8	0.049	0.053	0.003	0.002	0.83	0.81
849.5–917.0	8	0.057	0.051	0.003	0.004	0.82	0.78
920.2–987.1	8	0.046	0.047	0.005	−0.004	0.84	0.85
990.3–1,056.4	8	0.024	0.035	0.004	0.007	0.89	0.86
1,059.5–1,124.8	8	0.009	0.009	0.000	−0.003	0.92	0.92
703.3–1,124.8	8	0.453	0.628	0.013	0.024	0.78	0.77

[a]SEC, standard error of calibration; SEP, standard error of prediction.

Table 6.8 Influence of preprocessing of spectra on the prediction performance of PLS models of different sets of wavelength (Jha and Matsuoka 2004b)

		Calibration		Validation	
Wavelength range (nm)	Preprocessing methods	SEC	Correlation	SEP	Correlation
703.3–1,124.8	Second derivative	0.143	0.78	0.156	0.73
	MSC	0.129	0.79	0.121	0.75
	Smoothing	0.152	0.73	0.166	0.71
1,059.5–1,124.8	Second derivative	0.015	0.90	0.018	0.89
	MSC	0.011	0.91	0.011	0.90
	Smoothing	0.063	0.89	0.048	0.90
990.3–1,056.4	Second derivative	0.028	0.86	0.038	0.87
	MSC	0.026	0.88	0.035	0.89
	Smoothing	0.072	0.85	0.047	0.86

(0.009) and the value of *R* was the highest (0.92) for the wavelength range 1,059.5–1,124.8 nm, whereas for the full wavelength range (703.3–1,124.8 nm), the SEC, SEP, and bias were found to be the highest and the *R*-value was the lowest in both the cases, i.e., untreated and treated (preprocessed) models (Tables 6.7 and 6.8). The reason may be that the data from the entire range of wavelength may include many weak absorbance bands as compared with sets of wavelength of smaller range. The preprocessing of spectra such as computation of second order derivatives, MSC and smoothing of spectra could not improve the calibration models (Table 6.8), in contrast to some previous reports from other materials (Kawano et al. 1992, 1993), this was not the case for the model obtained directly from the original spectra without any treatment. However the treatment effect of MSC, based on SEC/SEP and *R*-values, was found to be the best, whereas it was the least for the smoothing. The effect of sample cell (test tube in this case) was not investigated, however, the NIR spectra of milk were affected in the same way as chemical components of the sample in the sample cell used (Chen et al. 1999).

The best calibration model was obtained by using PLS regression on the original spectra between the wavelengths from 1,059.5 to 1,124.8 nm. The reason for this may be that there is a strong absorption band of the acid contents of tomato juice and the parallelism of the majority of spectra after about 1,060 nm wavelength. If the spectra are parallel, the response of the detector for the sample is linear within the range of study, which in turn may give better results (Kawano et al. 1993). To check the performance of the calibration model, whose regression coefficients could be used directly in prediction, fifty-three validation samples were used. The predicted results for both original as well as preprocessed spectra of each segment are almost the same as the calibration results (Table 6.7). The calibration and validation results show that the SEC, SEP and correlation coefficients *R* are similar with no significant bias in either of the cases. Similarities in these values also dispel the confusion of over fitting of the model. In the literature, no model for ABR in tomato juice is available to compare with the present results. However, the performance of the model that has been developed in this work is better than a model that has been reported to be able to predict the soluble solids in intact tomatoes with a correlation coefficient of 0.92 for calibration, but with a very poor correlation coefficient (only 0.57) for prediction besides having larger SEC- and SEP-values (Peiris et al. 1998). This NIR model may be able to accurately determine the acid–brix ratio of tomato juice to give an indicator of taste using a single NIR model for practical usage.

(b) Prediction of taste of whole fruits

A numerous work on measurement of TSS and acidity of majority of fruits using NIRS has been reported in literature. Some work on apple and mango has also been reported from India. Experiments and their results for apple (Jha and Garg 2010) are reported hereunder for an exposure to the new entrants in this field.

(i) Sample collection

In order to find the taste of apple in terms of sweetness (TSS), sourness (titratable acidity %), and acid brix ratio, freshly harvested apples (*Malus domestica* Borkh) variety 'Golden Delicious', 'Red Delicious', 'Ambri' and 2 unknown varieties were procured from local fruit market, Ludhiana. The samples were brought to laboratory and screened manually to discard the damaged ones. Sound apples were wiped with muslin cloth to remove dirt and kept for 28 days at 32±0.5°C and 65±7% RH for accelerated changes in biochemical quality parameters. Three samples from each variety were randomly chosen bi-weekly for experimentation.

(ii) Spectra acquisition

Transmittance spectra in wavelength range of 900–1,700 nm of 118 apples were acquired using a portable NIR-spectrometer (model EPP 2,000-InGaAs, 2.25 nm resolution StellarNet Inc., USA) connected to 30 W halogen lamp and sample holder with 400 μm optical fibre cable and spectra wiz software (version 3.3). Dark and reference spectra for a standard supplied with the equipment were taken for 50 scan in 100 ms integration time. Apple fruit was then placed on sample holder arbitrarily from girth side in stable position by hand (Fig. 6.29). The probe (having both fibres for sending light and sensor for receiving the transmitted light) was fixed in the centre of the base of sample holder and transmittance spectra were acquired at an interval of 2.25 nm for the wavelength range of 900–1,700 nm.

(iii) TSS and acidity measurement

Immediately after recording the spectra, juice of the whole apple was extracted using domestic juicer at ambient room temperature (28–30°C) and filtered through a new piece of muslin cloth every time. The TSS of the filtered juice was measured thrice using a hand held digital refractometer (Pal-1, Atago, range 0–53°Brix, least count 0.2°Brix, Japan) and acidity was determined using standard titration method (AOAC 1990). Mean values were used for computation of acid-brix ratio and for NIR calibration and validation.

(iv) Data analysis

NIR spectral data were imported to MS-excel software from spectra wiz software, and then to Unscrambler (CAMO AS, Trondheim, Norway,

Fig. 6.29 NIR spectra acquisition set-up

version 8.0.5) software for multivariate analyses with TSS, acidity and acidity/TSS ratio. Spectral data were plotted to inspect the nature of the spectra. Four curves visually odd amongst the group were identified as outlier and were deleted. Altogether 114 samples were used for calibration and validation for prediction of TSS, acidity and acidity/TSS ratio.

Two methods of regression, partial least square regression (PLS) and multiple linear regressions (MLR) with the option of full cross validation available in the software were performed on the whole original spectra to develop the NIR model for predicting TSS, acidity and acidity/TSS ratio non-destructively. In order to search for a small and simple model, the whole range of spectra was divided into small groups of 35 wavelengths continuously at an interval of 2.25 nm and both PLS and MLR were performed on each group. The best models based on the standard error of calibration (SEC), multiple correlations coefficients (R) and standard error of prediction (SEP) were selected.

In order to improve the predictability of selected models, pre-processing of spectra such as smoothing (second order, S. Golay), full multiplicative scatter correction (MSC) and second order derivative (Savitzky-Golay, by averaging one point to the left and one point to the right and fitting a second order polynomial) of selected range of wavelengths were performed. A few outlier samples were also identified with the help of software and removed for further improvements in the models. To minimize the number of wavelengths further, the effect of individual wavelength by eliminating them from the model of best performing group of wavelengths on the root mean square error was investigated (Kawano et al., 1995). Scatter plots between measured and predicted parameters were plotted to know the actual predictability using NIRS non-destructively.

(v) Results and discussion

Typical spectral curves in the wavelength range of 900–1,700 nm for all five varieties (2 curves for each variety of apples) did not show any varietal differences in peaks and depressions (Fig. 6.30). The peaks and depressions in spectra show the strong and the weak transmittance characteristics of the apples, respectively within the range of the study. The relative values in other regions of spectra, however, are differed from sample to sample.

R values for calibration and validation of TSS in PLS regression were found to be 0.562 and 0.454, respectively for the wavelength range of 1,136.25–1,212.75 nm, whereas these values were 0.749 and 0.457 in case of MLR for the same range of wavelengths, which indicated that MLR is better for prediction of TSS. There is however a large difference in R values of calibration and validation and thus results may be unstable during prediction. Ventura et al. (1998) obtained higher R values for prediction of TSS as compared to this study. Lower values here are mainly due to use of 5 cultivars of apples which are distinctly different in characteristics. The present model is thus applicable to wide varieties of apple whereas it was only for one variety (cv. Jonagold) in case of Lammertyn et al. (1998).

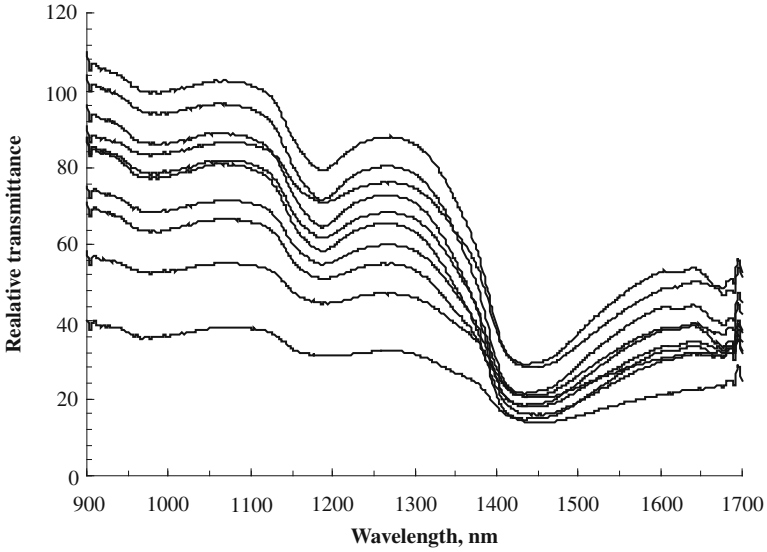

Fig. 6.30 Typical NIR spectra of different varieties of apple in wavelength range 900–1,700 nm

Effect of various pre-processing techniques for enhancement of predictability of the selected model showed that the MSC treatment yielded highest *R* values for calibration and validation, 0.889 and 0.745, respectively (for details reader can see the referred paper), which shows that after treatment, TSS can be predicted with reasonable accuracy. If no treatment is given even then we can predict the TSS but stability in prediction is at stake because of large difference in *R* values of calibration and prediction. Similar views have also been reported by Saranwong et al. 2004. Scatter plots of models after MSC treatments for the wavelength range of 1,136.25–1,212.75 nm are shown in Fig. 6.31, which indicate that slope of the curve is near to 45° and thus prediction is near to measured values.

Acidity can be predicted in the wavelength range of 900–976.5 nm using PLS as well as MLR. *R* values in case of PLS were found to be 0.736 for calibration and 0.66 for validation. So, prediction is stable but may not be so accurate as in MLR, where *R* values for calibration and validation were found to be 0.853 and 0.481, respectively. In this case large gap indicates that prediction may not be stable as in PLS. The predictability of selected MLR model was further enhanced after applying MSC and removing some outlier samples. The lowest SEC/SEP highest *R* values and biases for calibration and validation of MSC treated spectra were found to be 0.016, 0.890, –0.001 and 0.024, 0.752, –0.001, respectively. Negative biases indicate that predicted values may be lower than the actual values, but the lower SEC, SEP, higher *R* values and lower differences in them indicated that prediction of acidity was much better and stable. These parameters without

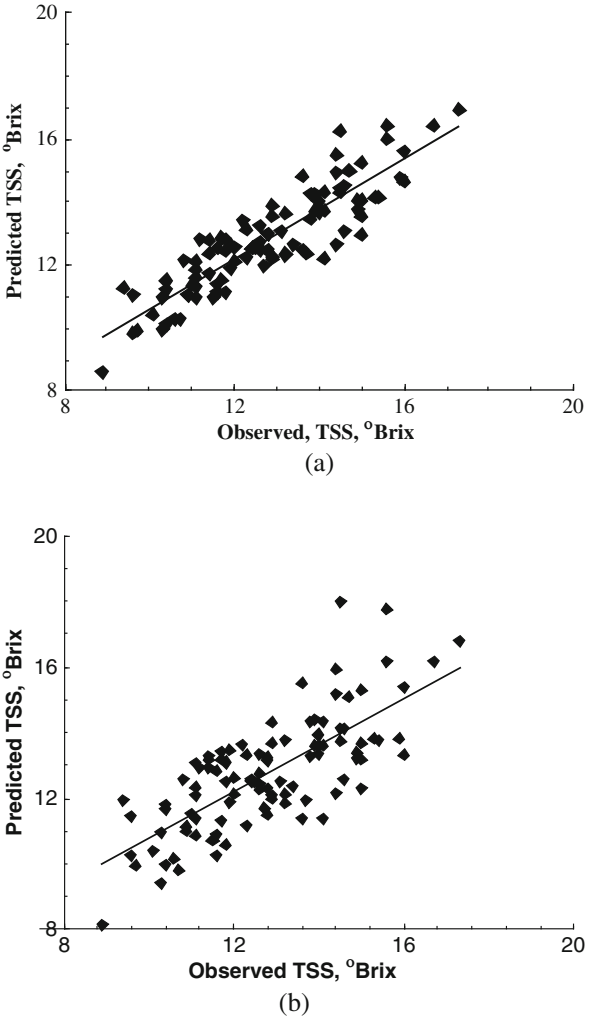

Fig. 6.31 Observed and predicted TSS in wavelength range of 1,136.25–1,212.75 nm after MSC treatment (**a**) for calibration (**b**) for validation set of apple samples

giving any treatments to data were also closer to the values of MSC treated data. Thus, one may choose spectra of wavelength range 900–976.5 nm without treatment or with MSC treatment depending upon the accuracy requirement for prediction of acidity. Prediction of acidity is better than that of TSS in case of apple.

Wavelength range (900–976.5 nm) and regression method (MLR) for prediction of acidity/TSS ratio was found to be the same as that of acidity. But after applying data treatment techniques not much improvement was found in *R* values. Thus model without data treatment whose SEC, SEP and

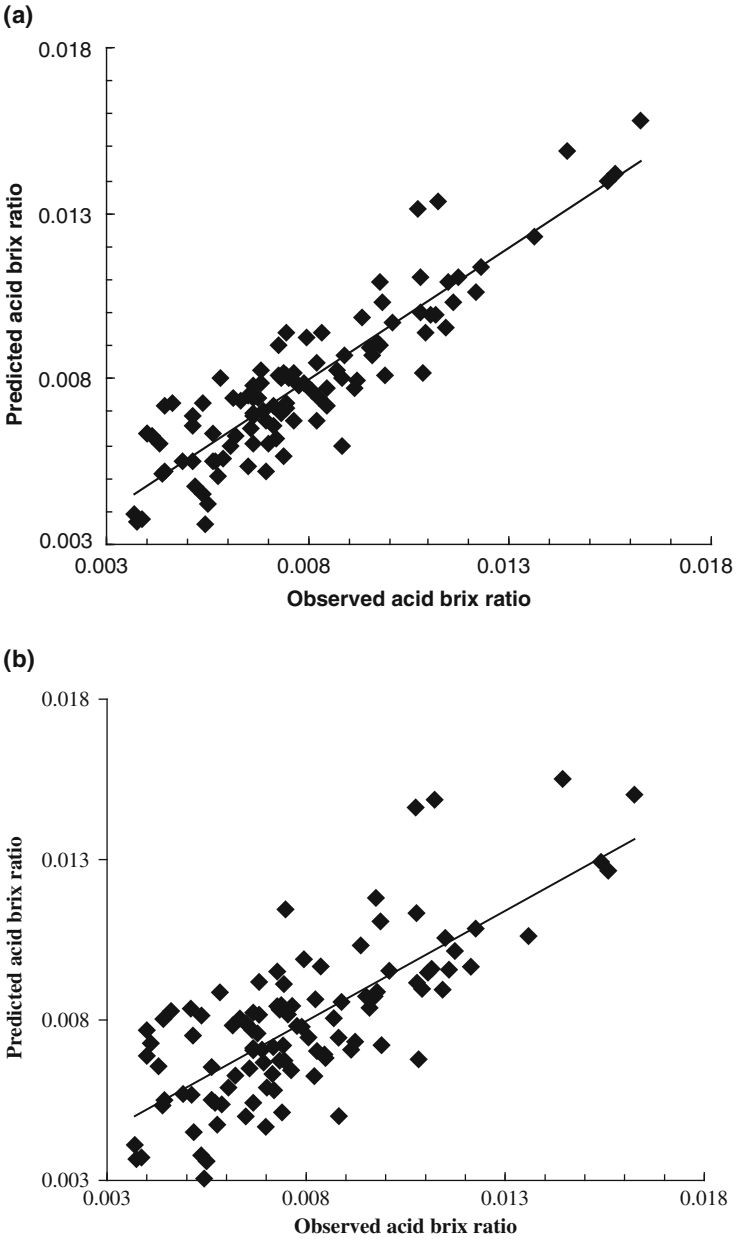

Fig. 6.32 Observed and predicted acid brix ratio of apple in wavelength range of 900–976.5 nm (**a**) calibration (**b**) for validation set of apple samples

R values were found to be 0.001, 0.002, 0.893 for calibration and 0.751 for validation, respectively may be used for prediction of acidity/TSS ratio. Comparison of statistical results indicated that quality of apple could better be judged using acidity rather than TSS. The taste of apple however could be

Fig. 6.33 NIR based fruit tester being used for checking the maturity of apple and muskmelon

judged with almost same accuracy as acidity, using acidity/TSS ratio, which include both acidity and TSS. Scatter plots for predicting acid/brix ratio are shown in Fig. 6.32. The multiple correlation coefficients in all cases are little lower than some of the reported values because of inclusion of five varieties to nullify the effect of varieties during commercial grading of apple. A commercial fruit tester (Fig. 6.33) manufactured by the Kubota, Japan is being used to check the maturity of apple and musk melon in the field.

6.4.2 Samples Classification

Adulteration of food materials especially fruit juices, milk, edible oil etc. is not new in food industries. Discriminate between authentic and adulterated sample is of crucial importance from regulatory perspective, number of work therefore have been reported to detect them. Adulteration of apple juice with high fructose corn syrup and sugar solutions has been detected using near infrared spectroscopy (Leoń et al. 2005) and synthetic apple juice had been monitored using FTIR-ATR spectroscopy (Irudayaraj and Tewari 2003). Different samples of apple juice adulterated by adding sugars have been classified between adulterated and unadulterated with 82.4–96% success (Kelly and Downey 2005).

Adulteration of juice by a less costly juice is also a common practice in food processing industries. Different markers to identify the adulteration of apple juice with pear juice were developed using HPLC (Thavarajah and Low 2006), and adulteration of pomegranate juice concentrate with grape juice was successfully detected using FTIR technique with R^2 of 0.975 (Vardin et al. 2008). Linda et al. 2005 differentiated the apple juice even based on the source of apples and heat treatment during processing using chemometrics and mid Infrared (MIR) and NIR data. Detection of sugars as adulterants in honey using FTIR and chemometrics has also been reported (Tzayhri et al. 2009). Classification of mango juice adulterated by added sugar has been performed by Jha and Gunasekaran (2010) using PLS discrimination analysis and PCA projection method as below:

Preliminary classification of samples was performed using PLS discrimination analysis. In this method unadulterated mango juice and adulterated samples in question were assigned values of 0 and 1, respectively. These values are called category variables. Discrimination was carried out using PLS regression on full raw spectra and the three peak regions of spectra and also by computing the second derivative (Savitzsky-Golay) and multiplicative scatter correction (MSC) of these spectral regions. A predicted value of 0.5 was selected as a cutoff for keeping the samples either in category of unadulterated or adulterated. To further verify the above classification, PCA projection method of classifications was used. For this purpose, whole samples were grouped into two categories: unadulterated and adulterated. Separate PCA for each category was performed and optimum numbers of principal components (same for both categories) were selected based on x-explained variance. These PCA models were used to develop classification tables using the classification module available in the Unscrambler software to assign each sample to either unadulterated or adulterated group.

It is evident from the summary of the analysis (Table 6.9) that all unadulterated samples have predicted category variables less than 0.5 and is higher than the same for all adulterated samples. Model developed using MSC treated data therefore correctly discriminated all samples between adulterated and unadulterated (Table 6.9). Best results however using PCA projection method did not discriminate 100% samples correctly (Table 6.10). Results showed that concentration of added sugar (AS) up to 1, 5, and 3% in sugar syrup, first lot and second lot of juice samples, respectively fell in both categories and therefore could not be classified correctly. In case of commercial juice, 20% samples having 3.6% AS concentration were correctly classified. In case of fresh juice samples higher percentage of AS as compared to pure sugar syrup could not be discriminated. It may be attributed to higher concentrations of natural sugars in these samples. Other commercial samples were having AS declared by the manufacturer on their packages, and concentrations were more than the limit of 3.6%. It therefore can be stated that commercial mango juice having AS of more than 3.6% could be easily identified as adulterated.

Table 6.9 Initial classification of prepared and commercial samples to adulterated and unadulterated groups using PLS discriminate analysis on full spectra after baseline offsetting and MSC

Sample type	Total number of samples	Number of samples with computed category variables		Correct classification (%)
		<0.5	>0.5	
Unadulterated	30	30	0	100
Adulterated	135	0	135	100

Table 6.10 Classification of prepared and commercial samples to adulterated and unadulterated groups using PCA projection method at 5% significance level in wavenumber range 1,476 to 912 cm^{-1} after baseline offset correction

Sample type	Added sucrose (%)	Total number of samples	Number of samples classified		Correct classification (%)
			Unadulterated	Adulterated	
Sugar solution	0	5	5	5	0
	1	5	5	5	0
	5	5	0	5	100
	9	5	0	5	100
	13	5	0	5	100
	17	5	0	5	100
	21	5	0	5	100
	25	5	0	5	100
Prepared juice-1	0	5	5	5	0
	1	5	5	5	0
	5	5	5	5	0
	9	5	0	5	100
	13	5	0	5	100
	17	5	0	5	100
	21	5	0	5	100
	25	5	0	5	100
Prepared juice-2	0	5	5	5	0
	3	5	5	5	0
	7	5	0	5	100
	11	5	0	5	100
	15	5	0	5	100
	19	5	0	5	100
	23	5	0	5	100
	27	5	0	5	100
Commercial juice-1	3.6	5	4	1	20
	7.1	5	0	5	100
	10.7	5	0	5	100
Commercial juice-2	12.8	30	0	30	100

References

AACC (1983, March) Approved methods of the American association of cereal chemists, 8th AACC, St Paul, MN

Anon (2010) Acousto-optical tunable filter. http://www.sciner.com/Acousto-Optics/acoustooptical_tunable_filters.htm. Accessed 20–21 July 2010

Bellamy LJ (1975) The infra-red spectra of complex molecules, 3rd Chapman and Hall, London

Born M, Wolf E (1977) Principles of optics. Pergamon Press, Oxford

Bureau S, Ruiz D, Reich M et al (2009) Application of ATR-FTIR for a rapid and simultaneous determination of sugars and organic acids in apricot fruit. Food Chem 115:1133–1140

Chen JY, Iyo C, Kawano S (1999) Development of calibration with sample cell compensation for determining the fat content of un-homogenized raw milk by simple near infrared transmittance method. J Near Infrared Spectrosc 7:265–273

Clancy PJ (2002) Transfer of calibration between on-farm whole grain analysers. In: RK Cho, AMC Davies (eds) Near Infrared Spectroscopy. Proceedings of the 10th international conference on Near Infrared Spectroscopy, Kuonjgu, Korea. NIR Publications, Chichester

Curcio JA, Petty CC (1951) The near infrared absorption spectrum of liquid water. J Opt Soc Am 41(5):302–304

Duarte IF, Barros A, Delgadillo I et al (2002) Application of FTIR spectroscopy for the quantification of sugars in mango juice as a function of ripening. J Agric Food Chem 50:3104–3111

Elliott A, Hanby WE, Malcolm BR (1954) The near infrared absorption spectra of natural and synthetic fibres. Br J Appl Phys 5:377–381

Fearn FRB (1982) Near infrared reflectance as an analytical technique, part 3. New Advances. Lab Pract 31(7):658–660

Foster GN, Row SB, Griskey RG (1964) Infrared spectrometry of polymers in the overtone and combination regions. J Appl Pol Sci 8:1357–1361

Glatt L, Ellis JW (1951) Near infrared pleochroism II. The 0.8–2.5 μ region of some linear polymers. J Chem Phy 19:449–457

Goddu RF (1960) Near-infrared spectrophotometry. Adv Anal Chem Instrum 1:347–417

Greensill CV, Walsh KV (2002) Standardization of near infrared spectra across miniature photodiode array-based spectrometers in the near infrared assessment of citrus soluble solids content. In: RK Cho, AMC Davies (eds) Near Infrared Spectroscopy. Proceedings of the 10th International conference on near infrared spectroscopy, Kuonjgu, Korea. NIR Publications, Chichester

Hammaker RM, Graham JA, Tilotta DC et al (1986) What is hammard transform spectroscopy. In:Durig JR (ed) Vibrational spectra and structure, vol 15. Elsevier, Amsterdam, pp 401–485.

Hecht KT, Wood DL (1956) The near infra-red spectrum of the peptide group. Proc R Soc Lond 235:174–188

Holland JK, Newnham DA, Mills IM (1990) Vibrational overtone spectra of monofluoroacetylene: a preliminary report. Mol Phy 70:319–330

Holman RT, Edmondson PR (1956) Near infrared spectra of fatty acids and related substances. Anal Chem 28:1533–1538

Irudayaraj J, Tewari J (2003) Simultaneous monitoring of organic acids and sugars in fresh and processed apple juice by Fourier transform infrared-attenuated total reflection spectroscopy. Appl Spectrosc 57(12):1599–1604

Iwamoto M, Uozumi J, Nishinari K (1987) Preliminary investigation of the state of water in foods by near infrared spectroscopy. In: Hollo J, Kaffka KJ, Gonczy JL (eds) Near infrared diffuse reflectance/transmittance spectroscopy. Akademiai Kiado, Budapest, pp 3–12

Jaquinot P (1958) Journal de Physique Radium 19:223

Jha SN (2007) Nondestructive determination of sweetness of orange juice using portable near infrared spectroscopy. *J Agric Engineering* 44(3): 10–14

Jha SN, Garg R (2010) Nondestructive prediction of quality of intact apple using near infrared spectroscopy. J Food Sci Technol 47(2):207–213

Jha SN, Gunasekaran S (2010) Authentication of sweetness of mango juice using Fourier transform infrared – attenuated total reflection spectroscopy. J Food Eng. 101(3):337–342

Jha SN, Narsaiah K, Sharma AD, Singh M, Bansal S, Kumar R (2010). Quality parameters of mango and potential of non-destructive techniques for their measurement – a Review. J Food Sci Technol 47(1): 1–14

Jha SN, Kingsly ARP, Chopra S (2006) Physical and mechanical properties of mango during growth and storage for determination of maturity. J Food Eng 72(1):73–76

Jha SN, Matsuoka T (2000) Non-destructive techniques for quality evaluation of intact fruits and vegetables. Food Sci Technol Res 6(4):248–251

Jha SN, Matsuoka T (2004a) Detection of adulterants in milk using near infrared spectroscopy. J Food Sci Technol 41(3):313–316
Jha SN, Matsuoka T (2004b) Nondestructive determination of acid brix ratio (ABR) of tomato juice using near infrared (NIR) spectroscopy. Int J Food Sci Technol 39(4):425–430
Jha SN, Matsuoka T, Kawano S (2001) A simple NIR instrument for liquid type samples. In: Proceedings of annual meeting of Japanese Society of Agriculture Structures, Paper No. C-20, pp 146–147
Kawano S, Abe H, Iwamoto M (1995) Development of a calibration equation with temperature compensation for determining the brix value in intact peaches. J Near Infrared Spectrosc 3: 211–218
Kawano S, Fujiwara T, Iwamoto M (1993) Nondestructive determination of sugar content in satsuma mandarin using near infrared (NIR) transmittance. J Jap Soc Hort Sci 62(2): 465–470
Kawano S, Watanabe H, Iwamoto M (1992) Determination of sugar content in intact peaches by near infrared spectroscopy with fibre optics in interactance mode. J Jap Soc Hort Sci 61: 445–451
Kaye W (1954) Near infrared spectroscopy I, spectral identification and analytical applications. Spectrochim Acta 6:257–287
Kaye W, Canon C, Devaney RG (1951) Modification of a Beckman model DU spectrophotometer for automatic operation at 210–2700 μm. J Opt Soc Am 41(10):658–664
Kelly JFD, Downey G (2005) Detection of sugar adulterants in apple juice using Fourier transform infrared spectroscopy and chemometrics. J Agric Food Chem 53:3281–3286
Krikorian SE, Mahpour M (1973) The identification and origin of N-H overtone and combination bands in the near-infrared spectra of simple primary and secondary amides. Spectrochim Acta 29A:1233–1246
Lammertyn J, Nieolai BO, Smedt VD et al (1998) Nondestructive measurement of acidity, soluble solids and firmness of jonagold apples using NIR-spectroscopy. Trans ASAE 41:1089–1094
Lauer JL, Rosenbaum EJ (1952) Near infrared absorption spectrophotometry. Appl Spectrosc 6(5):29–46
Law DP, Tkachuk R (1977) Near infrared diffuse reflectance spectra of wheat and wheat components. Cereal Chem 54(2):256–265
Leoń L, Kelly JD, Downey G (2005) Detection of apple juice adulteration using near-infrared transflectance spectroscopy. Appl Spectrosc 59(5):593–599
Liddel U, Kasper C (1933) Spectral differentiation of pure hydrocarbons: a near infrared absorption study. J Res Natl Bur Stand 11:599–618
Lijuan X, Ye X, Liu D, Ying Y (2009) Quantification of glucose, fructose and sucrose in bayberry juice by NIR and PLS. Food Chem 114:1135–1140
Linda MR, Tony W, Colm PO, Kelly JD, Downey G (2005) Differentiation of apple juice samples on the basis of heat treatment and variety using chemometric analysis of MIR and NIR data. Food Res International 38: 1109–1115
Lu R (2003) Detection bruises on apples using near-infrared hyperspectral imaging. Trans ASAE 46(2):523–530
Lu R (2004) Prediction of apple fruit firmness by near-infrared multispectral scattering. J Text Stud 35:263–276
Lu R, Ariana D (2002) A near infrared sensing technique for measuring internal quality of apple fruit. Appl Eng Agric 18:585–590
Lu R, Guyer DE, Beaudry RM (2000) Determination of firmness and sugar content of apples using near-infrared diffuse reflectance. J Text Stud 31:615–630
Lu R, Peng Y (2006) Hyperspectral scattering for assessing peach fruit firmness. Biosyst Eng 93:161–171
Luis ER-S, Fedrick SF, Michael AM (2001) Rapid analysis of sugars in fruit juices by FT-NIR spectroscopy. Carbohydr Res 336:63–74
McGlone VA, Kawano S (1998) Firmness, dry-matter and soluble-solids assessment of postharvest kiwifruit by NIR-spectroscopy. Postharvest Biol Technol 13:131–141

Meurens M (1984) Analysis of aqueous solutions by NIR reflectance on glass fibre. In: Proceedings of the third annual users conference for NIR Researchers. Pacific Scientific, Sliver Springs, MD

Morimoto S (2002) A nondestructive NIR spectrometer: development of a portable fruit quality meter. In: RK Cho, AMC Davies (eds) Near Infrared Spectroscopy. Proceedings of the 10th international conference on Near Infrared Spectroscopy, Kuonjgu, Korea. NIR Publications, Chichester

Morimoto S, McClure WF, Stanfield DL (2001) Handheld NIR spectrometry: part I. An instrument based upon gap-second derivative theory. Appl Spectrosc 55(1):182–189

Murray M (1987) The NIR spectra of homologous series of organic compounds in near infrared diffuse reflectance/transmittance spectroscopy. In: Hollo J, Kaffka KJ, Gonczy JL (eds). International NIR/NIT conference. Akademia Kiado, Budapest, pp 13–28.

Murray I (1988) Aspects of interpretations of near infrared spectra. Food Sci Technol Today 2: 135–140

Norris KH (1984) Multivariate analysis of raw materials. In: Chemrawn II, Shemilt LW (eds) Chemistry and world food supplies: the new frontiers. Pergamon Press, New York, pp 527–535

Osborne BG, Douglas S (1981) Measurement of the degree of starch damage in flour by near infrared reflectance analysis. J Sci of Food and Agriculture 32:328–332

Osborne BG, Fearn T, Hindle PH (1983) Practical NIR spectroscopy in food and beverage analysis. Longman Scientific and Technical, Harlow

Peiris KHS, DUll GG, Leffler RG, Kays SJ (1998) Near infrared spectrometric technique for non-destructive determination of soluble solids content in processing tomatoes. J American Society of Horticultural Sci 123: 1089–1093

Peng Y, Lu R (2006a) Hyperspectral scattering for assessing peach fruit firmness. Biosyst Eng 93(2):161–171

Peng Y, Lu R (2006b) Improving apple fruit firmness predictions by effective correction of multispectral scattering images. Postharvest Biol Technol 41(3):266–274

Peng Y, Lu R (2007) Prediction of apple fruit firmness and soluble solids content using characteristics of multispectral scattering images. J Food Eng 82:142–152

Rose FW Jr (1938) Quantitative analysis with respect to the component structural groups of the infrared (1 to 2 μ) molar absorptive indices of 55 hydrocarbons. J Res Natl Bur Stand 20: 129–157

Saranwong S, Sornsrivichai J, Kawano S (2004) Prediction of ripe-stage eating quality of mango fruit from its harvest quality measured non-destructively by near infrared spectroscopy. Postharvest Biol Technol 31:137–145

Thavarajah P, Low NH (2006) Adulteration of apple with pear juice: emphasis on major carbohydrates, proline, and arbutin. J Agric Food Chem 54:4861–4867

Tilotta DC, Hammaker RM, Fateley WG (1987) A visible-near-infrared hadamard transform spectrometer based on a liquid crystal spatial light modulator array: a new approach in spectroscopy. Appl Spectrosc 41(6):727–734

Tosi C, Pinto A (1972) Near-infrared spectroscopy of hydrocarbon functional groups. Spectrochim Acta 28A:585–597

Trott GF, Woodside EE, Taylor KG et al (1973) Physicochemical characterization of carbohydrate-solvent interactions by near-infrared spectroscopy. Carb Res 27(2):415–435

Tzayhri GV, Guillermo OS, Marlene ZL et al (2009) Application of FTIR-HATR spectroscopy and multivariate analysis to the quantification of adulterants in Mexican honeys. Food Res Int 42:313–318

Vardin V, Tay A, Ozen B et al (2008) Authentication of pomegranate juice concentrate using FTIR spectroscopy and chemometrics. Food Chem 108:742–748

Ventura M, Jager A, Putter H et al (1998) Non-destructive determination of soluble solids in apple fruit by near infrared spectroscopy. Postharvest Biol Technol 14:21–27

Wheeler OH (1959) Near infrared spectra of organic compounds. Chem Rev 59:629–666

Williams P, Norris K (1987) Near infrared technology in the agricultural and food industries. American Association of Cereal Chemists Inc., St Paul, MN, pp 247–290

Chapter 7
Ultrasonic Technology

Byoung-Kwan Cho

Ultrasonic has proven its merit as one of the most promising sensing methods for food quality evaluation due to its non-destructive, noninvasive, precise, rapid, and on-line potential. Ultrasonic is mechanical wave at frequencies above 20 kHz propagating by vibration of the particles in the medium and penetrating through optically opaque materials to provide internal or surface information of physical attributes, such as texture and structure. Ultrasonic non-destructive testing is a way of characterizing materials by transmitting ultrasonic waves into a material, and investigating the characteristics of the transmitted and/or reflected ultrasonic waves. For the purpose of quality measurement of materials, low-intensity ultrasonic with the power level of up to 1 W/cm^2 has been used. The low-intensity ultrasonic doesn't cause physical or chemical changes in the properties of the specimen when it transmits through the material. However, high-intensity ultrasonic of the power range above 1 W/cm^2 may produce physical/chemical disruption and alteration in the material through which the wave propagates. High-intensity ultrasonic is usually used in cleaning, promotion of chemical reactions, homogenization, etc

The two parameters that are mostly used in ultrasonic measurements are the ultrasonic velocity and attenuation coefficient. Among the parameters, velocity is the most widely used parameter because of its simplicity. However, a limitation of this method is the distance traveled by the wave must be known. Ultrasonic velocity and attenuation coefficient could serve as good indicators of material property or a change in material characteristics since they are dependent on the properties of the material, such as density, elastic modulus, and viscosity. Hence, the ultrasonic parameters can provide detailed information about physicochemical properties, such as structure, texture, and physical state of the components of the media. In addition, foreign objects such as bone, glass, or metal fragments residue in or on food products can be precisely detected using ultrasonic technique due to the strong ultrasonic reflection and refraction at the interfaces of the host tissue and foreign object interface.

B.-K. Cho (✉)
Chungnam National University, Daejeon, South Korea
e-mail: chobk@cnu.ac.kr

S.N. Jha (ed.), *Nondestructive Evaluation of Food Quality*,
DOI 10.1007/978-3-642-15796-7_7,

Conventional contact ultrasonic procedure uses a coupling medium between the transducer and the test specimen to overcome the high attenuation due to large acoustic impedance mismatch between air and the material. However, the use of couplant might change or destroy the liquid-sensitive, porous, and continuously formed food materials. In addition, the use of a couplnat makes the rapid measurement and process control cumbersome. Recently, several novel methods of non-contact ultrasonic have been developed. The advantage of the non-contact ultrasonic measurement is its ability to measure the ultrasonic velocity, attenuation coefficient, and thickness without contacting the sample. The non-contact ultrasonic became an exciting alternative of the conventional ultrasonic technique especially for a certain food quality evaluation. In this chapter, basic principles of both contact and non-contact ultrasonic and its applications to food products are explored.

7.1 Basic Concepts

The mechanism of ultrasonic wave propagation can be described with stress and strain. When stress is applied to a material, it produces elastic waves, which carry changes in stress and strain. Wave propagation is created by a balance between the stress and strain when fractions of a medium are distorted due to traction forces as shown in Fig. 7.1. From the definition of stress and strain (Eqs. 7.1 and 7.2), the wave equation can be derived as the Eq. (7.9).

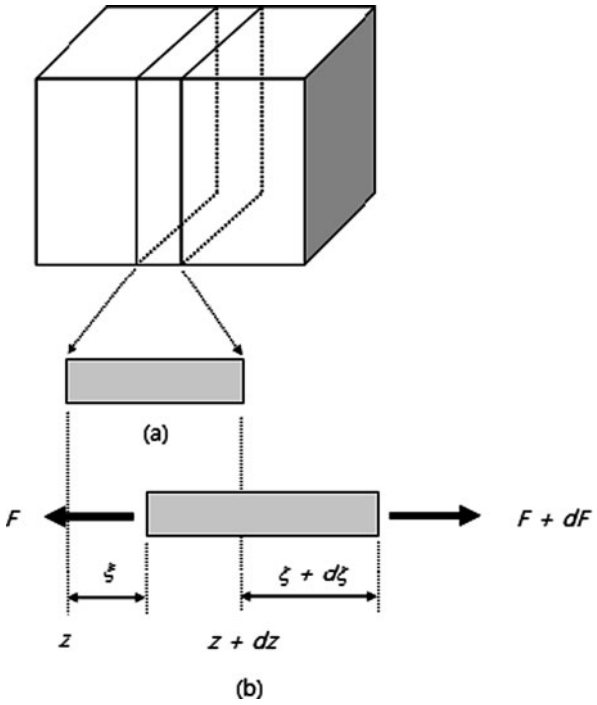

Fig. 7.1 Fraction of a medium (**a**) undistorted and (**b**) distorted

$$T = \frac{F}{A} \tag{7.1}$$

where T is the stress, F is the longitudinal force, and A is the cross-sectional area. If dz is assumed to be small

$$\xi + d\xi = \xi + \left(\frac{d\xi}{dz}\right) dz \tag{7.2}$$

$$d\xi = \left(\frac{d\xi}{dz}\right) dz \tag{7.3}$$

$$S = \frac{d\xi}{dz} = \frac{\left(\frac{d\xi}{dz}\right) dz}{dz} = \frac{d\xi}{dz} \tag{7.4}$$

where ξ is the longitudinal displacement of a particle, S is the strain, and z is the displacement in the longitudinal direction.

$$dF = (F + dF) - F = (F + \frac{\partial F}{\partial z} dz) - F$$

$$= \frac{\partial F}{\partial z} dz = A \frac{\partial T}{\partial z} dz \tag{7.5}$$

From the Newton's law

$$F = ma = \rho A dz \frac{\partial^2 \xi}{\partial t^2} = TA \tag{7.6}$$

$$\frac{\partial T}{\partial z} = \rho \frac{\partial^2 \xi}{\partial t^2} \tag{7.7}$$

$$T = \frac{F}{A}$$

where ρ is the density of a medium.

Particle velocity, v is obtained from the time derivative of particle displacement

$$v = \frac{\partial \xi}{\partial t} \tag{7.8}$$

Hence, the wave equation becomes

$$\frac{\partial T}{\partial z} = \rho \frac{\partial v}{\partial t} \tag{7.9}$$

The above equation is the one dimensional wave equation. This partial differential equation can be used to analysis for ultrasonic wave propagation in an elastic material.

7.2 Ultrasonic Parameters

The two parameters that are most widely used in ultrasonic measurements are the ultrasonic velocity and attenuation coefficient. The parameters are related to the physical properties of media, such as structure, texture, and physical state of the components.

7.2.1 Velocity

The ultrasonic velocity is a constant quantity for a material in a given state and depends on its physical properties. Velocity is a vector quantity that describes both the magnitude and the direction, while speed is a scalar quantity, which provides only the magnitude of velocity. In fact, ultrasonic speed is more accurate expression, however both terms have been used equally in engineering fields since the direction of ultrasonic velocity is always considered as the same direction with the ultrasonic propagation. In case of solid material, the ultrasonic velocity is related to modulus of elasticity, E and density, ρ of the solid material. The theoretical background of acoustic wave velocity in viscoelastic materials are as follows:

Stress, T, in a viscoelastic material is related to the elastic modulus and viscosity by the relationship,

$$T = ES + \eta \frac{dS}{\partial t} \tag{7.10}$$

where E is the elastic modulus and η is the viscosity.

$$\frac{\partial S}{\partial t} = \frac{\partial}{\partial t}\left(\frac{\partial \xi}{\partial z}\right) = \frac{\partial v}{\partial z} \tag{7.11}$$

Substituting Eq. (7.10) into Eq. (7.9)

$$\frac{\partial}{\partial z}\left(ES + \eta \frac{\partial S}{\partial t}\right) = \rho \frac{\partial v}{\partial t} \tag{7.12}$$

$$\frac{\partial^2}{\partial t \partial z}\left(ES + \eta \frac{\partial S}{\partial t}\right) = \rho \frac{\partial^2 v}{\partial t^2} \tag{7.13}$$

From Eq. (7.11),

$$\frac{\partial^2 S}{\partial z \partial t} = \frac{\partial^2 v}{\partial z^2} \tag{7.14}$$

Substituting Eqs. (7.11) and (7.14) into Eq. (7.13)

$$\rho \frac{\partial^2 v}{\partial t^2} = E \frac{\partial^2 v}{\partial z^2} + \eta \frac{\partial^3 v}{\partial t \partial z^2} \tag{7.15}$$

Assuming the solution is a plane wave, the velocity can be defined as,

$$v = Ce^{j(wt-\hat{k}z)} \tag{7.16}$$

where $\hat{k}$ is the wave number, w is the angular velocity ($= 2\pi f$), and C is a constant.

If attenuation by absorption is included, the only effect is that the wave number becomes complex. It can be assumed as,

$$\hat{k} = \beta - j\alpha \tag{7.17}$$

where α is the attenuation coefficient by absorption and β is the wave propagation constant defined as 2π divided by the wavelength ($= \frac{2\pi}{\lambda}$).

From Eq. (7.16),

$$\frac{\partial^2 v}{\partial t^2} = -w^2 v \tag{7.18}$$

$$\frac{\partial^2 v}{\partial z^2} = -\hat{k}^2 v \tag{7.19}$$

Substituting Eq. (7.18) and (7.19) into Eq. (7.15)

$$-\rho w^2 = -E\hat{k}^2 - j\eta\hat{k}^2 w \tag{7.20}$$

where

$$\hat{k}^2 = \beta^2 - \alpha^2 - j2\beta\alpha \tag{7.21}$$

Hence, Eq. (7.20) becomes

$$-\rho w^2 = -E\beta^2 + E\alpha^2 - 2\eta\beta\alpha w + j(2E\beta\alpha - \eta\beta^2 w + \eta\alpha^2 w) \tag{7.22}$$

Using the real part of Eq. (7.22),

$$-\rho w^2 = -E\beta^2 + E\alpha^2 - 2\eta\beta\alpha w \tag{7.23}$$

If $\eta, \alpha << \beta, w$, the acoustic wave velocity is obtained as

$$v_a = \frac{w}{\beta} = \sqrt{\frac{E}{\rho}} \tag{7.24}$$

The wave propagation in an extended solid medium implies that the lateral dimension of the material is more than 5 times greater than the wavelength of ultrasonic in the material and is denoted as bulk propagation. In this case, the modulus

of elasticity should be described by the combination of the bulk modulus and the shear modulus as the following equation (Kinsler 2000),

$$E = K + \frac{4}{3}G \tag{7.25}$$

where K and G are the bulk and shear modulus respectively.

Hence, the longitudinal ultrasonic velocity in solids is defined as,

$$v = \sqrt{\frac{(K + \frac{4}{3}G)}{\rho}} \tag{7.26}$$

Note that the Eq. (7.26) holds for plane longitudinal waves traveling in homogenous and isotropic solids.

In case of liquid medium, ultrasonic waves are different from those in solids because liquids in equilibrium are always homogeneous, isotropic, and compressible. In addition, the pressure in liquids is a scalar and uniform on a volume element. Hence, the shear modulus needs not to be considered, and only bulk modulus can be an appropriate modulus for longitudinal wave propagation in liquid medium. The ultrasonic velocity in liquid is simplified as,

$$v = \sqrt{\frac{B}{\rho}} = \sqrt{\frac{\gamma B_T}{\rho}} \tag{7.27}$$

where B is the adiabatic bulk modulus, B_T is the isothermal bulk modulus, and γ is the ratio of the specific heats.

Measurement of ultrasonic wave velocity: A simple experimental arrangement can be constructed as shown in Fig. 7.2 for measuring the ultrasonic wave velocity. The system consists of an ultrasonic transducer, a pulser-receiver, and a position control system linked to a personal computer. The measurement technique is pulse-echo method. The sample is placed in the bottom and the wave propagation velocity through the sample is computed. An electrical pulse generated from the pulser-receiver is converted into an ultrasonic pulse by the transducer. The ultrasonic pulse

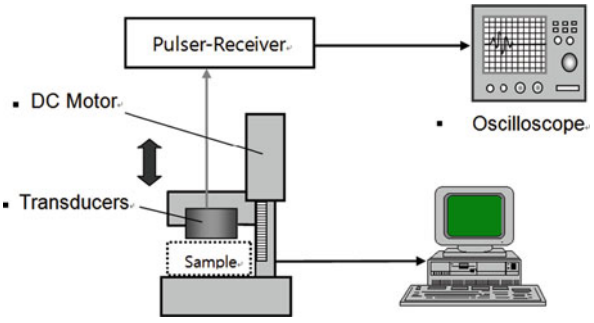

Fig. 7.2 Schematic diagram of ultrasonic system for velocity measurement (Cho et al. 2001)

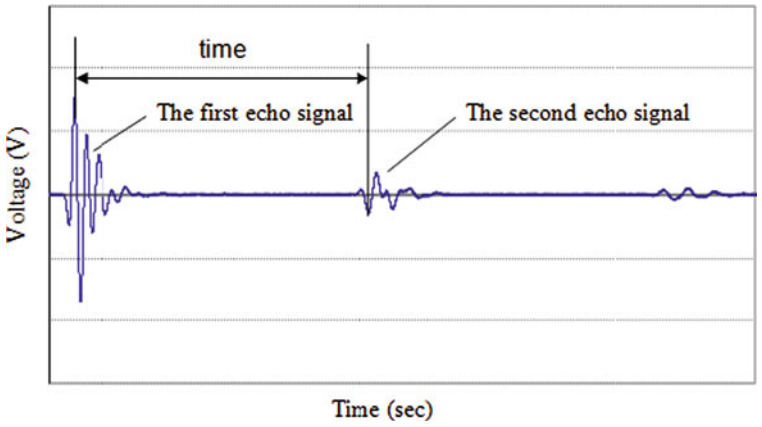

Fig. 7.3 Ultrasonic pulse-echo signal for a sample (Cho et al. 2001)

travel through the sample and reaches to the bottom where it is echoed back to the transducer. Reversely, the ultrasonic pulse is converted back into an electrical pulse by the transducer, and the electrical pulse is sent to the oscilloscope for display and further process. Velocity was calculated by dividing the total distance traveled by the time of flight. Time of flight is the time interval between the peak of the first pulse through the sample and the peak of the second pulse reflected from the bottom. Figure 7.3 shows a typical ultrasonic pulse-echo signal for measuring wave propagation velocity.

7.2.2 Attenuation

Attenuation is the amount of the decreasing power of a wave as it travels through a material. The major reasons of attenuation are due to absorption and scattering as the wave propagates through the medium. In the absorption process the ultrasonic energy is permanently converted into heat energy which may cause a temperature increase in the material. The absorption caused by a variety of mechanism, such as internal friction caused by viscosity, thermal conduction, and molecular relaxation. When an ultrasonic wave travels through a non-uniform medium, scattering occurs, in which part of the wave changes its initial direction and propagates separately from the original incident wave, distorting and interfering with the initial wave. Ultrasonic scattering does not decrease the mechanical energy, however it's difficult to be detected because the wave direction has been changed. The discontinuity within a medium, such as cracks, holes, and foams plays a role in scattering. The effect of scattering is lesser than that of absorption in homogeneous media. Also attenuation is affected by the frequency of the ultrasonic wave. In general, attenuation of ultrasonic signals increases as a function of frequency. Theoretically attenuation can be derived from the Eq. (7.22). From the imaginary part of equation we can write as

$$2E\beta\alpha - \eta\beta^2 w + \eta\alpha^2 w = 0 \tag{7.28}$$

If $\eta, \alpha << \beta, w$, the attenuation can be defined as

$$\alpha = \frac{\eta w \beta}{2E} = \frac{\eta w^2}{2v_a^3 \rho} \tag{7.29}$$

As shown in the above equation, attenuation is related to the wave velocity, density, viscosity, and frequency. When ultrasonic is propagated through a material, the total loss of the ultrasonic energy can be described as follows,

$$W = 20 \cdot \log\left(\frac{A_0}{A}\right) \tag{7.30}$$

where W is the total loss in dB, A_0 is the amplitude of the transmitted intensity without a test material in between the transducers, and A is the amplitude of the transmitted intensity through the test material.

It is assumed that the extent of attenuation is linearly dependent on the thickness of a material, while the other factors affecting the attenuation, such as reflection and coupling loss is not related with the thickness. The reflection and coupling loss for a material and transducer are constant. Hence, the total loss W can be expressed as,

$$W = \alpha \cdot x + \beta \tag{7.31}$$

where α is the attenuation coefficient (dB/mm), x is the thickness of the test matrial (mm), β is the reflection and coupling loss (dB).

Attenuations of two materials with different thickness are defined as follows,

$$W_1 = 20\log\left(\frac{A_0}{A_1}\right) = \alpha \cdot x_1 + \beta \tag{7.32}$$

and

$$W_2 = 20\log\left(\frac{A_0}{A_2}\right) = \alpha \cdot x_2 + \beta \tag{7.33}$$

where W_I is the total loss after traveling the distance x_I, W_2 is the total loss after traveling the distance x_2, A_I is the amplitude of the received signal after traveling the distance x_I and A_2 is the amplitude of the received signal after traveling a distance x_2.

The attenuation coefficient can be calculated by subtracting Eq. (7.32) from (7.33) as follows,

$$20\log(\frac{A_0}{A_2}) - 20\log(\frac{A_0}{A_1}) = \alpha(x_2 - x_1) \tag{7.34}$$

$$\alpha = \frac{20\log(A_1/A_2)}{x_2 - x_1} \tag{7.35}$$

There are two types of attenuation coefficient, apparent attenuation coefficient measured in time domain and frequency dependant attenuation coefficient. The

apparent attenuation coefficient is determined by measuring the peak amplitudes of transmitted ultrasonic pulses in time domain at two different sample thicknesses. If the frequency of the transducer is narrow-banded, the apparent attenuation is acceptable, however in case of broadband, the frequency dependent attenuation needs to be used.

7.3 Non-contact Ultrasonic (NCU) Measurement

To date, conventional contact ultrasonic procedure uses a couplant, such as a gel between the transducer and the test sample to overcome the high attenuation due to large acoustic impedance mismatch between air and the material. The use of a coupling media has the potential to change or destroy the liquid-sensitive, porous, and continuously formed food materials by absorption or interaction of liquid couplants and contributing to contamination and making the measurement process cumbersome.

The limitations of conventional contact ultrasonic techniques can be overcome by using non-contact (or air-coupled) ultrasonic transducers. The most important element in developing air-coupled transducer is the matching layer, which determines the efficiency of ultrasonic transmission from piezoelectric material to medium. For perfect transmission of ultrasonic, specific matching layer should be developed. The thickness of matching layer should be a quarter of a wavelength and a specific acoustic impedance of 0.1 Mrayls (Hayward 1997).

To overcome the high acoustic impedance mismatch between air and the test material, highly sensitive non-contact transducers need to be developed. Fox et al. (1983) developed non-contact ultrasonic transducers of 1 and 2 MHz central frequency using silicon rubber as the matching layer. They demonstrated the ability of the transducers to measure the distance in air from 20 to 400 mm with an accuracy of 0.5 mm. Haller et al. (1992) enhanced the transmission efficiency of the non-contact ultrasonic transducers using a specially designed matching layer with tiny glass spheres in the matrix of silicone rubber. Bhardwaj (1997, 1998) demonstrated the highly efficient acoustic matching layer for non-contact ultrasonic transducers using soft polymers.

7.3.1 NCU Velocity Measurement

The non-contact ultrasonic system can be constructed using two transducers, which can operate both as a transmitter and a receiver as shown in Fig. 7.4. Since the system has two channels for data acquisition (with two amplifiers and two analog I/O boards), it can provide four operation modes: two reflection (one for each of the two transducers) and two transmission modes (one used as transmitter and the other as receiver and vice-versa). After a simple calibration for the air velocity (V_a) using a known thickness calibration material, the thickness and ultrasonic velocity of a sample can be calculated directly by the following equations (Bhardwaj 2000).

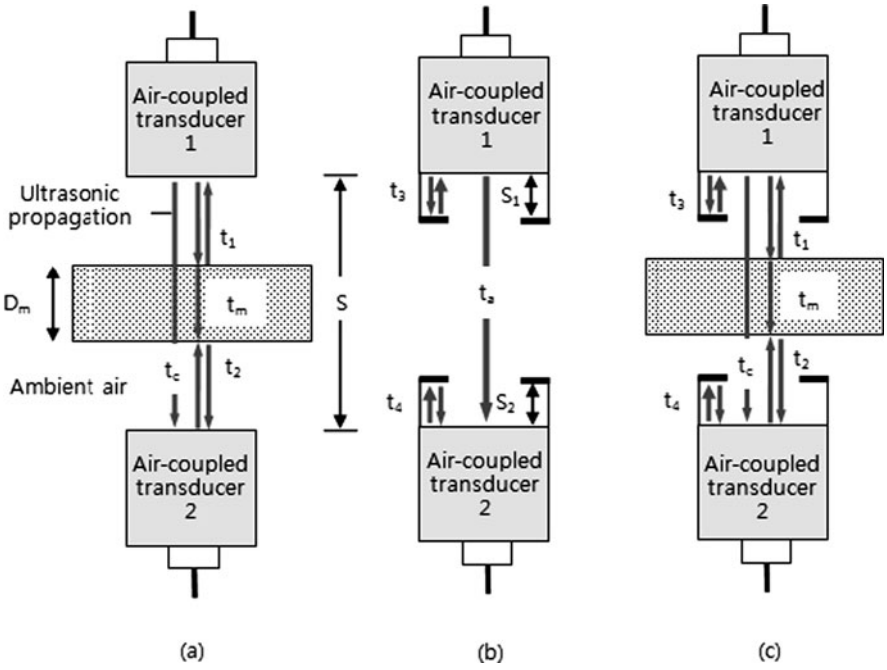

Fig. 7.4 Schematic of (**a**) the non-contact ultrasonic measurement with a sample material, and (**b**) the non-contact air instability compensation ultrasonic measurement (**b**) without and (**c**) with a sample material (Cho and Irudayaraj 2003c)

$$D_m = V_a\left(t_a - \frac{t_1 + t_2}{2}\right) = S - V_a\frac{t_1 + t_2}{2} \tag{7.36}$$

$$V_m = \frac{D_m}{t_m} = \frac{D_m}{t_c - \frac{t_1 + t_2}{2}} \tag{7.37}$$

where, D_m is the sample thickness, V_a and V_m are the respective velocities of ultrasonic in air and through the sample, S is the distance between transducer 1 and transducer 2, t_m is the time-of-flight in the test material, t_a is time-of-flight between transducer 1 and transducer 2 in air, t_c is time-of-flight between transducer 1 and transducer 2 with sample, t_1 is the round trip time-of-flight between the transducer 1 and sample, and t_2 is the round trip time-of-flight between the sample and transducer 2.

In case of food sample measurements, the signal of non-contact ultrasonic measurement is weak and mixed with a random noise, hence it is difficult to identify the original signal from the mixed signal in case the noise level is higher than the signal level. An original signal is shown as Fig. 7.5a and the simulated real signal is displayed as Fig. 7.5b, which is the combination of the random noise and the original signal with a time delay. The original signal is hidden in the random noise of which the level is twice that of the original signal amplitude. To eliminate the

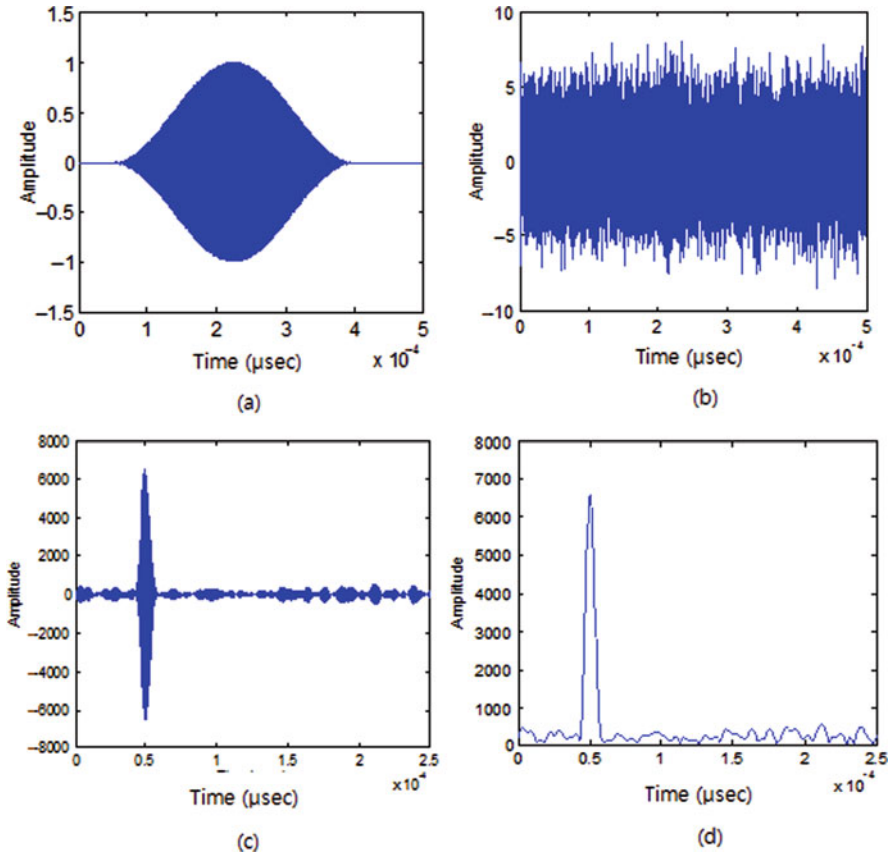

Fig. 7.5 Transmitted signal (**a**) which was (**b**) embedded in noise, (**c**) pulse compressed signal of (**b**), (**d**) enveloped signal of (**c**) (Cho and Irudayaraj 2003a)

random noise from the mixed signal cross-correlation method can be utilized. The correlated result is as shown in Fig. 7.5c in which the noise is much reduced. The advantages of the cross-correlation method are that it is not only reduces the noise but also estimates the time shift between the signals. Since the position of the maximum output correlation indicates the shifted time between the original signal and the transmitted signal at a time delay, time-of-flight of the ultrasonic wave through the sample can be determined by reading the location in time of the maximum peak. For precise identification, the maximum peaks from the correlated signal, the signal envelop was made using Hilbert transformation (Oppenheim et al. 1999). As shown in Fig. 7.5d the waveform clearly shows where the main peak is located. In addition, the area underneath the most significant peak above –6 dB from the transmitted signal in dB unit denoted as integrated response (IR) can be depicted as ultrasonic energy. The IR provides information of the energy attenuation during transmission of the ultrasonic wave through air and/or a specimen (Bhardwaj 2000).

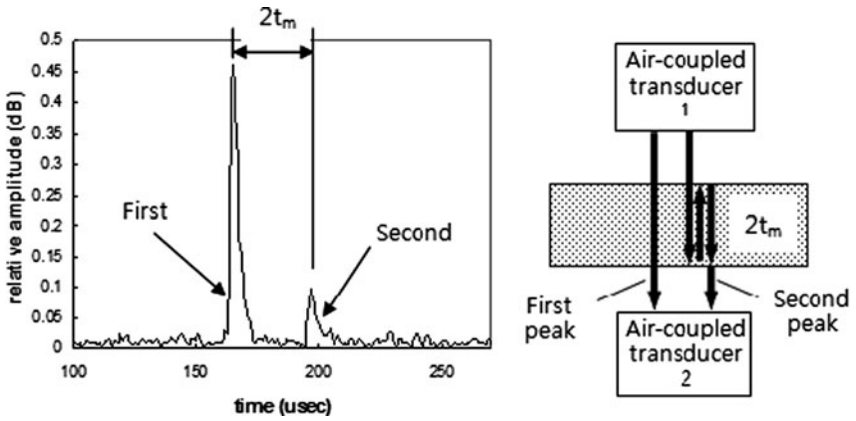

Fig. 7.6 A typical non-contact ultrasonic signal transmitted through a solid sample (Cho and Irudayaraj 2003a)

7.3.2 NCU Attenuation Measurement

A typical non-contact ultrasonic through-transmission signal of a solid material is shown in Fig. 7.6. The first peak is the transmitted signal through air and sample material directly while the second peak is caused by internal reflection of the transmitted signal. Other periodic peaks are multi-reflected peaks by a sample material, which are hardly observed in materials with high attenuation rate. The attenuation coefficient can be calculated by dividing the difference between the integrated response of the first and the second peak by the sample thickness.

7.3.3 Calibration of Ultrasonic Measurement

The non-contact ultrasonic system can be calibrated before measurement using a known property material, such as polystyrene block or a Dow Corning (DC) silicon fluid. After aligning the transducers parallel to each other and verifying the shape of the received signal, the polystyrene block was placed between the two transducers. The measured thickness was compared with the actual thickness. If the difference is not acceptable, the system parameters, such as the computer generated chirp used for a transmitted signal, and the parallelism of the transducers need to be adjusted within 0.1% error.

7.3.4 NCU Image Measurement

To obtain a non-contact ultrasonic image of samples, an X-Y positioning system to obtain ultrasonic image can be constructed as shown in Fig. 7.7. All scanning and data acquisition were controlled by a personal computer and a real-time

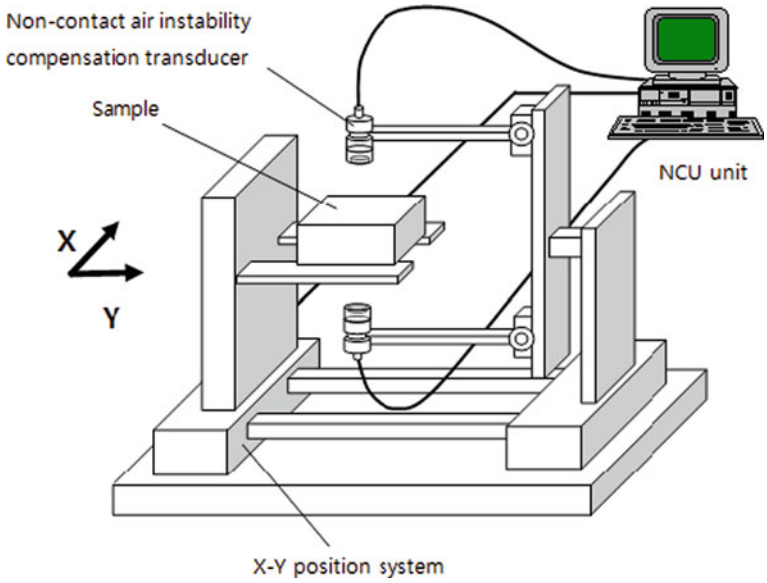

Fig. 7.7 Schematic of the non-contact ultrasonic imaging system (Cho and Irudayaraj 2003b)

operating system. The velocity and attenuation coefficient through the sample can be measured.

Figure 7.8 shows the ultrasonic attenuation images of a metal fragment in a poultry breast and cracks in cheese. Since the ultrasonic attenuation is more sensitive to the difference in product characteristics than velocity, the attenuation provides better images than those of velocity in general. The results of NCU images demonstrate its potential to detect the presence of foreign objects and defects inside food materials.

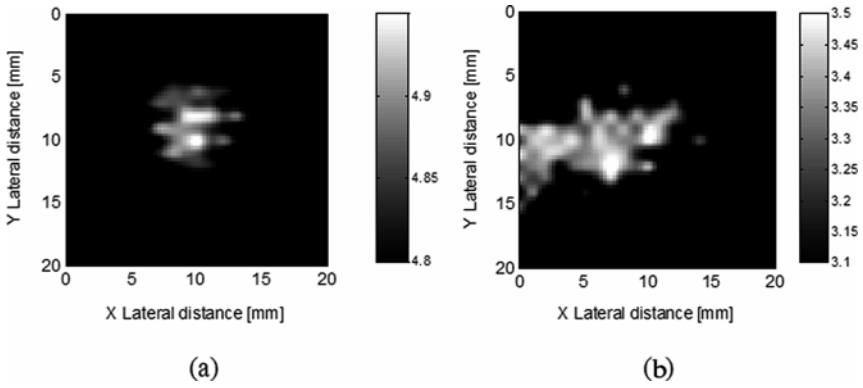

Fig. 7.8 Modified NCU attenuation images of a metal fragment (5×3 mm^2) (**a**) in a poultry breast and a crack in extra sharp cheddar cheese (**b**) (Cho and Irudayaraj 2003b)

7.4 Ultrasonic Image

Ultrasonic images are two-dimensional ultrasonic representation of the internal structure of materials. Of the ultrasonic imaging methods, a C-scan is the most common imaging type, which is a sequence of waveforms taken at points on a grid overlaid on the surface of a material, as illustrated in Fig. 7.9. The waveform to be imaged is defined through the use of an electronic gate. Along with the C-scan there are other two types of ultrasonic data display, A- and B-scans. An A-scan (Fig. 7.10) is a displayed waveform of ultrasonic signal for a point on a sample material, in which an axis represents the time and the other corresponds to the intensity of the signal. The A-scan provides one-dimensional depth information along the line of beam propagation. A B-mode stands for "brightness" modulation of the displayed signal. The B-scan is a sequence of A-scans taken at points along a line on the surface of a material, and displayed side-by-side to represent a cross-section of the material, as shown in Fig. 7.11. The scans can be made by using either pulse-echo or through-transmission inspection techniques.

Another widely used imaging type is a steered image which made by steered sweeping beams of a linear array of transducers. The measurement is performed in the pulse-echo mode so that there is no separate moving receiver. The beam is

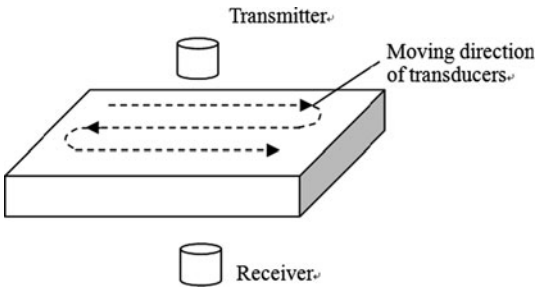

Fig. 7.9 Illustration of test arrangement for C-scan

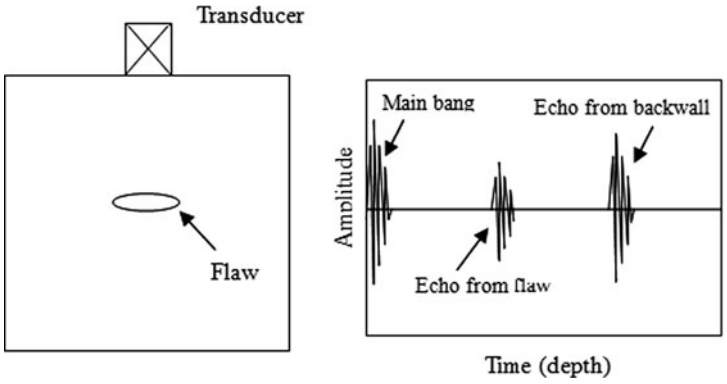

Fig. 7.10 Illustration of A-scan

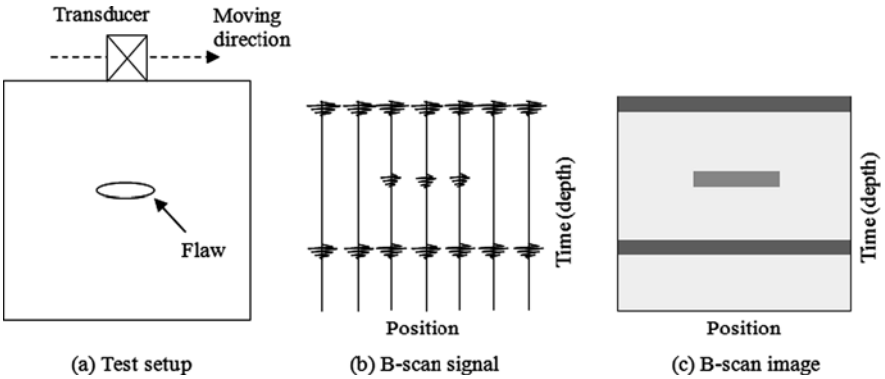

Fig. 7.11 Illustration of B-scan

Fig. 7.12 Steered wave

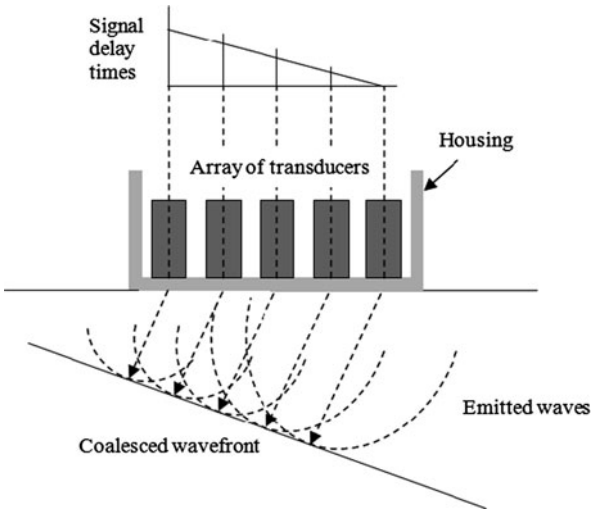

controlled by introducing successively increasing time delays across the transducer array as shown in Fig. 7.12. The orientation of the wavefront is steered by changing the excitation times across the array. The technique is usually operated in the pulse-echo mode and extensively used in medical imaging.

Ultrasonic imaging techniques have already been used to provide information about the meat quality, such as ratio of fat and lean tissue, both in live animal and in carcasses. Commercialized ultrasonic inspection systems for meat quality are widely used these days. Ultrasonic imaging was also applied to monitor creaming and sedimentation processes in emulsions and suspensions as well as detection of foreign objects in food materials.

7.5 Application of Ultrasonic to Food Quality Measurement

The application of ultrasonic to food quality measurement have increased due to its non-destructive, rapid, and automated potential. The most important ability of ultrasonic is that the waves can propagate through optically opaque samples and provide useful quality information. The early usage of ultrasonic techniques has been limited mostly for non-destructive measurement of medical and industrial materials. With the development of fabrication and measurement techniques, ultrasonic is broaden its application to various research fields including food quality assessment.

Previous researches using ultrasonic techniques on meat, fruits, and dairy products have explored the feasibility of noninvasive measurement. Lee et al. (1992) investigated shear wave ultrasonic spectra to measure the rheological properties of cheese and dough. The determined rheological values from ultrasonic were compared with traditional oscillating rheometry. Gunasekaran and Ay (1996) used ultrasonic attenuation to determine the optimum cutting time of cheese based on the degree of coagulation of milk. Results indicated that ultrasonic could be a potential non-destructive tool to measure the cutting time during cheese making. It was demonstrated that ultrasonic velocity could be a good indicator of cheese maturity (Benedito et al. 1999). Since ultrasonic velocity is closely related to the rheological properties of solid materials (Povey and McClements 1988), such as elastic modulus, it can be used to monitor and determine the maturity of cheese which is objectively represented by moisture and rheological parameters. Recently, non-contact ultrasonic technique was utilized for food quality measurements to avoid the use of a couplant which might change or destroy the liquid-sensitive, porous, and continuously formed food materials. The use of a coupling liquid limits the rapidity, on-line monitoring, measurement and process control severely. Cho and Irudayaraj (2003a) applied the non-contact ultrasonic technique to measurement of mechanical properties of cheeses. The ultrasonic velocity and attenuation coefficient of the different types of cheeses are shown in Table 7.1. They demonstrated that the ultrasonic velocity gradually increased with the increment of elastic modulus, hardness, and toughness. The relationship between ultrasonic velocity and mechanical properties of cheeses is shown in Fig. 7.13.

Theoretically, ultrasonic velocity is related to the square root of the elastic modulus (E) and density (ρ) of the solid material. As mentioned in previous section, the

Table 7.1 Ultrasonic parameters values of cheeses (Cho and Irudayaraj 2003a)

Cheese type	Ultrasonic velocity (m/s)	Attenuation coefficient (dB/mm)
Sharp cheddar	1,573.37 ± 2.0[a]	0.192 ± 0.012[a]
Reduced fat sharp cheddar	1,609.49 ± 6.0	0.226 ± 0.056
Asiago	1,618.09 ± 6.29	0.464 ± 0.229
Romano	1,651.77 ± 4.8	0.279 ± 0.102
Parmesan	1,648.12 ± 2.43	0.237 ± 0.02

[a]Standard deviation.

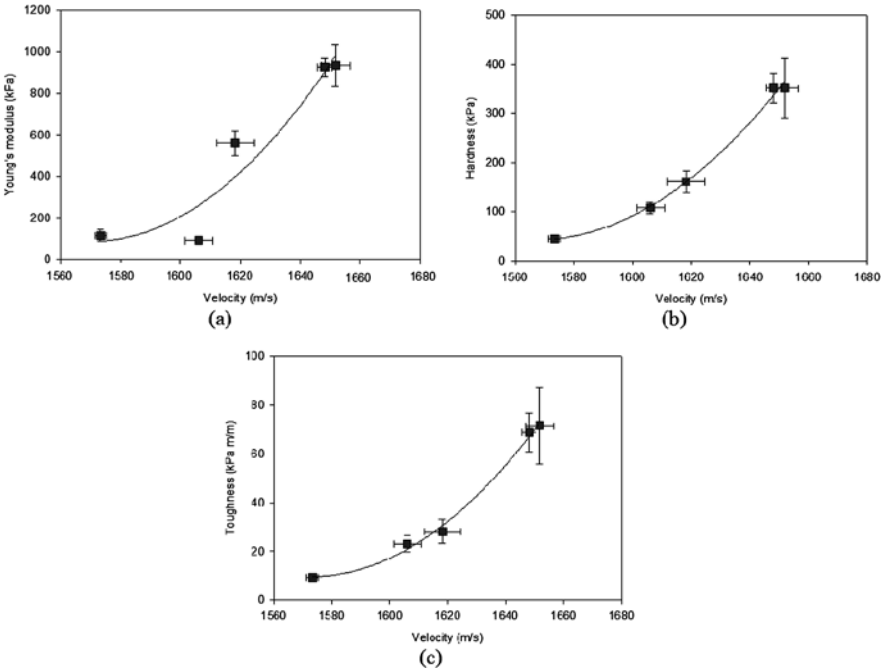

Fig. 7.13 Relationship between ultrasonic velocity and mechanical properties of cheese: (**a**) elastic modulus, (**b**) hardness, and (**c**) toughness (Cho and Irudayaraj 2003a)

elastic modulus can be replaced with the combination of bulk modulus and shear modulus for an isotropic solid material as shown in the following equation.

$$v = \sqrt{\frac{E}{\rho}} = \sqrt{\frac{B + \frac{4}{3}G}{\rho}} \tag{7.38}$$

where B is the bulk modulus and G is the shear modulus.

Since the bulk modulus is about 106 times greater than the shear modulus in a food system, the velocity is highly dependent on the bulk modulus (Povey and McClements 1988). The differences in density of cheeses are lower than those of elastic modulus. Thus, the ultrasonic velocity of cheeses is mainly determined by its bulk modulus which is not easy to measure non-destructively. Usually it is assumed that bulk modulus is closely related with the mechanical properties, such as elastic modulus, hardness, and toughness. Hence, the mechanical properties can be predicted using ultrasonic measurements. In general, the power of non-contact ultrasonic is very weak so that the relationship between strain and stress is linear. Thus, it's difficult to compare the ultrasonic parameters quantitatively with mechanical properties defined by the large strain level.

Although the attenuation coefficient is assumed to be related to the combination of the physical properties, such as viscosity, density, and ultrasonic velocity, the

correlation between ultrasonic attenuation coefficient and the mechanical parameters is not high. The reasons are that the sensitivity to sample surface unevenness, minor surface defects, and uneven component distribution in sample materials make it difficult to find the relationship between the attenuation coefficient and the mechanical property of cheeses.

The non-contact ultrasonic technique is able to measure the thickness of soft food materials without sample distortion. Figure 7.14 shows the compared result of thickness measured by non-contact ultrasonic and the actual thickness for three types of cheese, such as Sharp Cheddar ($n = 6$), Asiago ($n = 7$), and Romano ($n = 7$) with different thicknesses. The non-contact ultrasonic measured thickness values agreed well with the actual thickness values with an R^2-value > 0.999 and the standard error of estimation of 0.089 mm (Cho and Irudayaraj 2003a).

When the shape becomes complex and/or the sample surface are not parallel and smooth, the measurement cannot be made precisely. In addition, non-contact ultrasonic measurement is not practically suitable for very high acoustic impedance materials such as fruits and vegetables. For ultrasonic measurement of fruits and vegetables, specific contact ultrasonic transducer needs to be designed. Figure 7.15

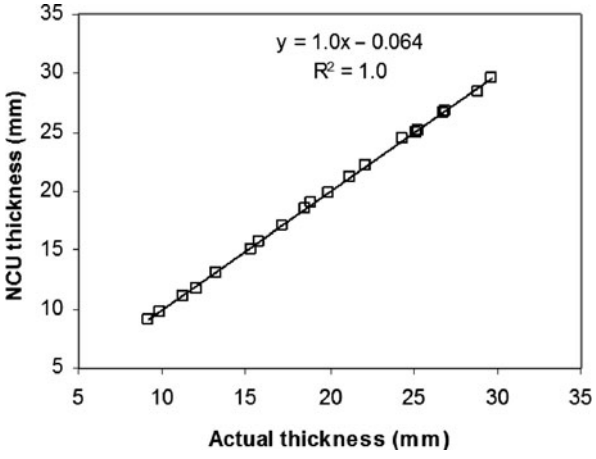

Fig. 7.14 NCU thickness measurement for cheese blocks (Cho and Irudayaraj 2003a)

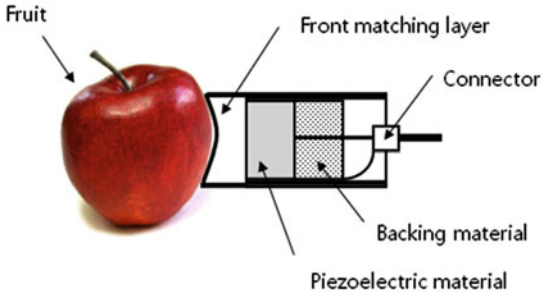

Fig. 7.15 Schematic of ultrasonic transducer designed for fruits

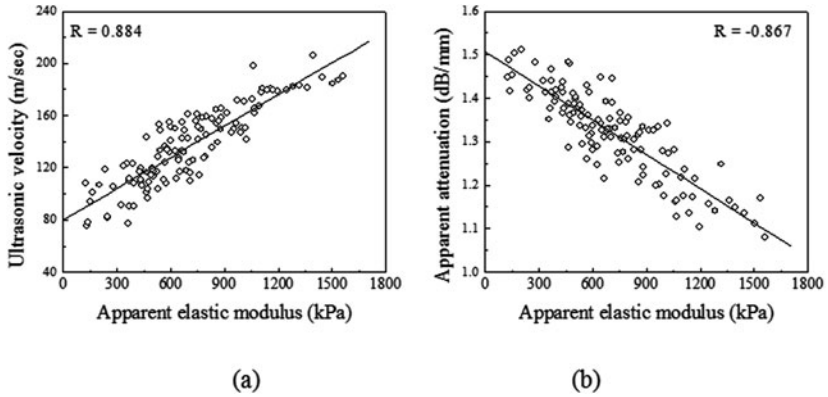

Fig. 7.16 The relationship between apparent elastic modulus of apple and ultrasonic parameters, (**a**) velocity and (**b**) attenuation coefficient (Kim et al. 2009)

is an example of the focusing contact type ultrasonic transducer specially designed for fruits with 100 kHz central frequency (Kim et al. 2004). The concave front matching layer of the transducer acts a role of acoustic lens which focus the power of ultrasonic wave to a designated area. The matching layer is made of Teflon with the dimension of 60 mm diameter and 4.3 mm thickness at the center.

The relationship between ultrasonic parameters and apparent elastic modulus is demonstrated in Fig. 7.16. The results show significant relationships between elastic modulus and velocity and attenuation coefficient with the correlation coefficients of 0.884 and –0.867, respectively. Ultrasonic velocity increased with the increment of the elastic modulus, while attenuation coefficient is in inverse proportion to the elastic modulus.

Mizrach et al. (1994a) developed continuous-touch systems for non-destructive quality evaluation of fruit and vegetables. The system consists of a two transducers having exponential beam-focusing elements, high-power low-frequency pulser-receiver, and a mounting structure for the transducers as illustrated in Fig. 7.17. The angle between the transducers was set to 120°, while the gap between the transducers could be adjusted.

An ultrasonic signal was transmitted from a transducer, and the transmitted signal through the sample was received by the other transducer. Ultrasonic pulse penetrated the peel and propagated through the underneath the peel along the gap between the two probes. The ultrasonic wave propagation velocity can be calculated by measuring the time of the ultrasonic pulse traveled between the two probes. The velocity v was obtained by the following equation,

$$v = \frac{l}{t} \tag{7.39}$$

where l is the distance and t is the traverse time between the two probe tips.

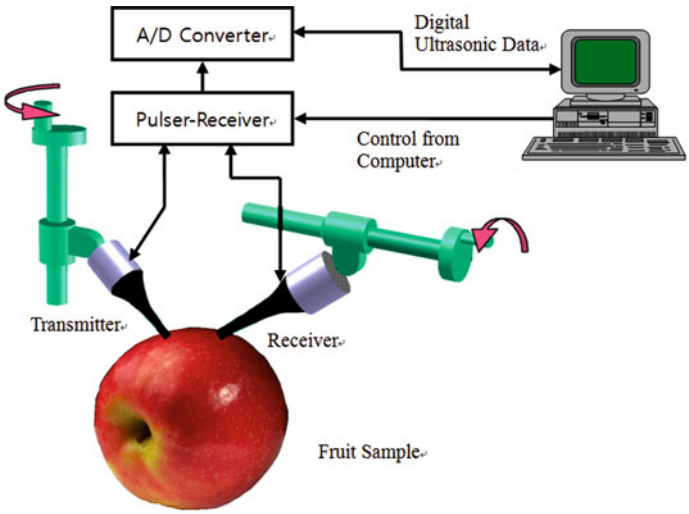

Fig. 7.17 Schematic diagram for non-destructive ultrasonic system for fruit and vegetables

The attenuation coefficient, was determined using the following equation,

$$\alpha = \frac{1}{l} \log \frac{A_0}{A} \tag{7.40}$$

where A_0 and A are the ultrasonic pulse amplitudes at the beginning and the end of the propagation through the specimen.

The non-destructive ultrasonic system has been used for the quality measurements of the variety of fruits and vegetables over the last decade. Mizrach and the colleagues (1999) studied non-destructive monitoring of physicochemical changes in whole avocado during maturation by the ultrasonic system. They demonstrated that ultrasonic attenuation coefficient could be used to monitor the change of dry weight (DW) which is an indicator of oil content in avocado. Since ultrasonic attenuation measurement could estimate the DW percentage during growth, it could be an evaluation method for harvest time of avocado. In addition, ultrasonic attenuation increased with the decrease of firmness regardless of storage temperatures (Mizrach et al. 2000). The results indicated that ultrasonic attenuation was good quality predictor for pre- and postharvest avocado. Mizrach et al. (2003) investigated the feasibility of the ultrasonic parameters for the measurement of mealiness levels for "Cox" apples, and indicated that the ultrasonic attenuation was well matched with the mealiness levels. The physicochemical properties of mango fruit were measured with the ultrasonic system (Mizrach et al. 1997). The ultrasonic attenuation and the firmness of mango were well fitted with a parabolic regression model (Fig. 7.18a). The relationship between attenuation and sugar content was expressed

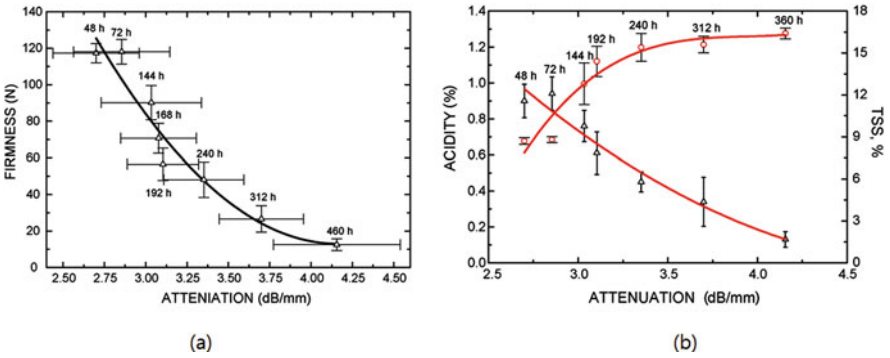

Fig. 7.18 Relationship between ultrasonic attenuation coefficient and (**a**) firmess, (**b**) sugar contents (○) and acidity (Δ) of mango fruits (Mizrach et al. 1997)

with a third-degree polynomial equation, and a parabolic model was selected for the relationship between attenuation and acidity (Fig. 7.18b). The internal quality parameters of melon, such as firmness and sugar contents were investigated using ultrasonic surface wave velocity and attenuation (Mizrach et al. 1994b). For the monitoring of the physicochemical changes of greenhouse tomatoes after harvest, Mizrach (2007) demonstrated that ultrasonic attenuation was linearly related to the firmness of the fruit during 8 days storage time. The studies demonstrated ultrasonic technology has a good potential for non-destructive evaluation of pre and postharvest quality of fresh fruit and vegetables.

The advantages of ultrasonic technology are its non-destructive, noninvasive, precise, rapid, and on-line potential. In addition, it can be applied to systems that are concentrated and optically opaque, which would be suitable for monitoring food processing operations. On the other hand, ultrasonic technology has disadvantages. One of those is that the presence of small porosities or bubbles in a sample attenuates ultrasonic energy so much that the ultrasonic signal cannot be preceded and hard to be acquired. The effect of the porosities can be reduced in pulse-echo measurements; however the signal from the porosities may complicate those from other components. Another disadvantage is that lots of thermophysical properties (e.g. density, compressibility, heat capacity, thermal conductivity, etc) of a material need to be defined to determine ultrasonic properties of the material theoretically. However the theoretical values of the material don't need to be considered if the same ultrasonic system is used in routine experiments. Non-contact ultrasonic has same limitations as the contact/immersion ultrasonic method. Moreover, the non-contact ultrasonic parameters are very sensitive to sample surface unevenness and minor surface defects. The technique is easily applicable to a sample with flat and smooth surface. However, when the shape becomes complex and/or the sample surface are not parallel and smooth, the measurement is very difficult to be made. Also, non-contact ultrasonic is not practically suitable for very high acoustic impedance materials such as fruits and vegetables.

References

Benedito J, Carcel J, Clemente G et al (1999) Cheese maturity assessment using ultrasonics. J Dairy Sci 83:248–254

Bhardwaj MC (1997, 1998) Ultrasonic transducer for high transduction in gases and method for ultrasonic non-contact transmission into solid materials. Int Patent

Bhardwaj MC (2000) High transduction piezoelectric transducers and introduction of non-contact analysis. The e-Journal of Nondestructive Testing & Ultrasonics [serial online]. 1:1–21. Available from NDT net: http://www.ndt.net. Posted Jan 2000

Cho B, Irudayaraj JMK (2003a) A non-contact ultrasound approach for mechanical property determination of cheese. J Food Sci 68:2243–2247

Cho B, Irudayaraj JMK (2003b) Foreign object and internal disorder detection in food materials using non-contact ultrasound imaging. J Food Sci 68:967–974

Cho B, Irudayaraj JMK (2003c) Design and application of a non-contact ultrasound velocity measurement system with air instability compensation. Trans ASAE 46:901–909

Cho B, Irudayaraj JMK, Omato S (2001) Acoustic sensor fusion approach for rapid measurement of modulus and hardness of cheddar cheese. Appl Eng Agric 17:827–832

Fox JD, Khuri-Yakub BT, Kino GS (1983) High frequency wave measurements in air. Proc IEEE Ultrason Symp 1:581–592

Gunasekaran S, Ay C (1996) Milk coagulation cut-time determination using ultrasonics. J Food Process Eng 19:63–73

Haller MI, Khuri-Yakub BT (1992) 1-3 Composites for ultrasonic air transducer. Proc IEEE Ultrason Symp 2:937–939

Hayward G (1997) Air coupled NDE – constraints and solutions for industrial implementation. Proc IEEE Ultrason Symp 1:665–673

Kim KB, Kim MS, Lee S et al (2004) Consideration of design parameters of ultrasonic transducer for fruit. Rev Prog Quant Nondestruct Evaluation 24A:1047–1053

Kim KB, Lee S, Kim MS et al (2009) Determination of apple firmness by nondestructive ultrasonic measurement. Postharvest Biol Technol 52:44–48

Kinsler LE, Frey AR, Coppens AB et al (2000) Fundamentals of acoustics, 4th edn. Wiley, New York, NY

Lee HO, Luan H, Daut DG (1992) Use of an ultrasonic technique to evaluate the rheological properties of cheese and dough. J Food Eng 16:127–150

Mizrach A (2007) Nondestructive ultrasonic monitoring of tomato quality during shelf-life storage. Postharvest Biol Technol 46:271–274

Mizrach A, Bechar A, Grinshpon Y et al (2003) Ultrasonic classification of mealiness in apples. Trans ASAE 46:397–400

Mizrach A, Flitsanov U, Akerman M et al (2000) Monitoring avocado softening in low-temperature storage using ultrasonic measurements. Comput Electron Agric 26:199–207

Mizrach A, Flitsanov U, El-Batsri R et al (1999) Determination of avocado maturity by ultrasonic attenuation measurements. Sci Hortic 80:173–180

Mizrach A, Flitsanov U, Fuchs Y (1997) An ultrasonic nondestructive method for measuring maturity of mango fruit. Trans ASAE 40:1107–1111

Mizrach A, Galili N, Rosenhouse G (1994a) A method and a system for non-destructive determination of quality parameters in fresh produce. Israel Patent No.109406

Mizrach A, Galili N, Teitel DC et al (1994b) Ultrasonic evaluation of some ripening parameters of autumn and winter-grown galia melons. Sci Hortic 56:291–297

Oppenheim AV, Schafer RW, Buck JR (1999) Discrete-time signal processing, 2nd edn. Prentice Hall, Upper Saddle River, NJ

Povey MJW, McClements DJ (1988) Ultrasonics in food engineering. Part 1: Introduction and experimental methods. J Food Eng 8:217–245

Chapter 8
Miscellaneous Techniques

Shyam N. Jha

Nondestructive way of determining the food quality is the need of the hour. Till now major methods such as colour measurements and their modeling; machine vision systems; X-ray, CT and MRI; NIR spectroscopy; electronic nose and tongue; and ultrasonic technology have been discussed in detail. These techniques, in general, are considered to be sophisticated and costly, and therefore probably are not being adopted as fast as it should be. I am however of the reverse opinion. While going through these techniques, it has been seen that majority of quality parameters have been measured and correlated with the signals obtained using different equipment. I am therefore of the opinion that any quality parameters or combination thereof can be correlated with the most simple parameters such as weight, electrical conductivity, magnetic properties, and even with days of storage etc., which can be measured with reasonable accuracy. Only important aspects of development of such techniques are quality of regression (calibration), validation and stability of prediction, which have been already dealt in previous chapters. This chapter illustrates the use of few other technologies such as electrical, thermal imaging, magnetic, and modeling of some quality parameters, hitherto estimated subjectively, for using in nondestructive way of measurement of different food quality.

8.1 Electrical Technology

Electrical characteristics of agricultural materials have been of interest for many years (Nelson 2006) and are being utilized in one or the other form. Electrical properties such as electrical conductance, resistance, capacitance, dielectric properties, pulsed electric fields, ohmic heating, induction heating, radio frequency, and microwave heating are important to develop instruments for determination of various quality parameters. Dielectric properties of various agri-foods and other biological materials are finding increasing application in their respective industries

S.N. Jha (✉)
Central Institute of Post-Harvest Engineering and Technology, Ludhiana 141004, Punjab, India
e-mail: snjha_ciphet@yahoo.co.in

S.N. Jha (ed.), *Nondestructive Evaluation of Food Quality*,
DOI 10.1007/978-3-642-15796-7_8,

and research laboratories (Venkatesh et al. 2004). Detailed theory of these properties have been dealt in various text books of electrical technologies, here however important ones are presented for convenience of readers interested in nondestructive methods of quality evaluation of food.

8.1.1 Electrical Conductivity

Electrical conductivity is a measure of electric current flows through a food of unit cross-sectional area A, unit length L, and resistance R. It is the inverse value of electrical resistivity (measure of resistance to electric flow) and is expressed in the following relation:

$$\sigma = \frac{L}{AR} \tag{8.1}$$

Electrical conductivity or specific conductance is thus a measure of a material's ability to conduct an electric current. When an electrical potential difference is placed across a conductor, its movable charges flow and consequently electric current produced. The conductivity σ is also defined as the ratio of the current density J to the electric field strength E:

$$J = \sigma E \tag{8.2}$$

It is also possible to have materials in which the conductivity is anisotropic and in such case σ is a 3×3 matrix (or more technically a rank-2 tensor). The *SI* and *CGS* unit of electrical conductivity is Siemens per metre ($S{\cdot}m^{-1}$) and inverse of second (s^{-1}), respectively. The electrical conductivity is commonly represented by a Greek letter σ, or κ (especially in electrical engineering science) or γ are also occasionally used.

One should not get confused with electrical conductance, which is a measure of an object's or circuit's ability to conduct an electric current between two points. Electrical conductance is dependent on the electrical conductivity and the geometric dimensions of the conducting object.

The conductivity of a material is generally measured by passing a known current at constant voltage through a known volume of the material and by determining resistance. Basic instruments involved in measurement of electrical conductivity are bridge networks (such as the Wheatstone bridge circuit) or a galvanometer. Nowadays many devices are available to measure it directly. An EC meter, for example, is used to measure conductivity of a liquid sample.

8.1.2 Dielectric Properties

A dielectric is a non-conducting substance, i.e. an insulator. Although "dielectric" and "insulator" are generally considered synonymous, the term "dielectric" is more

often used to describe materials where the dielectric polarization is important, such as the insulating material between the metallic plates of a capacitor, while "insulator" is more often used when the material is being used to prevent a current flow across it.

Dielectric is the study of dielectric materials and involves physical models to describe how an electric field behaves inside a material. It is characterized by how an electric field interacts with an atom and is therefore possible to approach from either a classical interpretation or a quantum one. Many phenomena in electronics, solid state and optical physics can be described using the underlying assumptions of the dielectric model. It could be understood that the same mathematical model can be used to describe different physical phenomena.

Dielectric properties of food materials are those electrical properties which measure the interaction of food with electromagnetic fields (Ahmed et al. 2007). Relative permittivity, dielectric loss factor, loss tangent and the alternate current conductivity are of concern in heating, drying and storage of grains. However, the first dielectric properties for grain were not reported until 45 years ago (Nelson 1965). Electrical permittivity is a dielectric property that determines the interaction of electromagnetic waves with matter and defines charge density under an applied electric field (Barbosa et al. 2006). In solids, liquids, and gases the permittivity depends on dielectric constant ε', which is related to capacitance of a substance and its ability to store electrical energy. The dielectric loss factor ε'' is related to energy losses when the food is subjected to an alternating electrical field i.e., dielectric relaxation and ionic conduction (Barbosa et al. 2006).

(a) Permittivity and loss factor

In foods, permittivity can be related to chemical composition, physical structure, frequency, and temperature, with moisture content being the dominant factor (Ryynanen 1995). The absolute permittivity of a vacuum is ε_0 and it is determined by the speed of light (c) and the magnetic constant (μ_0) which are linked together by the equation:

$$c^2 \mu_0 \varepsilon_0 = 1 \tag{8.3}$$

The numerical value for ε_0, is about 8.854×10^{-12} F/m and for μ_0 it is 1.26 $\mu \mathrm{Hm}^{-1}$. In other media (solid, liquid and gaseous), the permittivity has higher values and is usually expressed relative to the value in vacuum (Nyfors and Vainikainen 1989): $\varepsilon_{\mathrm{abs}} = \varepsilon_{\mathrm{r}} \varepsilon_0$ or the relative permittivity, ε_{r} of a material equal to $\varepsilon_{\mathrm{abs}}/\varepsilon_{0.}$ Where, $\varepsilon_{\mathrm{abs}}$ and ε_{r} are absolute and relative permittivity of a material.

High frequency and microwave fields are sinusoidal time dependent (time-harmonic) and common practice is to use complex notation to express them (Nyfors and Vainikainen 1989). Thus permittivity is also a complex quantity with real and imaginary components. The equation for complex permittivity is (Risman 1991):

$$\varepsilon = \varepsilon' - j\varepsilon'' \tag{8.4}$$

where, ε = relative complex permittivity, ε' = relative real permittivity (dielectric constant), ε'' = dielectric loss factor, j = imaginary unit.

The real component of permittivity (dielectric constant) is related to the capacitance of a substance and its ability to store electrical energy. The imaginary component, the dielectric loss factor is related to various absorption mechanisms of energy dissipation and is always positive and usually much smaller than dielectric constant. The substance is lossless if dielectric loss factor = 0 (Mudgett 1986, Nyfors and Vainikainen 1989). The ratio of dielectric loss factor to dielectric constant ($\varepsilon''/\varepsilon'$) is called the loss tangent (tan σ) or dissipation factor, a descriptive dielectric parameter, is also used as an index of the material's ability to generate heat (Mudgett 1986).

(b) Power density and penetration depth

The rate of heating can be expressed by the power equation:

$$P_v = 2Ef\varepsilon_0\varepsilon'' |E|^2 \tag{8.5}$$

where, P_v = energy developed per unit volume (W/m^3), f = frequency (Hz), and $|E|$ = electric field strength inside the load (V/m).

The electric field inside the load is determined by the dielectric properties and the geometry of the load, and by the oven configuration. Therefore, this equation is generally impractical as the determination of the electric field distribution is very complex (Buffler 1993). To gain a better practical understanding of the meaning of the values of the dielectric properties, a penetration depth should be calculated from the dielectric properties.

(c) Wave impedance and power reflection

Transmission properties, which are related to the dielectric and thermal properties of the medium, determine the distribution of energy (Mudgett 1986). Since dielectric constant (absolute permittivity) decreases with the speed of propagation, wavelength in the dielectric medium is shorter than in free space. This change in wavelength leads to a reflection at the interface between two media with different dielectric constant (Nyfors and Vainikainen 1989). The reflection phenomena can be analyzed in terms of characteristic wave impedances, ε (Ohlsson 1989):

$$\eta = \frac{\eta_0}{\sqrt{\varepsilon}} \tag{8.6}$$

where, η and η_0 are the characteristic wave impedance of material and free space (~377 Ω), respectively.

The reflection and transmission at a plane boundary are primarily related to $\sqrt{\varepsilon}$, and the principal determining factor for the magnitude of reflection is from the real permittivity of material. Characteristic impedance is important when different materials are heated simultaneously. The change in characteristic impedances at the food surface results in reflection of about 50% of microwave power falling on the surface. Most of this energy is reflected

back to food via metal cavity walls. For frozen food, the impedance matching is better, often resulting in higher power utilization for thawing than for heating (Ohlsson 1989). The impedance measurements of the real capacitor are the basis for the determination of material dielectric properties at low frequencies.

(d) Polarization of dielectrics

When two charges are separated by a distance, they constitute an electric dipole. The dipole can be represented by a vector called the dipole moment. Molecules with nonzero permanent electric dipole moments are called polar molecules. Non-polar molecules may acquire a dipole moment in an electric field as a result of the distortion of their electronic distributions and nuclear positions. The polarization is the average dipole moment per unit volume. The relation between permittivity and polarization is (Nyfors and Vainikainen 1989):

$$P = (\varepsilon - 1)\,\varepsilon_0 E \tag{8.7}$$

where, P = polarization, ε–1 = electric susceptibility, ε_0 = absolute permittivity of vacuum, E = electric field.

The relative permittivity ε (or electric susceptibility, ε–1) is thus a measure of the polarizing effect from an external field, that is, how easily the medium is polarized. There are four types of polarization: ionic, orientation, atomic and electronic polarization. Electronic polarization occurs in atoms, where electrons can be displaced with respect to the nucleus. This polarization occurs in all substances. In atomic polarization, the atoms can be moved in crystals or molecules. Electronic polarization together with atomic polarization gives most dry solids a permittivity in the order of ($\varepsilon < 10$). When only these two mechanisms are present, the material is almost lossless at microwave frequencies. Atomic or vibration polarization is closely related to electronic polarization but, because of the much greater mass to be moved, the resonant frequencies of atomic polarization are lower. Atomic polarization is found in the infrared band while electronic polarization is found in the optical band (Nyfors and Vainikainen 1989). In microwave or high frequency field, the dipoles try to follow the rapidly changing field. The energy is then lost to the random thermal motion of the water, which is equivalent to a temperature rise. This is orientation polarization. Hydrated ions try to move in the direction of electrical field and they transfer energy by this movement (Nyfors and Vainikainen 1989, Ohlsson 1989). Polarization can be due to various effects ranging from charge accumulation at the surfaces between materials with different electrical properties (interfacial polarization) to dipole orientation and other effects (Gerard et al. 1999).

(e) Factors affecting the dielectric properties

Various factors such as frequency of the applied alternating electric field, moisture content, bulk density, temperature (Icyer and Baysal 2004a, Nelson 1965, 1984, Ryynanen 1995, Venkatesh and Raghavan 2004) ionic nature, concentration (density), structure and constituents of food materials (Engelder

and Buffler 1991, Feng et al. 2002, Guan et al. 2004, Nelson 1991, 1992, Nelson et al. 1994, Nelson and Bartley 2002, Ohlsson et al. 1974a, Venkatesh and Raghavan 2004, Sipahioglu et al. 2003) influence the dielectric properties of food materials. Dielectric properties have been reported for different agricultural commodities, including grains and seeds (Nelson 1965), fruits and vegetables (Feng et al. 2002, Guan et al. 2004, Ikediala et al. 2000, Nelson 1983, Nelson et al. 1994, Wang et al. 2003), juice and wine (Garcia et al. 2004), baked foods and flours (Kim et al. 1998, Zuercher et al. 1990), dairy products (Green 1997, Herve et al. 1998), fish and meat (Bengtsson and Risman 1971, Lyng et al. 2005), egg white solutions and thermal denatured egg albumen gels (Lu et al. 1998). Possibilities of using dielectric properties for assessing the quality of agri-food products have been also explored (Nelson et al. 1995, Dev et al. 2008). The dielectric constant and conductivity of carrots depends largely on moisture content, frequency, temperature, density, and particle size. Although moisture content is important, carbohydrate, both ash and protein content can also affect the dielectric properties (To et al. 1974, Zhang et al. 2007). The principal state variables that influence the dielectric properties at a given frequency are temperature and moisture content. Effects of different parameters such as moisture content, temperature, bulk density and frequency on the dielectric properties of agri-food materials are summarized in Table 8.1. The relationship between these factors, composition and the dielectric properties of food and food products are discussed in the following sub-sections:

The influence of salt, fat and other constituents: At higher moisture and lower fat contents, the loss factor increased somewhat with temperature (Datta and Nelson 2000). Increase in fat/lipid content decreased the dielectric properties of different food and food products (Table 8.2). The influence of water and salt or ash content depends to a large extent on the manner in which they are bound or restricted in their movement by the other food components (Sun et al. 1995). The most common food products have a loss factor of less than 25, which implies a penetration depth (PD) of 0.6–1.0 cm. However, literature data are mostly limited to pure foods and food components. For complex and formulated foods, the dielectric properties must be measured or estimated (Ohlsson 1989, Buffler and Stanford 1991). An increase in flour slurry concentration of Indian Basmati rice, systematically reduced dielectric constants during the entire frequency range while variations in dielectric loss factor values were mixed (Ahmed et al. 2007). Addition of 1% salt markedly increased loss factor of slurries. Salt addition decreased dielectric constant (ε') and increased loss factor (ε'') in different food and food products (Table 8.3). Microwave permittivities of bread dough can be measured as a function of water-flour composition, proofing time, and baking time (Zuercher et al. 1990, Ohlsson et al. 1974). Influence of different water and salt content on dielectric properties was significantly larger, especially at 450 and 900 MHz. It was also found that dielectric constant decreased gently with temperature above 60°C, whereas loss factor increased,

Table 8.1 Effects of moisture content, temperature, bulk density and frequency on the dielectric properties of food and food products

Food/product source	Range of parameters	Comments	References
Food materials, salty foods	2,800 MHz freq.	At constant temperatures, dielectric constant (ε') and loss factor (ε'') of food materials increase with decreasing frequency. The penetration depth (PD) decreased with increasing frequency, temperature and moisture content. At higher microwave frequencies only salty foods show an increase in ε'' with temperature but at lower microwave frequencies there is a general increase in ε''. Both ε' & $\varepsilon''$of various foods increased with increasing moisture content	Bengtsson and Risman (1971), Ohlsson et al. (1974), Kent (1987)
Moist foods	3 GHz freq.	Loss factor (ε'') increases with falling frequency	Bengtsson and Risman (1971), Ohlsson et al. (1974), Nyfors and Vainikainen (1989), Ryynanen (1995)
Fruits and vegetables	Freq. (1–1,800 MHz), temp. (20–60°C)	Generally, ε' increases with temperature at lower frequencies but decreases at higher frequencies, whereas ε'' increased with increasing temperature at all frequencies	Calay et al. (1995), Nelson (2003), Sosa-Moralesa et al. (2009)
Mango	Freq. (1–1,800 MHz), temp. (20–60°C)	Dielectric properties values decreased with increasing frequency, but this reduction was larger for ε'' than for the dielectric constant. Loss factor increased but ε' decreased with increasing temperature. Both values decreased with storage time	Sosa-Moralesa et al. (2009)

Table 8.1 (continued)

Food/product source	Range of parameters	Comments	References
Grape juice & wine	Freq. 200 MHz and 3 GHz	Both ε' & ε'' of grape juice are greater than wine at 200 MHz. At 3 GHz, ε' of grape juice is slightly less than of wine, whereas ε'', at 3 GHz is practically the same for grape juice and wine	Garcia et al. (2004)
Apples	915 MHz or 2.45 GHz; moisture content range of 4–87.5% at 22 and 60°C	An increase in temperature at low moisture contents resulted in increased dielectric properties. The penetration depth increased as moisture was removed from the sample	Feng et al. (2002)
Garlic	Freq. 2,450 MHz, moisture content (6–185%, db), temp. (35–75°C)	Both ε' & ε'' directly proportional to moisture content. Both ε' & ε'' decreased with increase in temperature at higher moisture levels and a reverse trend in lower moisture range. The relationship of ε' as well as ε'' was found to be linear with temperature. PD of microwaves increased with decrease in moisture content and the temperature had the insignificant effect on it	Sharma and Prasad (2002)
Legume flours (chickpea, green pea, lentil and soybean flour)	Freq. (10–1,800 MHz), temp. (20–90°C) and m.c. (8–21 g/100 g)/ water activities (0.3–0.9)	Both ε' & ε'' of four legume flours decreased with increasing frequency but increased with increasing temperature and moisture content. At low frequencies with high temperature and moisture content, negative linear correlations for both ε' & ε''	Guo et al. (2008, 2010), Wenchuan et al. (2010)

Table 8.1 (continued)

Food/product source	Range of parameters	Comments	References
Common bean, nuts	Freq. (75 kHz–5 MHz), moisture content range from 13.4–15.5%w.b.	The value of relative permittivity at each moisture content decreased regularly with increasing frequency. The frequency dependence of ε'' and loss tangent was less regular than that of permittivity. Relative permittivity increased with moisture content at every frequency. Both ε' & ε'' of nuts increased regularly with moisture content at all frequencies and decreased as the frequency increased	Berbert et al. (2002), (Lawrence et al. 1992, 1998)
Flaxseed	Freq. (50 kHz–10 MHz), m.c. (5.92–22.18%, db)	Both ε' & ε'' increased with increase in moisture content and bulk density and decrease in frequency	Sacilik et al. (2006)
Safflower	Freq. (50 kHz–10 MHz); m.c. (5.33–16.48%, db)	The ε' increased with increase in moisture content and bulk density, whereas it decreased with an increase in frequency	Sacilik et al. (2007)
Fresh eggs	Freq. (10–1,800 MHz) at 24°C temp.	The ε' increases with temperature at lower frequencies but decreased at higher frequencies, whereas ε'' increased with increasing temperature probably at any frequency ε' at the higher frequencies	Guo et al. (2007b)
Ground beef	Freq. 915 MHz	Loss factor is independent of moisture content between 20% and 45% but increases linearly with moisture content between 20 and 45%	Van Dyke et al. (1969)

Table 8.1 (continued)

Food/product source	Range of parameters	Comments	References
Beef and beef products	2,800 MHz freq.	Both ε' & ε'' increase with decreasing frequency at constant temperature; however, ε' decreases and ε'' increases with increasing temperature at constant frequency	Bengtsson and Risman (1971), To et al. (1974)
Beef burgers	2,430 MHz freq.	Adding 15% water had no effect on ε' or ε'' as most of 15% water lost during deep frying	Lyng et al. (2002)
Aqueous and beef	27.12, 2,450 MHz freq.	25% water slightly increased both ε' & ε'' in beef blends at both frequencies	Lyng et al. (2005)
Tuna fish, Catfish and shrimp, Fish meal	2,450 and 915 MHz freq.	A sharp increase in dielectric properties was observed around the freezing point. Both ε' & ε'' increased with increased water content at constant temperature; ε' & ε'' of lean tuna were larger than those of fatty tuna. PD below the freezing point increased rapidly as the temperature decreased. ε' of marinated catfish and shrimp, generally decreased with increasing temperature whereas ε'' increased with temperature. Both ε' & ε'' of fish meal increased non-linearly with moisture content and also increased with temperature in a relatively linear manner	Liu and Sakai (1999), Zheng et al. (1998), Kent (1970, 1972)
Salmon fillets	Freq. (27–1,800 MHz), temp. (20–120°C)	At RF frequencies of 27 and 40 MHz, ε' decreased with increasing temperature. But at microwave frequencies (e.g., 915, 1,800 MHz), an opposite trend was observed. ε'' increased with increasing temperature over the tested frequency range	Wang et al. (2008)

Table 8.1 (continued)

Food/product source	Range of parameters	Comments	References
Macaroni and cheese	Freq. (915–1,800 MHz); 20–121°C temp.	ε' increased as temperature increased and ε'' increased sharply with increase in temperature	Wang et al. (2003)
Cheeses	Freq. (0.3–3 GHz); temp. (55–75°C)	Both ε' & ε'' decrease with increasing frequency. Dielectric constants generally decreased with increasing temperature, within this frequency range	Everard et al. (2006)
Sugar/starch H_2O	1,000, 3,000 MHz freq.	ε' increased with moisture content while ε'' changed with the addition of sugars and starch	Roebuck et al. (1972)
Pure honeys and water-added honey	Freq. (10–4,500 MHz) at 25°C temp., m.c. (18–42.6%)	ε' decreased monotonically with increasing frequency, and increased with increasing water content. Dielectric relaxation was evident in ε''. The critical frequency and the maximum ε'' increased with increasing water content	Guo et al. (2010)
Edible oils and fatty acids	Freq. (100 Hz–1 MHz), temp. (20–45°C), m.c. (0.02–0.31%)	Both ε' & ε'' of oils decreased with increasing temperature and ε' increased with increasing moisture content	Lizhi et al. (2008), Rudan-Tasic and Klofutar (1999)
Starch		ε'' decreases rapidly with increasing temperature, ε' increases slightly with decreasing frequency	Miller et al. (1991)
Powder potato starch, locust bean gum	Freq. 2.45 GHz; 0–20%m.c, wb	The dielectric properties increase regularly with moisture content	Nelson (1991)
Salt solutions	3,000, 10,000 MHz	ε' of the salt solutions decreased as temperature increased. For salt contents greater than 2%, the predicted ε'' increased with temperature, which is in accord with the behaviour of aqueous salt solutions	Hasted et al. (1948), Sun et al. (1995)

Table 8.1 (continued)

Food/product source	Range of parameters	Comments	References
Soy protein isolate	200–2,500 MHz concentration (5, 10 and 15 g/100 g water), temperature (20–90°C)	ε' decreased with temperature (except at 90°C) and frequency while increased with concentration. ε'' increased with frequency and concentration; however, temperature showed mixed effect. PD decreased with an increase in frequency, concentration, temperature and pH	Ahmed et al. (2008)
Potato flour-water dispersions (slurry)	500–2,500 MHz; concentration (10–25% w/w); temperature (20–75°C)	ε' decreased with temperature and frequency while increased with concentration. ε'' increased with frequency and concentration; however, temperature showed mixed effect. PD decreased with an increase in frequency and non-systematic with temperature. Addition of salt substantially reduced Penetration depth of potato slurry	Ahmed et al. (2009)

Table 8.2 Effect of fat/lipid content on dielectric properties of food and food products

Food/product source	Freq. (MHz)	Comments	References
Model meat emulsions	900	ε'' decreased with increasing fat faster between 15 and 35% vs. 0 and 15% fat	Ohlsson et al. (1974)
Potato	300–3,000	Lipid content of food depresses dielectric activity by volume exclusion	Mudgett et al. (1995)
Lard, corn oil	0.01–100	Both ε' & ε'' of fats are low and vary slightly with source	Ryynanen (1995)
Beef burgers	2,430	10% fat decreased both ε' and ε''	Lyng et al. (2002)
Pork fat and beef	27.12, 2,450	20% fat decreased both ε' & ε'' at both frequencies	Lyng et al. (2005)
Vegetable oils	–	ε'' found to increase with ash content and to decrease with fat content of oil	Rudan-Tasic and Klofutar (1999)

Table 8.3 Effect of salt or ash on dielectric properties of food and food products

Food/product source	Range of parameters	Comments	References
NaCl solutions	3,000, 10,000 MHz	Salt addition can decrease dielectric constant (ε')	Hasted et al. (1948)
Beef, pork	915 MHz	4% salt more than doubled loss factor (ε'') while 1% salt increased ε'' by 20%	Van Dyke et al. (1969)
Gravy	2,800 MHz	Adding 1% salt to gravy increased ε'' by about 20%and also slightly increased ε'	Bengtsson and Risman (1971)
Ham	2,450 MHz	Salt content (0.5–3.5%) increased ε'' while ε' remained relatively constant	Li and Barringer (1997)
0.27% Guar solution	30,100 MHz	Salt concentration (0.2–0.7%) was not significant vs. ε'' while ε' may be lowered	Piyasena and Dussault (1999)
Beef burgers	2,430 MHz	3% salt depressed ε' and ε''	Lyng et al. (2002)
Aqueous and beef	27.12, 2,450 MHz	Salt depressed ε'' and increased ε'' most noticeably at 5% and 27.12 MHz in aqueous solution	Lyng et al. (2005)
Flour slurry concentration of Indian basmati rice	500–2,500 MHz (temp. 30 and 80°C)	Addition of 1% salt markedly increased ε'' of slurries	Ahmed et al. (2007)

particularly at lower frequencies for salty foods (Bengtsoson and Risman 1971). A decreasing trend of dielectric constant and loss factor was observed in the lower moisture range for grapes (Tulasidas et al. 1995b). At higher microwave frequencies 2,800 MHz only salty foods showed an increase in dielectric loss, with temperature but at lower microwave frequencies there is a general increase in loss factor (Bengtsson and Risman 1971, Ohlsson et al. 1974). The dielectric loss factors increased with ash content and decreased with fat content of oil (Rudan-Tasic and Klofutar 1999). Microwave permittivities of bread dough were measured over the frequency range from 600 to 2.4 MHz as a function of water-flour composition. The dielectric constant and loss factor decreased with water content and reduction in baking time (Zuercher et al. 1990). The penetration depth of bread dough was, however, surprisingly low (8–10 mm) in comparison with normal foods (10–15 mm). As the volume expands during proofing, the penetration depth increased up to 16–19 mm (Mellgren et al. 1988). Both dielectric constant and loss factor of flour are low at microwave frequencies for lower water content (Kent 1987).

The influence of moisture content, temperature and frequency: Temperature dependence of dielectric properties was not seen for dried granular solids but increased dramatically at higher moisture contents over 9.4 GHz (Stuchly and Stuchly 1980). Both the dielectric constant and loss factor of various foods increased with increasing moisture content (Bengtsson and Risman 1971). The dielectric properties of fruits and vegetables as a function of moisture and temperature are reported by Calay et al. (1995). In general, dielectric constant increases with temperature, whereas loss factor may either increase or decrease depending on the operating frequency. Loss factor of fresh fruits and vegetables generally increased with increasing temperature (Nelson 2003, Sosa-Moralesa et al. 2009) and dielectric constant increased with temperature at lower frequencies, but decreased with temperature at higher frequencies. Temperature dependence of dielectric constant was minimal in the frequency range between 0.01 and 1.8 GHz (Nelson 2003). The dielectric constant and loss factor of flaxseed increased with an increase in moisture content and bulk density, and decreased with frequency (Sacilik et al. 2006). The rate of change of dielectric constant and loss factor with temperature depends on the free and bound water content of the food materials (Calay et al. 1995). The dielectric constant of fatty acids increased with an increase in the number of double bonds or molecular chain length. Both dielectric constant and dielectric loss of oils decreased with increasing temperature and dielectric constant increased with increasing moisture content (Lizhi et al. 2008). The loss factor increased with temperature and transition phase of solid to liquid (Stier 2004). The dielectric constant of oils decreased with increasing temperature (Rudan-Tasic and Klofutar 1999). Both the dielectric constant and loss factor of nuts increased regularly with moisture content at all frequencies and decreased as the frequency increased. At lower moisture contents, the temperature dependence was minimal, but both the dielectric constant and loss factor increased rapidly with temperature at high moisture levels (Lawrence et al.

1992, 1998). For salty foods at lower microwave frequencies, dielectric constant shows a sharp decrease with increasing temperature. For moist foods, loss factor increases with falling frequency (Bengtsson and Risman 1971, Ohlsson et al. 1974, Nyfors and Vainikainen 1989). At constant temperatures, dielectric constant and loss factor increase with decreasing frequency (Kent 1987) and penetration depth decreases with increasing frequency, temperature and moisture content. This was large enough at 27 MHz to develop large-scale industrial radio frequency (RF) treatments. Dielectric constants of many cereal grains and soybeans as functions of frequency, moisture content, and bulk density have been reported (ASAE 2000, Nelson 1987, Kraszewski and Nelson 1989). For moist foods, loss factor decreases with increasing frequency (Ryynanen 1995). Ohlsson et al. (1974) observed that dielectric constant and loss factor increased significantly with falling frequency for most foods tested and in most cases, dielectric properties increased sharply with temperature during the transition from –10 to 0°C (thawing). At temperatures below the freezing point, dielectric constants of codfish increases slightly before the abrupt increase depending on the frequency (Bengtsson and Risman 1971). Dielectric properties of fish meal as a function of the temperature and moisture content are reported by Kent (1970, 1972). Both the dielectric constant and loss factor increased non-linearly with moisture content and almost linearly with temperature (Kent 1970, 1972). The dielectric constant of marinated catfish and shrimp, generally decreases with increase in temperature whereas the loss factor increases with increase in temperature (Zheng et al. 1998). The dielectric constant and loss factor of tuna fish varies with the composition of a substance and the temperature (Liu and Sakai 1999). A sharp increase in dielectric properties was observed around the freezing point. The dielectric constant and loss factor increases with increased water content at constant temperature. The dielectric constant and loss factor of lean tuna were larger than those of fatty tuna. Penetration depths as the temperatures below the freezing point increased rapidly as the temperature decreased (Liu and Sakai 1999). For beef products, both dielectric constant and loss factor increase with decreasing frequency at constant temperature; however, dielectric constant decreases and loss factor increases with increasing temperature at constant frequency (To et al. 1974).

Physical structure of material: Dielectric properties vary with number of physical attributes including bulk density, particle size and homogeneity. Bulk density has been identified as a major source of variation for dielectric constant and loss factor (Kent 1977, Kent and Kress-Rogers 1986, Nelson 1983, 1984, Nelson and You 1989). The density dependence of the dielectric properties of materials must be accounted in elaborating functions determining grain moisture content and this relation could also be used in the control of continuous on-line processing of grains (Meyer and Schilz 1980).

(f) Measurement techniques

Measurement of dielectric properties has gained importance because it can be used for nondestructive monitoring of specific properties of materials

undergoing physical or chemical changes and is finding increasing application as a new electro-technology for use in agriculture and food processing industries. A comprehensive overview of different techniques can be found elsewhere (Venkatesh and Raghavan 2005). The dielectric properties of food materials in the microwave region can be determined by several methods using different microwave measuring sensors (Kraszewski 1980). Measurement techniques mainly can be categorized as reflection or transmission types using resonant or non resonant systems, with open or closed structures for sensing properties of samples (Kraszewski 1980). Waveguide and coaxial line transmission measurements represent closed structures while the free-space transmission measurements and open-ended coaxial-line systems represent open-structure techniques.

More practical measurement method appears to be utilizing the measurement of dielectric properties of the agri-food products and the grain; more specifically its relative permittivity and loss factor (Hlavacova 2003). These techniques include wave guide measurements, resistivity cell, parallel plate, lumped circuit, coaxial probe, transmission line, resonant cavity, free space, parallel plate capacitor, cavity resonator, and time domain spectroscopy. The lumped circuit techniques are only suitable for low frequencies and high loss materials. Each method is having unique advantages and disadvantages (Icyer and Baysal 2004b, Nyfors and Vainikainen 1989). Among these techniques, open-ended coaxial probes have been the most commonly used method to determine the dielectric properties of high loss liquid and semi-solid foods (Nelson et al. 1994, Herve et al. 1998), and fresh fruits and vegetables (Nelson and Bartley 2000). The choice of a method for any desired application depends on the nature of the dielectric material to be measured, sample physical state (liquid or solid), shape (thickness, flatness) and electrically desired range of frequency and the degree of accuracy required (Agilent Technologies 2005, Nelson 1999). The choices of measurement equipment and sample holder design depend upon the dielectric materials to be measured, the extent of research, available equipment, and resources for the studies. The advantages and disadvantages of various methods are compiled to aid selection of measuring technique in Table 8.4. The particular measurement methods used in agri-food sector are described here with their principles and limitations:

Cavity perturbation technique: The cavity perturbation technique is frequently used for measuring dielectric properties of homogeneous food materials because of its simplicity, easy data reduction, accuracy, and high temperature capability (Bengtsson and Risman 1971, de Loor and Meijboom 1966). The technique is also well suited to low dielectric loss materials and can be very accurate and are sensitive to low loss tangents (Hewlett-Packard 1992, Kent and Kress-Rogers 1986, 1987). The resonant cavities are designed in the standard TM (transverse magnetic) or TE (transverse electric) mode of propagation of the electro-magnetic fields. It is based on the shift in resonant frequency and the change in absorption characteristics of a tuned resonant cavity. The measurement is made by placing a sample completely through the centre of a

Table 8.4 Advantages and disadvantages of different dielectric properties measurement techniques

Technique	Advantages	Disadvantages
Cavity Perturbation technique	Frequently used for measuring dielectric properties of homogeneous food materials because of its simplicity, easy data reduction, accuracy, and high temperature capability. Also well suited to low dielectric loss materials. Can be very accurate and they are also sensitive to low loss tangents. Calculations are rapid. Sample preparation is relatively easy and a large number of samples can be measured in a short time. This method is also easily adaptable to high (up to + 140°C) or low (–20°C) temperatures. For liquid samples, both solid and liquid measurements can be accurately measured	The resonant cavity systems restrict the measurements to a single frequency
Open-ended coaxial probes	Most commonly used method to determine the dielectric properties of high loss liquid and semi-solid foods and fresh fruits and vegetables. Quite easy to use and can be used for liquid and semi-solid materials including biological and food materials. This method is convenient and often little or no sample preparation	Due to density variations in material, such techniques are not free of errors. Not suitable for determining permittivities of granular and pulverized samples
Transmission line technique	More accurate and sensitive than the more recent coaxial probe method. Liquids and viscous-fluid type foods can be measured. The dielectric properties can be easily and inexpensively obtained	Sample preparation is also more difficult and time consuming
Resonators and transmission line	The method applies to all liquid and solid materials	Not applies to gases since their permittivities are too low. Problems with the sample preparation of solid materials. The accuracy is not as good

Table 8.4 (continued)

Technique	Advantages	Disadvantages
Time domain spectroscopy/reflectometry	The measurement is very rapid and accuracy is high. The sample size used is very small and the substance to be measured must be homogeneous. They are excellent tools for advanced research on the interaction of electromagnetic energy and materials over a wide frequency range	These methods are expensive
Free space transmission techniques	Do not require special sample preparation, therefore they are particularly suitable for materials at high temperature and for inhomogeneous dielectrics. They may be easily implemented in industrial applications for continuous monitoring and control e.g., moisture content determination and density measurement. Accurate measurement of the permittivity over a wide range of frequencies can be achieved	
Six-port reflectometer (SPR) using an open-ended coaxial probe	SPR can provide non-destructive broadband permittivity measurements with accuracy comparable to commercial. Data acquisition and reduction are fully automatic	This method involves a more complex mathematical procedure in order to translate the signal characteristics into useful permittivity data
Colloid dielectric probe	It can measure dielectric properties of colloidal liquid materials in food, chemical, pharmaceutical, and biochemical industries quickly and accurately	
The lumped circuit techniques	All material types, except gases, can be measured	Not used widely because of suitablility only for low frequencies and high loss materials

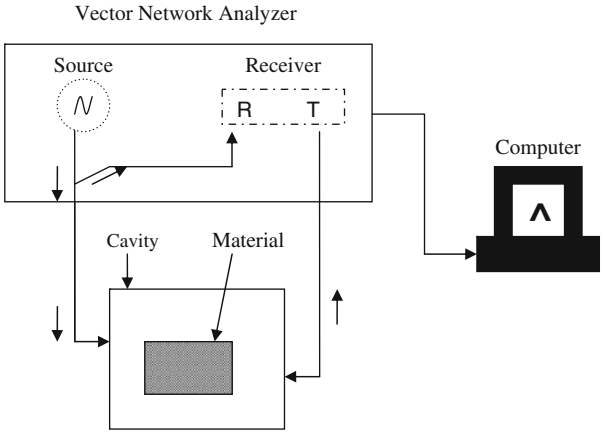

Fig. 8.1 Schematic representation of a resonant cavity method (R, reflected power, T, transmitted power) (Jha et al. 2010)

waveguide (rectangular or circular) that has been made into a cavity (Fig. 8.1). Changes in the centre frequency and width due to insertion of sample are related to dielectric constant. For ease of measurement, the vector network analyzer (VNA) can be used to automatically display changes in frequency and width (Engelder and Buffler 1991). The measurement details and the perturbation equations adapted for calculation of dielectric constant and loss factor along with accuracy information were reported by Liao et al. (2001) and Venkatesh (2002). The resonant cavity systems restrict the measurements to a single frequency. Each cavity needs calibration but, once the calibration curves have been obtained, calculations are rapid. Sample preparation is relatively easy and a large number of samples can be measured in a short time. This method is also easily adaptable to high (up to +140°C) or low (–20°C) temperatures (Ohlsson and Bengtsson 1975, Risman and Bengtsson 1971). Sharma and Prasad (2002) have used the cavity perturbation method to measure the dielectric properties of garlic at selected levels of moisture content and at 35–75°C temperature.

Open ended coaxial probe technique: The coaxial probe method is basically a modification of transmission line method. It uses a coaxial line, which has a special tip that senses the signal reflected from the material. The tip is brought into contact with the substance by touching the probe to a flat face of a solid or by immersing it in a liquid. The reflected signal is related to the dielectric properties of the substance. Though the method is quite easy to use and is possible to measure the dielectric properties over a wide range of frequencies (500 MHz–110 GHz) with limited accuracy particularly with materials with low values of absolute permittivity i.e. dielectric constant and loss factor (Engelder and Buffler 1991, Hewlett-Packard 1992). This technique is valid for 915 and 2,450 MHz, for materials with loss factors greater than one (Sheen and Woodhead 1999, Hewlett-Packard 1992). Typical open-ended probes utilize

3.5 mm diameter coaxial line. For measurement of solid samples, probes with flat flanges are suggested to use (Hewlett-Packard 1992).

This technique is also used to measure the dielectric properties as thermal treatments for controlling insects in fruits at temperature range of 20–60°C over a frequency range from 1 to 1,800 MHz (Wang et al. 2003). For liquid and semi-solid materials including biological and food materials, open-ended coaxial-line probes have been used for broadband permittivity measurements (Blackham and Pollard 1997, Grant et al. 1989). A similar technique is used for permittivity measurements on fresh fruits and vegetables (Nelson et al. 1994, Ohlsson et al. 1974). Due to density variations in material, such techniques are not free of errors. If there are air gaps or air bubbles between the end of coaxial probe and sample, this technique is not suitable for determining permittivity of granular and pulverized samples. This method is convenient, relatively easy to use, and often little or no sample preparations are required over a wide range of frequencies (Feng et al. 2002, Ikediala et al. 2000, Nelson 2003, Venkatesh and Raghavan 2004, Wang et al. 2003, 2005).

Transmission line technique: In transmission line methods, sample is put inside an enclosed transmission line and both reflection and transmission are measured. Although this method is more accurate and sensitive than the more recent coaxial probe method, it is useful in a narrower range of frequencies. As the sample must fill the cross-section of the transmission line (coaxial or rectangular), sample preparation is also more difficult and time consuming (Engelder and Buffler 1991, Hewlett-Packard 1992). When such methods are used to determine moisture content, the frequency used should be above 5 GHz to avoid the influence of ionic conductivity and bound water relaxation (Kraszewski 1996). Liquid and viscous-fluid type foods can be measured with this method by using a sample holder at the end of a vertical transmission line. The dielectric properties can be easily and inexpensively obtained by this technique, particularly if one utilizes a slotted line and standing wave indicator (Nelson et al. 1974). A more sophisticated implementation of the technique utilizes a swept-frequency network analyzer, where the impedance is measured automatically as a function of frequency. This technique is cumbersome because the sample must be made into a slab or annular geometry. At 2,450 MHz, the sample size is somewhat large, particularly for fats and oils (Venkatesh and Raghavan 2005).

Resonators and transmission line: A microwave resonator, partly or completely filled with a material, can also be used to determine permittivity. The resonator (perturbation technique) is usually calibrated with materials whose dielectric properties are known, usually with organic solvents such as methanol, ethanol, etc. The measurement frequency range is from 50 MHz to more than 100 GHz. If the transmission line is enclosed, the permittivity of a material can also be measured without the resonator by putting it directly inside the waveguide. The method applies to all liquid and solid materials, but not to gases since their permittivities are too low. There are, however, problems with the sample preparation of solid materials. The accuracy is not as good as that of the transmission line with resonator (Venkatesh and Raghavan 2005).

Waveguide and coaxial transmission line method: Early efforts to characterize the dielectric properties of materials were made at the Massachusetts Institute of Technology (Roberts and Von Hippel 1946) using this method. Coaxial-line and rectangular wave-guide sample holders are used with various microwave measurement systems assembled for dielectric properties determination on grain, seed, and fruit and vegetable tissue samples at frequencies from 1 to 22 GHz (Nelson 1973, 1983, 1991). The same sample holders are useful for measurements on pulverized coal and mineral samples (Nelson 1983) also.

Time domain spectroscopy/reflectometry (TDR) method: Time domain spectroscopy/reflectometry methods have been much developed in the 1980s. They cover a frequency range from 10 MHz to 10 GHz. This method also utilizes the reflection characteristic of the food material under test to compute the dielectric properties. The measurement is very rapid and accuracy is high, within a few percent error (Afsar et al. 1986). The sample size used is very small and the substance to be measured must be homogeneous. Although these methods are expensive, they are excellent tools for advanced research on the interaction of the electromagnetic energy and materials over a wide frequency range (Mashimo et al. 1987, Ohlsson et al. 1974). The dielectric properties of honey-water mixture have been investigated and tabulated using this technique in the frequency range of 10 MHz–10 GHz at 25°C by Puranik et al. (1991).

Free space transmission techniques: In this method sample is placed between a transmitting antenna and receiving antenna and the attenuation and phase shift of the signal are measured. The dielectric sample holders with rectangular cross-sections were placed between the horn antennas and a similar radiating element (Trabelsi et al. 1997). The usual assumption made during this technique is that a uniform plane wave is normally incident on the flat surface of a homogenous material, and that the planar sample has infinite extent laterally (Venkatesh and Raghavan 2005). Special sample preparations are not required in this method. Therefore, they are particularly suitable for materials at high temperature and for inhomogeneous dielectrics. In addition, they may be easily implemented in industrial applications for continuous monitoring and control e.g., moisture content determination and density measurement (Kraszewski 1980). Accurate measurement of the permittivity over a wide range of frequencies can be achieved by this technique.

Micro strip transmission line: Micro strips have long been used as microwave components suitable for use in dielectric permittivity measurement. It shows many properties and overcome some of the limitations. It is thus well known that the effective permittivity (a combination of the substrate permittivity and the permittivity of the material above the line) of a micro strip transmission line (at least for thin width to height ratios) is strongly dependent on the permittivity of the region above the line (Venkatesh and Raghavan 2005). This effect has been utilized in implementing microwave circuits and to a lesser extent investigation of dielectric permittivity. Furthermore, the measurement of effective permittivity is relatively straightforward and well suited for implementation in industrial equipment. Such a system could be based on determining the

effective permittivity of a micro strip line covered by an unknown dielectric substance (Keam and Holmes 1995).

Six-port reflectometer (SPR) using an open-ended coaxial probe: SPR can provide nondestructive broadband permittivity measurements with accuracy comparable to commercial one (Venkatesh and Raghavan 2005). Nondestructive broadband permittivity measurements using open-ended coaxial lines as impedance sensors are of great interest in a wide variety of biomedical applications (Ghannouchi and Bosisio 1989). The device under test is an open-ended coaxial test probe immersed in the test liquid kept at a constant temperature. Data acquisition and reduction are fully automatic. This effective transmission line method, used to represent the fringing fields in the test medium, provided a good model to interpret microwave permittivity measurements in dielectric liquids. Using such a model, the precision on relatively high-loss dielectric liquid measurements is expected to be good. However this method involves a more complex mathematical procedure in order to translate the signal characteristics into useful permittivity data (Venkatesh and Raghavan 2005).

Colloid dielectric probe: This electrical technology can quickly and accurately measure dielectric properties (permittivity) for evaluation of colloidal liquid materials in food, chemical, pharmaceutical, and biochemical industries. The advanced sensing technique provides permittivity vs. frequency characteristics. Its electromagnetic technique eliminates the electrode polarization effect, which causes measurement error when ionic materials are measured with metal electrodes (Venkatesh and Raghavan 2005).

Measurement of correct dielectric constant as envisaged from the preceding paragraphs is a difficult job. The relative static permittivity, ε_r, is measured for static electric fields as follows: first the capacitance of a test capacitor, C_0, is measured with vacuum between its plates. Then, using the same capacitor and distance between its plates the capacitance C_x with a dielectric between the plates is measured. The relative dielectric constant can be calculated as

$$\varepsilon_r = \frac{C_x}{C_0} \tag{8.8}$$

Various instrumental setups nowadays are available to measure the capacitance of a sample. Reader can choose the most suitable for their type of samples.

8.2 Thermal Imaging

Thermal imaging (TI) is an emerging, noninvasive process analytical technique suitable for the food industry. Originally it was developed for military applications, but has recently emerged as a powerful nondestructive measurement technique in other industries (Gowen et al. 2010). It is an emerging tool for food quality and safety assessment in the food industry too (Gowen et al. 2010). Thermal imaging is a technique to convert the invisible radiation pattern of an object into visible

images for feature extraction and analysis (Vadivambal and Jayas 2010). Thermal imaging or infrared (IR) thermography is a two-dimensional, noncontact diagnostic technique for measuring surface temperature of materials which can be usefully employed in non destructive quality evaluation (Giorleo and Meola 2002, Gowen et al. 2010). Thermal imaging utilizes the radiation emitted to produce a pseudo image of thermal distribution of a body surface. In thermography, a large number of point temperatures are measured over an area and processed to form a thermal map or thermogram of the target surface. Thermography with high spatial resolution is a powerful tool for analyzing and visualizing targets with thermal gradients. Research to date shows that opportunities exist for its potential application in food quality and safety control. Nondestructive evaluation using this technique provides information of product properties such as discontinuities and separations; structure; dimensions and metrology; physical and mechanical properties; composition and chemical analysis; stress and dynamic response; signature analysis and abnormal sources of heat (Giorleo and Meola 2002). It is a nondestructive, non-contact system of recording temperature by measuring infrared radiation emitted by a body surface (Arora et al. 2008). Food processors are increasingly investigating new and innovative technologies for food quality and safety profiling. Thermal imaging studies were limited due

Table 8.5 Advantages and disadvantages of selected measurement techniques

Technique	Principle	Advantages	Disadvantages
Visual testing	Mechanical-optical	Low cost, minimum training	Time consuming, low resolution, repeatability and high error
Radiographic testing	Penetrating radiation	Non-contact	Time consuming, hazardous
Nuclear magnetic resonance	Magnetic field	Quick, can be used in routine analysis	Expensive
Ultrasonic testing	Sonic-ultrasonic	Non-contact	Single point measurement, limited to acoustics impedance
Thermal imaging	Temperature and heat flow measurements	Non-contact, no harmful radiation, high portability, real-time imaging	Requires training, expensive
X-ray topography	Electromagnetic spectrum wavelength (<1 nm)	Non-contact	Time consuming, hazardous, not applicable to bulk flowing products
Hyperspectral imaging	Spectroscopy	Multi-constituent information Sensitivity to minor components	Requires training, expensive

to the poor sensitivity of the TI systems available (Gowen et al. 2010). With the advancement in computer, analytical tools with digitalized high-resolution imaging, it has found application in various other fields including medicine, material science and fire safety (Amon et al. 2008). In medical sciences, thermal imaging has been shown to be a useful method for analyzing patterns of temperature change, which can help to locate areas of maximum heat production (McCullagh et al. 2000). Thermal imaging quantifies the changes in surface temperature with high temporal and spatial resolution compared to single point measurements as in the case of other contact methods (e.g. thermocouples, thermometers). Recent advances and potential applications of TI for food safety and quality assessment such as temperature validation bruise and foreign body detection and grain quality evaluation are reviewed. Applications of TI for determining food quality and safety and comparison of this technique with other key nondestructive methods were reviewed by Gowen et al. (2010) and are presented in Table 8.5. Thermal imaging systems are suitable for a wide range of applications due to their portability, real-time imaging, noninvasive and noncontact temperature measurement capability. They can also be applied to real food systems without alteration (Nott and Hall 1999). Increasing demands for objectivity, consistency and efficiency within the food industry, have necessitated the introduction of computer-based image processing techniques which have already been discussed in Chap. 3.

8.3 Magnetic Methods

Magnetic materials are suitable for characterization of changes in structure of ferromagnetic materials, because their magnetization processes are closely related to the microstructure of the materials. This fact also make the magnetic measurements an evident candidate for nondestructive testing, for detection and characterization of any modification and/or defects in materials and manufactured products made of such materials. Structural non-magnetic properties of ferromagnetic materials have been nondestructively tested using various magnetic methods for a long time but with fair success only. The application of magnetic methods, therefore, in daily testing has not been succeeded.

The main research therefore in this method is focused towards clarification and quantification of relationship between microstructure and magnetism in materials and develop in-situ magnetic inspection techniques for quantitative nondestructive evaluation of components and structures including: (i) methods for evaluating performance related properties of materials from their structure sensitive magnetic properties (ii) new techniques and instrumentations for evaluation of materials conditions using magnetic properties, and (iii) models for description of magnetic properties and their dependence on structure.

A large number and quite different methods exist in this area. Few are: magnetic hysteresis loop measurements, barkhausen noise measurement, magnetic acoustic emission, micromagnetic, multiparameter, microstructure, and stress analysis,

magnetic flux leakage analysis, combination of conventional eddy current technique with magnetic field measurement, magneto-optical methods, magnetostrictive delay line technique and classic low frequency magnetometry. Majority of these methodologies are being tried in metallurgy and may be tried in food items to detect the presence of items having ferromagnetic characteristics and properties in food. Magnetic resonance imaging (MRI) is being tried world wide.

MRI primarily was developed and being used as a medical diagnostic tool. It is a technique for obtaining high-resolution images of internal structure by mapping the distribution of hydrogen nuclei. The principle of MRI is that all atomic nuclei with an odd number of protons are positively charged. As nuclei spin, they create micro-magnetic fields around themselves, so that each nucleus resembles a tiny bar magnet with the north and south poles along the axis of spin. Ordinarily, nuclei are oriented randomly so that there is no net magnetic field. However, if a strong and uniform external magnetic field is applied, the nuclei will line up to create a detectable magnetic field. This technique however is costly and requires special skill to use in field. This technique has been covered in detail in Chap. 5.

8.4 Modeling of Quality Attributes

Foods are numerous, so as the quality attributes too. It is therefore usually difficult to measure all the quality attributes of any food item. People therefore measure some important attributes and decide about the overall quality of a particular food. Here, two important quality parameters such as maturity and over all quality index of some fruits and freshness index of vegetables, which are often not measureable directly, have been reproduced from literature for understanding the modeling process of quality attributes.

8.4.1 Maturity Index

Maturity is a concept which is not easy to define quantitatively. For the purpose, three maturity indices of apple have been introduced: physiological maturity, Streif index and respiratory maturity (Peirs et al. 2005).

(a) Physiological maturity

Physiological maturity is defined as the number of days before the optimal harvest date. The harvest date is set equal to the mean of the period provided to the growers. Generally this period is 1–2 weeks longer, depending on the cultivar, and is predicted based on a comparison of time course of soluble solids content, acidity, background colour, size, firmness and Streif index with historical data. The disadvantage of this approach, however, is that the prediction is some extent a subjective interpretation and that the accuracy of the harvest prediction can only be verified based on the fruit quality after a few months

of storage and subsequent shelf-life, i.e., at consumption. In addition, the measurements are very time-consuming. Calibration models, which are based on the relation between historical spectral data and their respective harvest dates, would offer a tool to non destructively predict the harvest date of future fruit, a couple of weeks prior to harvest.

(b) Streif index

Streif index is an indirect measurement of the maturity, which is widely used by commercial growers in Belgium and other countries in Europe, and is a combination of three fruit attributes: firmness, soluble solids content and starch index. The Streif index is calculated using Eqn as follows (Streif 1996):

$$I_s = \frac{F}{R \times S} \tag{8.9}$$

Where, I_s is Streif index, F is firmness in kgcm^{-2}, R soluble solids content in ^{o}Brix and S is starch index.

The Streif index decreases exponentially during maturation of the fruit until reaching the cultivar-specific threshold value for optimal harvest. At this point, fruit destined for extended storage must be harvested. The Streif index latter on can be correlated with physiological maturity and may also be modeled with NIR spectral data for nondestructive prediction.

Based on the concept of relation between development of physiological maturity and soluble solids content, another simple maturity index for mango has been developed as expressed in the following Eqn (Jha et al. 2007):

$$I_m = \frac{T_s}{8} \times 100 \tag{8.10}$$

where, I_m is maturity index in percent, T_s is total soluble solids content in ^{o}Brix. This index may vary from about 50% maturity to even up to 250%. When values reach to about 100% it is assumed that mango is fully mature for harvesting. Beyond this value, it indicates over-maturity or states of ripeness. Highly ripped mango will have value of I_m as high as 250% or more.

(c) Respiratory maturity

Changes in respiration rate up to the respiration minimum are also used to monitor the change in maturity. The optimal harvest date is typically slightly later than this minimum. Respiration rate calculation is well known in the text so is not being presented here. The respiratory maturity was defined as the number of days between the measurement date and the day when the minimal respiration rate was reached. The minimum of this curve was determined by calculation of the derivative of the second-order polynomial that best fitted through the data points. The disadvantage of this technique is that the minimum is found rather late while the growers have to be informed a few weeks in advance. Further, it is not relevant to use NIR spectra to predict the respiration rate as the absolute minimal respiration rate might differ among the seasons. Therefore, it is

suggested to examine the relation between spectra and time remaining until the respiratory minimum is reached (Peirs et al. 2005).

8.4.2 Quality Index

Quality of food is a relative term and is judged subjectively. It has been described in detail in Chap. 1. For quantitative determination of quality, various factors (quality attributes) have to be taken together to formulate an index which would give the overall idea of the product quality. Sometimes it is also referred as freshness index which gives an idea of how old or new the products are, or what approximately remaining shelf life of the product will be?

(a) *Formulation of quality index (I_q)*: Jha et al. (2010b) modeled various quality parameters of apple to define the overall quality in terms of quality index (I_q). At the outset they assumed the index for a very good selected apple as one and then fourteen model expressions (Table 8.6) taking ideas from the trends of quality attributes such as TSS, titratable acidity, gloss, density, colour values, yellowness index etc. with physiological maturity were formulated. For the purpose, experience from literature (Jha et al. 2007) and preliminary trials on many other expressions, not shown here, were also considered. The I_q values were thereafter computed at each storage interval and matched with the trends of likeness of the sensory panel for selecting the best expression. The computed

Table 8.6 Possible models for computing overall quality index (I_q) of apple

Model no.	Model equations
1.	$D \times T_S \times G_{60}/Y_i$
2.	$G_{45} \times T_S/(L + a + b)$
3.	$G_{60} \times T_S/(L + a + b)$
4.	$T_S \times G_{60}/(\mathrm{T_S/A})$
5.	$A \times T_S/\lvert(a \times b)\rvert$
6.	$A \times T_S \times \mathrm{D}/\lvert(a \times b)\rvert$
7.	$T_S \times G_{45}/Y_i$
8.	$T_S \times G_{60}/Y_i$
9.	$T_S \times G_{60}/(T_S/A \times D)$
10.	$T_S \times G_{45}/(Y_i \times D)$
11.	$A \times T_S \times D \times G_{45}/(b \times Y_i)$
12.	$G_{45} \times G_{60} \times D/L$
13.	$A \times G_{60}/(b + Y_i)$
14.	$Y_i/(D \times T_S/A)$

T_s, total soluble solid in °Brix; A, acidity in %; G_{45} and G_{60} are gloss values at 45 and 60° angle in GU, respectively; D, density in $\mathrm{kgm^{-3}}$; L, a, b are colour values; Y_i, yellowness index.

Table 8.7 Computed quality index of apple using different model equations

	Storage period (days)									
Model no.	0	2	4	6	8	11	21	23	26	28
1.	1.050	0.544	0.350	0.451	0.446	0.490	0.451	0.459	0.397	0.345
2.	1.233	0.931	0.726	0.708	0.685	0.732	0.755	0.733	0.682	0.622
3.	1.096	0.616	0.407	0.506	0.440	0.521	0.471	0.492	0.418	0.384
4.	1.072	0.456	0.272	0.351	0.301	0.250	0.198	0.249	0.249	0.210
5.	1.008	0.659	0.533	0.553	0.514	0.344	0.281	0.369	0.260	0.267
6.	1.040	0.645	0.518	0.537	0.509	0.337	0.273	0.358	0.254	0.257
7.	1.168	0.839	0.642	0.652	0.701	0.703	0.743	0.704	0.663	0.580
8.	1.039	0.556	0.361	0.466	0.451	0.501	0.465	0.473	0.407	0.358
9.	1.060	0.466	0.280	0.361	0.304	0.257	0.204	0.256	0.255	0.218
10.	1.155	0.858	0.661	0.672	0.709	0.718	0.765	0.724	0.680	0.602
11.	1.015	0.506	0.352	0.334	0.292	0.232	0.195	0.233	0.230	0.218
12.	1.001	0.469	0.243	0.283	0.277	0.304	0.266	0.263	0.289	0.212
13.	1.038	0.426	0.250	0.314	0.277	0.222	0.167	0.212	0.210	0.177
14.	1.020	0.839	0.776	0.776	0.674	0.513	0.439	0.542	0.628	0.609

I_q from selected model was thereafter correlated to storage period and other measured parameters to know its predictability nondestructively.

Selection of expression for overall quality index: Computed I_q using various model equations were ranged between 1.001 and 0.177 (Table 8.7). The trends of computed values of I_q of model number 5 and 12 indicated that the initial values of quality index are very nearer to one as assumed, but values computed by model 12 declined suddenly after 2 days, during storage. The sudden fall in quality within 2 days of storage was not visible and was also not indicated by the sensory panel. It was probably because this model comprised of only physical parameters. The values computed by model 5, however, yielded gradual changes in quality index as compared to any other model and was comprised of both physical as well as biochemical parameters. Other researchers had have also indicated the importance of both physical and bio-chemical parameters on maturity. Therefore, model 5 was tentatively selected for further validation.

The range of quality index and percent of likeness of apple (Table 8.8) indicate that initially, majority of apples were either liked extremely or moderately. The degree of likeness was determined till 100% respondents extremely disliked the apples. The data indicated that "liked extremely" decreased to a level of 31% when predicted I_q was in the range of 0.69–0.60. The sensory scores also indicated that deterioration in apple is as gradual as the computed quality index. The trend of acceptability of apple was thus almost matching with the trend of predicted quality. Thus, the expression (model no. 5) (Table 8.6) was finally selected among all the expressions. The quality index of apple thus may be defined as the ratio of product of acidity (%) and TSS (°Brix) to the mode of product of *a* and *b* Hunter colour values of apple.

Table 8.8 Percentage of respondents for sensory scores with their predicted quality index (I_q) using model no. 5

Predicted quality index	Liked extremely (9[a])	Liked moderately (7[a])	Disliked moderately (3[a])	Disliked extremely (1[a])	Remarks
1.00–0.90	64	35	1	0	Good taste and appeal
0.89–0.80	58	33	7	2	Good taste but, not fresh
0.79–0.70	44	30	19	7	Fair appearance & taste
0.69–0.60	31	28	28	13	Dull colour and gloss Y
0.59–0.50	26	25	33	16	Shriveled, rotting spots
0.49–0.40	11	18	24	47	Partially rotten
0.39–0.30	0	0	8	92	Major portions rotten
0.29–0.20	0	0	0	100	Unacceptable, rejected

[a]Sensory scores (9 point hedonic scale).

Relationship between I_q and measured quality parameters: Regression equations viz. linear, logarithmic, power, second order polynomial and exponential were fitted to computed I_q and measured quality parameters and storage period to see the possibility of predicting I_q using either of these physico-chemical parameters nondestructively. Best fitted expressions with their respective correlation coefficients are presented in Table 8.9. It shows that I_q decreased inversely with storage period. Rate of decrease was initially faster (almost exponential)

Table 8.9 Regression equations with their corresponding correlation coefficient (R) for various measured quality parameters

Parameter	Regression equation	R
Total soluble solids	$-0.0006\ S_p^3 + 0.0225\ S_p^2 - 0.1332\ S_p + 12.927$	0.940
Acidity	$-7E{-}06\ S_p^3 + 0.0005\ S_p^2 - 0.0118\ S_p + 0.151$	0.956
Gloss at 45°	$-0.0009\ S_p^3 + 0.0432\ S_p^2 - 0.6143\ S_p + 7.136$	0.918
Gloss at 60°	$-0.001\ S_p^3 + 0.0502\ S_p^2 - 0.7098\ S_p + 5.8204$	0.859
Density	$-1E{-}05\ S_p^3 + 0.0005\ S_p^2 - 0.0072\ S_p + 1.0005$	0.808
L values	$-0.0011\ S_p^3 + 0.0238\ S_p^2 + 0.3277\ S_p + 49.319$	0.859
a values	$0.0016\ S_p^3 - 0.0495\ S_p^2 + 0.419\ S_p + 11.146$	0.937
b values	$-0.001\ S_p^3 + 0.0243\ S_p^2 + 0.213\ S_p + 18.317$	0.939
Yellowness index	$0.0011\ S_p^3 - 0.0452\ S_p^2 + 0.8507\ S_p + 86.032$	0.915

S_p, Storage period in days.

than at latter stages and reached to its minimum value of 0.26 after storage period of 23 days, and thereafter it became almost constant. It decreased with increase in TSS whereas, it increased with increase in acidity. This means that as the TSS increased with storage, the degree of likeness got reduced, whereas the apple with slightly acidic taste is preferred by the consumer. Similarly the I_q increased with increase in gloss and density of apple during storage period. This is due to the fact that glossy surface and non-shriveled fruit surface is always preferred. Density and gloss actually decreased with storage period and quality index follows the trend. At the end of storage period of 28 days the overall indices were about 0.26 and 0.3. These values are almost the same as those computed using storage period, yellowness index and at stage of rejection of apple by the sensory panel. The color values (L, a, b) and yellowness index was satisfactorily correlated with the computed quality index and decreased with the increase of these parameters. This is in line with the trend followed by the acceptability scores. This might be attributed to the perception that red, less green and less yellow apples are liked by the consumers. Comparison of results indicated that consumers might reject the apple even if the quality index comes about 0.25–0.3. Similar trends for the colour values with strong correlations with the consumer acceptability has also been reported by Vieira et al. (2009), Drogoudi et al. (2008), Iglesias et al. (2008), Orak (2007).

Based on respiration rate Joas et al. (2009) has developed a ripening class index (R_{ci}) of mango. The R_{ci} was used to study the impact of agronomic conditions such as leaf-to-fruit ratio and harvest stage on the changes in physicochemical criteria traditionally used as quality descriptors. Sugar content increases with the increase in carbon supply and the harvest stage, whereas the titratable acidity and the hue angle decrease during ripening. This type of index can be used to validate the relevance of harvest indicators by verifying the homogeneity of the changes in stored batches or for more effectively assessing the impact of a storage technique on fruit metabolism.

(b) *Freshness index* (I_f): The freshness index of eggplant was defined as the ratio of product of relative spectral reflectance (surface gloss) and stiffness ratio to the density ratio and was computed using mean surface gloss ratio (G_{sr}), stiffness ratio (S_r) and density ratio (D_r) of eggplant as below (Jha and Matsuoka 2002):

$$I_f = \frac{G_{sr} S_r}{D_r} \tag{8.11}$$

8.5 Practical Applications

8.5.1 Electrical Technology

The most common application of electrical technology is in the determination of moisture content of agricultural materials. One of the earliest applications of such electrical properties is the study of direct current (d.c.) and electrical resistance of grain for rapid determination of its moisture content. Jha and Matsuoka (2004)

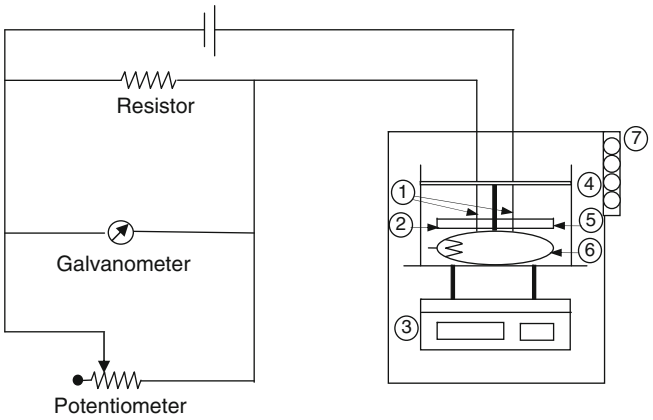

Fig. 8.2 Schematic arrangement of instruments used for measuring the electrical resistance of the eggplant: (*1*) platinum electrode; (*2*) insulated plate; (*3*) electronic balance; (*4*) sample holder; (*5*) cloth piece; (*6*) eggplant fruit; (*7*) constant temperature chamber (Jha and Matsuoka 2004)

determined the electrical resistances of eggplant fruits (Fig. 8.2) and correlated them with gloss, weight and storage period; and advanced applications of electrical resistance measurement was compiled by Leppack (1998). Later radio-frequency (RF) measurements (Kim et al. 2003, Nelson and Payne 1982, Nelson and Whitney 1960, Wang et al. 2006a, 2001), changes in the capacitance of sample-holding capacitors, when grain samples were introduced between the capacitor plates, were correlated with grain moisture content and used for grain moisture measurement (Nelson 1996, 2006). Dielectric properties of various agri-foods and biological materials are finding increasing application, as fast and new technology is adapted for use in their respective industries and research laboratories. Kato (1997) developed a sorting system based on soluble solids content of watermelon using the concept of electrical density and Bauchot et al. (2000) assessed the physiological condition of kiwifruit using electrical impedance spectroscopy. A convenient, simple, rapid and nondestructive method using electrical properties for evaluating the moisture content (Toyoda 2003) and monitoring the quality of various agricultural materials has been developed (Nelson 1991, 2005, Barbosa et al. 2006). Majority of the food materials, including oils and fat (Cataldo et al. 2010, Pace et al. 1968, Lizhi et al 2010, El-shaml et al 1992, Carey and Hayzen 2008, Fritsch et al 1979, Hein et al 1998, Inoue et al 2002), meat and poultry (Basaran et al. 2010, Li and Barringer 1997, Ragni et al. 2007, Castro-Giráldez et al. 2010, Ghatass et al 2008), fruits and vegetables (Garcia et al. 2001, Gordeev 1998, Guo et al. 2007a, Harker and Dunlop 1994, Harker and Forbes 1997, Harker and Maindonald 1994, Inaba et al 1995, Maezawa and Akimoto 1996, Nelson 1980, 2008, Nelson et al. 2007, 2006, Ikediala et al. 2001, Tran et al. 1984, Varlan and Sansen 1996, Bauchot et al 2000) and dairy products (Nunes et al. 2006, Kudra et al 1992, O'Connor and Synnot 1982, Prakash and Armstrong 1970, Rzepecka and Pereira 1974) are availablein literature and some of them are presented in Tables 8.1–8.3, 8.10.

Table 8.10 Dielectric property data for red meat and red meat products

Source	Frequency (MHz)		Product	Frequency (MHz)	Temperature (°C)	Dielectric constant	Dielectric loss factor
	RF (<300 MHz)	MW (>300 MHz)					
Van Dyke et al. (1969)	–	915	Beef	915	0–1	–	15
Bengtsson and Risman (1971)	–	3,000 (2,800)	Beef	2,800	0	47.8	16.5
				2,800	–10	5	2
				2,800	–20	4	1
To et al. (1974)	–	300	Beef	300	+5	48	58.4
		915		915	+5	56	21
		2,450		2,450	+5	52.5	17.5
Tran and Stuchly (1987)	100	–	Beef	100	+1.2	63.6	115.3
Sipahioglu et al. (2003)	–	2,450	Ham	2,450	–10	7	3
				2,450	+5	46.6	526.7
Zhang et al. (2004)	27.12	896	Pork	2,450	+5	36.08	17.14
	915		Luncheon, roll				

8.5.2 Thermal Imaging

Thermal imaging (TI) is well recognized as an important sensing technology for detection, monitoring and diagnosis in medical and military applications. However, recently, thermal imaging has found applications in other biological systems including agriculture and food processing for process monitoring, product development and storage analysis (Alchanatis et al. 2006, Chaerle and Van der 2000, Gowen et al. 2010, Lamprecht et al. 2002, Oerke et al. 2006, Stajnko et al. 2004, Sugiura et al. 2007, Vadivambal and Jayas Digvir 2010). Infrared thermal imaging was first developed for military purposes but later gained a wide application in various fields such as aerospace, agriculture, civil engineering, medicine, and veterinary. Infrared thermal imaging technology can be applied in all fields where temperature differences could be used to assist in evaluation, diagnosis, or analysis of a process or product. Potential use of thermal imaging in agriculture and food industry includes predicting water stress in crops, planning irrigation scheduling, disease and pathogen detection in plants, predicting fruit yield, evaluating the maturing of fruits, bruise detection in fruits and vegetables, detection of foreign bodies in food material and temperature distribution during cooking. Applications of thermal imaging in agriculture and food industry are presented in Tables 8.11

Table 8.11 Application of thermal imaging in food quality evaluation

Food product	Application	Reference
Chicken	Combined IR imaging-neural network method: Internal temperature of meat immediately following cooking	Ibarra et al. (2000)
Food simulant	Controlled heating and cooling cycles at the surface of food samples	Foster et al. (2006)
Wheat grain	Detection of infestations by six developmental stages (four larval instars, pupae and adults) of *Cryptolestes ferrugineus* inside wheat kernels	Manickavasagan et al. (2008c)
Apple	Detection of bruises in apples during forced convective heat transfer	Varith et al. (2003)
Apple	Surface quality analysis of apple	Veraverbeke et al. (2006)
Tomato	Bruise damage (soft spots)	Van Linden et al. (2003)
Potato, cauliflower	Ice nucleation and freezing of plants	Fuller and Wisniewski (1998)
Wheat	Wheat class identification	(Manickavasagan et al. 2008a, b)
Meat	Pig meat quality defects	Gariepy et al. (1989)
Walnut	Temperature–time history and surface temperature distributions of walnut kernels during radio frequency treatment	Wang et al. (2006)
Citrus drying	Determination of drying time for citrus fruit	Fito et al. (2004)

Table 8.12 Application of thermal imaging in post-harvest and food industry operations

Product	Problem	Results from IR thermal imaging studies	References
Apple (*Malus domestica*)	Bruise detection in fruits is a major issue in fruit quality	Possible to determine bruises at an early stage	Baranowski et al. (2008), Varith et al. (2003), Danno et al. (1977)
Apple, cherry tomato (*Solanum lycopersicum*) Japanese persimmon (*Disopyros kaki* L), Japanese pear (*Pyrus serotina* Rehder), tomato	Non-destructive method for maturity evaluation is not available	IR thermal imaging makes it possible to determine the maturity of fruits	Hellebrand et al. (2000), Offerman et al. (1998), Danno et al. (1980)
Wheat (*Triticum aestivum*)	Lack of rapid online method to determine varietal purity	IR imaging has a potential to identify wheat classes	Manickavasagan et al. (2008a, b)
Hazel nuts, chocolate chunks	Lack of system to determine all contamination in food irrespective of shape or size	Possible to determine all sorts of impurities such as leaves, stalks, pedicels, thorns, and foul nuts	Warmann and Märgner (2005), Ginesu et al. (2004)
Potato (*Solanum tuberosum*)	Maintaining optimum temperature in a storage facility is a challenge	Optimization of climate control in storage facility is feasible	Geyer et al. (2004)
Wheat (*T. aestivum*)	Rapid detection of insect infestation is a challenge	Insect infestation could be determined to certain accuracy in wheat using IR thermal imaging	Manickavasagan et al.(2008c)
Ground beef; grain	Temperature mapping not feasible	Temperature mapping enables safe cooking temperature and safe temperature to maintain seed quality	Berry (2000), Manickavasagan et al. (2006)
Citrus (*Citrus sinensis*)	Citrus surface drying results in reduced sensory quality and shelf life	Drying time could be established; fruit quality could be improved	Fito et al. (2004)
Packaging material	Non destructive technique to detect packaging defect not available	IR imaging has potential to detect cracks, delamination, and voids in packaging material	Liu and Dias (2002)

and 8.12. Thermal imaging has been employed to facilitate controlled heating and cooling cycles at the surface of food samples (Foster et al. 2006). Ibarra et al. (2000) estimated the internal temperature of chicken meat immediately after cooking using TI working within a spectral range of 3.4–5.0 μm. Application of thermal imaging can improve heat consumption and fruit quality control (Fito et al. 2004). Thermal imaging can be used to trace the ingress of potentially contaminated air to reduce the airborne contamination of foods (Burfoot et al. 2000).

(a) Fruits and vegetables' quality

Maturity evaluation of fruits and vegetables is a crucial operation in both pre-harvest and post-harvest stages. Even though several automatic methods are available for this purpose, visual inspection is followed in many parts of the world (Manickavasagan et al. 2005). This manual method of maturity evaluation is a time consuming process and human fatigue frequently influences the results (Danno et al. 1980). Thermal imaging has potential applications in many post-harvest operation such as quality evaluation of fruits and vegetables (e.g. bruise detection in fruits, maturity evaluation of fruits), quality testing of meat, detection of foreign materials in food, temperature mapping in cooked food and grain, drying, and detection of defects in packaging (Vadivambal and Jayas Digvir 2010). Bruising is the major factor for rejecting fruits during sorting because bruised fruits can cause significant damage to unbruised fruits during storage as well as consumers are not willing to purchase fruits with bruises. The existing sorting systems are not capable of effectively distinguishing fruit with bruises which has occurred at short time before inspection. Mechanically damaged fruits and vegetables result in significant economic losses for food processors due to impaired appearance, increased microbial contamination and accelerated ripening (Varith et al. 2003). With the advancement in imaging technology on-line detection of subtle bruises on fruits and vegetables is feasible. Non destructive methods for detecting bruised fruits using imaging technologies including hyperspectral imaging have been reported (Gowen et al. 2007, Ueno et al. 2008, Zhao et al. 2008). Thermal imaging also shows potential for objective quantification of bruise damage in fruits and vegetables. The first application of thermal imaging as a potential alternative technique for bruise detection in apples was reported by Danno et al. (1980). They monitored bruised apples under changes in temperature by means of natural convection. Varith et al. (2003) concluded that the bruise detection was mainly due to the variation in thermal diffusivity, not due to thermal emissivity differences since they observed no temperature differences between bruised and sound tissue under steady state conditions.

(b) Grain quality

Grain infestation by pests, microbial spoilage or contamination is a significant problem for the food industry. Manual inspection, sieving, cracking-floatation and Berlese funnels are used to detect insects in grain handling

facilities. However, these methods are not efficient and time consuming (Neethirajan et al. 2007) with poor accuracy for the developing life stages of pests. Detection of pest infestation in food commodities and in their storage premises is essential to ensure wholesome and acceptable produce for human consumption, for regulatory compliance, for diagnosis of incipient infestation and to ascertain the success of the control measures such as fumigants (Rajendran 1999). Application of thermal imaging for the detection of all insect post-embryonic stages is based on the temperature difference due to heat production during respiration compared to grain temperature (Emekci et al. 2002, 2004). This temperature difference due to infestation inside a kernel can be detected by thermal imaging. Manickavasagan et al. (2008c) studied the temperature distribution pattern of the infested wheat kernel and observed a strong correlation between the temperature distribution patterns of infested grain surface with the respiration rate of each insect developmental stage. These studies show the potential for on-line continuous detection of food grain infestation. Manickavasagan et al. (2006) studied the application of thermal imaging for detection of hot spots in grain storage silos, reporting that thermal imaging was possible only after coating the silo exterior with high emissivity paint. Recently Manickavasagan et al. (2008a,b) showed the potential of thermal imaging for classification of wheat cultivars which are difficult to distinguish by visual inspection. They observed higher accuracies in pair wise discrimination and concluded that thermal imaging approaches may have potential to develop classification methods for varieties and grain classification.

(c) Detection of foreign body in food

The presence of foreign bodies in food is a major safety concern and various methods are employed in the food industry. Visual inspection is commonly used but it is affected by several factors. Physical separation methods such as sieving, sedimentation, screening, filtering, and gravity systems are used and more sophisticated systems such as metal detectors, X-ray machines, optical sensors, and ultrasonic methods are used for the detection of foreign objects, which have been dealt in previous chapters. But there is no system capable of determining every contaminant regardless of size and shape. The presence of foreign bodies in food is a major food safety issue. The thermography technique may be used as a supplementary method to detect foreign materials, which could not be separated by mechanical and optical methods. Meinlschmidt and Maergner (2003) reported that thermography could be used to detect foreign substances in the food material very easily. The quality of detection was related to the physical behaviour of the food and the foreign body, their form, and the noise of the images. Ginesu et al. (2004) studied the potential of thermal imaging to detect foreign bodies in food products using a Thermosensorik CMT 384 thermal camera and concluded that results are promising and thermal imaging has a potential to detect foreign bodies in food materials.

8.5.3 Magnetic Properties

Various methods for using magnetic properties in nondestructive methods of quality evaluation have been indicated in previous paragraphs. Till now no application in food, however, has been reported, except work based on magnetic resonance imaging, which has already been covered in Chap. 5.

8.5.4 Modeling of Quality Attributes

Quality attributes such as invisible surface bruises, colour, gloss, firmness, density, volume expansion of processed food (Jha and Parsad 1996) etc. are important in first instance when consumer proceed for selection of food items. Often they select food materials, particularly fruits and vegetables by judging these parameters visually. Multiple efforts have been made to determine these parameters visually. A fluorescence technique was used to detect invisible surface bruises on Satsuma mandarins (Uozumi et al. 1987). They also tested this method successfully to know the freshness of cucumbers and eggs.

Glossiness and colour, in fact, are the only visual attributes for measuring the quality of fruits and vegetables. A unique gloss meter for measuring the gloss of curved surfaces was used in parallel with a conventional, flat surface glossmeter to measure peel gloss of ripening banana (Ward and Nussinovitch 1996). Usually banana ripeness is judged by the colour of the peel. The new glossmeter is able to measure the peel correctly which helps in predicting the correct time and level of ripening. This is also able to measure the gloss of other fruits and vegetables such as green bell pepper, orange, tomato, eggplant and onion. Jha et al. (2002) measured the gloss using spectroradiometer, light source and computer (Fig. 8.3) and correlated the same with weight for easy and nondestructive prediction of freshness of eggplant fruits.

Different forms of equation, viz., linear, power, exponential, and second order polynomial were fitted to the data of I_f and weight ratio, density ratio, stiffness ratio, surface gloss ratio, and storage period and best empirical models were found as below (Jha and Matsuoka 2002):

$$I_f = 0.979\left(\frac{w}{w_0}\right)^{19.303} \tag{8.12}$$

$$I_f = 0.919\left(\frac{\rho}{\rho_0}\right)^{-6.27} \tag{8.13}$$

$$I_f = 1.01e^{-0.0194\theta} \tag{8.14}$$

$$I_f = 1.05S_r - 0.107 \tag{8.15}$$

$$I_f = 12.905G_{sr}^2 - 18.71G_{sr} + 6.83 \tag{8.16}$$

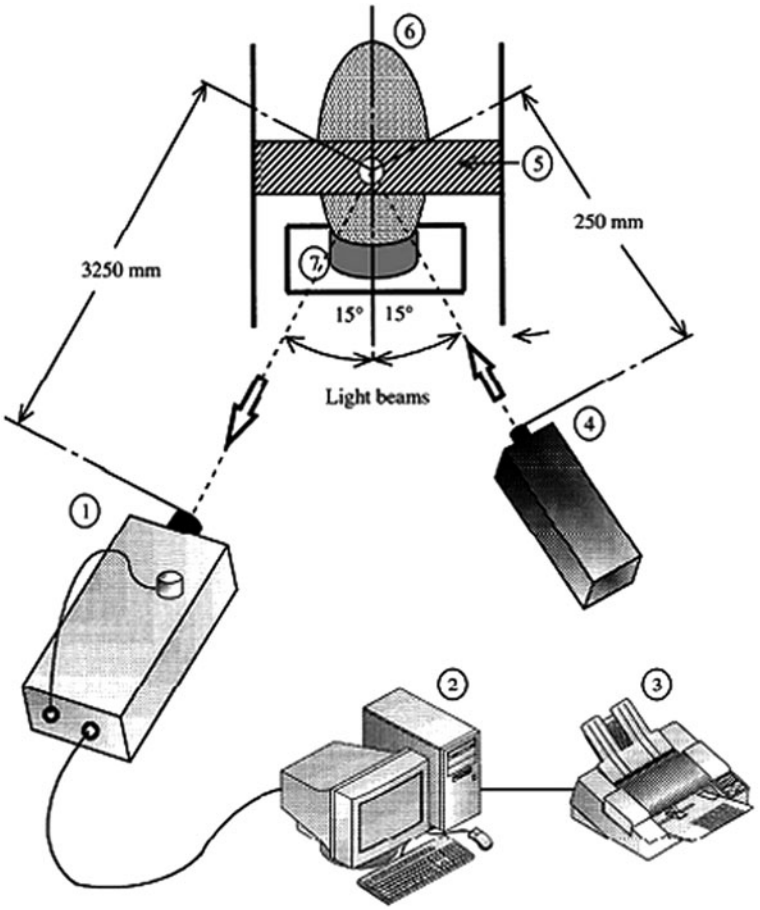

Fig. 8.3 Schematic arrangement of instruments used for the measurement of surface reflectance (spectral radiation): (*1*) spectroradiometer; (*2*) computer; (*3*) printer; (*4*) light source; (*5*) sample holder; (*6*) sample eggplant; (*7*) sample table (Jha et al. 2002)

Where w, ρ, θ, are weight, density and time at any storage period W_o, $\rho_{o\,at}$ and zero storage period, respectively, whereas S_r, and G_{sr} are stiffness ratio and surface gloss ratio of eggplant fruits during storage. I_f of another group of samples including the fresh one was then computed using above equations and were plotted against price variation in local vegetable markets to know the price of stored eggplant fruits based on quality parameters or storage period.

Another property that helps a consumer in deciding the quality is firmness. Takao (1988) developed a fruit hardness tester that can measure the firmness of kiwifruit nondestructively. The tester is called a "HIT counter" after the three words, hardness, immaturity and texture. By just setting the sample in the tester, the amount of change in shape is measured and a digital reading within a few seconds indicates

about the freshness. Based on the same principle another on-line prototype HIT counter, fruit hardness sorting machine has also been developed (Takao and Omori 1991). A computer driven testing system to measure the firmness and other physical properties of fruit and vegetables was reported by Duprat et al. (1995). The system had multiple functions and was used for a range of crops in either destructive or non destructive mode. Measurements made include skin firmness or rupture strength, flesh firmness at any given depth, compressibility, modulus of elasticity, energy absorption during a loading cycle, and compression strength between flat platens. The system consisted of a computer with a multi-function input/output card and two computer controlled stepper motors which drove a vertical column up to 4 mm s^{-1}. Various indenters were attached to the column to compress or crush the fruit sample. The specimen to be sampled was placed on a load cell under the indenter column, and the output from the load cell was fed to the computer at a sampling rate of 40 kHz through an analogue/digital converter. The computer was programmed to conduct the required test measurements as soon as the specimen was detected. In this way, measurements could be taken by inexperienced personnel too. Each test took under 30 s to complete, and results were fed back to the user immediately. System had successfully been tested for tomatoes, apples and cherries.

In addition to above, a novel fruit firmness index has been proposed (Cherng and Ouyang 2003) for solid ellipsoids with one long and two equal short principal axes, usually possessed by the most of fruits. The developed index is dependent on the mass, density, and two natural frequencies of the lowest spherical modes (under free boundary conditions) moving along long and short axes, respectively. In fact, the new index is a generalization of the conventional firmness index for a sphere, because the two natural frequencies for an ellipsoid become equal for a sphere. This newly developed index extends the firmness estimation for fruits or vegetables from a spherical to an ellipsoidal shape. The formula was developed using the following steps: (1) assign mode shape functions observed from a finite element model; (2) approximate the potential energy and kinetic energy over the whole volume; (3) apply Rayleigh's quotient to determine natural frequencies in a simple form; and (4) deduce an appropriate mathematical equation relating firmness (equivalent to modulus of elasticity) with natural frequencies, mass, and density. Detailed derivations are provided, together with finite element models for verifications of the new firmness index. Satisfactory results from simulations show that the proposed formula is quite suitable for predicting the firmness of ellipsoidal fruits or vegetables.

In an interesting study, McGlone et al. (2002) have compared the prediction of dry matter and soluble solids content of unripe and ripe kiwifruit using density and NIR modeling and have reported that use of density rendered fairly similar accuracy for unripe fruit at harvest with root mean square standard error of prediction of 0.53%. This means, modeling of density accurately may successfully be used to develop nondestructive method to predict the harvest stage of fruit. Use of density has also been demonstrated for sorting of watermelon. An optimum range of density was first determined and then a new automatic density sorting system was developed to measure the hollowness of watermelon with cavities or deteriorated porous flesh to be removed and permits estimation of the soluble solids content of

this fruit. Gamma-absorption technique combined with a scanning device for continuous non destructive crop mass and growth measurement in the field has given promising results (Gutezeit 2000). The accuracy of the measurement was found to be in agreement with the direct weighing system. This method has made it possible to assess the reaction of plants and their dependence on environmental factors by growth analysis.

Six sensory attributes such as crunchiness, chewiness, touch resistance, mealiness, juiciness and fondant of apple were modeled using multi regression method which showed that some sensory parameters, like touch resistance and fondant, could be predicted reasonably with one measured parameter while for other more complex and more number of variables are needed (Mehinagic et al. 2004). Numerous softwares for modeling and solving the model are available. Neural network however has lately gained popularity as an alternative to regression models to characterize the biological processes. Its decision-making capabilities can best be used in image analysis of biological products where the shape and size classification is not governed by any mathematical function. Many neural network classifiers have been used and evaluated for classifying agricultural products, but multi-layer neural network classifiers perform such tasks best.

Preceding sections indicate that very limited work on nondestructive methods using electrical, magnetic and modeling of quality attributes have been reported. It however has demonstrated that various (physical, electrical, magnetic etc.) properties, which may be measured without harming the sample, can very easily be modeled to predict some internal quality parameters such as maturity, total soluble solids content, dry matter, sweetness, hollowness etc and possibly has removed the thinking that only high-tech techniques such as NIR and FTIR spectroscopy, X-ray, CT, MRI, ultrasonic etc. can be used for nondestructive prediction of quality of foods. One in fact needs to research which properties are important for predicting which quality parameters of ones product.

References

Afsar MN, Birch JR, Clarke RN et al (1986) Measurement of dielectric properties of materials. IEEE Trans Instrum Meas 74(1):183–199

Agilent Technologies (2005) Agilent 16452A Liquid test fixture operation and service manual, pp 3–15

Ahmed J, Ramaswamy HS, Raghavan VGS (2007) Dielectric properties of Indian basmati rice flour slurry. J Food Eng 80:1125–1133

Ahmed J, Ramaswamy HS, Raghavan VGS (2008) Dielectric properties of soybean protein isolate dispersions as a function of concentration, temperature and pH. J Food Sci 41(1):71–81

Ahmed J, Seyhun N, Ramaswamy HS et al (2009) Dielectric properties of potato puree in microwave frequency range as influenced by concentration and temperature. Int J Food Prop 12(4):896–909

Alchanatis V, Cohen Y, Cohen S et al (2006) Fusion of IR and multispectral images in the visible range for empirical and model based mapping of crop water status. Amer Soc Agric Biol Eng Paper no. 061171

Amon F, Hamins A, Bryner N et al (2008) Meaningful performance evaluation conditions for fire service thermal imaging cameras. Fire Safety J 43:541–550

Arora N, Martins D, Ruggerio D et al (2008) Effectiveness of a non-invasive digital infrared thermal imaging system in the detection of breast cancer. Am J Surg 196:523–526
ASAE (2000) Dielectric properties of grain and seed. In: ASAE Standards 2000. ASAE, St Joseph, MI, pp 549–558
Baranowski P, Lipecki J, Mazurek W et al (2008) Detection of water core in 'gloster' apples using thermography. Postharvest Biol Technol 47(3):358–366
Barbosa-Canovas GV, Juliano P, Peleg M (2006) Engineering properties of foods in food engineering. In: Encyclopaedia of Life Support Systems. Developed under Auspices of the UNESCO, EOLSS Publishers, Oxford, UK. http://www.eolss.net
Basaran P, Basaran-Akgul N, Rasco BA (2010) Dielectric properties of chicken and fish muscle treated with microbial transglutaminase. Food Chem 120(2):361–370
Bauchot AD, Harker FR, Arnold WM (2000) The use of electrical impedance spectroscopy to assess the physiological condition of kiwifruit. Postharvest Biol Technol 18:9–18
Bengtsson NE, Risman PO (1971) Dielectric properties of food at 3 GHz as determined by a cavity perturbation technique. II. Measurements on food materials. J Microw Power Electromagn Energy 6(2):107–123
Berbert PA, Queriroz DM, Melo EC (2002) Dielectric properties of common bean. Biosyst Eng 83(4):449–462
Berry BW (2000) Use of infrared thermography to assess temperature variability in beef patties cooked from the frozen and thawed states. Food Res Int 12(4):255–262
Blackham DV, Pollard RD (1997) An improved technique for permittivity measurements using a coaxial probe. IEEE Trans Instrum Meas 46(5):1093–1099
Buffler CR (1993) Viscosity and dielectric property measurements. J Food Sci 63:983–986
Buffler CR, Stanford MA (1991) Effects of dielectric and thermal properties on the microwave heating of foods. Microw World 12(4):15–23
Burfoot D, Brown K, Xu Y et al (2000) Localized air delivery systems in the food industry. Trends Food Sci Technol 11:410–418
Calay RK, Newborough M, Probert D (1995) Predictive equations for the dielectric properties of foods. Int J Food Sci Technol 29:699–713
Carey AA, Hayzen AJ (2008) The dielectric constant and oil analysis. http://www.noria.com/learning_center/category_article.asp?articleid=226 & relatedbookgroup=OilAnalysis. Accessed 29 Nov 2009
Castro-Giráldez M, Fito PJ, Fito P (2010) Application of microwaves dielectric spectroscopy for controlling pork meat (*Longissimus dorsi*) salting process. J Food Eng 97(4):484–490
Cataldo A, Piuzzi E, Cannazza G et al (2010) Quality and anti-adulteration control of vegetable oils through microwave dielectric spectroscopy. Measurement. doi:10.1016/j.measurement.2010.02.008
Chaerle L, Van der SD (2000) Imaging techniques and the early detection of plant stress. Trends Plant Sci 5(11):495–501
Cherng A-P, Ouyang F (2003) A firmness index for fruits of ellipsoidal shape. Biosyst Eng 86(1):35–44
Danno A, Miyazato M, Ishiguro E (1977) Quality evaluation of agricultural products by infrared imaging method: grading of fruits for bruise and other surface defects. Memoir Facul Agr Kagoshima Univ 14, 123–138
Danno A, Miyazato M, Ishiguro E (1980) Quality evaluation of agricultural products by infrared imaging method. III. Maturity evaluation of fruits and vegetables. Memoir Facul Agr Kagoshima Univ 16, 157–164
Datta AK, Nelson SO (2000) Fundamental physical aspects of microwave absorption and heating in handbook of microwave technology for food applications. CHIPS Publications, USA
De Loor GP, Meijboom FW (1966) The dielectric constant of foods and other materials with high water contents at microwave frequencies. J Food Technol 1:313–322
Dev SRS, Raghavan GSV, Gariepy Y (2008) Dielectric properties of egg components and microwave heating for in-shell pasteurization of eggs. J Food Eng 86(2):207–214

Drogoudi PD, Michailidis Z, Pantelidis G (2008) Peel and flesh antioxidant content and harvest quality characteristics of seven apple cultivars. Sci Hortic 115:149–153
Duprat F, Grotte M-G, Pietri E et al (1995) A multi-purpose firmness tester for fruits and vegetables. Comput Electron Agric 12:211–223
EI-Shaml SM, Selim IZ, EI-Anwar IM et al (1992) Dielectric properties for monitoring the quality of heated oils. J Am Oil Chem Soc 69(9):872–875
Emekci M, Navarro S, Donahaye E et al (2002) Azrieli, respiration of *Tribolium castaneum* (Herbst) at reduced oxygen concentrations. J Stored Prod Res 38:413–425
Emekci M, Navarro S, Donahaye E et al (2004) Respiration of *Rhyzopertha dominica* (F) at reduced oxygen concentrations. J Stored Prod Res 40:27–38
Engelder DS, Buffler CR (1991) Measuring dielectric properties of food products at microwave frequencies. Microw World 12(2):6–15
Everard CD, Fagan CC, O'Donnell CP et al (2006) Dielectric properties of process cheese from 0.3 to 3 GHz. J Food Eng 75(3):415–425
Feng H, Tang J, Cavalieri RP (2002) Dielectric properties of dehydrated apples as affected by moisture and temperature. Trans ASAE 45:129–135
Fito PJ, Ortolá MD, De los Reyes R et al (2004) Control of citrus surface drying by image analysis of infrared thermography. J Food Eng 61(3):287–290
Foster AM, Ketteringham LP, Swain MJ et al (2006) Design and development of apparatus to provide repeatable surface temperature–time treatments on inoculated food samples. J Food Eng 76:7–18
Fritsch CW, Egberg DC, Magnuson JS (1979) Changes in dielectric constant as a measure of frying oil deterioration. J Am Oil Chem Soc 56(8):746–750
Fuller MP, Wisniewski M (1998) The use of infrared thermal imaging in the study of ice nucleation and freezing of plants. J Therm Biol 23:81–89
Garcia A, Torres JL, De Blas M (2001) Dielectric properties of fruits. J Food Eng 48:203–211
Garcia A, Torres JL, De Blas M et al (2004) Dielectric characteristics of grape juice and wine. Biosyst Eng 88(3):343–349
Gariepy C, Amiot J, Nadai S (1989) Ante-mortem detection of PSE and DFD by infrared thermography of pigs before stunning. Meat Sci 25:37–41
Gerard H, Markx C, Davey L (1999) The dielectric properties of biological cells at radiofrequencies: applications in biotechnology. Enzyme Microb Technol 25:161–171
Geyer S, Gottschalk K, Hellebrand HJ et al (2004) Application of a thermal imaging measuring system to optimize the climate control of potato stores. In: Agricultural Engineering conference, Leuven, Belgium, 12–16 Sept 2004, pp 1066–1067
Ghannouchi FM, Bosisio RG (1989) Measurement of microwave permittivity using a six-port reflectometer with an open-ended coaxial line. IEEE Trans Instrum Meas 38(2):505–508
Ghatass ZF, Soliman MM, Mohamed MM (2008) Dielectric technique for quality control of beef meat in the range 10 kHz–1 MHz. Am Euras J Sci Res 3(1):62–69
Ginesu G, Giusto D, Märgner V et al (2004) Detection of foreign bodies in food by thermal image processing. IEEE Trans Ind Electron 51:480–490
Giorleo G, Meola C (2002) Comparison between pulsed and modulated thermography in glass–epoxy laminates. NDT E Int 35(5):287–292
Gordeev AS (1998) Electro-physical criteria of fruit quality in Russia. Mechaniz Elektr Sel' Choz 7:10–16
Gowen AA, O'Donnell CP, Cullen PJ et al (2007) Hyperspectral imaging: an emerging process analytical tool for food quality and safety control. Trends Food Sci Technol 18(12): 590–598
Gowen AA, Tiwari BK, Cullen PJ et al (2010) Applications of thermal imaging in food quality and safety assessment – review. Trend Food Sci Technol 21(4):190–200
Grant JP, Clarke RN, Symm GT et al (1989) A critical study of the open-ended coaxial line sensor technique for RF and microwave complex permittivity measurements. J Phys Electron Sci Instrum 22:757–770

Green AD (1997) Measurements of the dielectric properties of cheddar cheese. J Microw Power Electromagn Energy 32(1):16–27
Guan D, Cheng M, Wang Y et al (2004) Dielectric properties of mashed potatoes relevant to microwave and radio-frequency pasteurization and sterilization processes. J Food Sci 69(1):30–37
Guo W, Nelson SO, Trabelsi S et al (2007a) 10–1800 MHz dielectric properties of fresh apples during storage. J Food Eng 83:562–569
Guo W, Tiwari G, Tang J et al (2008) Frequency, moisture and temperature-dependent dielectric properties of chickpea flour. Biosyst Eng 101:217–224
Guo W, Trabelsi S, Nelson SO et al (2007b) Storage effects on dielectric properties of eggs from 10 to 1800 MHz. J Food Sci 72:E335–E340
Guo W, Wang S, Tiwari G et al (2010) Temperature and moisture dependent dielectric properties of legume flour associated with dielectric heating. Food Sci Technol 43:193–201
Guo W, Zhu X, Liu Yi et al (2010) Sugar and water contents of honey with dielectric property sensing. J Food Eng 97(2):275–281
Gutezeit B (2000) Non-destructive measurement of fresh plant mass by the gamma-scanning technique applied to broccoli. J Agri Eng Res 75:251–255
Harker FR, Dunlop J (1994) Electrical impedance studies of nectarines during cool storage and fruit ripening. Postharvest Biol Technol 4:125–134
Harker FR, Forbes SK (1997) Ripening and development of chilling injury in persimmon fruit: an electrical impedance study. N Z J Crop Hortic Sci 25:149–157
Harker FR, Maindonald JH (1994) Ripening of nectarine fruit: changes in the cell wall, vacuole, and membranes detected using electrical impedance measurements. Plant Physiol 106:165–171
Hasted JB, Ritson DM, Colic CH (1948) Dielectric properties of aqueous ionic solutions. Part 1 and 2. J Chem Phys 16(1):1–21
Hein M, Henning H, Isengard HD (1998) Determination of total polar with new methods for the quality survey of frying oils and fats. Talanta 47:447–454
Hellebrand HJ, Linke M, Beuche H et al (2000) Horticultural products evaluated by thermography. In: Agricultural Engineering 2000, Paper No. 00-PH-003, University of Warwick, UK, 2–7 July 2000
Herve AG, Tang J, Luedecke L et al (1998) Dielectric properties of cottage cheese and surface treatment using microwaves. J Food Eng 37(4):389–410
Hewlett-Packard (1992) Basics of measuring the dielectric properties of materials. Application Note 1217–1221
Hlavacova Z (2003) Low frequency electric properties utilization in agriculture and food treatment. Agric Eng Res 49(4):125–136
Ibarra JG, Tao Y, Xin H (2000) Combined IR imaging-neural network method for the estimation of internal temperature in cooked chicken meat. Opt Eng 39(11):3032–3038
Icyer F, Baysal T (2004a) Dielectric properties of food materials-2: measurement techniques. Crit Rev Food Sci Nutr 44:473–478
Icyer F, Baysal T (2004b) Dielectrical properties of food materials: factors affecting and industrial uses. Crit Rev Food Sci Nutr 44:465–471
Iglesias I, Echeverria G, Soria Y (2008) Differences in fruit colour development, anthocyanin content, fruit quality and consumer acceptability of eight Gala apple strains. Sci Hortic 119:32–40
Ikediala JN, Tang J, Drake SR et al (2000) Dielectric properties of apple cultivars and codling moth larvae. Trans ASAE 43(5):1175–1184
Ikediala JN, Tang J, Drake SR et al (2001) Dielectric properties of apple cultivars and codling moth larvae. Trans ASAE 43(5):1175–1184
Inaba A, Manabe T, Tsuji H et al (1995) Electrical impedance analysis of tissue properties associated with ethylene induction by electric currents in cucumber (*Cucumis sativus* L.) fruit. Plant Physiol 107:199–205

Inoue C, Hagura Y, Ishikawa M et al (2002) The dielectric property of soybean oil in deep fat frying and the effect of frequency. J Food Sci 67:1126–1129
Jha SN, Chopra S, Kingsly ARP (2007) Modeling of colour values for nondestructive evaluation of maturity of mango. J Food Eng 78:22–26
Jha SN, Matsuoka T (2002) Development of freshness index of eggplant. Appl Eng Agric 18(5):555–558
Jha SN, Matsuoka T (2004) Changes in electrical resistance of eggplant with gloss, weight and storage period. Biosyst Eng 87(1):119–123
Jha SN, Matsuoka T, Miyauchi K (2002) Surface gloss and weight of eggplant during storage. Biosyst Eng 81(4):407–412
Jha SN, Narsaiah K, Basedia A et al (2010a) Measurement techniques and application of electrical properties for nondestructive quality evaluation of foods – a review. J Food Sci Technol. Accepted for publication
Jha SN, Parsad S (1996) Determination of processing conditions of gorgon nut (*Euryale ferox*). J Agric Eng Res 63:103–112
Jha SN, Rai DR, Rajiv R (2010b) Physico-chemical quality parameters and overall quality index of apple during storage. J Food Sci Technol. Accepted for publication
Joas J, Caro Y, Lechaudel M (2009) Comparison of postharvest changes in mango (cv Cogshall) using a ripening class index (Rci) for different carbon supplies and harvest dates. Postharvest Biol Technol 54:25–31
Kato K (1997) Electrical density sorting and estimation of soluble solids content of watermelon. J Agric Eng Res 67(2):161–170
Keam RB, Holmes WS (1995) Uncertainty analysis of measurement of complex permittivity using micro strip transmission line. In: Proceedings SBMO/IEEE MTT-S, Rio de Jenerio, Brazil
Kent M (1970) Complex permittivity of white fish meal in the microwave region as a function of temperature and moisture content. J Phys D Appl Phys 3:1275–1283
Kent M (1972) Microwave dielectric properties of fishmeal. J Microw Power Electromagn Energy 7(2):109–116
Kent M (1977) Complex permittivity of fishmeal: a general discussion of temperature, density and moisture dependence. J Microw Power Electromagn Energy 12(4):341–345
Kent M (1987) Electrical and dielectric properties of food materials. A bibliography and tabulated data. A COST 90bis production. Science and Technology Publishers, Hornchurch
Kent M, Kress-Rogers E (1986) Microwave moisture and density measurements in particulate solids. Trans Instrum Meas Control 8(3):167–168
Kent M, Kress-Rogers E (1987) The COST 90bis collaborative work on the dielectric properties of foods. In: Jowitt R, Escher F, Kent M, McKenna B, Roques M (eds) Physical properties of foods. 2. COST 90bis. Final Seminar proceedings, Elsevier Applied Science, London
Kim KB, Lee SS, Noh MS (2003) On-line measurement of grain moisture content using RF impedance. Trans ASAE 46(3):861–867
Kim YR, Morgan MT, Okos MR et al (1998) Measurement and prediction of dielectric properties of biscuit dough at 27 MHz. J Microw Power Electromagn Energy 33(3):184–194
Kraszewski A (1980) Microwave aquametry. J Microw Power Electromagn Energy 15:209–220
Kraszewski A (1996) Microwave aquametry: electromagnetic interaction with water containing materials. IEEE Press, Piscataway, NJ, Volume 47 2005 Canadian Biosystems Engng 7.29
Kraszewski AW, Nelson SO (1989) Composite model of the complex permittivity of cereal grain. J Agric Eng Res 43:211–219
Kudra T, Raghavan SV, Akyel C et al (1992) Electromagnetic properties of milk and its constituents at 2.45 MHz. J Microw Power Electromagn Energy 27(4):199–204
Lamprecht I, Schmolz E, Blanco L, Romero CM (2002) Flower ovens: thermal investigations on heat producing plants. Thermochim Acta 391(1–2):107–118
Lawrence KC, Nelson SO, Bartley PG Jr (1998) Coaxial dielectric sensor for cereal grains. Institute of Electrical and Electronics Engineers. IEEE IMTC Proc 1:541–546
Lawrence KC, Nelson SO, Kraszewski AW (1992) Temperature dependence of the dielectric properties of pecan. Trans ASAE 35(1):251–255

Leppack E (1998) Advanced application of resistance measurement. Kartoffelbau 49:150–154
Li A, Barringer SA (1997) The effect of salt on the dielectric properties of ham at sterilization temperatures. IFT Annu Meet Book Abstr 55(5):155
Liao X, Raghavan GSV, Meda V et al (2001) Dielectric properties of supersaturated a-D-glucose aqueous solutions at 2450 MHz. J Microw Power Electromagn Energy 36(3):131–138
Liu Y, Dias R (2002) Evaluation of package defects by thermal imaging. In: Proceedings from the 28th international symposium for Testing and Failure Analysis, Phoenix, Arizona, 3–7 Nov 2002
Liu C, Sakai N (1999) Dielectric properties of tuna at 2450 MHz and 915 MHz as a function of temperature. J Jpn Soc Food Sci Technol 20:42–45
Lizhi Hu, Toyoda K, Ihara I (2008) Dielectric properties of edible oils and fatty acids as a function of frequency, temperature, moisture and composition. J Food Eng 88:151–158
Lizhi Hu, Toyoda K, Ihara I (2010) Discrimination of olive oil adulterated with vegetable oils using dielectric spectroscopy. J Food Eng 96(2):167–171
Lu Y, Fujii M, Kanai H (1998) Dielectric analysis of hen egg white with denaturation and in cool storage. Int J Food Sci Technol 33:393–399
Lyng JG, Scully M, McKenna BM (2002) The influence of compositional changes in beef burgers on their temperatures during microwave heating and their thermal and dielectric properties. J Muscle Food 13:123–142
Lyng JG, Zhang L, Brunton NP (2005) A survey of the dielectric properties of meats and ingredients used in meat product manufacture. Meat Sci 69:589–602
Maezawa S, Akimoto K (1996) Characteristics of electrical conductivity of low-temperature sensitive vegetables. Res Bull Fac Agric Gifu Univ Jpn 61:81–86
Manickavasagan A, Jayas DS, White NDG et al (2005) Thermal imaging of a stored grain silo to detect a hot spot. The Canadian Society for Engineering in Agriculture Biological Systems. Paper No. 05-002
Manickavasagan A, Jayas DS, White NDG et al (2006) Thermal imaging of a stored grain silo to detect a hot spot. Appl Eng Agric 22(6):891–897
Manickavasagan A, Jayas DS, White NDG et al (2008a) Wheat class identification using thermal imaging. Food Bioprocess Technol. doi: 10.1007/s11947-008-0110-x
Manickavasagan A, Jayas DS, White NDG et al (2008b) Wheat class identification using thermal imaging: a potential innovative technique. Trans ASABE 51(2):649–651
Manickavasagan A, Jayas DS, White NDG (2008c) Thermal imaging to detect infestation by *Cryptolestes ferrugineus* inside wheat kernels. J Stored Prod Res 44(2):186–192
Mashimo S, Kuwabara S, Yagihara S et al (1987) Dielectric relaxation structure of bound water in biological materials. J Phys Chem 91(25):6337–6338
McCullagh JJP, Setchell DJ, Gulabivala K et al (2000) A comparison of thermocouple and infrared thermographic analysis of temperature rise on the root surface during the continuous wave of condensation technique. Int Endod J 33:326–332
McGlone VA, Jordan RB, Seelye R et al (2002) Comparing density and NIR methods for measurement of kiwifruit dry matter and soluble solids content. Postharvest Biol Technol 26:191–198
Mehinagic E, Royer G, Symoneaux R et al (2004) Prediction of the sensory quality of apples by physical measurements. Postharvest Biol Technol 34:257–269
Meinlschmidt P, Maergner V (2003) Thermographic techniques and adapted algorithms for automatic detection of foreign bodies in food. In: Conference Thermosense XXV, Orlando, FL, pp 168–176
Mellgren E, Ohlsson T, Risman PO et al (1988) Dielectric properties of wheat bread dough. In: Asp N-G (ed) Cereal Science and Technology in Sweden, Proceedings from an international symposium, Ystad, Sweden, 13–16 June 1988, pp 322–324
Meyer W, Schilz W (1980) A microwave method for density independent determination of the moisture content of solids. J Phys D Appl Phys 13:1823–1836
Miller LA, Gordon J, Davis EA (1991) Dielectric and thermal transition properties of chemically modified starches during heating. Cereal Chem 68(5):441–448

Mudgett RE (1986) Electrical properties of foods. In:Rao MA, Rizvi SSH (eds) Engineering properties of foods. Marcel Dekker, New York, pp 329–390
Mudgett RE (1995) Dielectric properties of food. In: Decareau RV (ed) Microwaves in the food processing industry. Academic Press, Orlando, pp 15–37
Neethirajan S, Karunakaran C, Jayas DS et al (2007) Detection techniques for stored-product insects in grain. Food Control 18:157–162
Nelson SO (1965) Dielectric properties of grain and seed in the 1 to 50-MC range. Trans ASAE 8(1):38–43
Nelson SO (1973) Electrical properties of agricultural products – a critical review. Trans ASAE 16:384–400
Nelson SO (1980) Microwave dielectric properties of fresh fruits and vegetables. Trans ASAE 23:1314–1317
Nelson SO (1983) Dielectric properties of some fresh fruits and vegetables at frequencies of 2.45 to 22 GHz. Trans ASAE 26:613–616
Nelson SO (1984) Moisture, frequency, and density dependence of the dielectric constant of shelled, yellow-dent field corn. Trans ASAE 30(5):1573–1578, 1585
Nelson SO (1987) Models for the dielectric constants of cereal grains and soybeans. J Microw Power Electromagn Energy 22:35–39
Nelson SO (1991) Dielectric properties of agricultural products measurements and applications. IEEE Trans Dielectr Electr Insul 26(5):845–869
Nelson SO (1992) Microwave dielectric properties of fresh onions. Trans ASAE 35:963–966
Nelson SO (1996) Review and assessment of radio-frequency and microwave energy for stored grain insect control. Trans ASAE 39(4):1475–1484
Nelson SO (1999) Dielectric properties measurement techniques and applications. Trans ASAE 42(2):523–529
Nelson SO (2003) Frequency and temperature dependent permittivities of fresh fruits and vegetables from 0.01 to 1.8 GHz. Trans ASAE 46:567–574
Nelson SO (2005) Dielectric spectroscopy in agriculture. J Non Cryst Solids 351:2940–2944
Nelson SO (2006) Agricultural applications of dielectric measurements. IEEE Trans Dielectr Electr Insul 13:688–702
Nelson SO (2008) Dielectric properties of agricultural products and some applications. Agric Eng Res 54(2):104–112
Nelson SO, Bartley PG (2000) Measuring frequency and temperature dependent dielectric properties of food materials. Trans ASAE 43(6):1733–1736
Nelson SO, Bartley PG Jr (2002) Frequency and temperature dependence of the dielectric properties of food materials. Trans ASAE 45:1223–1227
Nelson SO, Forbus WR Jr, Lawrence KC (1994) Permittivities of fresh fruits and vegetables at 0.2 to 20 GHz. J Microw Power Electromagn Energy 29:81–93
Nelson SO, Forbus WR Jr, Lawrence KC (1995) Assessment of microwave permittivity for sensing peach maturity. Trans ASAE 38:579–585
Nelson SO, Guo W, Trabelsi S et al (2007) Dielectric spectroscopy of watermelons for quality sensing. Meas Sci Technol 18:1887–1892
Nelson SO, Payne JA (1982) RF dielectric heating for pecan weevil control. Trans ASAE 25(2):456–458, 464
Nelson SO, Stetson LE, Schlaphoff CW (1974) A general computer program for precise calculation of dielectric properties from short-circuited wave-guide measurements. IEEE Trans Instrum Meas 23(4):455–460
Nelson SO, Trabelsi S, Kays SJ (2006) Dielectric spectroscopy of honeydew melons from 10 MHz to 1.8 GHz for quality sensing. Trans ASABE 49:1977–1981
Nelson SO, Whitney WK (1960) Radio-frequency electric fields for stored-grain insect control. Trans ASAE 3:133–137
Nelson SO, You TS (1989) Microwave dielectric properties of corn and wheat kernels and soybeans. Trans ASAE 32(1):242–249

Nott KP, Hall LD (1999) Advances in temperature validation of foods. Trends Food Sci Technol 10:366–374
Nunes AC, Bohigas X, Tejada J (2006) Dielectric study of milk for frequencies between 1 and 20 GHz. J Food Eng 76:250–255
Nyfors E, Vainikainen P (1989) Industrial microwave sensors, Chapter 2. Artech House, Norwood, MA
O'Connor JF, Synnot EC (1982) Seasonal variation in dielectric properties of butter at 15 MHz and 4°C. J Food Sci Technol 6:49–59
Oerke EC, Steiner U, Dehne HW et al (2006) Thermal imaging of cucumber leaves affected by downy mildew and environmental conditions. J Exp Bot 57(9):2121–2132
Offermann S, Bicanic D, Krapez JC et al (1998) Infrared transient thermography for noncontact, non-destructive inspection of whole and dissected apples and of cherry tomatoes at different maturity stages. Instrum Sci Technol 26(2&3):145–155
Ohlsson T (1989) Dielectric properties and microwave processing. In: Singh RP, Medina AG (eds) Food properties and computer-aided engineering of food processing systems. Kluwer Academic Publishers, Norwell, MA
Ohlsson T, Bengtsson NE (1975) Dielectric food data for microwave sterilization processing. J Microw Power Electromagn Energy 10:93–108
Ohlsson T, Bengtsson NE, Risman PO (1974a) The frequency and temperature dependence of dielectric food data as determined by a cavity perturbation technique. J Microw Power Electromagn Energy 9:129–145
Ohlsson T, Henriques M, Bengtsson N (1974b) Dielectric properties of model meat emulsions at 900 and 2800 MHz in relation to their composition. J Food Sci 39:1153–1156
Orak HH (2007) Total antioxidant activities, phenolics, anthocyanins, polyphenoloxidase activities of selected red grape cultivars and their correlations. Sci Hortic 111:235–241
Pace W, Westphal WB, Goldblith SA (1968) Dielectric properties of commercial cooking oils. J Food Sci 33:30–36
Peirs A, Schenk A, Bart MN (2005) Effect of natural variability among apples on the accuracy of VIS-NIR calibration models for optimal harvest date predictions. Postharvest Biol Technol 35:1–13
Piyasena P, Dussault C (1999) Evaluation of a 1.5 kW radio frequency heater for its potential use in a high temperature short time (HTST) process. In: CIFST annual conference, Kelowna, BC, June
Prakash S, Armstrong JG (1970) Measurement of the dielectric constant of butter. Dairy Ind 35(10):688–689
Puranik S, Kumbhakarne AK, Mehrotra S (1991) Dielectric properties of honey-water mixture between 10 MHz and 10 GHz using time domain technique. J Microw Power Electromagn Energy 24(4):196–201
Ragni L, Al-Shami A, Galina M et al (2007) Dielectric characterization of hen eggs during storage. J Food Eng 82:450–459
Rajendran S (1999) Detection of insect infestation in stored food commodities. J Food Sci Technol 36(4):283–300
Risman PO (1991) Terminology and notation of microwave power and electromagnetic energy. J Microw Power Electromagn Energy 26:243–250
Risman PO, Bengtsson NE (1971) Dielectric properties of food at 3 GHz as determined by a cavity perturbation technique. J Microw Power Electromagn Energy 6:101–106
Roberts S, Hipple AV (1946) A new method for measuring dielectric constant and loss in the range of centimetres waves. J Appl phys 17:610–616
Roebuck BD, Goldblith SA, Westphal WB (1972) Dielectric properties of carbohydrate–water mixtures at microwave frequencies. J Food Sci 37:199–204
Rudan-Tasic D, Klofutar C (1999) Characteristics of vegetable oils of some Slovene manufactures. Acta Chim Slov 46(4):511–521

Ryynanen S (1995) The electromagnetic properties of food materials: a review of the basic principles. J Food Eng 26:409–429
Rzepecka MA, Pereira M (1974) Permittivity of some dairy products at 2450 MHz. J Microw Power Electromagn Energy 9(4):277–288
Sacilik K, Tarimci C, Colak A (2006) Dielectric properties of flaxseeds as affected by moisture content and bulk density in the radio frequency range. Biosyst Eng 93(2):153–160
Sacilik K, Tarimci C, Colak A (2007) Moisture content and bulk density dependence of dielectric properties of safflower seed in the radio frequency range. J Food Eng 78(4):1111–1116
Sharma GP, Prasad S (2002) Dielectric properties of garlic (*Allium sativum* L.) at 2450 MHz as function of temperature and moisture content. J Food Eng 52(4):343–348
Sheen NI, Woodhead IM (1999) An open-ended coaxial probe for broad-band permittivity measurement of agricultural products. J Agric Eng Res 74:193–202
Sipahioglu O, Barringer SA, Bircan C (2003) The dielectric properties of meats as a function of temperature and composition. J Microw Power Electromagn Energy 38(3):161–169
Sosa-Moralesa ME, Tiwari G, Wang S et al (2009) Dielectric heating as a potential post-harvest treatment of disinfesting mangoes, Part I: relation between dielectric properties and ripening. Biosyst Eng 103:297–303
Stajnko D, Lakota M, Hocevar M (2004) Estimation of number and diameter of apple fruits in an orchard during the growing season by thermal imaging. Comput Electron Agric 42(1):31–42
Stier RF (2004) Tests to monitor quality of deep-frying fats and oils. Eur J Lipid Sci Technol 106:766–771
Streif J (1996) Optimum harvest date for different apple cultivars in the 'bodensee' area. In: de Jager A, Johnson D, Hohn E (eds) The postharvest treatment of fruit and vegetables: determination and prediction of optimum harvest date of apple and pears, COST 94, Brussels, Belgium, pp 15–20
Stuchly MA, Stuchly SS (1980) Dielectric properties of biological substances-tabulated. J Microw Power Electromagn Energy 15:19–25
Sugiura R, Noguchi N, Ishii K (2007) Correction of low-altitude thermal images applied to estimating soil water status. Biosyst Eng 96(3):301–313
Sun E, Datta A, Lobo S (1995) Composition-based prediction of dielectric properties of foods. J Microw Power Electromagn Energy 30(4):205–212
Takao H (1988) HIT counter. Noryu Giken Kaihou 180:7–9 (in Japanese)
Takao H, Omori S (1991) Quality evaluation of fruits and vegetables using light transmittance. Noryu Giken Kaihou 145:14–16 (in Japanese)
To EC, Mudgett RE, Wang DIC et al (1974) Dielectric properties of food materials. J Microw Power Electromagn Energy 9(4):303–316
Toyoda K (2003) The utilization of electric properties. In: Sumio K (ed) The handbook of non-destructive detection. Science Forum, Tokyo, pp 108–126
Trabelsi S, Kraszewski A, Nelson SO (1997) Simultaneous determination of density and water content of particulate materials by microwave sensors. Electron Lett 33(10):874–876
Tran VN, Stuchly SS (1987) Dielectric properties of beef, beef liver, chicken and salmon at frequencies from 100 to 2500 MHz. J Microw Power Electromagn Energy 22(1):29–33
Tran VN, Stuchly SS, Kraszewski AW (1984) Dielectric properties of selected vegetables and fruits 0.1–10 GHz. J Microw Power Electromagn Energy 19(4):251–258
Tulasidas TN, Raghavan GSV, Mujumdar AS (1995b) Microwave drying of grapes in a single mode cavity at 2450 MHz-II: quality and energy aspects. Drying Technol 13(8–9): 1973–1992
Ueno A, Shu Z, Takahashi T (2008) Determination of spectral wavelengths for detecting bruise defects on apple fruits. J Jpn Soc Agric Mach 70(5):63–68
Uozumi J, Kawano S, Iwamoto M et al (1987) Spectrometric systems for the quality evaluation unevenly coloured food. Nippon Shokuhin Kagyo Gakkaishi 34:163–170
Vadivambal R, Jayas Digvir S (2010) Applications of thermal imaging in agriculture and food industry – a review. Food Bioprocess Technol. doi: 10.1007/s1194701003335

Van Dyke D, Wang DIC, Goldblith SA (1969) Dielectric loss factor of reconstituted ground beef: the effect of chemical composition. Food Technol 23(7):944–946
Van Linden V, Vereycken R, Bravo C et al (2003) Detection technique for tomato bruise damage by thermal imaging. Acta Hortic (ISHS) 599:389–394
Varith J, Hyde GM, Baritelle AL (2003) Non-contact bruise detection in apples by thermal imaging. Innov Food Sci Emerg Technol 4:211–218
Varlan AR, Sansen W (1996) Nondestructive electrical impedance analysis in fruit: normal ripening and injuries characterization. Electro Magnetobiol 15:213–227
Venkatesh MS (2002) Development of integrated dual frequency permittivity analyzer using cavity perturbation concept. Unpublished Ph.D thesis, Department of Agricultural and Biosystems Engineerings, McGill University, Montreal, QC
Venkatesh MS, Raghavan GSV (2004) An overview of microwave processing and dielectric properties of agri-food materials. Biosyst Eng 88:1–18
Venkatesh MS, Raghavan GSV (2005) An overview of dielectrical properties measuring techniques. Can Biosyst Eng 47:715–730
Veraverbeke EA, Verboven P, Lammertyn J et al (2006) Thermographic surface quality evaluation of apple. J Food Eng 77:162–168
Vieira FGK, Borges GDC, Copetti C (2009) Physico-chemical and antioxidant properties of six apple cultivars grown in southern Brazil. Sci Hortic 122:421–425
Wang S, Birla SL, Tang J (2006a) Postharvest treatment to control codling moth in fresh apples using water assisted radio frequency heating. Postharvest Biol Technol 40(1):89–96
Wang S, Ikediala JN, Tang J (2001) Radio frequency treatments to control codling moth in in-shell walnuts. Postharvest Biol Technol 22(1):29–38
Wang S, Monzon M, Gazit Y et al (2005) Temperature dependent dielectric properties of selected subtropical and tropical fruit and associated insect pests. Trans ASAE 48(5):1873–1881
Wang Yu, Tang J, Rasco B et al (2008) Dielectric properties of salmon fillets as a function of temperature and composition. J Food Eng 87(2):236–246
Wang S, Tang J, Sun T et al (2006) Considerations in design of commercial radio frequency treatments for postharvest pest control in in-shell walnuts. J Food Eng 77:304–312
Wang Y, Wig TD, Tang J et al (2003) Dielectric properties of foods relevant to RF and microwave pasteurization and sterilization. J Food Eng 57:257–268
Ward G, Nussinovitch A (1996) Peel gloss as a potential indicator of banana ripeness. Lebenson Wiss Technol 29:289–294
Warmann C, Märgner V (2005) Quality control of hazel nuts using thermographic image processing 3-17, MVA2005 IAPR conference on Machine Vision Applications, Tsukuba Science City, Japan, 16–18 May 2005
Wenchuan G, Shaojin W, Tiwari G et al (2010) Temperature and moisture dependent dielectric properties of legume flour associated with dielectric heating. Food Sci Technol 43:193–201
Zhang Lu, Lyng James G, Brunton NP (2007) The effect of fat, water and salt on the thermal and dielectric properties of meat batter and its temperature following microwave or radio frequency heating. J Food Eng 80:142–151
Zhang L, Lyng JG, Brunton N et al (2004) Dielectric and thermo physical properties of meat batters over a temperature range of 5–85°C. Meat Sci 68:173–184
Zhao JW, Liu JH, Chen QS et al (2008) Detecting subtle bruises on fruits with hyperspectral imaging. Trans Chin Soc Agric Mach 39(1):106–109
Zheng M, Huang, YW, Nelson SO et al (1998) Dielectric properties and thermal conductivity of marinated shrimp and channel catfish. J Food Sci 63(4):668–672
Zuercher JL, Hoppie R, Lade S et al (1990) Measurement of the complex permittivity of bread dough by open-ended coaxial line method at ultra-high frequency. J Microw Power Electromagn Energy 25(3):161–167

Index

S.N. Jha (ed.), *Nondestructive Evaluation of Food Quality*,
DOI 10.1007/978-3-642-15796-7,